Elucidation of multinumerous centrosomes and their impact on migration in dendritic cells

Dissertation

zur

Erlangung des Doktorgrades (Dr. rer. nat.)

der

Mathematisch-Naturwissenschaftlichen Fakultät

der

Rheinischen Friedrich-Wilhelms-Universität Bonn

vorgelegt von

Mirka Homrich

aus

Siegen

Bonn, 2023

Angefertigt mit Genehmigung der Mathematisch-Naturwissenschaftlichen Fakultät
der Rheinischen Friedrich-Wilhelms-Universität Bonn

1. Gutachterin: Prof. Dr. Eva Kiermaier

2. Gutachter: Prof. Dr. Oliver Gruß

Tag der Promotion: 14.06.2023

Erscheinungsjahr: 2023

Contents

Preliminary remarks

I hereby declare that I have written the present doctoral thesis without sources other than indicated in the main text and without help from third parties. I have designed and conducted all the experiments described in this thesis, except for

- cell sorting according to DNA content and FACS experiments with DNA content and surface marker analysis

- automated analyses of distances between centrioles and centrosomes in untreated BMDCs, manual verification of part of the results and creation of a representative figure using Matlab

which were conducted and kindly provided by Ann-Kathrin Weier and Robert Hauschild, respectively.

Data presented in figures 16 (a) and 19 (a) were generated with the help of a master's student, as indicated in the figure legends.

According to the common practice in English scientific writing, this thesis is drafted using the first-person plural narrator.

Parts of this dissertation were published in a peer-reviewed journal article with shared first authorship (*):

Multiple centrosomes enhance migration and immune cell effector functions of mature dendritic cells. Ann-Kathrin Weier*, Mirka Homrich*, Stephanie Ebbinghaus, Pavel Juda, Eliška Miková, Robert Hauschild, Lili Zhang, Thomas Quast, Elvira Mass, Andreas Schlitzer, Waldemar Kolanus, Sven Burgdorf, Oliver J. Gruß, Miroslav Hons, Stefan Wieser, Eva Kiermaier. *J Cell Biol* 2022; 221 (12): e202107134. doi: 10.1083/jcb.202107134

List of abbreviations

2D, 3D	two-dimensional, three-dimensional
2N, 4N	diploid, tetraploid
ac-tub	acetylated tubulin
ACKR4	atypical chemokine receptor 4
ANOVA	analysis of variance
APC	antigen-presenting cell
APC/C	anaphase-promoting complex/cyclosome
Arp2/3	actin related protein 2/3
BCZ	B cell zone
BMDC	bone marrow-derived dendritic cell
BSA	bovine serum albumin
Bub3	budding uninhibited by benzimidazoles 3
BubR1	Bub1-related kinase
C-NAP1	centrosomal NEK2-associated protein 1
CCL	C-C motif chemokine ligand
CCR7	C-C motif chemokine receptor 7
CD	cluster of differentiation
Cdc	cell division cycle
cDCs	conventional/classical dendritic cells
Cdk	cyclin-dependent kinase
Cdk5Rap2	Cdk5 regulatory subunit-associated protein 2
CDP	common dendritic cell progenitor
Cdt1	chromatin licensing and DNA replication factor 1
CEP	centrosomal protein
CETN2-GFP	centrin-2-green fluorescent protein
CLP	common lymphoid progenitor
CMP	common myeloid progenitor
CP110	centriolar coiled-coil protein of 110 kDa
CPAP	centrosomal P4.1-associated protein
Cy3	cyanine dye 3
DAMPs	danger-associated molecular patterns
DAPI	4',6-diamidino-2-phenylindole dihydrochloride
DC	dendritic cell
ddH_2O	double distilled water
DI water	deionized water

DMSO	dimethyl sulfoxide
DNA	deoxyribonucleic acid
e.g.	for example (from Latin: *exempli gratia*)
ECL	enhanced chemiluminescence
ECM	extracellular matrix
EdU	5-ethynyl-2′-deoxyuridine
et al.	and others (from Latin: *et alii*)
F-actin	filamentous actin
FACS	fluorescence-activated cell sorting
FCS	fetal calf serum
Fig.	figure
FUCCI	fluorescent ubiquitination-based cell cycle indicator
γ-TuRC	γ-tubulin ring complex
g	g-force (relative centrifugal force)
GEF	guanine nucleotide exchange factor
GM-CSF	granulocyte-macrophage colony-stimulating factor
GTPase	guanosine triphosphatase
HEVs	high endothelial venules
HRP	horseradish peroxidase
HSC	hematopoietic stem cell
HSET	human spleen embryonic tissue and testis
i.e.	that is (from Latin: *id est*)
ICAM-1	intercellular adhesion molecule 1
IF	immunofluorescence
Ig	immunoglobulin
KIPs	kinase inhibitor proteins
LECs	lymphatic endothelial cells
LPS	lipopolysaccharide
Mad2	mitotic-arrest deficient 2
MCC	mitotic checkpoint complex
MHC(-I/II)	major histocompatibility complex (class I/II)
MLC	myosin light chain
mo-DCs	monocyte-derived DCs
MSD	mean square displacement
MT	microtubule
MTOC	microtubule organizing center
na	nuclear area

NEDD1	neural precursor cell expressed developmentally downregulated 1
PAGE	polyacrylamide gel electrophoresis
PAK1	p21-activated kinase 1
PAMPs	pathogen-associated molecular patterns
PARP1	poly-ADP-ribose polymerase 1
PBS	phosphate-buffered saline
PCM	pericentriolar material
pDC	plasmacytoid DC
PDMS	polydimethylsiloxane
PFA	paraformaldehyde
pH3	phospho-histone H3
PI3K	phosphatidylinositol 3-kinase
PIP3	phosphatidylinositol-3,4,5-trisphosphate
Pixα	PAK-interacting exchange factor α
PLK	Polo-like kinase
pre	precursor
PRRs	pattern recognition receptors
PTMs	post-translational modifications
R10/R20	full medium used for cell culture (see *Material and methods*)
Rac1	Ras-related C3 botulinum toxin substrate 1
Rb	retinoblastoma protein
RhoA	Ras homolog family member A
ROCK1	Rho-associated protein kinase 1
ROI	region of interest
RPMI	Roswell Park Memorial Institute (cell culture medium)
RT	room temperature
SAC	spindle assembly checkpoint
SAS-6	spindle assembly abnormal protein 6
SCS	subcapsular sinus
SD	standard deviation
SDS-PAGE	sodium dodecyl sulfate polyacrylamide gel electrophoresis
t	timepoint
TBS	Tris-buffered saline
TBS-T	Tris-buffered saline with Tween
TCZ	T cell zone
TECs	tumor endothelial cells
TGS	Tris-glycine-SDS

TLR	Toll-like receptor
Tris	Tris(hydroxymethyl)aminomethane
vs.	versus
WT	wildtype
XCR1	XC-chemokine receptor 1

List of units

°C	degree Celsius
A	Ampere
h, hrs	hour, hours
kDa	kilodalton
µg	microgram
µL	microliter
µm	micrometer
µM	micromolar
mg	milligram
min	minute(s)
mL	milliliter
mm	milimeter
ng	nanogram
nm	nanometer
sec	second(s)
V	volt

Summary

Centrosomes act as major *microtubule organizing center* (MTOC) in most animal cells and are well known for their role in building up the mitotic spindle during cell division. Core structure of the centrosome are two tubulus shaped centrioles, which are connected by linker fibers and surrounded by a protein-rich matrix (*pericentriolar material*, PCM). The centrosome duplicates precisely once during the cell cycle leading to the presence of one centrosome in G1 phase and two centrosomes after centriole duplication in S phase. However, studies in our lab showed that about 20-30 % of mature murine *bone marrow-derived dendritic cells* (BMDCs) and dermal dendritic cells (dermal DCs) harbor more than one centrosome in G1 phase. The phenomenon of additional centrosomes has so far only been described for very few non-malignant cells, but is commonly observed in solid and haematological malignancies. In some cancer types, the degree of centrosome amplification is positively associated with tumor aggressiveness partly explainable by the fact that extra centrosomes can contribute to the development of metastasis. Prerequisite for the dissemination of primary tumor cells is the acquisition of a migratory phenotype.

Against this backdrop, our findings of multinumerous centrosomes shed new light on DCs – cells specialized in trafficking through complex and versatile environments –, raising the question of whether the presence of excess centrosomes in DCs has any impact on the cells' migratory behavior. In order to elucidate the origin of additional centrosomes in murine DCs we took a closer look at the cell cycle and studied centrosomes *in vitro*, *ex vivo* and *in situ*. We found that supernumerary centrosomes are neither the consequence of ongoing cell proliferation nor the result of culturing conditions. Instead, we revealed that mature DCs arrest in G1 phase of the cell cycle. Moreover, we unraveled that extra centrosomes occur by accumulation due to a modified cell division cycle or cytokinesis failures, leading to tetraploid cells with a surplus of centrosomes. Diploid cells with multiple centrosomes, on the other hand, were found to arise from a process of centriole overduplication.

We examined the functionality of multinumerous centrosomes regarding their role as MTOC and investigated DCs with different centrosome numbers during cell locomotion. Our data show that multiple centrosomes are functional by terms of microtubule (MT) nucleation and carry significantly higher numbers of MT filaments compared to DCs with only one centrosome. Furthermore, we observed that DCs with extra centrosomes show enhanced persistent locomotion, and we succeeded in demonstrating that there is a causal relationship.

Additionally, we unveiled that excess centrosomes form and maintain tight clusters during DC migration. To address the question of whether centrosomal clustering is required for proper

migration, we made use of declustering agents to chemically disturb the clustered configuration of multiple centrosomes. Declustering drugs are mainly used in mitosis experiments in cancer cell science and are seen as a hope for new therapeutic approaches. However, in contrast to the proclaimed drug specificity for (cancer) cells with supernumerary centrosomes, we also found an effect on BMDCs with only one centrosome and observed severe side effects on DCs' cytoskeleton and PCM. Therefore, observed migration effects after drug treatment could not be attributed to the declustering of multiple centrosomes making it necessary to search for alternative approaches.

Taken together, we have contradicted the paradigm of one centrosome in G1 phase of the cell cycle when observing that a non-negligible proportion of DCs carries more than one centrosome in this phase. In addition to the excess of centrosomes, the clustering of extra centrosomes was the second observed phenomenon, which is mainly known from cancer cells. However, while multinumerous centrosomes in tumor cells increase malignancy, thus being disadvantageous for the organism, DCs do not seem to acquire adverse features from additional centrosomes. On the contrary, with regard to migration *in vitro*, even rather beneficial effects are emerging by a surplus of centrosomes making further studies worthwhile.

1 Introduction

1.1 Dendritic cells

1.1.1 Ontogeny and development

Dendritic cells (DCs) belong to the leukocyte family and are the most professional antigen-presenting cells (APCs) besides macrophages and B cells[1]. DCs are found in all tissues, especially in so-called barrier organs at the interface between the body and the external environment, such as skin, lung, and intestine, but also in lymphoid organs. The main task of DCs is to monitor tissues and call the adaptive immune system into action when danger signals are detected[2], thus acting as a link between innate and adaptive immunity[2,3]. In this context, the characteristic features of DCs include **antigen uptake** and **processing** in the periphery, efficient **directional migration** toward tissue-draining lymph nodes, and the potential to **stimulate naïve T cells** by presenting antigenic peptides on *major histocompatibility complex* (MHC)-molecules[4], thus initiating (adaptive) immune responses.

Approximately 2-4 % of all leukocytes in any tissue are DCs[5]. However, DCs are a heterogeneous group of cells and there exist many different attempts of and characteristics for classification, such as ontogeny, developmental requirements, surface protein expression, functional properties or *in vivo* localization[6]. A common classification divides DCs into ”conventional” or ”classical” DCs (**cDCs**) and plasmacytoid DCs (**pDCs**)[7,8] based on the fact that the cells arise from discrete committed precursors and their development depends on distinct sets of transcription factors[7]. While cDCs are classical APCs, in particular, for activating naïve T cells, pDCs morphologically resemble plasma cells and play a crucial role in innate immunity being able to rapidly produce large amounts of type I interferons in response to viral stimuli[9–11]. However, upon stimulation, pDCs differentiate into immunogenic DCs that can prime T cells against viral antigens[8,11]. For the sake of completeness, *monocyte-derived DCs* (mo-DCs) and Langerhans cells should be mentioned as a further group of “non-classical” DCs, although they should not be the focus of attention here[4,12].

The first steps of DCs’ ontogeny take place in the bone marrow: Starting from a self-renewing *hematopoietic stem cell* (HSC), *multipotent progenitors* (MPPs) develop from which both *common lymphoid progenitors* (CLPs) and *common myeloid progenitors* (CMPs) ermerge – the first branching between cells of the myeloid and lymphoid lineages[13–15] (Fig. 1). CLPs give rise to B, T and natural killer cells and are assumed to develop into *precursor pDCs* (pre-pDCs) that later become pDCs[16,17]. In the myeloid development branch, the emergence of DCs

originates from CMPs, which also give rise to granulocytes, erythrocytes, monocytes and thrombocytes. After passing through several intermediate stages, CMPs become common DC progenitors (CDPs) that can take two paths and develop into pre-pDCs or into pre-cDCs[18,19]. From the latter, another branching leads to the two DC-subsets pre-cDC1 and pre-cDC2. Whether cDCs could also evolve from CLPs is still controversial[12].

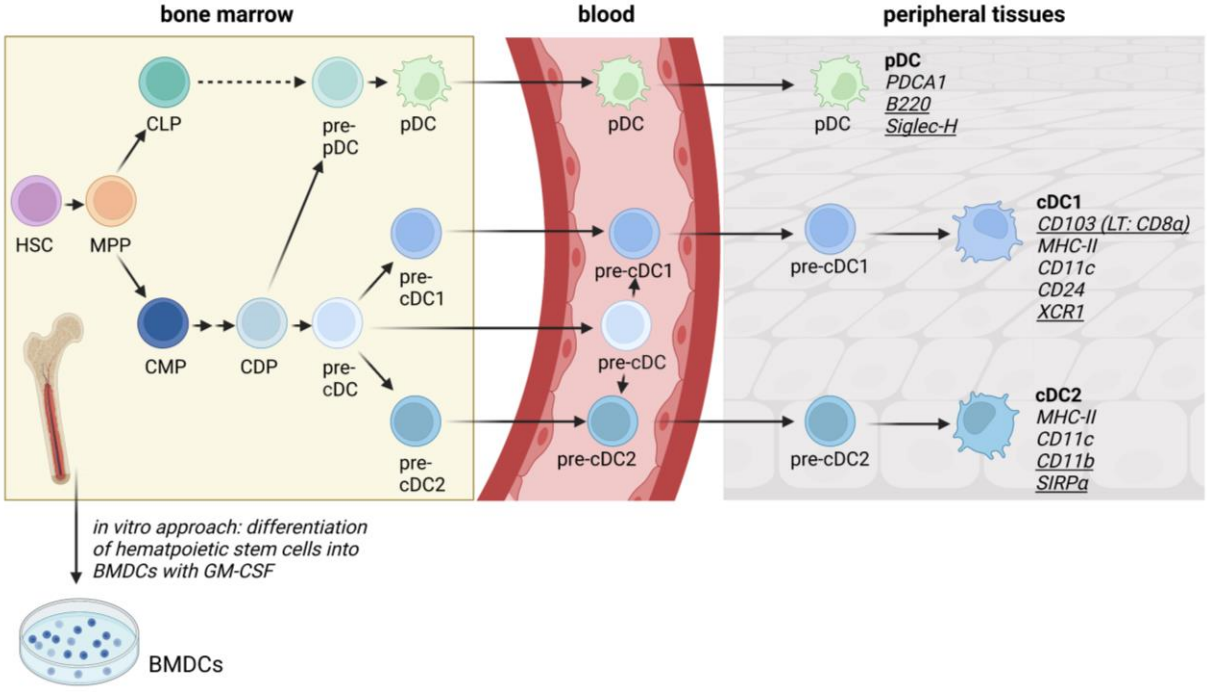

Figure 1. Ontogeny and development of dendritic cells

Conventional/classical dendritic cells (cDCs) and *plasmacytoid DCs* (pDCs) develop from precursor cells derived from *common lymphoid* and *common myeloid progenitors* (CLPs, CMPs). Their common root are *hematopoietic stem cells* (HSCs). The developmental steps take place in different tissues. BMDCs: bone marrow-derived dendritic cells; GM-CSF: granulocyte-macrophage colony-stimulating factor; LT: lymphoid tissue. Created with BioRender.com.

Unlike pDCs, whose development is completed in the bone marrow resulting in terminal differentiated cells, DCs of the myeloid branch are still in a precursor stage[18,20]. Mature pDCs leave the bone marrow into the blood stream, where they circulate, or colonize peripheral lymphoid organs[5]. Pre-cDCs migrate through the vascular system to settle lymphoid and most non-lymphoid tissues, where they locally finish their differentiation into **cDC1** and **cDC2** cells[12,21–24] (Fig. 1).

Although cDCs1 and cDCs2 constitutively express the hematopoietic markers *cluster of differentiation* (CD)45, MHC class II (MHC-II) and CD11c on their surface[8], the two subsets can be distinguished by the expression of distict surface marker combinations. cDC1 cells in peripheral (non-lymphoid) tissues are characterized by the surface protein CD103[25,26], while

the equivalent population residing in murine lymphoid organs expresses CD8α instead[27,28]. Irrespective of their localization, cDC1 cells are negative for CD11b (CD11b$^-$), but express CD24 and the *XC-chemokine receptor 1* (XCR1)[29]. While CD24 and CD103 expression are not unique to this subset[30,31], XCR1 serves as a unifying marker of cDCs1 in both human and mice[32–34]. cDC2 cells on the other hand, do not express XRC1, but *signal regulatory protein α* (SIRPα)[29]. Furthermore, cDCs2 most often lack the integrin CD103 and express the integrin CD11b (CD11b$^+$)[8]. pDCs are identified by the expression of *plasmacytoid dendritic cell antigen 1* (PDCA1)[5], B220 and *sialic acid binding Ig-like lectin H* (Siglec-H) (Fig. 1).

Due to the limited number of DCs in murine tissues, suitable *in vitro* models have been established to obtain reasonable numbers of DCs for experimental processes. One widely used protocol cultures murine bone marrow with *granulocyte-macrophage colony-stimulating factor* (GM-CSF)[8,35–38] (Fig. 1) leading to large numbers of CD11c$^+$ and MHC-II$^+$ *bone marrow-derived dendritic cells* (BMDCs) that resemble cDCs and mo-DCs, whereas pDCs do not arise[35,36,39,40]. Like DCs isolated from tissues, BMDCs derived from GM-CSF cultures are able to respond to microbial stimuli, undergo a maturation process, migrate directionally in response to chemokine stimuli and present exogenous antigens to T cells[8,41]. In the present work, BMDCs are referred to as *primary cells* to distinguish them from cell lines.

1.1.2 Tasks and specificity of cDCs

After development in the bone marrow, pre-cDCs enter the blood stream and are distributed to lymphoid organs (such as the thymus, spleen and lymph nodes, Fig. 2, path a) and non-lymphoid organs (such as the skin, Fig. 2, path b)[10]. The final cell differentiation into immature DCs is thought to take place after the cells leave the blood circulation and enter the tissues[22,23].

Circulating pre-DCs enter lymphatic tissues via *high endothelial venules* (HEVs)[2,22] and differentiate into immature DCs followed by maturation upon antigen encounter[10,22] (Fig. 2, path a). cDCs developing within secondary lymphoid organs are usually referred to as ‘lymphoid tissue-resident’ cDCs and are thus delimited from ‘non-lymphoid tissue-derived’ or ‘migratory’ cDCs homing via afferent lymph vessels into draining lymph nodes[10].

DC progenitors that populate peripheral tissues, such as mucosal surfaces, the skin and most solid organs, enter their target tissues via resting or inflamed post-capillary venules[10] (Fig. 2, path b). Here, they differentiate into immature DCs that act as sentinels of the immune system by constantly monitoring the tissues for damage or danger signals and sensing environmental stimuli[8]. Pre-cDCs that have entered murine tissue were shown to proliferate under steady-

state conditions (absence of inflammatory signal), while differentiated cDCs possess only low proliferative capacity[42].

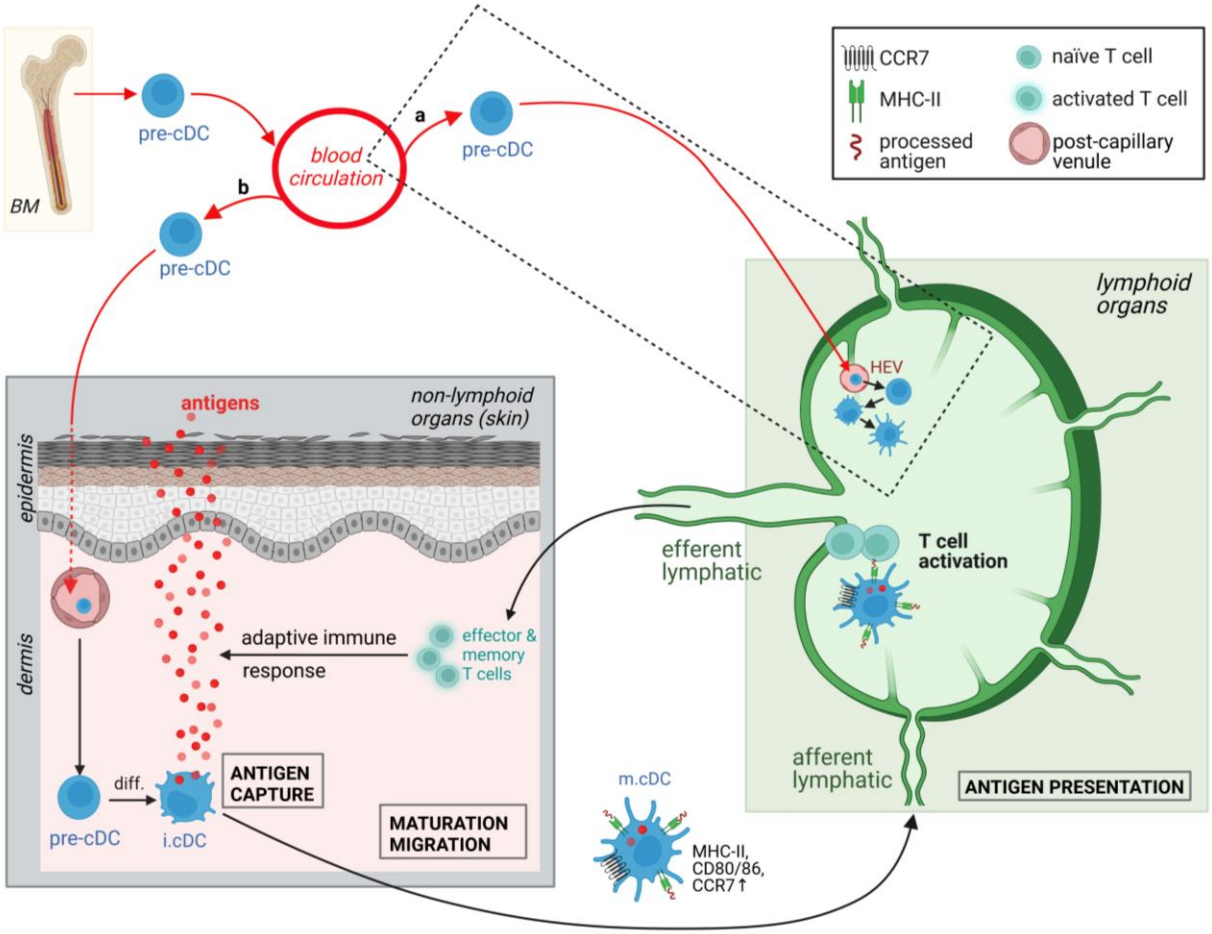

Figure 2. Distribution and tasks of conventional dendritic cells in the organism

Precursor conventional/dendritic cells (pre-cDCs) leave the bone marrow and enter the blood stream, from where they take different pathways. a) pre-cDCs enter lymphoid organs, differentiate into immature cDCs and mature upon antigen contact. b) pre-cDCs enter non-lymphoid tissues, such as the skin, where they differentiate into immature cDCs that monitor the tissue for antigens. Upon antigen uptake and processing, cDCs mature and migrate to the draining lymph node to present antigen fragments to naïve T cells inducing their activation and an adaptive immune response. BM: bone marrow; diff: differentiation; i.cDC: immature cDC. m.cDC: mature cDC. Created with BioRender.com.

The characteristic stellate extensions of immature DCs allow the cells to make expansive movements and establish a dense cellular network that enables them to detect invading pathogens[4]. At peripheral sites such as the mouse ear[43] and the gut[44], immature DCs have been shown to be motile, but highly developed mobility and motility are exhibited only by mature DCs. Immature cDCs are specialized in the sampling of foreign (and self-) antigens and use different mechanisms of antigen acquisition, such as receptor-dependent endocytosis[45,46] and phagocytosis[47,48] (for apoptotic cell material, bacteria, viruses and parasites) or micropinocytosis (in case of soluble antigens)[49]. In this context, *pattern recognition receptors* (PRRs) play a crucial role enabling the cell to distinguish between self- and foreign antigens[50,51]. PPRs, including *Toll-like receptors* (TLRs), *retinoic acid-inducible gene* (RIG)-like receptors, *nucleotide oligomerization domain* (Nod)-like receptors and C-type lectin receptors, are associated with plasma or endosomal membranes, reside in the cytosol or are localized in the nucleus[51–54] being able to sense microbial stimuli (*pathogen-associated molecular patterns*, PAMPs) or endogenous stress signals (*danger-associated molecular patterns*, DAMPs). PAMPs are highly conserved structures of pathogens and include, for instance, bacterial *lipopolysaccharide* (LPS)[55,56] which signals via TLR4[57] and is often used as stimulus for DCs in experimental settings to induce maturation. DAMPs include aberrantly expressed self-molecules, for example from dying cells or in case of necrosis or cancer[58,59], or adenosine triphosphate whose tissue concentration is normally very low but increases upon cellular damage[60].

Upon **antigen capture**, immature DCs start a process of **maturation**, thereby transforming from a resting and residing phagocytotic cell into an activated and motile antigen-presenting cell[3,61] (Fig. 2). The maturation process involves major phenotypic and genotypic changes in DCs. This includes the formation of dendrites and the upregulation of cell surface molecules related to antigen presentation, such as MHC proteins and the co-stimulatory molecules CD40, CD80, CD86[3,62,63]. Moreover, molecules for directional **migration** are increasingly expressed, including *C-C motif chemokine receptor 7* (CCR7)[64,65], which is important for the initiation of an adaptive immune response[63,64,66]. While at the beginning of the maturation process DCs' potential for antigen internalization is enhanced, this property decreases during maturation in favor of the migratory capacity so that the lymphoid organs can be reached[67,68].

After antigen uptake in the periphery, DCs process the antigen into peptide fragments and load them on MHC molecules for presentation to and activation of antigen-specific T cells in draining lymph nodes[69] (Fig. 2). Extracellular antigens, such as bacteria, are internalized and degraded in endosomes/phagosomes, before peptide fragments are bound to MHC-II molecules and transported to the DC surface[70] where they remain stable for days being available for recognition by antigen-specific $CD4^+$ T cells after the DC has reached the draining lymph

node[71]. Intracellular antigens, such as viral proteins or tumor antigens, can be presented by all cells to $CD8^+$ T cells, but to trigger a cytotoxic immune response, antigen-specific $CD8^+$ T cells first have to be primed by APCs, such as DCs[72]. Of note, MHC molecules and MHC peptide complexes are 10- to 100-fold more abundant on DCs than on other APCs[73]. After proteasomal degradation in the cytosol of DCs, resulting fragments of intracellular antigens are complexed to MHC-I molecules in the endoplasmatic reticulum and transported to the plasma membrane for presentation to $CD8^+$ T cells[72]. Moreover, DCs, along with a few other cell types, have the special property of presenting extracellular antigens on MHC-I molecules to $CD8^+$ T cells – a process called *cross-presentation*[74], which is particularly important for antiviral and antitumor immune responses[74,75].

Guided by CCR7 ligands, mature migratory DCs travel through the interstitium and enter the draining lymphoid organs via afferent lymphatic vessels[76,77] (Fig. 2). In the process of **antigen presentation**, the DCs present antigen-peptide fragments on MHC molecules to naïve T cells inducing their activation[78,79]. Of the main tasks of DCs described above, the following will focus on the process of migration.

1.2 Dendritic cell migration

1.2.1 Basics

1.2.1.1 Principles of dendritic cell migration

Like all other leukocytes, DCs are characterized by their high motility[10,80–82]. In the organs and tissues they have colonized[83], immature DCs patrol and search for danger associated antigens, which induce DC maturation and trafficking of migratory DCs to the draining lymphoid organs to initiate an adaptive immune response (see section 1.1.2). Thereby, DCs have to move within a plethora of tissue types and cross barriers requiring adaption of their motility mechanisms[3,62,80,84–86]. Main parameters in the plastic process of migration are confinement and adhesiveness[87], with the nature of the environment influencing the mode of migration.

Cell migration occurs under various geometric conditions, which include, for example, two-dimensional (2D) environments where motile cells migrate on flat surfaces (x-y plane)[81] (Fig. 3 a). This 2D environment occurs very rarely in the organism and is found, for instance, during organogenesis, when epithelial cells migrate along 2D sheets of basement membranes[88]. In addition, 2D migration is found in leukocytes that patrol along the luminal surface of blood vessels[89] or crawl across inner body surfaces, such as the peritoneum or the bronchial tract[90]. Predominant in the organism, however, is a three-dimensional (3D), structurally complex

environment (x-y-z dimension), where cells, such as DCs, are usually embedded in cell-rich compartments (e.g., in the lymph nodes) or collagen-rich interstitial matrices[91] (Fig. 3 b). Here, the environment provides confinement, which is a significant difference to 2D environments. Under 3D circumstances, at least one dimension of the environment is smaller than the average DC, which means that the cell has to deform in order to locomote[77]. Another significant difference between 2D and 3D migration is that in 2D environments no change of direction in the z dimension is possible.

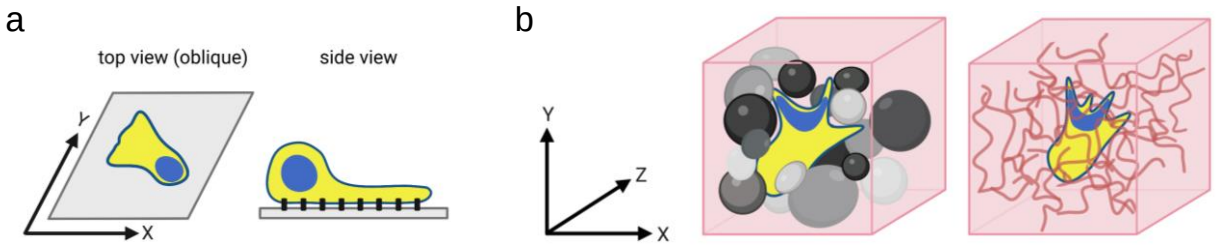

Figure 3. Models of cell migration in different environments

(**a**) 2D migration: Motile cell migrating on a flat surface using cell adhesion molecules (side view: black rectangles). (**b**) 3D migration: Motile cell migrating between cells (left) or navigating through dense tissue (right; curly lines: collagen fibers). Created with BioRender.com.

Principal elements for migration in any environment are **force generation** (membrane protrusion and contraction by molecular motors) and **force transmission/transduction** (contact interaction with the environment)[77], where the shifting of the balance between adhesive, contractile and protrusive forces produces different modes of movement[81]. Accordingly, two migration modes – among other types of migration – can be distinguished: Adhesion-dependent migration is predominantly used by mesenchymal cells (**mesenchymal migration**) and typically occurs with the help of transmembrane receptors of the integrin family, which anchor the cell to the extracellular substrate[81,92,93]. In addition to fibroblasts, which are considered the prototypical mesenchymal cells, macrophages, myoblasts and certain cancer cells and cancer cell lines also exhibit this locomotion behavior[94]. For DCs, the mesenchymal migration mode plays a minor role and only immature but not mature DCs have proteolytic capacity – a common feature of “classical” mesenchymal cells that make their way by proteolytic degradation of their environment[85,95]. Integrin-independent migration is the predominant locomotion mode of DCs in tissues[96] and the cells are characterized by gliding, weak to no cell-substrate interaction, constant shape changes and the formation of a defined front-back morphology (cell polarization, see section 1.2.1.2)[91,97]. These morphodynamic characteristics are reminiscent of the migration of the amoeba *Dictyostelium discoideum*[98]

(**amoeboid migration**), a migration mode practiced by other leukocytes besides DCs, such as neutrophils[99,100] and lymphocytes[96,100,101], and also by some tumor cells[102].

Besides, migration modes can be categorized according to the form of the present chemoattractant (CCR7 ligands): In the absence of attracting signals, random migration (non-directed locomotion) occurs, which is enhanced in the presence of homogeneous chemokine fields leading to increased random cell motility[103]. Depending on whether the cue is immobilized or soluble the moving behavior of the cells is termed "**haptokinesis**" or "**chemokinesis**", respectively[85,96,104–107] (Fig. 4 a). In case of a signal presented in the form of a gradient, cells switch from random to directional migration being guided toward the signal source[104,108]. Directional migration is characterized by the cells' ability to extend, retract, and stabilize membrane protrusions in a defined direction. If the chemokine gradient is immobilized, the cells approach via "**haptotaxis**", in contrast to soluble gradients, which induce "**chemotaxis**" of cells[85,96,104–107] (Fig. 4 b). While the migratory pattern of chemokinesis helps DCs to scan large tissue volumes[105], directed movement caused by attractant gradients enables them to efficiently reach secondary lymphoid organs[62]. For DC migration, mainly *C-C motif chemokine ligand* (CCL)19 and CCL21 play a role, differing by an elongated positively charged C-terminus, which is only present in CCL21. This "extension" increases the binding affinity to proteoglycans in the *extracellular matrix* (ECM) and on cell surfaces[109] enabling the formation of long-lasting stationary chemokine concentration gradients[110,111]. Both chemokines are abundantly expressed by stromal cells within the paracortical zone of the lymph node[112–114], but the obligate soluble CCL19 is expressed at much lower levels[115]. Moreover, CCL21 is also present on afferent *lymphatic endothelial cells* (LECs)[116] (see Fig. 6). While CCL21 is indispensable for guiding mature DCs to the lymphatic tissue[63,110,117], CLL19 is assumed to play a subordinate role in *in vivo* migration[118], although it is difficult to detect for the reasons mentioned above, making reliable conclusions about its role difficult.

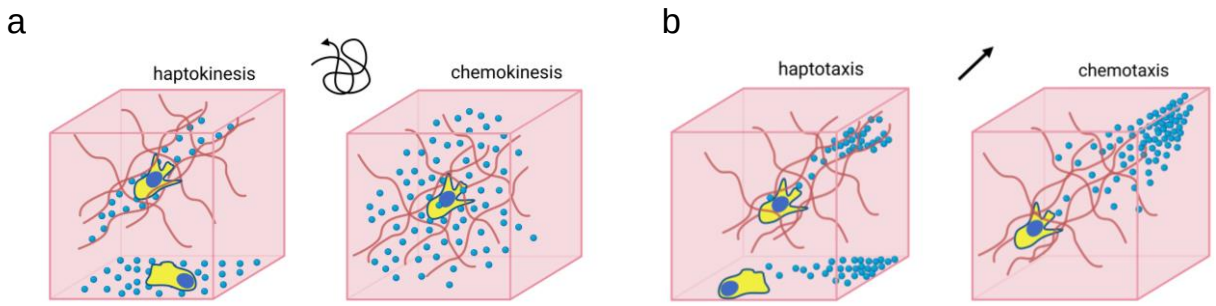

Figure 4. Cell migration behavior in relation to the presence of the chemokine

(**a**) Haptokinesis: cell moves in a field of a homogeneously distributed chemokine immobilized on structures of a 3D environment (here: collagen fibers) or on a surface (2D). Chemokinesis: cell moves in a field of a homogeneously distributed soluble chemokine. In both cases, random migration takes place (curled arrow). (**b**) Haptotaxis: cell moves along a chemokine gradient immobilized on structures of a 3D environment (here: collagen fibers) or on a surface (2D). Chemotaxis: cell moves along a soluble chemokine gradient. In both cases, directed migration takes place (straight arrow). Created with BioRender.com.

1.2.1.2 Prerequisite for migration: Cytoskeletal rearrangements

The first prerequisite for a cell to initiate migration is the acquisition of a polarized morphology that allows the translation of intracellularly generated forces into net cell movement[119]. In the process of **polarization**, cells become elongated and morphological changes occur that break cell symmetry leading to the emergence of a cell front (leading edge) and a cell back (trailing edge)[85]. The shape change can occur as spontaneous self-polarization without any external signal[120] or is induced by chemical signals in the form of chemokines, that are – in the case of DCs – ligands of the DC-transmembrane receptor CCR7[121,122].

Mainly responsible for cell polarization is the rearrangement of actin and microtubule (MT) filaments[91,119,123]: Formerly cortical *filamentous* (F) actin (Fig. 5, left) concentrates in the anterior part of the cell (Fig. 5, right), causing the cell to lose its spherical shape[124,125]. MTs in DCs are mainly organized by the centrosome-containing *microtubule organizing center* (MTOC)[126] at which polar MT filaments are anchored with their minus ends and grow predominantly at their plus ends toward the cell cortex leading to a radial symmetric array[127,128]. During polarization, the MTOC leaves its position in the center of the cell and reorients toward the uropod, where it is predominantly – but depending on the environment or the migration mode (see sections 1.2.2.1 and 1.3.3.2) – located close behind the nucleus during migration[91,129–131]. *In vitro* studies have shown that MTs in polarized DCs align and grow along the axis of migration, with the number of MT filaments radiating from the MTOC to the trailing edge being higher than the number of filaments extending to the leading edge[126]. DCs are able to change their polarity frequently and rapidly, which means, for example, that the cell front forms relatively quickly in a different location from the previous one. This capability distinguishes DCs from stationary polarized cells, such as neurons or epithelial cells[91].

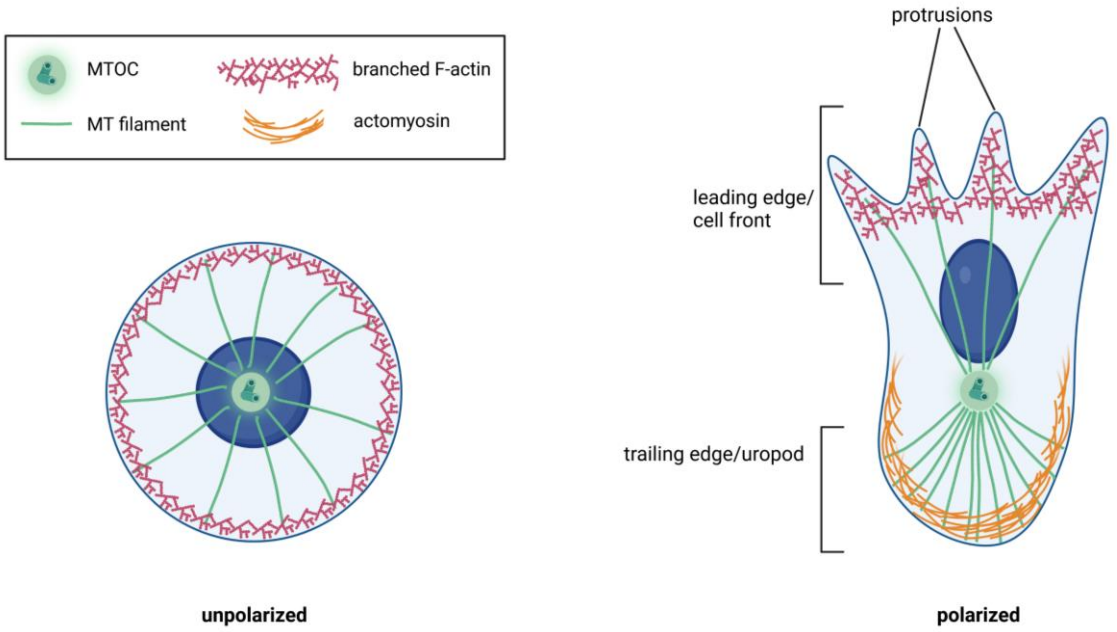

Figure 5. Polarization of an amoeboid migrating cell

Unpolarized cell (left): Symmetric distribution of cytoskeleton components with central positioning of the nucleus and the *microtubule organizing center* (MTOC). *Microtubule* (MT) filamets project evenly distributed into the cell periphery. Branched actin filaments concentrate at the cell cortex. Polarized cell (right): Symmetry is broken, forming a cell front/leading edge composed of actin-rich membrane protrusions and a cell back/trailing edge, where actomyosin concentrates. The MTOC has moved toward the back of the cell, with more MT filaments radiating to the cell back than to the leading edge. Created with BioRender.com.

Central player in the process of migration is the actomyosin cytoskeleton. In non-adherent 3D environments, the front of a polarized DC with its rich occurrences of branched actin filaments forms membrane extensions that extend/protrude into the open space without mechanical anchorage, often referred to as "**protrusions**"[131–133] (Fig. 5, right cell and Fig. 3b right).

Actin filaments have a plus (barbed) end facing the membrane and a minus (pointed) end and grow only at the former[134]. Polymerizing actin filaments push and protrude the plasma membrane forward[135] thereby acting as the main driving force of DC locomotion[82,87,136]. MT dynamics can also generate pushing forces[136–140], but MT expansion does not contribute appreciably to membrane protruding in DCs compared with growing actin filaments[80,139,140]. However, MTs primarily have other roles, such as pathfinding and cell shape control (see sections 1.2.2.1 and 1.3.3.2), and they provide the infrastructure to deliver components for membrane growth, actin-regulating factors, molecular motors, polarity factors, and others to the leading edge[123,141–143]. The tail-like projection at the trailing end of polarized DCs is called "**uropod**" and contains contractile fibers of non-muscle myosin II that help to propel the cell body forward[119,144,145] (Fig. 5, right cell).

1.2.2 Migration in different environments

1.2.2.1 Adhesion-independent amoeboid migration

The migration mode of DCs in 2D and 3D environments may be different. DCs migrating over flat **2D** substrates require adhesion receptors to anchor them to the surface, most likely since gravity is not strong enough to confine the non-adherent cells to planar surfaces and allow the transduction of traction forces[96]. The process of **adhesion-dependent** migration is characterized by repetitive, intersecting or overlapping cycles of leading-edge protrusion, adhesion, transmembrane force coupling by adhesion receptors and contraction of the cell rear to promote de-adhesion[146–149]. Ongoing repetition of these cycles produces a new cell extension at the leading edge again, resulting in a coordinated multistep process of binding/detachment from the substrate and extension/retraction of cellular extensions[97,119,146,150–152].

Locomotion in **3D** occurs much more frequently in the organism and means completely different requirements and challenges for cells than migration in 2D. While migration of cells such as DCs and T cells on 2D substrates depends on integrin-mediated surface anchoring, their locomotion in a 3D environment can be both dependent and independent of adhesion molecules[100,101] with the latter mode dominating. When embedded in complex 3D non-adhesive tissues and tightly surrounded by fibrils or surfaces the need for surface anchoring decreases[96,100]. The cells experience enough confinement sufficiently immobilizing them and shift their mode of migration to an **adhesion-independent** manner[96,100,153], illustrating the importance of environmental geometry for the migration mode of DCs. The flexibility to switch between adhesion-dependent and adhesion-independent migration is termed "**migration plasticity**". In addition to DCs, neutrophils, macrophages and T cells are also able to change their migration mode very rapidly[85]. This plasticity enables DCs to flexibly adapt to the local microenvironment, so that they can pass almost any tissue without remodeling or digesting their environment[154]. Switching between adhesive and non-adhesive migration modes was also observed in tumor cells[155] facilitating metastasis[156].

The relative complexity of a 3D microenvironment forces the cell to navigate through a complex network of ECM proteins, overcome obstacles, and cope with ECM pores that are considerably smaller than themselves[157] (Fig. 3 b). It is noteworthy that mature DCs only very rarely use path-generating mechanisms such as pericellular proteolysis during migration in 3D structures[76,81,158]. To deal with the challenge of the surrounding environment, migrating DCs are able to drastically deform and squeeze their bodies allowing them to translocate through very small interstitial spaces[81,158] (**amoeboid migration**)**.** In the amoeboid migration mode with the strong polarization and unhindered by interactions with the ECM, remarkably higher

velocities are achieved (~4-25 µm/min) than in mesenchymal migrating cells (~0.1-0.5 µm/min)[90,106,159], with DCs exhibiting velocities of about 10 µm/min[90].

Main driver of the integrin-independent amoeboid migration mode is the force of the anterior actin network expansion, which runs via F-actin polymerization[81,160] and promotes the protrusive "**flowing**" of the leading edge, which is accompanied by passive movement at the trailing edge[96]. However, myosin II-dependent contraction of the uropod ("**squeezing**") is particularly required to propel the rigid nucleus through narrow gaps in connective tissues[96,161]. It was shown in *in vitro* assays with DCs that MTs at the leading edge are relatively stable showing a low turnover, while at the trailing edge filament shrinking occurs more frequently[126]. As MT depolymerization triggers actomyosin contractility[162] leading to the retraction of the uropod, this high dynamic of the backward oriented MTs plays an importat role in the regulation of local cellular retraction events[126] (see section 1.2.3).

When navigating through maze-like 3D microenvironments, DCs try to navigate along the most efficient path while sensing chemical stimuli such as the chemokine CCL21 that guides DCs to and within lymphatics[10]. In this context, DCs are also guided by the mechanical properties of the surrounding matrix: While moving through complex environments, DCs typically encounter multiple pores and it has been shown *in vitro* that DCs prefer paths of larger pore sizes, which facilitates nuclear passage[131]. The nucleus here serves as mechanical gauge for larger pores[131] (Fig. 3 b) that probes dense tissue, estimates the available space and finds the path of least resistance, enabling rapid locomotion in tissues[131]. In line with this procedure and conversely to mesenchymal cells[163], the nucleus in amoeboid migrating cells/DCs is characteristically located in front of the MTOC (Fig. 5, right cell)[81,131,164].

Summary: DCs are able to switch between adhesion-mediated and adhesion-independent migration thus adapting to the conditions of their environment. Independent of the mode, actin polymerization and myosin II mediated contraction are the main driving forces for locomotion. MTs are not so much required for cell movement per se, but rather specify the direction of movement by locally remodeling cell morphology. On 2D substrates and under adhesive conditions in 3D, i.e., in the presence of integrin ligands, DCs rely on integrins for anchorage and migration. Under non-adhesive circumstances, DCs are able to locomote without integrins. The forward positioned nucleus acts as mechanical gauge helping the cell to choose the path of least resistance when navigating through dense tissues.

1.2.2.2 Dendritic cell migration in(to) lymph nodes

A “classical” migration route for tissue resident DCs is their way from the tissue to the draining lymph node. The cells take this pathway after antigens have triggered their activation through PRR stimulation, which is accompanied by the upregulation of CCR7 and a switch from a mainly endocytotic activity toward a more migratory behavior allowing the cells to reach the lymphatic system. Irrespective of the prevailing conditions (steady-state or inflammation), the process of reaching the terminal lymphatics depends on CCR7 on DCs and its ligand CCL21, expressed by LECs[64,66,165,166], while CCL19 is not required for this process[110] (Fig. 6 a). Via its positively charged C-terminus, CCL21 gets immobilized on cell and ECM surfaces[110,118], resulting in a perilymphatic haptotactic chemokine gradient decaying from the lymphatic vessels[110,111] (Fig. 6 a, magnification). With the help of these stable “routes”, activated DCs find the closest lymphatic capillary which they subsequently enter (intravasation)[110,167]. It was shown in mouse ear skin that the immobilized gradient begins at a distance of about 90 µm from the initial lymphatic capillaries – a point, at which DCs change their mode of locomotion from a random fashion to a directional and persistent movement migrating along the haptotactic gradient toward the vessel[110] (Fig. 6 a, magnification).

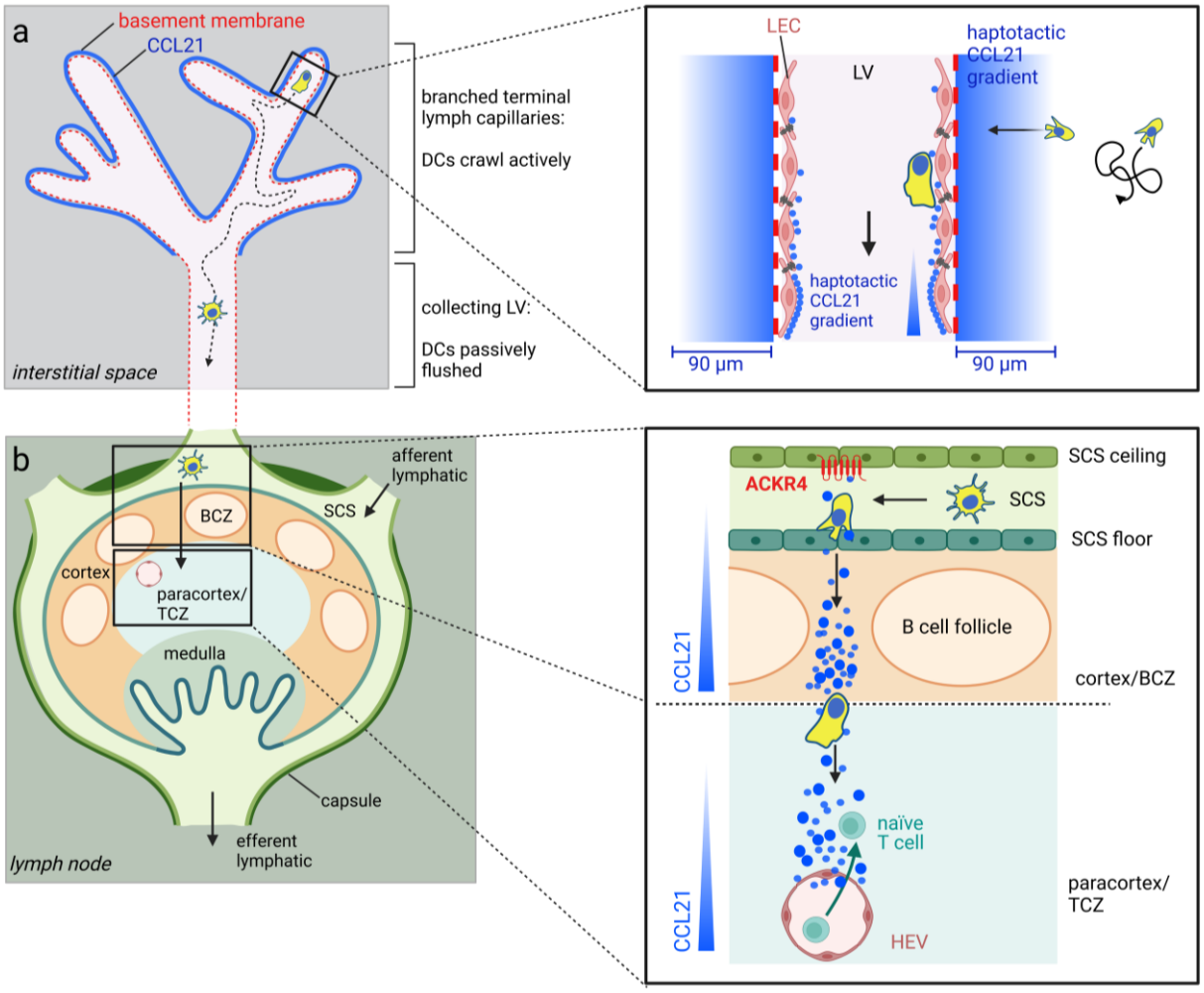

Figure 6. **Migration of dendritic cells to and within the lymph node**

(**a**) Antigen-loaded DCs approach afferent lymphatic vessels with the help of a *C-C motif chemokine ligand* (CCL)21 gradient that surrounds terminal lymphatics and induces a change in migration mode from random to directed migration. After passing the basement membrane of the lymphatics and a layer of *lymphatic endothelial cells* (LECs), DCs crawl along an intraluminal CCL21 gradient and reach the collecting lymph vessel, from where they are flushed into the *subcapsular sinus* (SCS). (**b**) Due to the *atypical chemokine receptor* (ACKR)4, which scavenges chemokines, another CCL21 gradient is created attracting DCs into the *T cell zone* (TCZ) of the lymph node. Here, DCs encounter naïve T cells that have entered the paracortex via *high endothelial venules* (HEVs). A CCL21 gradient originating from HEVs that attracts DCs is suspected. DCs present their antigens potentially inducing T cell activation. LV: lmypahtic vessel. Created with BioRender.com.

Terminal lymphatics are blind-ended branched capillaries that merge with larger collecting vessels and are characterized by a discontinuous basement membrane[168] (Fig. 6 a). The next "barrier" for DCs on their way to the vessel lumen is a monolayer of LECs that are discontinuously joined by specialized junctions[169,170] (Fig. 6 a, magnification) enabling the attachment of DCs to LECs and subsequent crossing of the LEC monolayer (transmigration)[170–172]. After arrival in the lymphatic vessel lumen, it takes DCs 1-3 days to reach the draining lymph node[62,79]. Intralymphatic DC locomotion occurs through a combination of initial active crawling along the inner vessel wall and being passively flushed by the lymphatic flow[65,173,174] (Fig. 6 a). Via this flush, DCs reach the *subcapsular sinus* (SCS)[65,173,174] (Fig. 6 b) that has an asymmetric distribution of the *atypical chemokine receptor 4* (ACKR4) (only the outer layer of LECs is positive for ACKR4)[175] (Fig. 6 b, magnification). By scavenging CCL21 a chemokine gradient is generated which points toward the paracortex/ T cell zone (TCZ) allowing directional DC migration into this region. On their way to the TCZ, DCs pass the B cell zone (BCZ), where B lymphocytes are organized in follicles[175,176] (Fig. 6 b).

The encounter of T cells and DCs takes place in the vicinity of paracortical HEVs[177], through which most naïve T cells enter the lymph node[178,179]. It was shown that CCL21 is expressed by HEV cells[9,76,79,83] probably establishing an interstitial gradient that attracts antigen loaded DCs[9,76,79] (Fig. 6 b, magnification), which subsequently concentrate around HEVs[177]. Findings on CCL19 involvement in this process are conflicting[9,76,83,180,181].

1.2.3 Intracellular key players in directional dendritic cell migration

Proper and well-coordinated migration of mature DCs from peripheral tissues to draining lymphoid organs is essential for protecting the organism against pathogens as well as for inducing immune tolerance. Inducer of DC migration from the site of infection/injury to lymphoid organs is the maturation process that is initiated upon antigen uptake[182]. A central role in this process is played by **CCR7**, a seven-transmembrane domain G-protein-coupled surface

receptor which is upregulated by mature DCs (upon stimulation by pathogenic or inflammatory signals) and semi-mature DCs (under steady-state conditions) being crucial for DC migration to regional lymphatic tissues[63,64,66,78,122].

There are several models of motility to describe the locomotion behavior of cells. To describe the behavior of DCs in the absence of external directional cues under steady-state conditions, the persistent random walk model fits best for amoeboid migrating DCs during their search for pathogens[77,183]. In this biphasic random migration mode, phases of persistent walks along curved trajectories alternate with periods of "diffuse migration", which represents pauses in the forward movement (Fig. 7). During the latter phase, DCs show short irregular displacements randomly fluctuating around their specific location[183]. While during persistent migration the velocity of DCs was shown to be remarkably higher than during diffusive migration[183], the pause intervals enable the cells to search locally for pathogens.

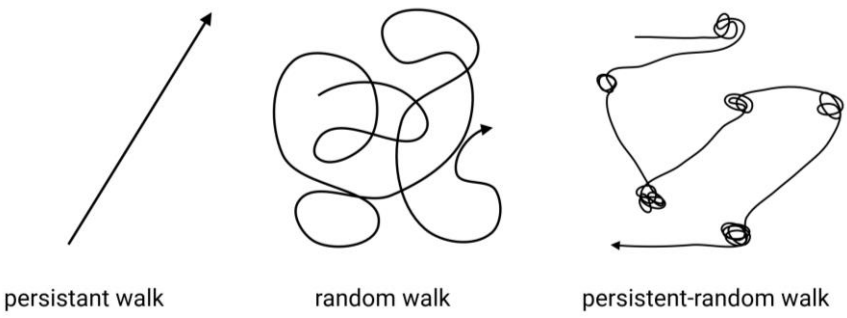

Figure 7. Schematic illustration of different motility models

Persistant walk refers to a movement in any direction that occurs without deflection in any other direction. In contrast, the random walk does not show any directness or directionality and is characterized by many successive changes of direction. The persistent random walk can be regarded as a mixture of the first two models. In this process, deflection-free, persistent migration phases alternate with phases in which random movement takes place, during which there is no significant locomotion from the spot. Created with BioRender.com.

Since the most abundant mode of DC locomotion in the organism is adhesion-free haptotaxis, the following will describe the rough signaling pathways for amoeboid migrating cells. Much of the knowledge about this comes from studies with neutrophils.

Downstream of CCR7, activation of heterotrimeric G-proteins by the intracellular part of the receptor occurs at the leading edge after extracellular chemokine binding[184] (Fig. 8). After dissociation of the activated G proteins into α- and βγ-subunits, the latter activate *phosphatidylinositol 3-kinase* (PI3K)[185,186]. This translocates together with its product *phosphatidylinositol-3,4,5-trisphosphate* (PIP3) to the leading protrusion[187,188], where **PIP3** activates the small *guanosine triphosphatase* (GTPase) *Ras-related C3 botulinum toxin*

substrate 1 (**Rac1**) by means of specific *guanine nucleotide exchange factors* (GEFs)[189], such as P-Rex1[190]. Rac, which was shown in neutrophils to be a central and essential player in leukocyte migration[191], regulates the *suppressor of cAR* (**SCAR**)[192–194], which stimulates the *actin related protein* (Arp) 2/3[189] (Fig. 8). Local activation of the **Arp2/3** complex leads to actin nucleation followed by branched actin polymerization at the cell front, resulting in the development and expansion of protrusions that grow in a specific direction, which is the basis for directional migration[160,189].

This sets the stage for the cell to move forward, however, for the unidirectional bias of locomotion, which occurs along gradients and is THE hallmark of haptotaxis/chemotaxis, another player seems essential: It was shown in many cell types that in the absence of the Rho-GTPase *cell division cycle 42* (Cdc42) leukocytes exhibit a random walk rather than directed migration when placed in a chemotactic gradient[195–199]. After activation of *p21-activated kinase 1* (**PAK1**) by $G_{\beta\gamma}$-subunit signaling, the Cdc42 specific GEF *PAK-interacting exchange factor α* (Pixα)[200] is recruited and activates **Cdc42** (Fig. 8). This small GTPase positively regulates PAK1 in a feedback loop ensuring high Cdc42 acitivity at the leading edge[201] (not shown for overview reasons), and activates the *Wiskott-Aldrich syndrome protein* (**WASP**)[202], which in turn stimulates Arp2/3 resulting in actin nucleation followed by actin polymerization at the leading edge of the cell[189,201,203]. It has been shown in DCs under *3D in vitro* conditions as well as *in vivo* that Cdc42 is indispensable for the temporal and spatial regulation of cell protrusions at the leading edge[107]. At least in neutrophils and in the presence of PIP3, the $G_{\beta\gamma}$-subunit seems to activate the Rac- and Cdc42-specific GEFs P-Rex1 and Pixα directly[204] (Fig. 8). The two active GTPases, Rac and Cdc42, in concert with polymerized actin enhance the recruitment of PIP3 to the leading edge by building a positive feedback loop[205] (not shown for overview reasons).

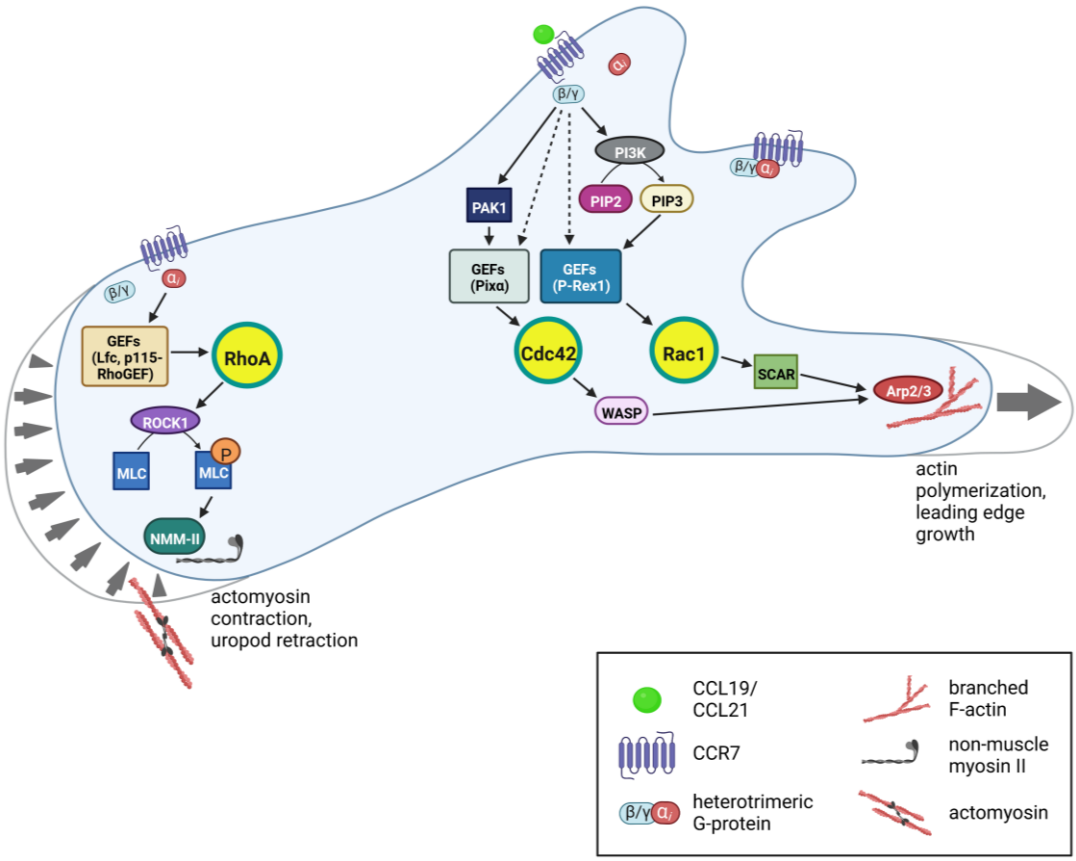

Figure 8. Intracellular signaling pathways in an amoeboid migrating cell (simplified representation)

The movement of an amoeboid migrating cell results mainly from actin polymerization at the leading edge supported by actomyosin contraction at the trailing edge. Both processes are based on complex signaling pathways that influence each other (not shown). Key players at the cell front are the small GTPase *Ras-related C3 botulinum toxin substrate 1* (Rac1) and the GTPase *cell division cycle 42* (Cdc42), which are responsible for regulating actin polymerization and leading edge coordination, respectively. At the uropd, the small GTPase *Ras homolog family member A* (RhoA) dominates the action, activating actomyosin via the kinase *Rho-associated protein kinase 1* (ROCK1). Created with BioRender.com.

In the signaling cascades that occur predominantly at the uropod after chemokine binding, the small GTPase *Ras homolog family member A* (**RhoA**) plays an important role. The G_{α}-subunit is able to activate RhoA via Rho specific GEFs[206,207], such as the MT associated Rho-GEF *Lfc*, which is released upon MT depolarization[126,208,209], or p115Rho-GEF[210] (Fig. 8). Effector of RhoA is the serine/threonine kinase *Rho-associated protein kinase 1* (**ROCK1**), which provides *myosin light chain* (**MLC**) phosphorylation, leading to activation of **non-muscle myosin II** (NMM-II) and active retraction of local cell parts, such as the uropod[126], by **actomyosin contractility**[184,211,212] (Fig. 8). This process of local contractions is needed, for example, for squeezing contractions of the cell's trailing edge to propel the nucleus forward when migrating through dense tissues[96]. The signaling cascade via MLC phosphorylation is also run to retract

protrusions that occur in parallel during exploration of complex 3D environments to find the path of least resistance[126,131].

Summary: Rac1 and Cdc42 act at the cell front, with the former regulating actin polymerization to promote protrusion and the latter controlling direction in response to extracellular signals. RhoA acts in the cell body and especially at the rear, causing contraction/retraction via actomyosin activation. The two signaling pathways involving either Rac or Rho have opposing effects, with Rac dominating RhoA signaling at the leading edge and vice versa at the cell's rear[213]. Although, or rather because, both GTPases suppress the other's activity, they act in concert to generate functional and morphological cell polarity and maintain directed migration[134,206].

1.2.4 *In vitro* models and quantification of dendritic cell migration

Many insights into cell migration come from *in vitro* migration assays, which simulate the physiological conditions in the body. For instance, adhesive 2D migration is experimentally mimicked by ligand-coated surfaces to study, for example, the rolling and crawling of neutrophils during extravasation[214]. As a technical setup, microfluidic devices and chamber-slides are used, which are coated accordingly[215]. Integrin-independent migration can be mimicked *in vitro* by collagen assays in which 3D maze-like structures are created that resemble the physiological situation[121,216]. However, replicable *in vitro* simulation of 3D physiological environments is difficult[118], not least because of the increased complexity, which manifests itself, for example, in the fact that changes in the protein concentration of the 3D matrices affect stiffness, matrix pore size, cell confinement, and fiber crosslinking. In addition, the techniques research groups use to produce 3D gels can vary greatly[217].

In addition to 3D *in vitro* and *in vivo* experiments, there are dedicated 2D *in vitro* settings to examine integrin-independent locomotion[96,132,218]. The prerequisite for this is the confinement of the cells between non-adherent surfaces. This is the case, for example, when cells are covered by a ceiling during migration, such as a layer of agarose (under agarose migration assay)[219], or during migration in microchannels whose design allows confinement of the cells (for 2D migration: only one axis confined)[77,80,220]. A comfortable tool for assays that provide cell confinement in the z dimension are microfabricated devices made of the silicone elastomer *polydimethylsiloxane* (PDMS). With the help of PDMS-devices it is possible to not only create simple setups, such as channels, but also more complex structures of almost any geometry and architecture[133,220–227]. Since migration in the mentioned channel types or under agarose only occurs in one plane, these assays are also termed "2.5D assays"[80] (confinement as it is

the case in a physiological 3D environment, but movement only possible in 2D). However, in the present work, we use the term “2D assays“.

Cell movement can be quantified and analyzed by collecting migration parameters such as **velocity**, **directionality** and **persistence**. Videos of moving cells generated by time-lapse video microscopy from 2D or 3D *in vitro* assays allow tracking of individual cells and subsequent derivation of the corresponding parameters with the help of suitable software[121,228]. For example, it is possible to distinguish between non-directional cell motility (random cell movement) and directional cell migration. Velocity provides information about how fast a cell moves per unit of time and can be used synonymously with speed. Persistence is also called *directness* and results from the ratio of displacement of a cell (Euclidean distance: length of a straight line between start and end point) to total path length (accumulated distance) being a measure of the straightness of the trajectories of a cell[229,230] (Fig. 9 a).

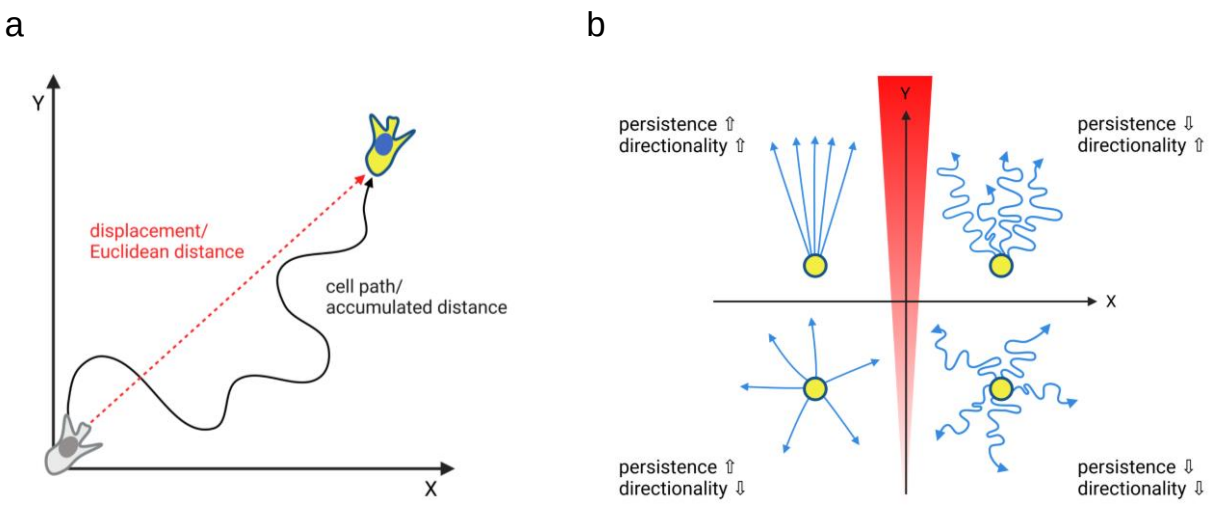

Figure 9. Definition and differentiation of the cell migration parameters persistence and directionality

The definition of cell migration parameters in terms of straightness and direction varies in the literature. (**a**) In the present work, we use the term "persistence" (or “directional persistence”) to make statements about the straightness/directness of a cell during its migration and thus to obtain information about the degree of deviation from its route. "Directional persistence" is defined as the quotient of displacement (or *Euclidean distance* as the length of the direct connection between starting and destination point) and total path length (which is the accumulated distance/the distance actually traveled). In contrast, the definition of "directionality" includes the direction of migration relative to the gradient direction, which is the ratio of the displacement in the gradient direction to total displacement (see b). (**b**) Relationship of persistence and directionality to each other in direct comparison. Created with BioRender.com.

In the present work, we use the term “(directional) persistence”, which is not to be confused with *directionality* (sometimes also called *chemotactic index*, *CI*). *Persistence* is a parameter that provides information about the extent to which a cell moves in random directions or heads

for a destination without detours. In contrast, *directionality/CI* includes the direction of migration (angle) relative to the gradient direction (ratio of the displacement in the gradient direction to total displacement) helping to quantify accuracy of the migration process (Do the cells move in the actual gradient direction or in a different direction?)[229] (Fig. 9 a, b).

1.3 Centrosomes

1.3.1 Structure

The centrosome is an organelle found in most animal somatic cells, where it serves predominantly as the main MTOC[94]. Core components of the centrosome are two barrel-shaped structures, called mother and daughter centriole, that are connected by flexible linker fibers[231,232], and the surrounding *pericentriolar material* (PCM) that enables MT nucleation (Fig. 10 a). Only the mother centriole carries distal and subdistal appendages at its distal end[233]. Each centriole consists of α- and β-tubulin subunits forming nine symmetrically arranged sets of MT triplets (Fig. 10 b), resulting in a cylinder of about 500 nm length and 130 nm and 250 nm inner/outer diameter in human cells, respectively[94,234,235]. The MT triplets transition to a doublet pattern at the distal ends of the two centrioles[236] (not shown). Most proliferating mammalian somatic cells harbor one centrosome in G1 phase that is mainly located in close proximity to the nucleus[237–239]. There is evidence of a structural connection between the two organelles probably including the MT minus-end directed motor dynein[237,240–242].

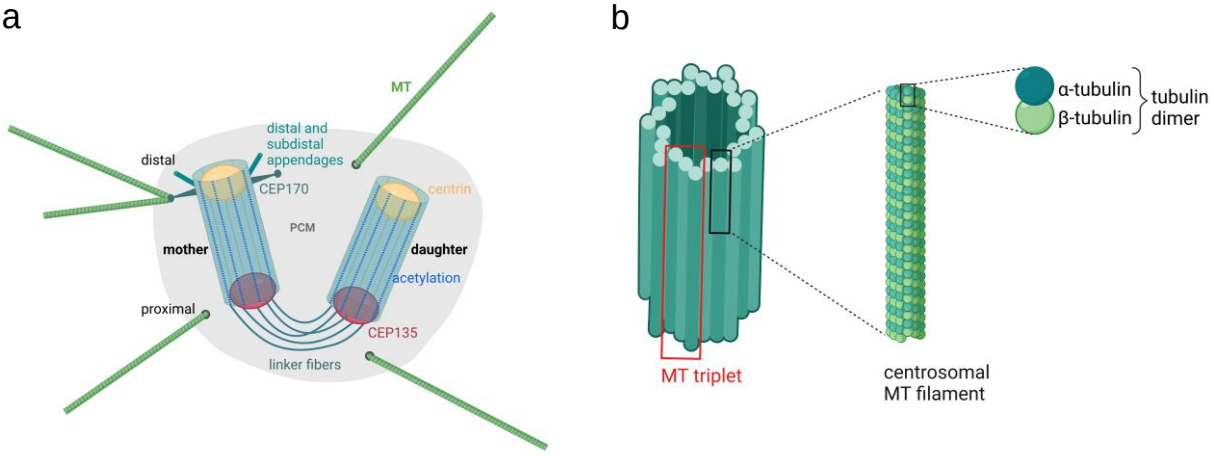

Figure 10. Structur of the centrosome

(**a**) The centrosome consists of two cylinders called mother and daughter centriole, the former bearing distal and subdistal appendages allowing the two centrioles to be distinguished. The cylinders are connected by proteinaceous linker fibers and surrounded by a variety of proteins, the latter forming the *pericentriolar material* (PCM).

Centrioles are highly acetylated and have characteristic proteins, such as centrin and the *centrosomal protein of 135 kDa* (CEP135). In leukocytes, the centrosome nucleates and anchors *microtubule* (MT) filaments. (**b**) Structure of a centriole: 9 MT triplets (red boxed) form a hollow cylinder, the centriole. Each MT filament consists of α- and β-tubulin dimers (black boxed). Created with BioRender.com.

Centriolar proteins exhibit numerous *post-translational modifications* (PTMs) such as acetylation, glutamylation, glycylation, phosphorylation and (de)tyrosination, with tubulin carrying most of the known PTMs[243–245]. It is now well known where different PMTs are located along the centriolar sub-regions, and some of the modifications are used for centriole visualization by antibody stainings (see Fig. 10 a, 12 c-e, 13 a and c). Although the function of the centriolar PMTs has not been fully elucidated yet, they primarily appear to play a role in MT nucleation and depolymerization, centriole/centrosome stability (especially acetylation[246] and polyglutamylation[247]), and are thought to be involved in regulating interactions between centriolar MTs and associated proteins[243]. In addition to the PTMs, the particular triplet and/or doublet structure of the centriolar MTs is believed to be the reason for the high stability of centriolar MTs, which resist, for example, cold, MT destabilizing agents, pressure and/or heat[246–250].

Similar to, but more specific than PMTs, there are centrosomal key proteins that characterize specific regions of the organelle, making them a suitable tool in research for indirect immunofluorescent-based visualization of the centrosome/centrioles: In the very proximal inner part of both centrioles the *centrosomal protein of 135 kDa* (CEP135) can be found (Fig. 10 a), while *spindle assembly abnormal protein 6* (SAS-6) is only present in the inner proximal end of newly emerging centrioles (“procentrioles”, see section 1.3.2). Here, both proteins are involved in the assembly of the cartwheel. Centrin concentrates at the distal lumen of each centriole (Fig. 10 a), where *centriolar coiled-coil protein of 110 kDa* (CP110) forms a cap structure at each centriolar tip. *Polo-like kinase 4* (PLK4) accumulates at the outer proximal region of the parental centriole where it binds to the centriole-surrounding scaffolding proteins CEP152 and CEP192[234,235,251]. *Centrosomal P4.1-associated protein* (CPAP), however, is located within the proximal lumen of each centriole. Cep164 and CEP83 belong to the group of proteins that specifically localize to distal appendages, while subdistal appendages can be characterized for instance by CEP170 (Fig. 10 a), CEP128 and ninein[234,235].

As part of the centrosome, the PCM plays a central role in MTOC activity, being a decisive structure for anchoring and nucleating cytoplasmic MTs during both interphase and mitosis[252]. Although the PCM consists of more than 100 constituents, seven major components have been identified, i.e., CEP120, CEP192 and CEP152, *Cdk5 regulatory subunit-associated protein 2* (Cdk5Rap2), *neural precursor cell expressed developmentally downregulated 1* (NEDD1), γ-tubulin and pericentrin[94,253]. PCM proteins are organized in an ordered structure

of concentric layers occupying discrete spatial regions around the centrioles[253,254]. Some of the mentioned proteins are suitable for staining the PCM and partially even make individual centrioles visible (Fig. 12, c-e).

1.3.2 Duplication cycle

Usually cells are born with one centrosome, which subsequently duplicates once per cell cycle[255]. Since centrioles replicate in a semi-conservative manner, each newly replicated unit contains both new and old components, i.e., in a centrosome there is an older centriole – inherited as fully grown centriole from the previous cell division cycle – and a younger one, that has just emerged in the previous cycle nucleating at a preexisting centriole (Fig. 11)[94,233,249,256]. Differentiation between the two cylinders is possible due to the distal and subdistal appendages that are present only at the parent centriole[233] (Fig. 10 a and 11). The distal appendages are assumed to play a role in the recruitment of basal bodies to the membrane during cilia formation, while subdistal appendages are involved in anchoring MTs[257,258].

The centrosome duplicates in S phase of the cell cycle simultaneously with DNA replication, resulting in two centrosomes with two centrioles, respectively. Centriole duplication is tightly regulated to ensure that the formation of new centrioles can only occur once per cell cycle guaranteeing the correct number of centrioles. Of note, the linkage between the two cycles is also reflected in the fact that in case of a delay in one of the two cycles, the other stops in order to avoid errors[259]. Moreover, some proteins have been identified that play a dual role being involved in both the DNA duplication and the centriole duplication cycle, namely PLK1, *cyclin-dependent kinase* (Cdk) 1 and Aurora A. These mitotic kinases phosphorylate components of the centrosome and mitotic machinery and also regulate each other[260–265].

The **centrosome cycle,** which is the canonical way of centriole generation in most proliferating cells, can be divided into four consecutive steps[233,234,242,252] (Fig. 11). A newly born cell harbors one centrosome consisting of two orthogonally engaged centrioles. (**1**) Upon exit from mitosis, the two cylinders move apart (disengagement), so that early G1 phase contains a mother and a daughter centriole that have lost their orthogonal arrangement but are connected at their proximal ends by protein linker fibers. (**2**) Driven by PLK4, as key regulator of centriole biogenesis[266,267] that is recruited to each centriole by CEP152[268], and with the help of SAS-6 and CEP135 in late G1/early S phase, a new centriole forms perpendicular to the wall of the mother and daughter centriole, respectively. In addition, at the G1-S-transition PLK2 is activated, which was shown to be required for centriole duplication in mammalian cells[269]. The newly arising centrioles are daughters, called ‘procentrioles’ until about mitosis when they are almost fully grown, and emanate from a structure known as cartwheel, which serves as scaffold

for the newly emerging centrioles[235] thus only being found on procentrioles[270]. The former daughter centriole has now become a parent centriole itself – although it is still immature and has no appendages yet (Fig. 11). After the initiation of procentriole assembly, the cell blocks further centriole duplication (reduplication) until mitosis has ended and the next S phase is reached[271]. (**3**) The procentrioles elongate under the control of CPAP[272,273] during passage through S and G2 phase leading to four centrioles per cell from late S phase on. In M phase, procentrioles have reached about 80 % of their final length, which they acquire in a maturation process during the next cell cycle[242,274]. The linker that connects mother and daughter centriole in G1 phase has now become a structure that links two parent centrioles or two nascent centrosomes. (**4**) At G2/M transition, the two centrosomes separate by a Cdk1-dependent mechanism[275] that is induced by phosphorylation of the *centrosomal NEK2-associated protein 1* (C-NAP1) which is located at the proximal ends of the centrioles[276–278]. C-NAP1 binds the linker fiber forming molecule rootletin and its phosphorylation leads to resolvement of the linker[276,277] allowing the two centrosomes to move to the two cell poles for organizing the spindle apparatus. Simultaneously, the PCM expands enormously in mitosis and acquires MTOC activity[279,280] ("centrosome maturation"). This process occurs when Cdk1 levels are high and requires the phosphorylation (activation) of the two serine/threonine kinases Aurora A and PLK1[263,281]. The following PLK1 mediated phosphorylation of pericentrin, Cdk5Rap2, and Cep192, and others, then entails the recruitment of further PCM proteins[263,265,279,281,282]. As a result, MT nucleation is increased and the mitotic spindle forms. Finally, the two centrosomes are divided between the two newly formed daughter cells. (**1**) Upon exit from mitosis and in preparation of the following duplication process, the two centrioles within each centrosome disengage which is mediated by the cysteine protease separase and PLK1. Centriolar disengagement licences centriole duplication in the next cycle[283,284].

For the sake of completeness, it should be mentioned that in some cases centrosomes can form *de novo* when centrioles are absent[256,285,286].

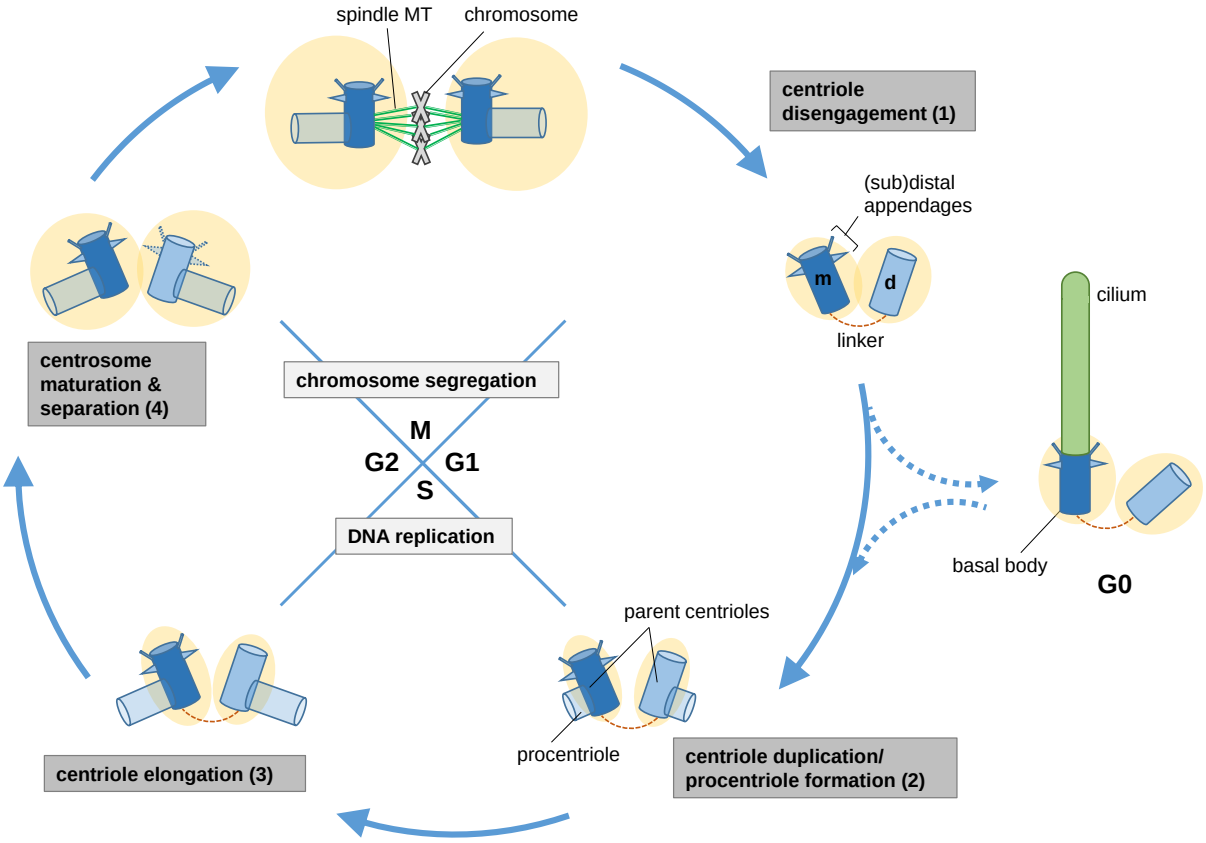

Figure 11. The centrosome duplication cycle

The centrosome duplicates once during the cell cycle, which occurs in parallel with DNA replication. In G1 phase, mother and daughter centriole are connected by the centriolar linker. At the G1/S transition, a procentriole emanates from each existing centriole transforming the previous daughter into a parent centriole. During S and G2 phase, the newly formed procentrioles elongate and further mature, accompanied by an increase in PCM. At G2/M transition, dissolvement of the linker fibers and separation of the two newly formed centrosomes takes place as well as further expansion of the PCM. In M phase, the two centrosomes mediate the formation of the mitotic spindle and are distributed to the two nascent daughter cells. With the disengagement of the two centrioles and the formation of the linker fibers, a new cycle begins. Created with Microsoft PowerPoint.

1.3.3 The centrosome as main microtubule organizing center

1.3.3.1 Microtubule nucleation and anchoring

The centrosome functions as major MTOC in most animal cells, where it influences MT dependent processes in cell division and interphase[234]. During the former, the MTOC's main task is to coordinate the spindle apparatus while MTs ensure chromosome separation, whereas in non-dividing cells the centrosome/MTOC has a crucial role in cilia assembly, formation of the immunological synapse and migration[94,251,260,287]. During cell locomotion, the MTOC contributes to cell polarity with nucleated MTs regulating cell's motility and controlling cell shape. Moreover, MTs also play a role for intracellular transport and organelle positioning by serving as tracks[288].

With regard to MTs, centrosomal MTOC function can be divided into a **nucleating** and an **anchoring** activity, whereby there are also cell types in which MTs grow from the centrosome (nucleation), for example, but then (partially) do not attach to it, but are anchored to membrane organelles or are not anchored at all lying freely in the cytoplasm[289–291] (see below). It is assumed that centrioles themselves are less or not important for the formation of MTs (which is/starts with MT nucleation), but for control of the aggregation of PCM components, MT anchoring and assembly of cilia and flagella[94,259]. For the latter task, centrioles move to the cell membrane in G0 phase, where the mother centriole serves as basal body for cilia and flagella (a conversion process that is possible in both directions in many cell types) with distal appendages mediating docking to the plasma membrane (Fig. 11)[292,293]. However, cDCs do not have cilia or flagella, so this feature of the centrioles will be neglected here.

MT nucleation takes place in the PCM of centrosome's immediate environment[294]. For this purpose, centrioles recruit PCM[234,235,295] and loss of centrioles has been shown to lead to fragmentation of the PCM, emphasizing the fundamental role of centrioles for centrosome integrity[296]. The actual process of PCM associated MT nucleation by the centrosomal MTOC begins with the *γ-tubulin ring complexes* (γ-TuRCs), small ring-shaped structures of 25-30 nm in diameter that are enriched at the centrosome and embedded in the PCM building the functional core of the centrosome[297–299]. The γ-TuRC unit serves as template for MT formation[300] and consists of the special tubulin isoform γ-tubulin[301], which directly binds to MT minus ends[302] (MT minus-end cap), as well as several other proteins. Together they form the basis from which MTs grow radially by polymerization of α- and β-tubulin dimers, resulting in the typical hollow tube structure of MTs (Fig. 10). Mainly responsible for the recruitment of γ-TuRC is NEDD1[303], while Cdk5Rap2 is considered to be an activator of nucleation by γ-TuRCs[304] and is required for the attachment of γ-TuRC to the centrosome/MTOC and the recruitment of many other PCM proteins, thereby interacting with γ-tubulin, pericentrin and

CEP192[253,305]. In addition to γ-TuRC, the MT nucleation site accumulates factors for MT growth while MT growth and shrinkage is controlled by a variety of MT associated proteins which regulate the dynamic behavior at both MT ends[304,306].

Beyond MT nucleation, the MTOC has to stabilize and anchor MT minus ends at the centrosome which is indispensable for maintaining a radial MT array in interphase[128] and usually takes place with the participation of γ-TuRC[300]. Subdistal appendages of the mother centriole are considered the main structure of MT anchoring[299]. The here located protein ninein seems to play a crucial role in connecting the mother centriole and γ-TuRC[299]. Moreover, NEDD1 seems to be mandatory for anchoring γ-TuRC-associated MTs[302,307]. In addition to the subdistal appendages, the PCM itself is being discussed as anchoring site[252,259], as is a transient anchorage by γ-TuRC units alone[299].

Although MTOCs are present in all eukaryotic cells[94], not all cell types use centrosomal MTOCs as site for MT nucleation and anchoring as leukocytes do[304]. While a radial MT configuration is useful for cells that rapidly change their polarity, such as immune cells, in some differentiated, stably polarized cells, a non-radial MT configuration is better suited for new cellular functions, such that the MTOC function is shifted to non-centrosomal sites. During neuronal development, for example, the centrosome is inactivated after an initial phase of MT nucleation and loses its function as MT nucleator[308,309], while differentiated muscle cells were shown to use the Golgi apparatus for MT nucleation as well as the nuclear envelope for both MT nucleation and anchoring[310–313]. Moreover, many polarized epithelial cells, for instance, switch off the centrosome[304,307,314] and exhibit non-centrosomal MT arrays in which the filaments are aligned linearly along the apical-basal axis of the cell nucleating from and anchored at the apical site with their minus ends[304,314–316].

In the cases, in which the centrosome continues to nucleate MTs, there is evidence that newly nucleated MTs are cut at their minus ends, probably by MT severing proteins such as katanin[314,316–320]. Subsequently, MT filaments are released from their nucleation site into the cytoplasm as it is reported from neurons in their initial differentiation[319,321]. Another possibility is that cut MTs are translocated to sites of anchoring, such as subdistal appendages of the mother centriole (nucleation *and* anchoring at the centrosome), apical parts in epithelial cells or the Golgi apparatus (nucleation at the centrosome, anchoring elsewhere[322,323])[233,317,319]. In addition to cell differentiation, such severing processes play a role for the remodeling of MTs at the transition from interphase to mitosis[233,316].

1.3.3.2 Centrosomes in cell migration

Almost all leukocytes, including DCs, typically use the centrosome for the nucleation and anchoring of MT filaments[304,324]. The tasks of the centrosomal MTOC plays a crucial role in cell locomotion, which requires high flexibilty and plasticity of MT organization to allow migrating DCs to adapt flexibly to different environmental demands.

Even before the actual process of locomotion, MTOCs and MTs play a crucial role, as they contribute significantly to the process of polarization[91]. Here, the MTOC leaves its central position and moves toward the uropod, where it is usually positioned behind the nucleus in amoeboid migrating cells/DCs, and in front of the nucleus in mesenchymal migrating cells[81,131,163,164]. The former conformation enables DCs migrating in complex environments to use the nucleus – the largest and most rigid cell organelle – as a mechanical sensor to find larger (convenient) pores (see section 1.2.2.1). Therefore, DCs simultaneously extend multiple front and side protrusions into several closely spaced pores and do the same with nuclear protrusions. Once the nucleus has translocated into the cell protrusion in the larger pore, the MTOC follows[131] and the cell decreases MT growth in the probing cytoplasmic protrusions[126]. Triggered by local MT depolymerization, activation of RhoA leads to local actomyosin skeleton contraction[126,208,211] resulting in the retraction of competing protrusions and the trailing edge, the latter process initiating translocation of the entire cell body[126,131]. In this way, a causal link between MTOC passage/MT (depolymerization) and cellular retractions could be established, emphasizing MTOCs'/MTs' important role in pathfinding/directional selection during locomotion through complex environments[126,131]: While the preceding nucleus probes pore sizes, the posterior passage of the MTOC together with the withdrawal of MTs from all but the leading protrusion likely stabilize the direction the cell has taken[126,325]. The purpose of MT controlled protrusion retraction is to prevent cell protrusions from becoming too long or ramified, which might lead to cell entanglement[126]. Since MTs might have problems to enter such protrusions due to their relatively stiff structure and straight growth, they induce the retraction of such protrusions[91,126]. Amoeboid-like migrating DCs use MTOC-nucleated MTs as a "sensor" to survey and possibly correct cell shape[126] highlighting that MTs are involved in physical coordination processes rather than individual processes of force generation or substrate interactions (as is the case with actin filaments)[152].

In addition to MT filaments, actin is one of the scaffold elements coordinated, at least in part, by the centrosomal MTOC, which promotes actin filament assembly (nucleation)[91,326,327]. The main role of actin during cell polarization and migration is to generate protrusive and contractile forces that move the cell forward[91,134] but the specific role of the centrosome as an actin organizer has not yet been deciphered.

1.4 Aim of the present work

The number of centrosomes in most non-malignant proliferating cells is restricted to one in G1 phase and two from S phase. Although multiple centrosomes are usually not tolerated in non-transformed cells[328], previous data from our lab show that a proportion of murine DCs contain multinumerous centrosomes. The centrosome in DCs is the main MTOC that plays a crucial role during interphase when DCs perform one of their major tasks, which is to migrate.

Until now, supernumerary centrosomes were mostly associated with pathological processes such as cell transformation and tumorigenesis[329–333]. Many cancer cells harbor two and more centrosomes[334–336] and excess centrosomes in cancer cells have been shown to confer beneficial tumor progression-driving features to the cells, such as enhanced invasion/ metastasis, making the cells more aggressive and leading to a poor prognosis[330,336,337].

Against this background, the question of the role of extra centrosomes in DCs arises. While in cancer cells, some mechanisms for the generation of multinumerous centrosomes have been revealed[338–344], nothing is known about the emergence of multiple centrosomes in DCs. Thus, one aim of the present work was to demonstrate the existence of excess centrosomes in different types of DCs and to decipher their origin. In addition, a special focus was placed on the role of multiple centrosomes in functional aspects of DCs investigated in the process of migration. In this context, we also tried to shed light on spatial and geometrical facets of extra centrosomes. Ultimately, we were also interested in whether there are further parallels between DCs and cancer cells other than the mere fact that there are multiple centrosomes, or what differences can be found.

2 Material and methods

2.1 Material

2.1.1 Laboratory equipment

Device and model	Source / Manufacturer
Autoclave: *VX-150*	Systec
CO_2 incubator: *CB210*	Binder
Centrifuges: *8510R, 5415R, 5424R, 5810R* *Galaxy MiniStar silverline*	 Eppendorf VWR
Chambers for SDS-PAGE: *Mini-PROTEAN Tetra Cell, Mini Trans-Blot® Cell*	 Bio-Rad Laboratories
Counting chamber: *Neubauer improved*	Marienfeld
Fluid aspiration system: *BioChem-VacuuCenter (BVC)*	Vacuubrand
Gel and blot imaging sytem: *ChemiDoc MP Imaging*	Bio-Rad Laboratories
Heating and shaking block: *ThermoMixer C*	Eppendorf
Heating cabinet: *venticell 55*	MMM Medcenter
Heating chamber for microscopy: *P Lab-Tek™ S*	Pecon
Hotplate: *Cimarec+™* *SD 160*	 Thermo Fisher Scientific Carl Roth
Hotplate stirrer: *HSC*	VELP Scientifica
Immunoblot transfer system: *Trans-Blot® Turbo™*	Bio-Rad Laboratories
Laminar flow hood: *BDK-SK1800*	BDK
Microscope stages (motorized)	Applied Scientific Instrumentation (ASI), Märzhäuser
Microscopes: Confocal laser scanning microscope: *LSM880* + Airyscan Phase contrast microscope: *Eclipse TS100* Spinning-disc confocal system: *Dragonfly 505* installed on an *Eclipse Ti2* inverted microscope Spinning-disc confocal system: *CSU-X1* installed on the inverted fluorescence microscope *Axio Observer* Widefield microscopes: *Eclipse TE 2000, Eclipse Ti2*	 Zeiss Nikon Andor, Nikon Yokogawa, Zeiss Nikon
Microwave: *MWG 786*	Clatronic
Objective heating: *Objective Heater 2000*	Pecon
pH meter: *MP220*	Mettler-Toledo
Pipette controller: *accu-jet® pro*	Brand®
Pipettes (2.5-1000 µL): *Eppendorf Research® plus*	Eppendorf
Planetary centrifugal mixer (mixer/defoamer): *ARE-250*	Thinky
Plasma cleaner: *PDC-002*	Harrick Plasma
Scales: *JB2002-G/FACT*, *AG285*	 Mettler Toledo
Shaker-rocker system: *Mini Blot Mixer*	VWR
Silicon wafer for *polydimethylsiloxane* (PDMS) device production	kindly provided by the group of Michael Sixt

Temperature control unit for microscopy: *TempController 2000-2*	 Pecon
Tilt shakers: *WS-5, WS-10*	 Edmund Bühler
Ultrasonic bath: *Sonorex RK 31*	Bandelin Electronic
Vacuum desiccator: *SP Scienceware*™	Bel-Art™
Vacuum suction system: *AC02 HLC*	BioTec
Vortex mixers: *Vortex-Genie® 2* *VM-3000* *ZX3*	 Carl Roth VWR VELP Scientifica
Waterbath: *VWB2*	VWR

SDS-PAGE: sodium dodecyl sulfate polyacrylamide gel electrophoresis

2.1.2 Consumables

Item	Source / Manufacturer
Adhesive tape: *Scotch Magic*™ (19 × 13 mm)	3M
Cannula: *Sterican®* 0.40 × 20 mm, 0.45 × 25 mm, 0.90 × 40 mm	 Braun
Cell culture dishes (Ø 60 mm) and multiwell plates (6/12-well) with hole (Ø 17 mm) in the middle of the bottom	In-house production (IST Austria)
Cell culture multiwell plates: *cellstar®* 6-well 24-well 48-well	Greiner Bio-One 657160 662160 677180
Cell strainer: *EASYstrainer*™ (40 and 70 µm)	Greiner Bio-One
Cotton earswabs	JES Collection®, TEDI®
Coverslips (glass): round (Ø10 mm), 0.13-0.16 mm	Carl Roth, Marienfeld
Coverslips (glass) #1.5: square (22 × 22 mm), 0.13-0.16 mm	VWR
Coverslips (glass, gridded): grid repeat distance 50 µm	Ibidi
Dental modeling wax sheets (toughened): *Anutex®*	Kemdent
Glass bottom dishes (Ø 35 mm): Ø glass 14 and 20 mm	MatTek
Glass bottom plate (6-well): Ø glass 20 mm	MatTek
Object slides: 76 × 26 × 1 mm	Marienfeld
Petri dishes (round, sterile): Ø 35 mm Ø 60 mm Ø 100 mm	Greiner Bio-One 627161 628161 633161
Petri dish (quadratic): 120 × 120 × 17 mm	Carl Roth
Plastic tips: 10, 200, 1000 µL 10 µL	 Carl Roth Eppendorf
Radiographic (x-ray) films *Amersham Hyperfilm™ ECL*	GE Healthcare
Reaction tubes: 0.5, 1.5, 2 mL 5 mL 15, 50 mL	 Starlab Biozym Scientific, Roth Greiner Bio-One
Serological pipettes: *cellstar®* (2, 5, 10, 25 mL)	Greiner Bio-One
Syringes: *Injekt® Solo* (10 mL), *Omnifix® Luer Lock Solo* (10 mL)	 Braun

Syringe filters:	
ROTILABO® (pore size 0.22 µm)	Carl Roth
Millex®*-HP*	Millipore
Precast protein gels for SDS-PAGE:	
4-20 % Mini-Protean® *TGX*™	Bio-Rad Laboratories
Nitrocellulose transfer packs for immunoblotting:	
Trans-Blot Turbo Mini 0.2 µm	Bio-Rad Laboratories

IST: Institute of Science and Technology

2.1.3 Chemicals and reagents

Chemical / reagent	Source / Manufacturer
Acetic acid (96 %)	Carl Roth
Agarose *UltraPure*	Invitrogen
Ascorbic acid	Sigma-Aldrich
β-mercaptoethanol (for cell culture)	Thermo Fisher Scientific
β-mercaptoethanol (for protein gel electrophoresis)	Bio-Rad Laboratories
Blotting-grade blocker (non-fat dry milk)	Bio-Rad Laboratories
Bovine serum albumin (BSA)	Sigma-Aldrich
CCL19 and CCL21 (recombinant mouse)	R & D systems
Collagen type I solution *PureCol*® (bovine), 3 mg/mL	Advanced BioMatrix
Declustering agent *GF-15*	Sigma-Aldrich
Declustering agent *PJ-34 hydrochloride hydrate*	Sigma-Aldrich
Deionized water (DI water)	In-house production (LIMES)
Developing solution for x-ray films: *Adefo Citroline2000*	Adefo-Chemie
Dimethyl sulfoxide (DMSO)	Sigma-Aldrich
Distilled water *UltraPure*™, DNase/RNase free	Invitrogen
Double distilled water (ddH_2O)	In-house production (LIMES)
Ethanol (≥ 99.5 %)	Carl Roth
Fetal calf serum (FCS)	Thermo Fisher Scientific
Formaldehyde (solution, 16 %), methanol free	Thermo Fisher Scientific
Isopropanol	Merck
Recombinant human intercellular adhesion molecule 1 (ICAM-1)	Thermo Fisher Scientific
LPS from *Escherichia coli*	Sigma-Aldrich
Mounting medium *Fluoromount-G*™ with/without DAPI	Thermo Fisher Scientific
Paraffin wax	Sigma-Aldrich
Penicillin/streptomycin	Thermo Fisher Scientific
Phosphatase inhibitor tablets *PhosSTOP*™	Roche
Ponceau S	Sigma-Aldrich
Protease inhibitor tablets *cOmplete*™	Roche
Sodium hydrogencarbonate (solution, 7.5 %)	Sigma
Triton™ X-100	Sigma-Aldrich
Tween-20	Sigma-Aldrich
Silicone glue: *Aquarium Silicone Sealant*	Marina

DAPI: 4',6-diamidino-2-phenylindole dihydrochloride; LIMES: Life and Medical Sciences Instiute

2.1.4 Buffer and media

Media and buffers	Source / Manufacturer
Cell lysis buffer: *radioimmunoprecipitation assay* (RIPA) buffer 10×	Cell Signaling
GM-CSF (supernatant from hybridoma cells), 150 ng/mL	produced by Stephanie Ebbinghaus, Kiermaier lab
HBSS 10× (with/without phenol red, with calcium, magnesium, glucose, without sodium hydrogencarbonate)	Thermo Fisher Scientific
Minimum Essential Medium (MEM) 10× (with phenol red, without L-glutamine, HEPES and sodium hydrogencarbonate)	Thermo Fisher Scientific
Phosphate-buffered saline (PBS), pH 7.4	Thermo Fisher Scientific
Protein sample buffer *Laemmli* 4×	Bio-Rad Laboratories
Roswell Park Memorial Institute (RPMI) 1640 Medium (with/without phenol red, with L-glutamine, without HEPES)	Thermo Fisher Scientific
Tris-buffered saline (TBS) 20×	Thermo Fisher Scientific
Tris-glycine-SDS (TGS) 10×	Bio-Rad Laboratories

GM-CSF: granulocyte-macrophage colony-stimulating factor; HEPES: 4-(2-hydroxyethyl)-1-piperazine-ethane-sulfonic acid; Tris: Tris(hydroxymethyl)aminomethane

2.1.5 Kits and standards

Kits and standards	Source / Manufacturer
Cell proliferation kit: *Click-iT™ Plus EdU*, Alexa Fluor™ 555 dye	Thermo Fisher Scientific
Immunoblotting substrate (Western blot): *Pierce™ ECL Plus*	Thermo Fisher Scientific
Protein standard: *Precision Plus Protein Dual Color*	Bio-Rad Laboratories
Silicone elastomer (PDMS) kit: *SYLGARD® 184*	Ellsworth Adhesives

2.1.6 Solutions

Solutions for cell culture, immunofluorescence analyses and cell migration assays

R10 (R20)

RPMI 1640 medium
10 % (20 %) FCS
100 U/mL penicillin
100 µg/mL streptomycin
50 µM β-mercaptoethanol

Solution for coverslip coating

1× PBS
10 % of 1:1 (vol:vol) mixture of ICAM-1 (100 µg/ml) and CCL21 (25 µg/ml)

Solution for cell permeabilization

1×PBS
0.2 % Triton™ X-100

Formaldehyde 2 / 3 / 4 %

1× PBS
12.5 / 18,9 / 25 % of formaldehyde solution 16 %

Solution for blocking and antibody dilution

1× PBS
1 % BSA

2× HBSS

distilled water UltraPure™
20 % 10× HBSS

Solutions and buffer for SDS-PAGE and immunoblotting

10× *PhosSTOP*™ phosphatase inhibitor stock solution for cell lysis buffer

1 tablet in 1 mL distilled water *UltraPure*™

25× *cOmplete*™ protease inhibitor solution for cell lysis buffer

1 tablet in 2 mL distilled water *UltraPure*™

Cell lysis buffer

DI water
10 % 10× RIPA
10 % of 10× *PhosSTOP*™ phosphatase inhibitor solution
4 % of 25× *cOmplete*™ protease inhibitor solution

inhibitors were added freshly

Loading buffer

4× *Laemmli* buffer
10 % β-mercaptoethanol

TBS-Tween (TBS-T)

1× TBS
0.1 % Tween-20

Ponceau S staining solution

ddH_2O
0.2 % Ponceau
3 % acetic acid (96 %)

Solution for blocking and antibody dilution

TBS-Tween (0.1 %)
5 % non-fat dry milk or 5 % BSA

2.1.7 Antibodies and staining substances

Primary IgG antibodies for immunofluorescence stainings

Target	Host	Clonality	Conjugate	Dilution	Company and product ID
α-tubulin	rat	mono		1:500	Thermo Fisher Scientific (MA1-80017)
acetylated tubulin	mouse	mono		1:600	Sigma-Aldrich (T7451)
BubR1	rab	mono		1:100	Abcam (ab254326)
CEP135	rabbit	poly		1:600	Abcam (ab75005)
γ-tubulin	mouse	mono		1:500	Sigma-Aldrich (T6557)
γ-tubulin	rabbit	mono		1:500* 1:800**	Abcam (ab11317)
LYVE-1	rat	mono		1:200	Thermo Fisher Scientific (14-0443-82)
MHC-II	rat	mono	biotin	1:400	Thermo Fisher Scientific (13-5321-82)
p21	rab	mono		1:300	Abcam (ab188224)

phospho-histone H3 (pH3) (Ser10)	rabbit	mono	1:500	Cell Signaling (9701)
pH3 (Ser10)	mouse	mono	1:600	Cell Signaling (9706)

*ear sheets; **isolated cells

Secondary polyclonal antibodies for immunofluorescence stainings

Target	Host	Conjugate	Dilution	Company and product ID
mouse IgG (H+L)	donkey	Alexa Fluor™ 488 (A488)	1:400	Jackson ImmunoResearch (715-546-151)
rabbit IgG (H+L)	goat	A488	1:400	Thermo Fisher Scientific (A11008)
rat IgG (H+L)	donkey	A488	1:400	Jackson ImmunoResearch (712-546-150)
rat IgG (H+L)	donkey	A568	1:400	Invitrogen (A78946)
mouse IgG (H+L)	donkey	A647	1:400	Jackson ImmunoResearch (715-606-150)
rabbit IgG (H+L)	donkey	A647	1:400	Jackson ImmunoResearch (711-606-152)
rat IgG (H+L)	donkey	A647	1:400	Jackson ImmunoResearch (712-606-150)
mouse IgG (H+L)	donkey	cyanine dye 3 (Cy3)	1:400	Jackson ImmunoResearch (715-166-151)
rabbit IgG (H+L)	goat	Cy3	1:400	Jackson ImmunoResearch (111-165-144)
rat IgG (H+L)	donkey	Cy3	1:400	Jackson ImmunoResearch (712-165-150)

Additional staining substances

Substance	Target	Conjugated fluorescent dye	Dilution	Company and product ID
Hoechst 33342	DNA		1:2000	Invitrogen (H3570)
phalloidin	F-actin	A546	1:200 1:400	Thermo Fisher Scientific (A22283)
streptavidin	biotin	Cy3	1:400	Jackson Immunoresearch (016-160-084)
streptavidin	biotin	A647	1:400	Jackson Immunoresearch (016-600-084)

Primary IgG antibodies for SDS-PAGE

Target	Host	Clonality	Dilution	Company and product ID
BubR1	rabbit	mono	1:1000 BSA	Abcam (ab254326)
cyclin A2	rabbit	mono	1:2000 milk	Abcam (ab181591)

cyclin B1	rabbit	mono	1:1000 milk	Abcam (ab181593)
cyclin E	rabbit	mono	1:1000 BSA	Cell Signaling (20808)
Cdk2	rabbit	mono	1:1000 milk	Abcam (ab32147)
Cdk4	rabbit	poly	1:500 milk	Abcam (ab137675)
GAPDH	mouse	mono	1:4000 milk	Abcam (ab125247)
p21	rabbit	mono	1:1000 milk	Abcam (ab188224)
p27	rabbit	poly	1:1000 BSA	Cell Signaling (2552S)
vinculin	mouse	mono	1:40000 milk	Sigma-Aldrich (V9131)

Secondary polyclonal antibodies for SDS-PAGE

Target	Host	Conjugate	Dilution	Company and product ID
mouse IgG (H+L)	goat	horseradish peroxidase (HRP)	1:10000	Bio-Rad Laboratories (1706516)
rabbit IgG (H+L)	goat	HRP	1:10000	Bio-Rad Laboratories (1706515)

2.1.8 Organisms

Organism	Source
centrin 2 (CETN2)-green fluorescent protein (GFP) mice (CB6-Tg(CAG-EGFP/CETN2)3-4Jgg/J)	Jackson Laboratory
GM-CSF producing hybridoma cells	Prof. Dr. Michael Sixt, IST Austria
WT mice (C57BL/6JRcc)	Genetic Resources Center, LIMES Institute

2.1.9 Software and online tools

Software and web applications	Company / URL
BioRender	https://app.biorender.com/
custom built software for laser cutting using LabView[345]	National Instruments
FIJI[346] / ImageJ[347] (1.48s and 1.53c)	https://imagej.net/software/fiji/ https://imagej.nih.gov/ij/
Fusion 2.2	Andor
ilastik v1.3.3	https://www.ilastik.org/about.html
iQ2	Andor
NIS-Elements AR 2.30	Nikon
NIS Elements 4.0	Nikon
GraphPad Prism 7	Graphpad Software
ZEN Black 2.3 SP1	Zeiss

2.2 Methods

Unless otherwise stated, all experiments were performed at room temperature (RT) and with single-concentration (1×) solutions and buffers.

2.2.1 Animal experimental techniques and cell culture methods

2.2.1.1 Mice

All mice used in the present studies were on a C57BL/6J background (wildtype (WT) and CETN2-GFP) and kept at the animal facility of the LIMES in accordance with the German law for animal experimentation. CETN2-GFP mice were purchased from Jackson Laboratory.

2.2.1.2 Generation and cultivation of ear explants

4-6-week-old female WT or CETN2-GFP reporter mice were sacrificed and their ears were cut off with scissors near the head. Using forceps, ears were separated into a dorsal and a ventral sheet[348], which were placed on 500 µL of full medium (R10: RPMI 1640 medium, 10 % FCS, 100 U/mL penicillin, 100 µg/mL streptomycin, 50 µM β-mercaptoethanol) in a 48-well plate. For declustering experiments, drugs were added to the medium in the indicated concentrations. Due to the mechanical stimulus of rupturing the ears in half, skin DCs are activated, which is accompanied by increased migratory capacity. According to the planned assay, ear sheets were fixed immediately (timepoint 0 hrs) or incubated at 37 °C and 5 % CO_2 in a humidified atmosphere for 24 or 48 hrs until fixation for the respective experimental runs. During this incubation period, 500 µL of R10 (+ declustering agents) were added daily. For fixation, medium was removed and replaced with 2 % *paraformaldehyde* (PFA) in PBS. After overnight storage at 4 °C, ear sheets were washed 3× 15 min with PBS while placed on a shaking plate. *Immunofluorescence* (IF) stainings were performed as described in section 2.2.2.3.

2.2.1.3 Isolation and cultivation of dermal DCs from ear explants

Ears of 8-12-week-old WT or CETN2-GFP reporter mice were cut off and split into two sheets as described above. Ear sheets were placed inside-out on 500 µL of full medium (R10) supplemented with 25 µg/mL CCL19 in a 24- or a 48-well plate and incubated for 3 days at 37 °C and 5 % CO_2 in a humidified atmosphere to let dermal DCs crawl out into the medium. 500 µL R10 and CCL19 were added daily before the non-adherent cells were harvested and fixed for IF staninigs, lyzed for immunoblot analyses or used in migration assays.

2.2.1.4 Isolation of bone marrow and generation of BMDCs

Femurs and tibias from 8-12-week-old WT or CETN2-GFP reporter mice were taken and placed in ethanol (70 %) for 2 min. The ends of the bones were cut with scissors, and bone marrow was flushed out with PBS, RRPMI or R10 using a syringe and 26-27 gauge needle. The cell suspension was filtered through a sterile strainer (70 µm) and centrifuged at 300× g for 5-10 min at 4 °C. For differentiation into DCs, cells were seeded in 100 mm Petri dishes (2×10^6 cells/dish) in R10 supplemented with 10 % GM-CSF in a total volume of 10 mL. Cells were kept at 37 °C, 5 % CO_2 and 80 % humidity. On day 3, cells were fed with R10 containing 20 % GM-CSF in a total volume of 10 mL leading to a total culture volume of 20 mL. On day 6, 10 mL of cell suspension was removed, discarded, and replaced with R10 containing 20 % GM-CSF in a total volume of 10 mL, again resulting in a culture volume of 20 mL per dish. Non-adherent cells were harvested and reseeded (2×10^6 cells/dish) in R10 and 10 % GM-CSF in a total volume of 20 mL. Stimulation was performed using 200 ng/ml LPS added to the cell cultures for 16 hrs. For experiments with immature DCs, cells from days 6 and 7 were used (unstimulated cells), whereas mature DCs were used from day 8 and 9 of cell cultivation (stimulated cells).

2.2.2 Cell based assays

2.2.2.1 Edu incorporation assay

For EdU labelling, immature and mature WT BMDCs as well as ear sheets from WT and CETN2-GFP mice from indicated time points were incubated with 10 µM EdU in R10 medium for 1 h at 37 °C, 5 % CO_2 and 80 % humidity. Subsequently, cells were immobilized on coverslips. Immobilized cells and ear sheets were fixed with PFA (see sections 2.2.1.2 and 2.2.2.2) and permeabilized before EdU detection using the Click-iT EdU Imaging Kit according to the manufacturer's protocol. Since Edu of the kit is coupled to a fluorophore (Alexa Fluor 555 dye), EdU-positive cells were identifiable and were imaged using a laser scanning microscopy.

2.2.2.2 Immunofluorescence stainings *in vitro*

In the case of non-migrated cells, round glass coverslips were coated with 2 µL of a 1:1 (vol:vol) mixture of ICAM-1 and CCL21 (see section 2.1.6) for 10 min before they were placed into a 24-well plate. 1-3 µL of DCs in full medium were transferred onto each coated coverslip, incubated for 5 min at 37 °C on a hotplate and fixed with 250 µL 4 % PFA/PBS at 4 °C for 20 min. Afterwards, cells were washed with PBS (3× 10 min).

In the case of migrated DCs, cells that have migrated on uncoated coverslips under agarose (see section 2.2.3.1) were fixed by adding 500 µL of 4 % PFA/PBS on top of the agarose. After over night incubation at 4 °C, remaining PFA solution on top of the agarose was removed before the agarose pad was carefully lifted off using a coverslip-tweezer. Coverslips were transferred into a 24-well plate and washed 3× 10 min with PBS.

Coverslips with migrated and non-migrated cells were incubated with 250 µL 0.2 % Triton X-100/PBS for 20 min to permeabilize the cells. A washing step of 2× 10 min with PBS was potentially followed by EdU staining with the Click-iT EdU Imaging Kit, concluding with a washing step (2× 10 min of PBS). Prior to antibody staining, a blocking step was performed to prevent non-specific binding. Therefore, samples were incubated in 250 µL blocking solution (1 % BSA/PBS) for 1 h. Primary antibodies diluted in 200 µL blocking solution were added overnight (only exception: CEP135-antibody which was incubated for 30 min) at 4 °C. Coverslips were washed for 3× 10 min with PBS and incubated with secondary antibodies in 200 µL blocking solution for 1 h in the dark. Finally, samples were washed again with PBS for 3× 10 min before the coverslips were placed upside down on a glass object slide with a drop of non-hardening mounting medium containing DAPI. Samples were sealed with nail polish. Storage was at 4 °C in the dark.

2.2.2.3 Immunofluorescence stainings *in situ*

After overnight fixation at 4 °C and washing with PBS for 3× 15 min (see section 2.2.1.2), ear sheets were incubated with 0.2 % Triton/PBS for 20 min. Explants were washed again with PBS for 2× 15 min. This step was followed by a potential EdU staining with the Click-iT EdU Imaging Kit, which was completed with a washing step (3× 10 min with PBS). Regardless of the following assay, all samples were incubated with 250 µL of blocking solution (1 % BSA/PBS) for 1 h which was followed by primary antibody treatment with 200 µL of biotin-coupled MHC-II-antibody diluted in blocking solution for 120 min to stain dermal DCs.

For centrosome visualization, single centrioles were parallelly stained with an antibody against ac-tubulin when using ears of WT mice. Depending on the experiment, the PCM was co-stained using an antibody against γ-tubulin. After a PBS washing step for 3× 10min, samples were incubated with the respective secondary antibodies in blocking solution for 90 min and washed again with PBS for 3× 10 min. Nuclear staining was performed using Hoechst dye 1:2000 in PBS for 30 min, followed by a final washing step with PBS (3× 10 min).

In assays study Edu incorporation of dermal DCs *in situ*, a washing step (3× 10 min with PBS) was performed after incubation of the primary antibody, followed by incubation of the

secondary antibody (streptavidin-coupled fluorophore) for 90 min. A final wash step of 3× 10 min with PBS prepared the samples for conservation (see below).

For joint visualization of dermal DCs and lymphatic vessels, a 120 min incubation with primary antibodies was performed after the blocking step with 1 % BSA/PBS to stain dermal DCs (MHC-II biotin) and lymphatic vessels (LYVE-1). This was followed by washing with PBS for 2× 15 min. Since both antibodies were from the same species (rat), an additional “blocking” step was performed with a streptavidin-coupled fluorophore diluted in 200 µL blocking solution (1 h). Immediately thereafter, explants were incubated for 90 min with secondary antibodies diluted in 200 µL blocking solution. Subsequently, samples were washed with PBS for 3× 15 min.

Ear sheets were placed on microscopy slides (stained side up) where they were drizzled with a drop of PBS or non-hardening mounting medium with or without DAPI. Finally, explants were covered with a round glass coverslip sealed with nail polish. Storage was at 4 °C in the dark.

2.2.2.4 BubR1 staining in immature cells under agarose

To microscopically investigate mitotic abnormalities, BubR1 and other relevant intracellular structures of BMDCs in M phase were imaged. Injection of cells under a pad of agarose results in a very flat shape of the cells, allowing target structures to be subsequently visualized clearly using IF stainings. To have enough or more mitotic events, immature cells were used. According to the cultivation protocol (see section 2.2.1.4), immature WT BMDCs were fed on day 6. After 8 hrs, cells were harvested and injected under agarose onto a coverslip as described in section 2.2.3.1. For the easier performance of the injection, a hole was punched on the opposite side, but this was not filled with chemokine as is the case in the under agarose migration assays. Since the (mechanical) process of injection induces a partial activation of the cells, resulting in the cells evolving from a more proliferative to a more migratory state, cells were fixed directly after injection using prewarmed 4 % PFA/PBS. Dishes were stored in a humidifed incubator at 37 °C and 5 % CO_2 for 5-20 min until further fixation at 4 °C over night. Staining was done as described in section 2.2.2.2. For mounting, a non-hardening medium containg DAPI was used.

2.2.2.5 Actin staining and quantification

To visualize centrosomal actin, mature (d9) WT and CETN2-GFP BMDCs that had previously migrated under agarose were fixed, permeabilized, and blocked as described previously. Samples were then treated with Alexa Fluor 546 (A546) coupled phalloidin (1:200 and 1:400)

over night at 4 °C. In parallel, the PCM was co-stained with an antibody against γ-tubulin. In the case of WT cells, centrioles were additionally co-stained using an antibody against ac-tubulin. After staining with secondary antibodies the next day, samples were preserved in non-hardening mounting medium containing DAPI. Quantification of centrosomal actin was performed only in diploid cells to exclude ploidy-related effects. Identification of 2N cells was based on the nucleus size as described in sections 3.2.3 and 3.3.2. The amount of centrosomal actin was determined using integrated Phalloidin-A546 fluorescence intensity. Normalization was performed in ImageJ by defining a *region of interest* (ROI) to mark areas for measurement. The defined ROI was then used to mark the area around the centrosome and an area of same size in the cytosol. Subsequently, the quotient of centrosomal actin signal (fluorescence intensity centrosome) and non-centrosomal actin signal (fluorescence intensity cytosol) was calculated for each cell.

2.2.2.6 Quantification of nuclear p21

In cell cycle analysis, the amount of nuclear p21 in fixed WT BMDCs of different maturation stages was determined by IF analysis. For this purpose, p21 was stained and the nuclei counterstained with DAPI. All images were acquired under the same settings with a confocal laser scanning microscope (LSM880) and processed in FIJI. An oval ROI was defined that was large enough to label as much of each nucleus as possible, but small enough to "fit" into most nuclei. The ROI was applied to all nuclei of an image and the integrated fluorescence density of the p21 signal was measured in the marked area. Cells with nuclei smaller than the ROI were not analyzed.

2.2.2.7 Inhibition of centrosomal clustering *in vitro*

Mature CETN2-GFP expressing BMDCs from day 9 (maturated over night from day 8 to 9) were harvested. To reduce the number of non-DCs and dying cells, allow recovery from LPS treatment, and reduce the amount of drug required, cells were reseeded in a 24-well plate (0.4×10^6 cells/well) and treated with declustering drugs and appropriate control for the indicated time at 37 °C and 5 % CO_2 in a humidified atmosphere. Depending on the following experiments, the next steps differ:

For analysis of declustering potency of the two drugs, cells were harvested, immobilized on coated coverslip (see section 2.2.2.2) and fixed with 4 % PFA/PBS. Afterwards, samples were conserved in non-hardening mounting-medium containing DAPI and analyzed for inter- and intracentrosomal distances using laser scanning microscopy.

For analysis of cytoskeletal structures, particularly MTs, and PCM after drug treatment, cells were harvested and injected onto an uncoated coverslip under a block of agarose, which contains the respective declustering drug. A chemokine gradient was used to induce directional migration, resulting in a flat morphology of the cells so that intracellular structures could be easily visualized. In a state of stable migration, cells were fixed through the agarose and stained as described in section 2.2.2.2.

To analyze the migration behavior of drug treated DCs, the cells were harvested and used in collagen and under agarose migration assays, in which the respective declustering drug was also added to the collagen/agarose (see sections 2.2.3.1 and 2.2.3.2).

2.2.3 Migration assays and pertubation of cell locomotion

2.2.3.1 2D under agarose migration assay

2D under agarose migration assays were performed for two different purposes: to generate migrating DCs that were fixed during migration to obtain flat cells for staining intracellular structures, or to monitor cells live during imaging. In both cases, mature (day 9) WT or CETN2-GFP expressing BMDCs were harvested and reseeded in a 24-well plate (0.4×10^6 cells/well). In the case of declustering experiments, cells were treated with the respective agents and appropriate controls for the indicated time in a humidified atmosphere at 37 °C and 5 % CO_2. For experiments without declustering drugs, cells were allowed to sit for approximately 55 min. Dermale DCs emigrated from ears sheets for 3 days were not reseeded but harvested directly from the 24-well plate for subsequent injection under agarose (see below).

For IF stainings, migration chambers were constructed from 35 or 60 mm Petri dishes and a plastic ring approximately 12 mm in diameter that was glued to the center of each dish with heated paraffin wax. A round coverslip with a diameter of 10 mm was placed on the dish bottom in each ring (see Fig. 16 c). For following the migration process, glass bottom dishes with optical properties for high-resolution microscopy were used instead of plastic Petri dishes and coverslips, allowing live imaging of moving cells. To prevent microbial contamination and regardless of the planned assay, the constructs were irradiated with UV light under a sterile laminar flow hood for 20 min.

To prepare agarose pads, 4 % agarose was heated and dissolved in nuclease-free distilled water and mixed with phenol red-free R20 (see section 2.1.6) and Hanks' Balanced Salt Solution (HBSS) (pH 7.2) in a ratio of 1:3 (final agarose concentration: 1 %). In the case of live cell fluorescent imaging, ascorbic acid (final concentration: 50 µM) was added as radical

scavenger. If declustering experiments were performed, the agarose mixture was added with the declustering drug or the appropriate control. Subsequently, 500 µl of the agarose-medium-mixture was poured into the glued rings. After a solidification time of about 5 min, a hole of about 1.5 mm diameter was punched into the agarose near the edge using a cut earswab (see Fig. 16 c). The part of the dish surrounding the plastic ring was filled with ddH_2O to create a humid environment for subsequent agarose equilibration at 37 °C, 5 % CO_2 and 80 % humidity.

After approximately 55 min, any water in the holes was removed, CCL19 was diluted in phenol red-free R20 (final concentration: 2.5 µg/mL) (depending on assay + declustering agents/control) and filled into the prepared holes to create a soluble chemokine gradient that attracts DCs. In parallel, DCs in the 24-well plate were harvested, centrifuged for 5 min at 300× g, and concentrated to 0.6-0.8×10^6 cells/µL R20 before 0.4-0.8 µL of the cell suspension was injected under the agarose on the opposite side of the chemokine hole. The purpose of the injection was to confine the cells between agarose and coverslip. Successful injection was monitored with a phase contrast microscope (Nikon Eclipse TS100). Suitable dishes were incubated for 2-3 hrs at 37 °C, 5 % CO_2 to allow the cells to recover and achieve a state of stable migration. Via microscope, cells were checked for proper confinement and migration status. It should be noted that if simple fixation and no live cell imaging is planned, the complete medium may contain phenol red and only 10 % FCS instead of 20 %.

Depending on the assay, the next steps differ: For IF experiments, cells were fixed with 500 µL of 4 % PFA/PBS added on top of the agarose and incubated over night at 4 °C. For next steps, see section 2.2.2.2. Live cell imaging was performed on a confocal laser scanning microscope, widefield systems or a spinning-disc confocal system, all equipped with an incubator or a heating chamber to provide the best possible physiological conditions (see section 2.2.4).

2.2.3.2 3D collagen migration assay

Chambers for 3D collagen migration devices were assembled with strips of dental wax that were formed into a U-shape and pressed onto an object slide[121]. A square coverslip (18 × 18 or 22 × 22 mm) was placed on the U and the construct was warmed up at 60 °C for 1 min to allow the coverslip to be gently pressed onto the U to fix it in place (see Fig. 12 a).

Mature WT BMDCs (day 9) and dermal DCs that migrated out of the ears of CETN2-GFP-expressing mice for 3 days were harvested and reseeded into a 24-well plate (0.3×10^6 cells/well). Cells were stored at 37 °C and 5 % CO_2 for at least 30 min for recovery or, in the case of declustering experiments, treated with declustering agents and an appropriate control for the indicated time. After recovery/incubation time, cells were harvested, centrifuged

for 5 min at 300× g, and resuspended in 100 µL R10 leading to a cell concentration of 0.3×10^6 cells/100 µL.

Collagen gels for U-shaped devices were prepared by mixing sodium hydrogencarbonate solution (7.5 %), 10× Minimum Essential Medium (MEM) and collagen type I solution (3 mg/mL) in a ratio of 1:2:15 resulting in a collagen gel of 1.7 mg/mL[121]. For each U-shaped migration chamber, 200 µL of the collagen mixture was calculated. The collagen mixture was next mixed with the cell suspension in a ratio of 2:1 and filled into the U-shaped chamber until it was two-thirds full (80-200 µL). Devices were placed in a slide holder (upright) and stored in a humidifed incubator at 37 °C and 5 % CO_2 for at least 45 min to allow polymerization of the gel. After this time, CCL19 diluted in R10 medium (final concentration: 0.625 µg/mL) was placed on top of the gel (40-100 µL) forming a chemotactic gradient that induces directional cell migration; the open top of the chamber was tightly sealed with heated paraffin wax (see Fig. 12 a). Images were acquired with a widefield microscope using time-lapse video microscopy.

2.2.3.3 Migration in Y-shaped micro-fabricated channels

Silanized wafer as moulds for the production of *polydimethylsiloxane* (PDMS) based devices were kindly provided by the group of Prof. Michael Sixt, *Institute of Science and Technology* (IST) Austria[126,154,226,227]. For the production of PDMS-devices (see also [227]), the wafer with Y-channel designs (channel size: 4 × 4 µm) was placed in a round tray of aluminium foil and overlayed with a mixture of silicone elastomer base and silicone elastomer curing agent (kit Sylgard184) in a ratio of 10:1 after the two components were mixed and degassed in a planetary centrifugal mixer for 4 min. After degassing with a vacuum desiccator for about 3× 3 min, the the PDMS was cured at 80-85 °C over night.

The next day, the PDMS part was separated from the wafer and cut into small rectangular pieces according to the distribution of the Y-channel designs. Using a puncher, two holes of 2 mm diameter were punched in the PDMS: The hole for the cells was punched close to the bottom of the Y (single arm), while the hole for the chemokine was punched above the ends of the two arms of the Y. Afterwards, PDMS pieces were cleaned with scotch tape.

Rectangular glass coverslips (#1.5) were cleaned in an ultrasonic bath with isopropanol, ethanol and DI water for 5 min each and then dried. Subsequently, coverslips and PDMS pieces were plasma cleaned for approximately 2 min before the PDMS pieces were placed on the coverslips with the features facing down. After gentle pressing, coverslips with PDMS were placed on a hotplate (85 °C) for 1 h to achieve proper bonding. Aquarium glue was used to glue coverslip bound PDMS devices into a custom-made Petri dish/mutiwell plate having a hole in the center. The glue was left to cure overnight at RT or in warming oven at 85 °C.

For the equilibration of the devices and all subsequent steps, R20 medium without phenol red was used to provide the best possible conditions for the migration of cells under fluorescence conditions. Therefore, ascorbic acid (final concentration: 50 µM) was also added to the medium. This mixture is called "medium" in this chapter. Dishes/wells were filled with prewarmed medium until the devices were fully covered. Devices were additionally flushed through the two holes. To avoid or remove air bubbles inside the devices, dishes/plates were degassed in a vacuum desiccator for 5-10 min. Medium from top of the devices was removed and dishes were stored in a humidifed incubator at 37 °C and 5 % CO_2 over night. All medium from the dishes/wells and chemokine holes was removed and 7-10 µL CCL19 diluted in medium (final concentration: 2.5 µg/mL) was filled in the chemokine holes. Then the hole for cells was emptied, which sucked the chemokine into the system.

Mature CETN2 BMDCs (day 9), previously harvested and then seeded for a recovery time of at least 45 min in a 24-well plate, were harvested from the multiwell plate, adjusted to approximately 6×10^4/µL, and carefully pipetted into the cell hole of the PDMS device (7-10 µL). After about 10 min, dishes/wells were filled with medium until the devices were covered completely. Devices were incubated in a humidifed incubator at 37 °C and 5 % CO_2 at for 1-3 hrs before fluorescence imaging began using a widefield microscope.

2.2.3.4 Laser ablation of centrosomes

During 2D migration under agarose, mature CETN2-GFP BMDCs were exposed to different laser treatments, distinguishing between 3 scenarios: 1) “full” or “complete” centrosomal ablation: complete centrosomes were ablated. 2) “partial” ablation: one centrosome of multiple centrosomes was ablated. 3) “control ablation”: laser shots hit the cytoplasm near the centrosome, but not the organelle itself. To determine the area of exposure, the software used allowed the definition of a ROI, which was always the same size when placed around the centrosome (full, partial ablation) or near it (control ablation).
Imaging of the cells at least 4 min before and after (control) ablation allowed analysis of migration velocity and persistence before and after the intervention. Therefore, cells were tracked manually using the ImageJ plugin *Manual Tracking*. The data obtained were fed into the *Chemotaxis and Migration Tool*, another ImageJ plugin, to quantify cell velocity and persistence. Results were presented as change in parameters between pre/post intervention.
As part of the efficiency analysis of centriole depletion, maximum intensity Z-stack projections of CETN2-GFP signals prior to and after the ablation process were recorded. Subsequently, fluorescence intensity of the GFP signal was quantified in FIJI by defining a ROI that marked the area of the centrosome before and after the ablation process.

Gridded glass coverslips were used for IF experiments in which MT filaments were stained, to retrieve those cells that had undergone complete laser or control treatment. MT filaments were counted after centrosomal laser ablation and compared with MT numbers of untreated cells. Similarly, the configuration of MT filaments (length, straightness) in laser exposed and control treated cells was quantified. For this purpose, MT were tracked semi-manually using the FIJI plugin *NeuronJ*. The obtained "traces" were used to calculate straightness ((distance start-end divided by filament length) weighted by filament length).

2.2.4 Microscopy

2.2.4.1 Imaging of fixed samples on a confocal laser scanning microscope

Fixed cells for IF analyses were imaged at RT with an inverted confocal laser scanning microscope (LSM880) equipped with a motorized stage (Märzhäuser), an Airyscan module, a photomultiplier tube and laser lines of 488, 561, and 633 nm wavelength. The associated software (ZEN Black 2.3 SP1) comes from Zeiss, as do all the previously mentioned components. Image acquisition of immobilized BMDCs and dermal DCs emigrated from skin explants was performed using a Plan-Apochromat 63×/1.4 oil objective. *In situ*, i.e., in ears sheets, the same imaging conditions were used for visualization of centrosomes, whereas localization of dermal DCs with respect to lymphatic vessels and determination of the percentage of Edu-positive cells were performed with a Plan Neofluar 20×/0.50 air objective. During image acqusition with a 63× objective, 200 nm sections in the Z-dimension were captured (covering a range of 4-8 µm), while during imaging with a 20× magnification sections of 2 µm were taken. Z-images were subjected to maximum intensity Z-stack projections using FIJI. In some image sections of ear sheets, only the indicated z-planes were projected to more clearly show structures of interest.

For the identification and quantification of centrioles in BMDCs and emigrated dermal DCs, the colocalized presence of ac-tubulin/CETN2-GFP and γ-tubulin staining or ac-tubulin/CETN2-GFP and CEP135 staining was used as a criterion. Structures that did not show a colocalization of the two markers were not considered as centriole and were therefore excluded from the analyses (only exception: quantification of centrioles in immature and mature WT BMDCs, as shown in Fig. 14 a; here, only ac-tubulin positive foci were used for quantification). Centrioles were counted manually after maximum z projections.

Image acquisition of cells to visualize MT filaments and actin was conducted in the Airy Mode and images were afterwards treated by deconvolution. For the quantification of MTs and actin, only 2N cells were used to exclude effects due to ploidy. Conclusions about ploidy were

obtained from nuclear sizes recorded with FIJI after DAPI staining, as described in sections 3.2.3 and 3.3.2. Following maximum intensity Z-stack projections, MTs emanating from the centrosome/s were counted manually using FIJI/Image. Quantification of actin is described in section 2.2.2.5. Quantification and graphical representation of cell and migration related parameters was performed using GraphPad Prism.

2.2.4.2 Live cell imaging on a confocal laser scanning microscope

The inverted confocal laser scanning microscope LSM880 and associated ZEN software have also been used for live cell imaging studies on a single cell level. For this purpose, the microscope system was expanded to include a portable heating chamber, which was inserted into the stage and set to 37 °C, and an objective heating. Mature (day 9) CETN2-GFP expressing BMDCs and dermals DCs collected from ears sheets of CETN2-GFP mice after 3 days of emigration were injected under agarose in glass bottom dishes and stored in a humidifed incubator at 37 °C and 5 % CO_2 as described in section 2.2.3.1. When the cells reached a state of stable migration, the dishes were successively transferred from the incubator to the previously humidified heating chamber.

Image acquisition was performed at 2 sec intervals for 10 min. With the 63×/1.4 oil DIC objective, individual centrioles were clearly visible, allowing discrimination of DCs with different centrosome numbers (1 vs. ≥ 2 centrosomes). Only diploid cells were included in the subsequent analyses of migration parameters to exclude ploidy-related effects. Migrating diploid and tetraploid cells were distinguished by measuring nuclear areas, which was possible despite the absence of nuclear staining, as the area of the nucleus was readily identifiable due to the lack of GFP signal.

Using ImageJ, images were processed and migration parameters of 2N cells with one and multiple centrosome(s) were determined. Therefore, each migrating cell was manually tracked using the plugin *Manual Tracking*. The data obtained were fed into the plugin *Chemotaxis and Migration Tool*, to determine cell velocity and directional persistence of the cells. Maximum intensity projection over time was performed using FIJI. Cells that interacted with other cells during migration as well as cells with unclear centriole numbers were excluded from the analysis. Quantification and graphical representation of cell and migration related parameters was performed using GraphPad Prism.

2.2.4.3 Live cell imaging on widefield microscopes

Non-fluorescent time-lapse video microscopy of cells in 3D collagen and 2D under agarose migration assays was performed with an inverted Nikon Eclipse widefield microscope (TE 2000) equipped with a stationary heating box, a motorized stage (Märzhäuser), and a CCD-1300 camera (Vosskühler). The software used (NIS-Elements AR 2.30) was also from Nikon. Dermal DCs migrating in collagen gels were monitored in a humidified environment at 37 °C over a period of 4 hrs by capturing images every 60 sec using a C-Apochromat 20×/0.5 PH1 air objective. Image acquisition of migrating drug treated WT BMDCs was performed under the same climate conditions for 4 hrs at 60 sec intervals (collagen gels) or 40 sec intervals (under agarose) using the same objective. Cells were manually tracked using the ImageJ plugin *Manual tracking*, and the obtained data were analyzed with the ImageJ *Chemotaxis and Migration Tool* plugin to determine average velocity and persistence (bulk cell analysis). Thereby, each individual cell track is based on the mean value of the average parameter of the individual measurement points, i.e., frames.

Fluorescent time-lapse video microscopy of BMDCs in PDMS-based microchannels and 2D under agarose migration assays was performed with an inverted Nikon Eclipse widefield microscope (Ti2) equipped with a stationary incubation chamber with a gas mixer (Ibidi), a motorized stage (Nikon), a Plan-Apochromat 40×/0.95 objective, a DS-Qi2 camera, and a *Spectra X* light source (Lumencor). The Nikon software used was NIS Elements 4.0 and the plugin module *JOBS*. For all assays performed, the incubation chamber was humidified and set at 37 °C and 5 % CO_2.

Analysis of intra- and intercentrosomal distances during migration was conducted in mature (day 9) CETN2-GFP expressing BMDCs migrating under agarose and was performed by Robert Hauschild. Intracentrosomal distances in cells with one centrosome were determined via centriole segmentation using pixel classification of the software *ilastik*. The centriole locations were found for each time point by a three-step procedure: segmentation of the centriole-probability output, particle size filtering, calculation of the center of mass. Afterwards, centrioles were tracked over time. Via the *Kuhn-Munkres algorithm*, a combinatorial optimization algorithm, problems with assignment were solved. Filtering by minimum track length and track duration was the final step of this process. Based on the condition that two centrioles move predominantly in parallel and are in close proximity to each other during the migration track pairs of centrioles were automatically identified. To filter out cells with extra centrosomes the distance to the closest third centriole was determined. To validate the automatical method, cells were analyzed manually. To determine intra- and intercentrosomal distances of extra centrosomes, centrioles were tracked using the ImageJ plugin *Manual*

Tracking. Obtained data allowed the calculation of the intercentrosomal distance (distance between the centers of centriole pairs). Maximum intensity projection over time was performed using FIJI. If not stated otherwise, quantification and graphical representation of cell and migration related parameters was performed using GraphPad Prism.

For studies of mature (day 9) CETN2-GFP BMDCs in PDMS based Y-shaped decision channels, images were aquired at 60 sec intervals for at leat 2.5 hrs. In addition to fluorescence imaging, also transmitted light images were acquired. Images were processed using FIJI.

2.2.4.4 Live cell imaging on a spinning disc confocal microscope

Laser ablation experiments with mature (day 9) CETN2-GFP BMDCs migrating under agarose were performed on an Andor spinning-disc confocal system (*Confocal Scanner Unit* (CSU): CSU-X1, Yokogawa) installed on an inverted Axio observer microscope (Zeiss). The system was equipped with a motorized stage (Applied Scientific Instrumentation, ASI), an incubation chamber with gas mixer (Ibidi) and an in-hose producted objective heating. To create physiological conditions for cell migration, the incubation chamber was humidified and set to 37 °C and 5 % CO_2. Visualization was done using a 50 mW 488 nm laser, a C-Apochromat 63×/1.2WKorr UV-VIS-IR objective (Zeiss) and the Andor camera *iXon897*. Cells were imaged at single cell level at 5 sec intervals for at least 4 min before and after laser intervention. Laser treatment consisted of complete or partial centrosome ablation or a control shot into the cytosol adjacent to the centosome with a 355 nm pulsed laser (pulse length: 350 ps, intensity: 1 [≙10.8 µW during shot]; pulses/shot: 5; pulse rate: 1 kHz; shots/µm^2: 1). Images were obtained with Andor software. Maximum intensity projection over time was performed using FIJI. Analysis and graphical representation were done with GraphPad Prism. For further details, see section 2.2.3.4.

2.2.4.5 Imaging of fixed samples on a spinning disc confocal microscope

Imaging of fixed and stained BMDCs that have migrated under agarose on gridded coverslips in laser ablation experiments was performed using a spinning-disc confocal system (Dragonfly 505, Andor) installed on a Nikon Eclipse Ti2 inverted microscope. The system was equipped with a motorized stage (ASI), a Plan Apochromat λ 60×/1.4 oil objective (Nikon) and 405, 488, and 561 nm laser lines. Images were acquired as Z-stacks (0.15 µm step size) in the range of 3 µm using *Zyla sCMOS* camera (4.2 Megapixel) and the software *Fusion 2.2* (both Andor). Image processing and data analysis were done with FIJI, quantification and graphical representation of the analyzed parameters were performed using GraphPad Prism.

2.2.5 Biochemical assays

2.2.5.1 Cell lysis and protein extraction

For the preparation of protein lysates, WT BMDCs of indicated differentiation/maturation stages or time points and dermal DCs emigrated from ear sheets of WT mice for 3 days were harvested, counted, and washed with PBS. Immature and mature BMDCs from CETN2-GFP mice, sorted by DNA content (2N, 4N,) were counted and provided in PBS. Cells were taken up in cell lysis buffer to which phosphatase inhibitor and protease inhibitor were added freshly as described in section 2.1.6. After incubation on ice for 30 min followed by centrifugation (14000× g for 10 min at 4 °C), the supernatant was separated and mixed with 4× sample buffer (4× Laemmli + 10 % β-mercaptoethanol) in a ratio of 3:1. Subsequently, samples were boiled at 95 °C for 5 min and centrifuged briefly.

2.2.5.2 Electrophoretic separation of proteins and immunoblotting

Proteins were separated by *sodium dodecyl sulfate polyacrylamide gel electrophoresis* (SDS-PAGE). Precast gradient gels (4-20 %) were used, which were placed in an electrophoresis chamber filled with *Tris-glycine-SDS* (TGS) running buffer. To compare different conditions, equal cell numbers were loaded on the lanes. A protein standard (5-7 µL) was loaded at least once on each gel. Gels were run at 80 V for the first 15 min before the voltage was increased to 100 V and gels were run until the blue dye front reached the bottom of the gels. For immunoblotting, pre-prepared transfer packs containing pre-incubated nitrocellulose membranes and filter papers were used. Proteins were transferred from the gel onto the membranes in a semi-dry manner using an automated transfer system. The transfer was run at 25 V, 1.3 A for 7 min. Subsequently, membranes were stained with Ponceau S solution for 3 min to visualize protein bands and to check for the efficiency of protein transfer. Destaining was performed in PBS on a hot plate (approximately 80 °C).

2.2.5.3 Immunodetection

After eventual cutting of the membranes according to the planned antibody treatment, the membranes were incubated for 90 min in blocking solution (5 % BSA/TBS-T or 5 % non-fat dry milk/TBS-T) with gentle shaking on a tilt shaker. Subsequently, primary antibodies against the target proteins were diluted in the appropriate blocking buffer (see section 2.1.7) and incubated with the membranes at 4 °C over night on a tilt shaker. After a washing step of 3× 10 min with TBS-T, membranes were incubated for 1 h with HRP-coupled secondary antibodies diluted in the same blocking solution as the respective primary antibodies. This was followed by a first

washing step of 3× 10 min with TBS-T. To remove residual Tween, the membranes were briefly washed with TBS (3× 10 sec.). Visualization of proteins was performed by *enhanced chemiluminescence* (ECL) detection. Therefore, membranes were drizzled with 200-400 µL substrate solution, which was prepared freshly according to manufacturer's instruction. Wrapped between two foils, the membrane was analyzed in a digital system (ChemiDoc, Biorad) to visualize protein bands or covered with an x-ray film, which was developed in the dark room.

2.2.6 Statistical analysis

Statistical analysis was done using GraphPad Prism 7. To test for Gaussian distribution *D'Agostino-Pearson normality test* was applied. The statistical test used for each experiment as well as the sample size are indicated in the figure legends. Graphs display mean values ± standard deviation (SD). The significance level was specified as *, $P < 0.05$; **, $P < 0.01$; ***, $P < 0.001$ and ****, $P < 0.0001$; detailed values are given in the figure legends.

3 Results

3.1 Dendritic cells carry multinumerous centrosomes

3.1.1 Bone marrow derived and peripheral dendritic cells harbor multiple centrosomes

The majority of cells carries one centrosome in G1 phase, which duplicates once during S phase resulting in two centrosomes in G2 and M phase[255,349]. However, preliminary studies in our lab revealed that a distict proportion of murine DCs harbors two or more centrosomes – a phenomenon which is more known from cancer cells than from non-malignant cells[336,337]. To study centrosomes in murine DCs in more detail, we worked with *wildtype* (WT)- and *centrin-2-green fluorescent protein* (CETN2-GFP)-reporter mice[350] and made use of various antibodies against centriolar structures and components of the PCM. Since centrioles are highly acetylated[351,352] we chose an antibody against acetylated tubulin (ac-tubulin) allowing us to stain individual centrioles. However, ac-tubulin is not a genuine centriolar marker, which has moved us to counterstain centrosomes with an antibody against the centriolar protein CEP135. To visualize the PCM we stained for γ-tubulin, the major MT nucleating component of the PCM[353] (Fig. 10 a).

For gaining large numbers of cells, we generated primary DCs from bone marrow of WT and CETN2-GFP mice (BMDCs) and matured the cells with LPS over night. To expand the spectrum of DCs beyond cells originating from bone marrow, we also examined peripheral DCs isolated from murine skin explants (dermal DCs). Therefore, ears from WT mice were split into two sheets incubated upside down on culture medium supplemented with CCL19 allowing the cells to leave the tissue and migrate into the medium. In contrast to BMDCs, crawled out cells received no stimulus such as LPS since mechanical rupture of the two ear sheets induces inflammation thus leading to activation of the cells[354]. After harvesting and *fluorescence-activated cell sorting* (FACS) analysis revealing a high abundance of DC-typical cell surface molecules such as CD11c and MHC-II, the cells were examined for their migratory behavior to confirm their identity as DCs. Therefore, we conducted an *in vitro* 3D collagen migration assay, for which we constructed devices on object slides as flat chambers that were filled with collagen and cells. A layer of chemoattractant (CCL19) on top of the collagen cell mixture provided a chemotactic gradient (Fig. 12 a). Time-lapse video microscopy (not shown) and subsequent manual cell tracking revealed that the cells could efficiently migrate toward a chemokine source (Fig. 12 b) indicating their identity as (activated) DCs with high CCR7 expression.

For counting centrosomes, we immobilized the cells on coverslips and conducted indirect *immunofluorescence* (IF) stainings as described in section 2.2.2.2. Ac-tubulin, CEP135, and CETN2-GFP make individual centrioles visible as single foci in mature WT and CETN2-GFP BMDCs as well as in dermal DCs whereas the PCM appears as rather diffuse structure (Fig.12, c-e). Additionally, the merged panel not only shows a clear colocalization of centrioles and PCM but also a colocalization of the different markers used to visualize single centrioles. For quantification of centrosomes in WT cells, foci positive for ac-tubulin and γ-tubulin and foci positive for ac-tubulin and CEP135 were counted manually. In CETN2-GFP BMDCs, CETN2-GFP/γ-tubulin positive and CETN2-GFP/CEP135 positive foci were used for quantification of centriole numbers. In the light of centrosome structure (Fig. 10 a) two centrioles correspond to one centrosome whereas four or more centrioles correlate to two or more centrosomes, respectively.

Quantification of centriole positive foci revealed a similar distribution of centrosome numbers between the three analyzed cell types (Fig.12, c-e, right panel). While the majority of all cells harbored one centrosome, around 18-19.5% of mature WT BMDCs, 19.5-23% of mature CETN2-GFP BMDCs and 13.5-19% of dermal DCs contained two centrosomes. Additionally, we also found cells with more than two centrosomes: about 2.3% of WT BMDCs, 5-7.3% of CETN2-GFP BMDCs and 1.3-6.5% of dermal DCs carried more than two centrosomes. Taken together, quantification of centrosome numbers showed that approximately 15-30% of mature BMDCs and dermal DCs from ear explants carry two or more than two centrosomes.

a

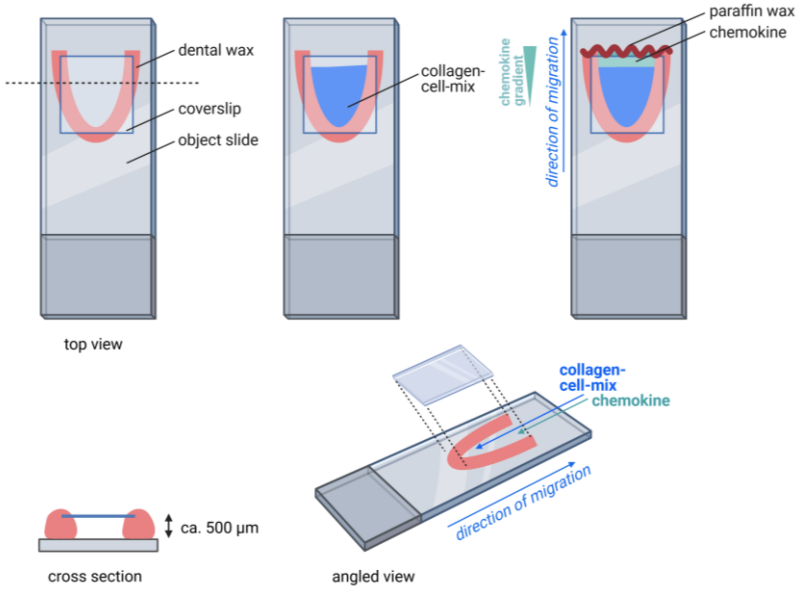

b

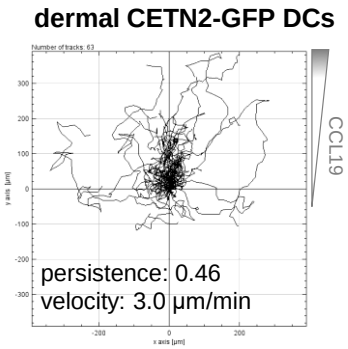

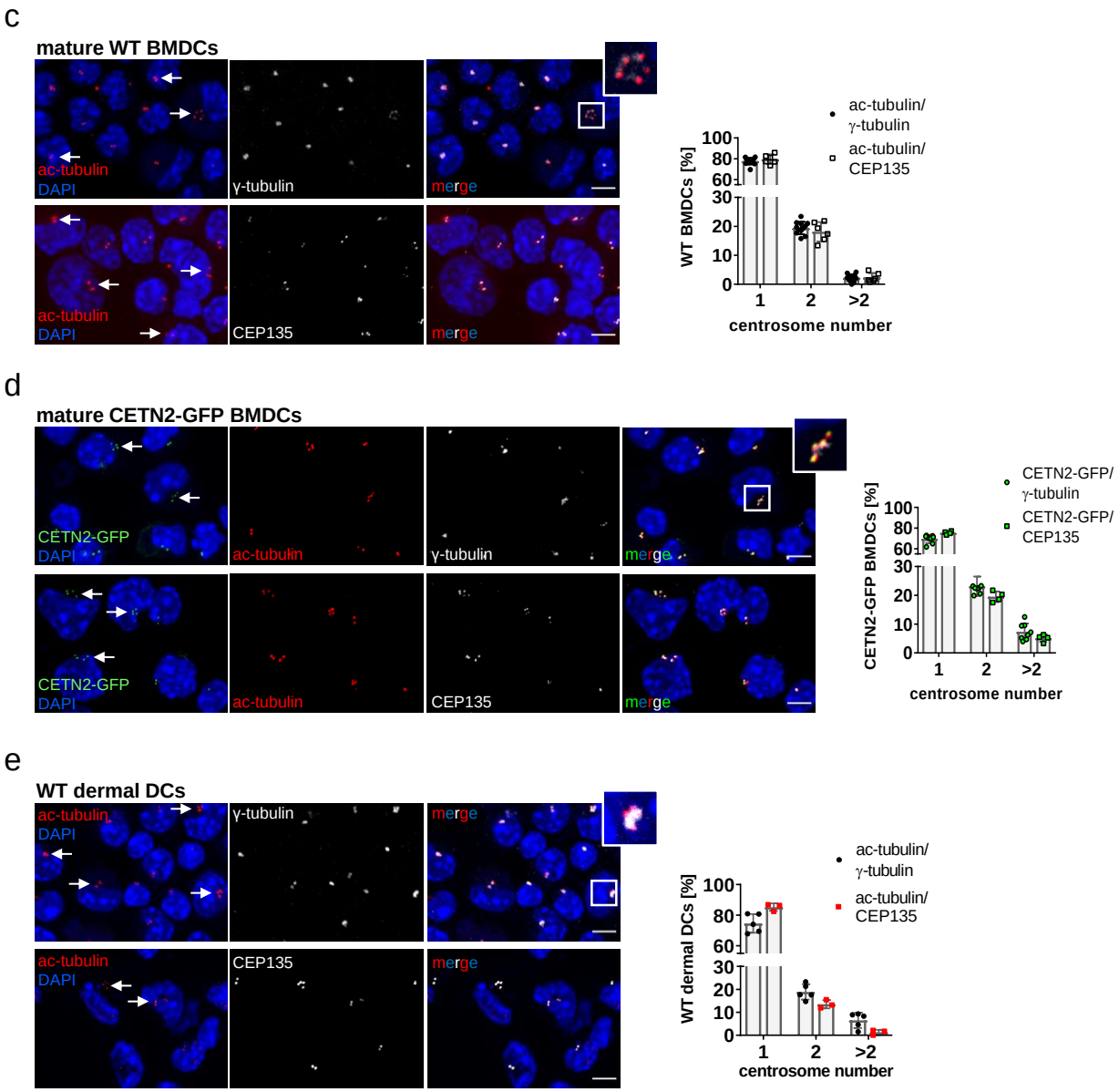

Figure 12. Murine BMDCs and isolated skin DCs carry two or more centrosomes

(**a**) Schematic illustration of a 3D collagen migration assay (created with BioRender.com). (**b**) Single-cell tracks of dermal CETN2-GFP DCs migrating along CCL19 gradients in 3D collagen gels (N = 63 cells pooled from 2 independent experiments). (**c**) Left: IF staining of centrioles and PCM (represented by γ-tubulin and CEP135) in mature WT BMDCs. Individual and merged channels of ac-tubulin (pseudocolored in red), γ-tubulin (pseudocolored in grey) and CEP135 (pseudocolored in grey) are shown. Right: quantification of centrosome numbers according to ac-tubulin/γ-tubulin and ac-tubulin/CEP135 positive foci. Graph shows mean values ± SD of 12 independent experiments (ac-tubulin/γ-tubulin) with N = 344/274/154/146/131/232/200/175/184/224/151/268 cells analyzed per experiment and 6 independent experiments (ac-tubulin/CEP135) with N = 270/254/206/207/222/225 cells analyzed per experiment. (**d**) Left: IF staining of centrioles and PCM in mature CETN2-GFP expressing BMDCs. Individual and merged channels of CETN2-GFP (green), ac-tubulin (red), γ-tubulin (grey) and CEP135 (grey) are depicted. Right: quantification of centrosome numbers by CETN2-GFP/γ-tubulin and CETN2-GFP/CEP135 positive foci. Graph displayes mean values ± SD of 8 independent experiments (CETN2-GFP/γ-tubulin) with N = 261/248/305/298/180/150/258/152 cells analyzed per experiment and 4 independent experiments (CETN2-GFP/CEP135) with N = 335/366/222/184 cells analyzed per experiment. (**e**) Left: IF staining of centrioles and PCM in WT dermal DCs. Individual and merged channels of ac-tubulin (red), γ-tubulin (grey) and CEP135 (pseudocolored in grey) are represented. Right: quantification of centrosome numbers by ac-tubulin/γ-tubulin and ac-tubulin/CEP135 positive

foci. Graph shows mean values ± SD of 5 and 3 independent experiments with N = 96/90/109/131/108 cells (ac-tubulin/γ-tubulin) and N= 129/285/238 (ac-tubulin/CEP135) cells pooled from ears of 3 different mice for each experiment. Nuclei were stained with DAPI (blue). Arrows mark multinumerous centrosomes (≥ 4 ac-tubulin positive foci in WT cells, CETN2-GFP positive foci in CETN2-GFP BMDCs). White boxes mark area of magnification showing multiple centrosomes and colocalization of centrioles and PCM. Scale bar: 5 µm.

3.1.2 Excess centrosomes arise *in vivo* and are not caused by culture conditions

To examine centrosomes in a more physiological environment and exclude that our findings are due to culturing conditions, we analyzed tissue resident DCs *in situ* using mouse ear explants. After splitting ears from WT and/or CETN2-GFP mice, the obtained sheets were placed on full medium for 24 hrs before the whole tissue was fixed and stained according to the IF staining protocol (see section 2.2.2.3). DCs were activated mechanically by rupturing the ears into two sheets, which eliminated the need for additional stimulation. Antibodies against MHC-II were used to identify DCs while ac-tubulin or CETN2-GFP visualized centrioles as described above; γ-tubulin serves as marker for the PCM.

Similar to BMDCs, also in peripheral DCs *in situ*, single centrioles could be visualized via ac-tubulin and CETN2-GFP (Fig. 13, a-c). Comparable to the situation in isolated dermal DCs, dermal DCs within tissue show multinumerous centrosomes (Fig. 13, a and b, magnification) and a colocalization of centrioles and PCM (Fig. 13 c, right panel). Our findings demonstrate that also DCs within tissue carry multiple centrosomes illustrating that this phenomenon is not due to the culture conditions of BMDCs or caused by the process of emigration from the dermis of the ear.

Taken together, we could show that DCs carry a surplus of centrosomes *in vitro*, *ex vivo* and *in situ*. These findings indicate that the phenomenon of supernumerary centrosomes – mainly known from malignant cells – is a robust event in mature DCs and not an artifact.

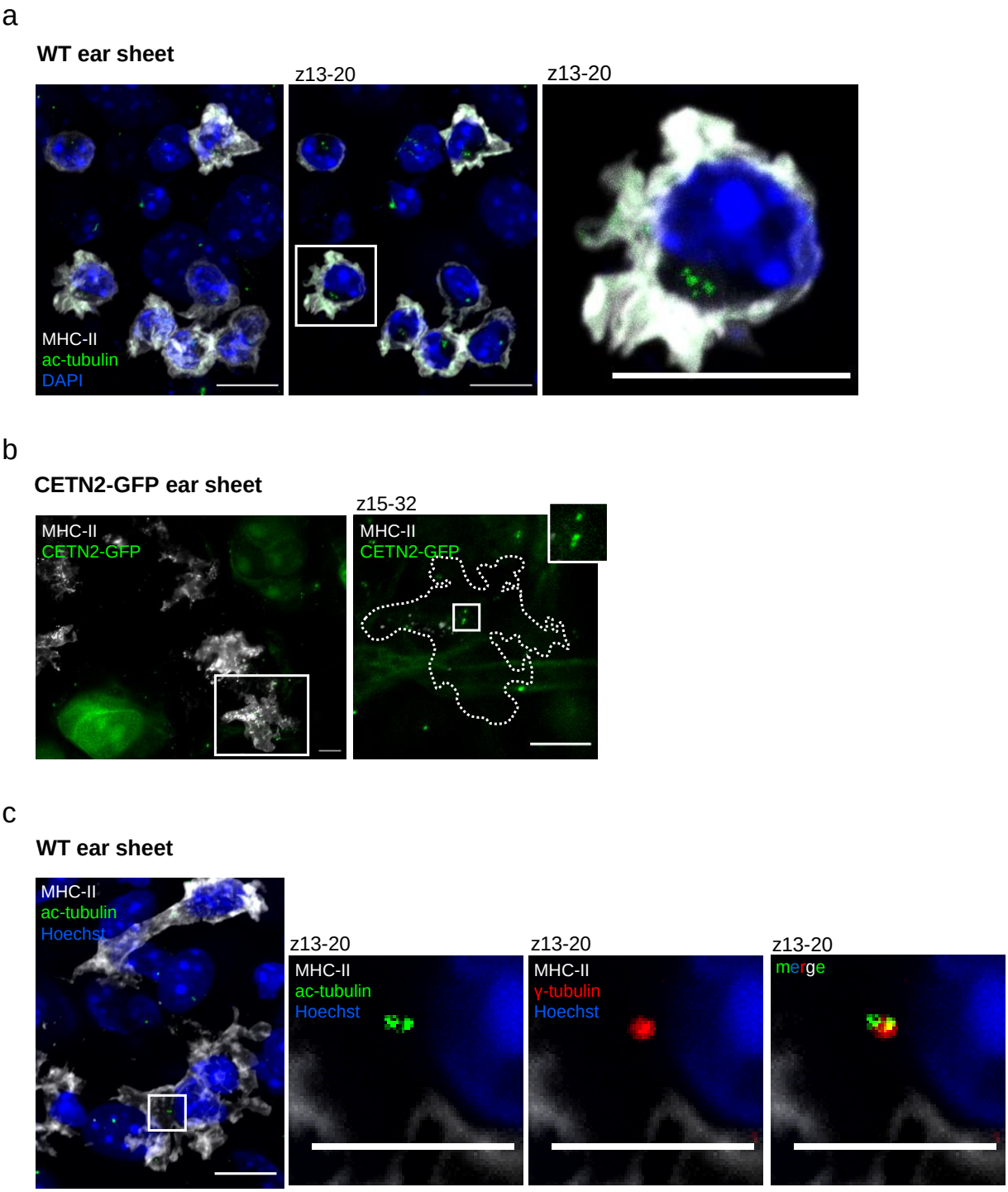

Figure 13. DCs in murine ear skin harbor multiple centrosomes

(**a, b**) IF stainings of centrioles in ear explants from WT and CETN2-GFP expressing mice. Merged channels of ac-tubulin (green) or CETN2-GFP (green) and MHC-II (pseudocolored in grey) are shown. Left: complete Z-stack (maximum projection), middle/right: projection of indicated z-planes. White boxes show area of magnification. Nuclei were stained with DAPI (**a**), dotted line marks cell outline (**b**). Scale bars: 10 µm. (**c**) IF stainings of centrioles and PCM in ear explants from WT mice. Left: overview shows merged channels of MHC-II (grey) and ac-tubulin (green). Nuclei were counterstained with Hoechst (blue). Scale bar: 10 µm. Right: magnification of boxed region consisting of indicated z-plane projections. Merged channels of MHC-II (grey) and ac-tubulin (green), MHC-II (grey) and γ-tubulin (red) and all of them are depicted. Scale bar: 5 µm.

3.2 The cell cycle is involved in the development of extra centrosomes

3.2.1 Multiple centrosomes are not a consequence of ongoing cell proliferation

The occurrence of two centrosomes (four centrioles) constitutes a physiogical event in cycling cells, which progress through S/G2/M phase in order to build up the mitotic spindle during cell division[255,349]. Mature BMDCs and tissue resident DCs are terminally differentiated cells that only have a low turn-over rate[42], however, we found that a proportion of those cells carries multiple centrosomes. Therefore, we next checked whether the presence of DCs with two centrosomes might be a consequence of ongoing cell proliferation. For this purpose, we made use of the markers *5-ethynyl-2'-deoxyuridine* (EdU) for S phase and *phospho-histone H3* (pH3) for G2-M transition in immature and mature BMDCs as well as in dermal DCs resident in murine ear sheets. BMDCs were co-stained for centrioles using ac-tubulin to compare their numbers in immature and mature states while ear sheets required staining of MHC-II to identify DCs.

IF stainings of mature BMDCs revealed that – in contrast to immature BMDCs – almost all cells stained were negative for EdU and pH3 (97 %, respectively) (Fig. 14 a, left and middle panel) indicating that the vast majority of those cells did not proliferate. The same applied for DCs *in situ*, which were very rarely double-positive for MHC-II and EdU (Fig. 14 b, left panel, magnification) and exhibited a similar proportion of EdU-negative cells 24 hrs after splitting of ears (98.5 %) (Fig. 14 c). Analogous to the comparison of immature and mature BMDCs we analyzed the proportion of proliferating DCs in ears 0 and 24 hrs after splitting the ears into two sheets. As characteristic for a barrier organ such as the skin, partially-activated DCs dominate at timepoint 0 hrs whereas the splitting of the ear skin corresponds to an inflammatory event leading to a complete activation of the cells. We found that the number of EdU-positive cells was generally low directly after splitting but 3-fold higher than 24 hrs after splitting (2.3 vs. 0.7 %) (Fig. 14 b, right panel) indicating a very low proliferative capacity of partially-activated cells, which decreased even further with progressing maturation.

We counted centrosome numbers in WT BMDCs and found that the proportion of cells with multinumerous centrosomes was considerably higher in mature than in immature cells (18.6 vs. 4.2 %) (Fig. 14 a, right panel). To avoid including cells that naturally have more than one centrosome due to an ongoing cell cycle, we considered in an additional count only those cells with extra centrosomes that stained negative for EdU and/or pH3 and found that the difference between mature and immature BMDCs in terms of centrosome number became even greater (17.4 vs. 1.1 %) (Fig. 14 a, right panel).

These data show and confirm that mature primary DCs from bone marrow and tissue resident DCs do not proliferate to a notable extent[42] demonstrating that supernumerary centrosomes are not the result of ongoing cell proliferation. Furthermore, the fact that we found DCs with more than two centrosomes (Fig. 14 a, lower panel, right picture), i.e., with a number exceeding the double content that naturally occurs in cycling cells due to centriole duplication, argues against a (regularly) ongoing cell cycle as (sole) reason for additional centrosomes. Moreover, the phenomenon of excess centrosomes is more present in mature than in immature BMDCs suggesting that the emergence of extra centrosomes is associated with the process of cell activation.

a

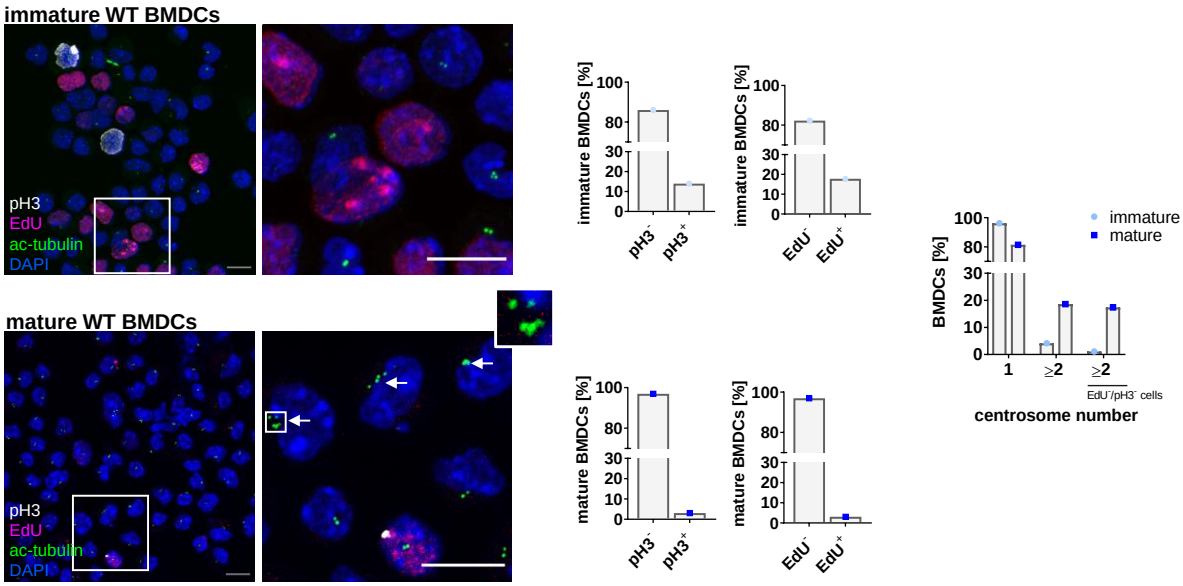

b

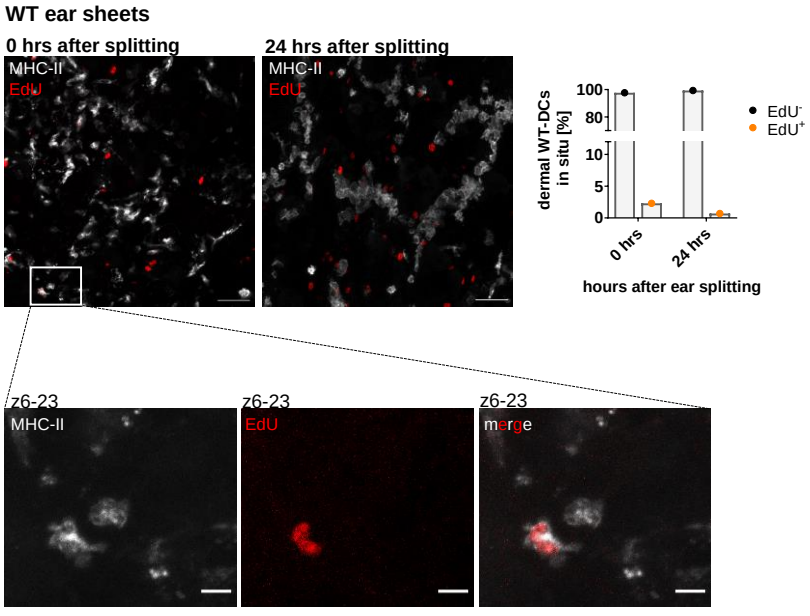

c

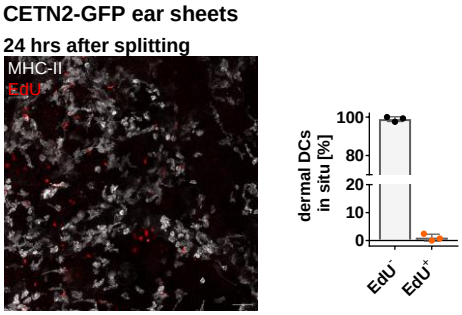

Figure 14. The proliferative capacity of DCs is extremely low *in vitro* and *in situ*

(**a**) Left: IF stainings of immature (upper panel) and mature (lower panel) WT BMDCs against centrioles and pH3 after EdU incorporation. Merged channels of ac-tubulin (green), EdU (pink) and pH3 (grey) are shown. Boxes mark regions of magnification. Arrows point to excess centrosomes (≥ 4 ac-tubulin positive foci). Nuclei were stained with DAPI (blue). Scale bar: 10 µm. Middle: quantification of pH3 and EdU positive cells. Graphs show mean values of 1 experiment with N = 265 immature and N = 328 mature BMDCs. Right: quantification of centrosome numbers according to ac-tubulin positive foci comparing distribution when counting all cells and after exclusion of EdU/pH3 positive cells. Graph shows mean values of 1 experiment with with N = 265 immature and N = 328 mature BMDCs. (**b**) Left: IF images of ear explants from WT mice stained against MHC-II and labeled for EdU-incorporation directly after ear splitting (0 hrs) and 24 hrs later. Merged channels of MHC-II (grey) and EdU (red) are shown. Scale bar: 50 µm. White box indicates area of magnification (lower panel): Individual and merged channels of MHC-II (grey) and EdU (red) are depicted. Only indicated z-planes were projected. Scale bar: 10 µm. Right: quantification of EdU positive dermal (MHC-II positive) DCs at the two indicated timepoints. Graph shows mean values of one experiment with N = 728 (0 hrs timepoint) and N = 715 (24 hrs timepoint) dermal DCs in ear explants from 3 different WT mice. (**c**) Left: IF staining against MHC-II and EdU-incorporation in ear explants of CETN2-GFP expressing mice 24 hrs after the splitting process. Merged channels of MHC-II (grey) and EdU (red) are shown. Scale bar: 50 µm. Right: quantification of EdU positive dermal (MHC-II positive) DCs. Graph displays mean values ± SD of 3 independent experiments with N = 262/2703 (CETN2-GFP expressing mice) and N = 715 (WT mice) cells analyzed per experiment pooled from 2 CETN2-GFP expressing mice and 3 WT mice.

3.2.2 Dendritic cells arrest during the cell cycle

The lack of proliferation markers in mature BMDCs and tissue resident DCs (Fig. 14, a-c) suggests that those cells have stopped proliferating and may be arrested in the cell cycle. In order to test this hypothesis, we examined the levels of cyclins, Cdks and Cdk-inhibitors in different maturation states and DC-types.

Cyclins and Cdks act as Cdk/cyclin-heterodimers and are the main proteins responsible for driving the cell cycle[355]. Unbound Cdks are typically inactive, but after binding a cyclin, they become able to exert their kinase activity and phosphorylate different target structures[356]. While Cdks are expressed constitutively, the expression of cyclins depends on the phase of the cell cycle[356] (Fig. 15 a).

While in proliferating cells cyclin A binds Cdk2 in late G1/S phase and Cdk1 in late S/G2 phase[357], it accumulates from late G1 on during S phase reaching highest expression levels in

mid-G2[358]. Cyclin B in combination with Cdk1, is considered the primary cell cycle regulator in G2 phase[356]. In proliferating cells, cyclin B1 accumulates during G2 phase reaching its maximum at G2-M transition. Cyclin E1, binding partner of Cdk2, mainly acts in G1 and S phase of the cell cycle[359] with an expression peak at the G1/S phase transition point enabling entry into S phase[360]. The resulting fluctuating expression pattern helps us to draw conclusions about which phase cells are in (Fig. 15 a). We used immature and mature BMDCs as well as dermal DCs emigrated from ear sheets for immunoblot analysis and tested for cyclin A2, B1, E1, Cdk2 and 4 and the Cdk inhibitors p21 and p27.

Immature BMDCs were characterized by the presence of cyclin A2 (Fig. 15, b and c) which ensures entry into and completion of S phase as well as transition to M-phase[361]. However, this cyclin was not detectable in mature BMDCs and dermal DCs. The same band pattern was prominent for cyclin B1, which regulates G2-M transition. Cyclin E1 was found in immature and mature BMDCs as well as in dermal DCs (Fig. 15, b and c). Cdk2 was analyzed in BMDCs and showed a similar band pattern to cyclin E1 (Fig. 15 b). In conjunction with Cdk4 and 6 cyclin D1 promotes cell cycle entry, progression through G1 phase and transition from G1 to S phase[362,363]. We found that its binding partner Cdk4[359] was present in immature DCs and to a lesser extent in mature DCs (Fig. 15 b).

The cyclin expression pattern in immature cells revealed strong activity of cyclins typically acting in S/G2/M phase, namely cyclin A2 and B1, also known as “mitotic cyclins”[364], indicating that these cells are cycling. The presence of cyclin E in those cells reflects the process of transitioning through G1/S during the cycling process. In contrast, mature BMDCs and dermal DCs lack the expression of cyclin A2 and B1 but were positive for cyclin E1 (and Cdk2) pointing to a G1-arrest. Considering the expression pattern of cyclin A2, B1 and E1, the presence of Cdk4 in immature BMDCs indicates the passage of G1 during the cycling process, while the presence of Cdk4 in mature cells suggests a G1 arrest.

To support the assumption of a cell cycle arrest in G1 phase, we analyzed the Cdk inhibitors p21$^{CIP1/WAF1}$ and p27^{KIP1} which belong to the group of *kinase inhibitor proteins* (KIPs; Cip/Kip family)[365,366] and negatively regulate G1-cyclin-Cdk complexes causing a G1-arrest[367].

Without inhibition, activated cyclin D-Cdk4/6 and cyclin E-Cdk2 complexes phosphorylate the *retinoblastoma protein* (Rb) (Fig. 15 d) leading to its inactivation. This results in a release and activation of the transcription factor E2F which subsequently activates the expression of genes whose products are responsible for entry into S phase[368]. Increase in p21$^{CIP1/WAF1}$ and p27^{KIP1} levels leads to the inhibition of cyclin D-Cdk4/6 and cyclin E-Cdk2 activity providing information about a potential G1 arrest[369].

We investigated the levels of $p21^{CIP1/WAF1}$ and $p27^{KIP1}$ in immature and mature BMDCs as well as in dermal DCs by immunoblot analysis. Additionally, we conducted IF stainings of immature and mature BMDCs using an antibody specific for $p21^{CIP1/WAF1}$.

Immunoblot analysis revealed considerable levels of $p27^{KIP1}$ in dermal DCs as well as $p21^{CIP1/WAF1}$ in mature BMDCs while immature cells showed much lower levels (Fig. 15, e and f) indicating a G1 arrest triggered by inhibition of cyclin D-Cdk4/6 and cyclin E-Cdk2. In line with these findings, the quantification of p21 in IF stainings via fluorescence intensity showed a gradual increase with progressive maturation which is also reflected in immunoblot analysis (Fig. 15 f).

In essence, our data demonstrate that mature BMDCs and dermal DCs arrest in G1 phase of the cell cycle confirming that extranumerous centrosomes are not a product of an ongoing cell cycle. Moreover, the fact that it is G1 phase in which the cells are arrested – a phase normally characterized by cells with one centrosome – strongly supports the assumption that proliferation is not the originator for the appearance of multiple centrosomes: While a proportion of cells with two centrosome would be expected from cells arrested in G2 phase, the presence of extra centrosomes in G1 phase is rather unusual, so we suggested that there must be another cause for the occurrence of supernumerary centrosomes.

a

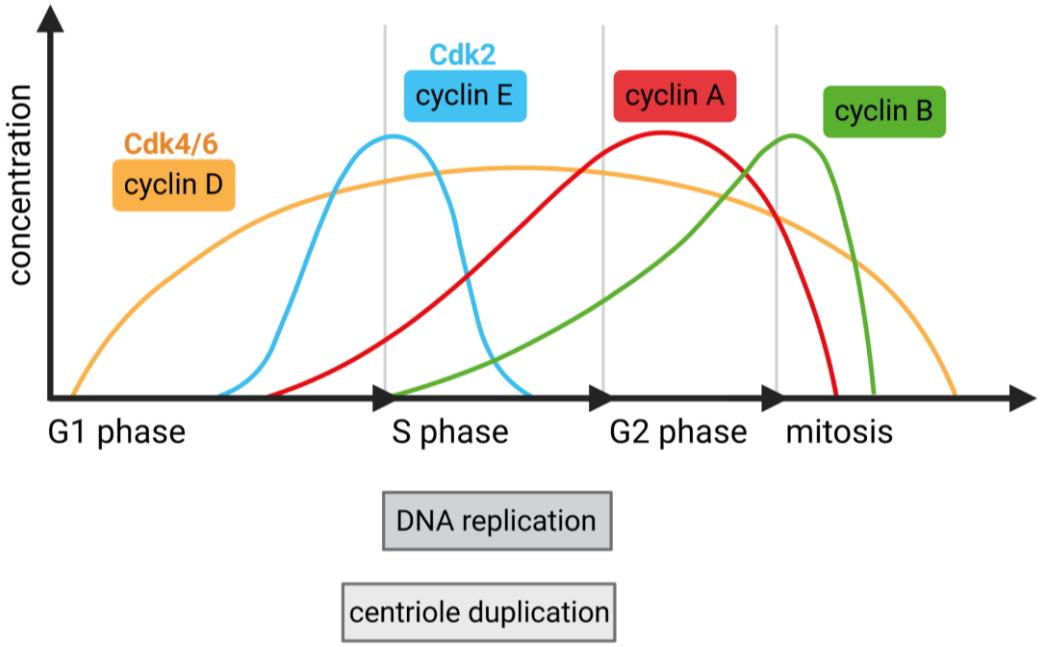

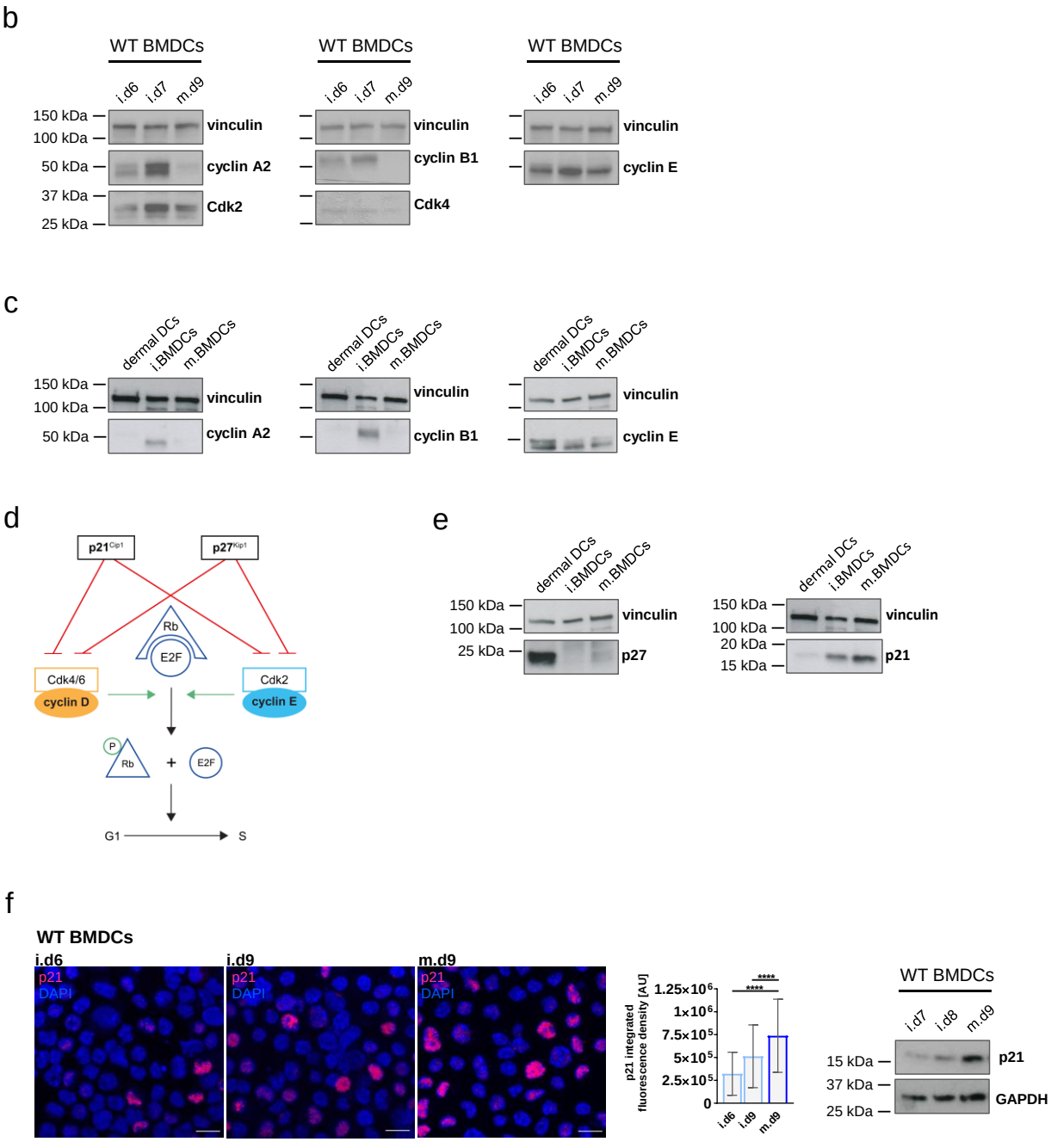

Figure 15. Mature BMDCs and dermal DCs arrest in G1 phase of the cell cycle

(**a**) Schematic illustration of the expression pattern of Cdks and cyclins during the cell cycle. (**b**, **c**) Immunoblot analysis of cyclins and Cdks in lysates generated from WT BMDCs and WT dermal DCs of indicated differentiation and maturation stages. Vinculin serves as loading control. One representative experiment out of three is shown. (**d**) Schematic illustration of the interplay between Cdk inhibitors (p21, p27), Cdks and cyclins and their role in regulating the cell cycle. (**e**) Immunoblot analysis of Cdk inhibitors in lysates generated from immature and mature WT BMDCs and WT dermal DCs, respectively. Vinculin serves as loading control. One representative experiment out of three is shown. (**f**) Left: IF stainings of Cdk inhibitor p21 (pink) in WT BMDCs from indicated differentiation and maturation stages. Nuclei were stained with DAPI (blue). Scale bar: 10 µm. Middle: corresponding quantification of nuclear p21 levels by fluorescence signal intensity. Graph shows mean values ± SD from three independent experiments with N = 253/177/222 cells (i.d6), 173/242/262 (i.d9) and 274/232/217 (m.d9) cells pooled from 3 mice. ****, P < 0.0001 (Kruskal-Wallis test followed by Dunn's test). Right: immunoblot analysis of p21 in lysates generated from WT BMDCs of indicated differentiation and maturation stages. GAPDH serves as loading control. One representative experiment out of three is shown. AU: arbitrary unit; d6/7/8/9: day 6/7/8/9; i.: immature; m.: mature. Figure parts a) and d) were created with Microsoft PowerPoint.

3.2.3 G1 arrested cells are composed of two different subpopulations

When analyzing centrosome numbers in mature BMDCs and dermal DCs it became obvious that the cells greatly differ in the size of their nuclei (Fig. 16 a, upper panel). Besides a remarkable occurrence of large nuclei, we also found few binucleated cells (Fig. 16 b), indicating that a proportion of cells became tetraploid.

To unravel whether DCs are composed of diploid (2N) and tetraploid (4N) cells we measured the nuclear area in cells containing one and multinumerous centrosomes. For the analysis of BMDCs, we used microscope images of mature BMDCs that have migrated under a layer of agarose and therefore show a flat morphology facilitating (nuclear) stainings and analyses. For these “2D under agarose migration assays”, cells were injected under a pad of agarose in a dish where they migrated on an uncoated glass coverslip, attracted by a chemokine (Fig. 16 c). Due to the “ceiling” of agarose, the cells experience confinement in the z-dimension, which, together with a soluble gradient (CCL19) induces directed chemotactic migration in an amoeboid manner. After the cells reached a state of stable migration, they were fixed through the agarose and their nuclei were stained with *4',6-diamidino-2-phenylindole dihydrochloride* (DAPI) (Fig. 16 a, upper left panel). The flat structure of the confined cells in this 2 D setting in combination with high-resolution confocal microscopy enabled us to reliably determine the *nuclear area* (na). Additionally, we determined nuclei sizes in BMDCs that were injected and fixed under agarose after sorting according to DNA content leading to a population of pure 2N cells.

Nuclear areas of unsorted cells, depicted as frequency distribution, showed two populations pointing to 2N and 4N cells (Fig. 16 a, lower left panel) while the histogram of nuclear areas in sorted 2N cells (Fig. 16 a, orange bars) coincides relatively closely with the distribution of nuclear areas from cells with one centrosome. The distribution of unsorted cells with one centrosome follows a normal distribution and 98 % of this population overlap with sorted 2N cells. Nuclear areas of unsorted cells with two or more centrosomes appear as two Gaussian curves in a histogram: the first, small one goes along with 2N cells whereas the second, broader bell curve represents 4N cells.

For the corresponding analysis with isolated dermal DCs, we measured nuclear areas *during* migration of the cells under agarose along chemokine gradients. For this purpose, we used dishes with a glass bottom instead of plastic dishes with a coverslip under the agarose (Fig. 16 c). These glass bottom dishes have the optical properties for high-resolution microscopy allowing live imaging of the migration process. Due to the flat morphology of the cells and the optimal signal-to-noise ratio, we were able to determine the nuclear area of cells even without a corresponding staining (Fig. 16 a, upper right panel). However, frequency distribution

revealed that – at least with this limited number of dermal DCs – it was not possible to work out different cell populations indicative for 2N and 4N cells (Fig. 16 a, lower right panel) as we did for BMDCs.

From our observations regarding nuclear appearance during IF stainings and subsequent analysis of nuclear areas we were able to show that mature BMDCs are composed of a mixed population of 2N and 4N cells.

As previously shown (see section 3.2.2), activated DCs arrest in G1 phase – a phase which is characterized by diploid DNA content. Therefore, the presence of tetraploid cells, typical for S/G2/M phase, was suprising and warranted further investigation. To verify this unexpected result, DNA content analysis of mature BMDCs and dermal DCs was performed using FACS. FACS data revealed that the majority of the cells was diploid (> 80 %), as expected for cells in G1; however, a smaller proportion of 4N cells was detected as well[370]. To confirm that diploid and tetraploid cells were in the same cell cycle stage, mature 2N and 4N BMDCs were separated and enriched by FACS based on DNA content before they were analyzed for the expression of cyclin-Cdk complexes in immunoblot assays. Just like mature 2N BMDCs, also mature 4N cells did not show any expression of S/G2/M-cyclins A2 and B1 but were found to express cyclin E (Fig. 16 d) revealing that both subpopulations arrest in G1 phase of the cell cycle.

In summary, our experiments show that the population of mature DCs contains diploid and tetraploid cells both arresting in G1 phase of the cell cycle. While the occurrence of two centrosomes in 4N cells is expected in principle, the mere presence of 4N cells in G1 phase is an unusual event providing evidence of irregularities in M phase. In contrast, the presence of 2N cells in G1 phase is expected, but not the existence of more than one centrosome in these cells. Based on these findings, we hypothesized that there are different ways of origin for extra centrosomes.

a

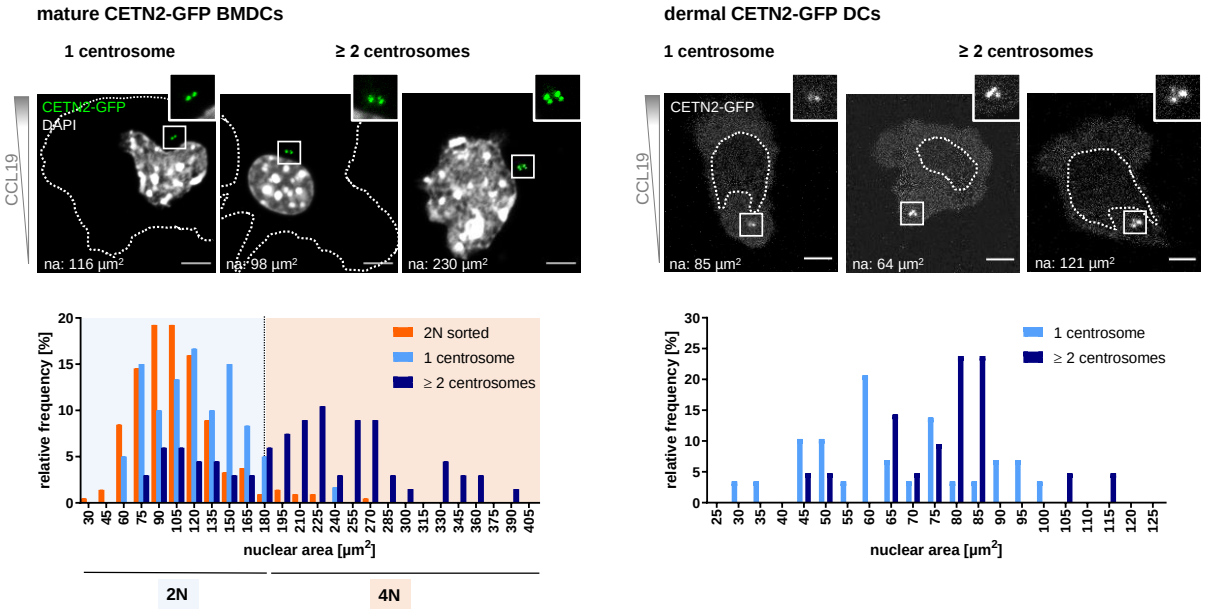
mature CETN2-GFP BMDCs
1 centrosome
≥ 2 centrosomes
CETN2-GFP
DAPI
CCL19
na: 116 µm²
na: 98 µm²
na: 230 µm²
dermal CETN2-GFP DCs
1 centrosome
≥ 2 centrosomes
CETN2-GFP
CCL19
na: 85 µm²
na: 64 µm²
na: 121 µm²
relative frequency [%]
2N sorted
1 centrosome
≥ 2 centrosomes
nuclear area [µm²]
2N
4N
relative frequency [%]
1 centrosome
≥ 2 centrosomes
nuclear area [µm²]

b

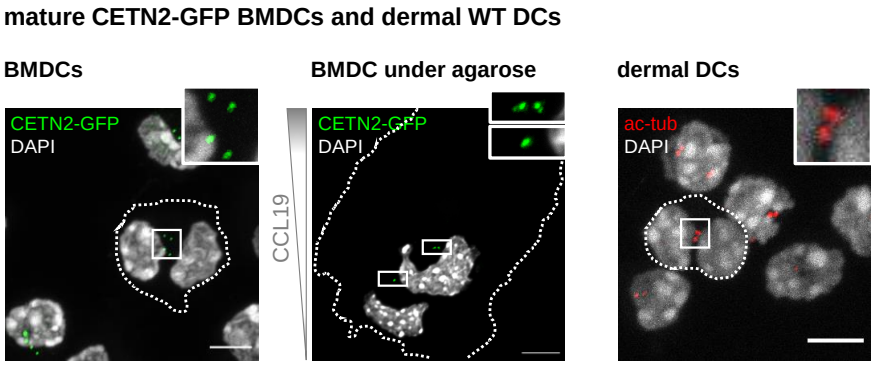
mature CETN2-GFP BMDCs and dermal WT DCs
BMDCs
CETN2-GFP
DAPI
BMDC under agarose
CETN2-GFP
DAPI
CCL19
dermal DCs
ac-tub
DAPI

c

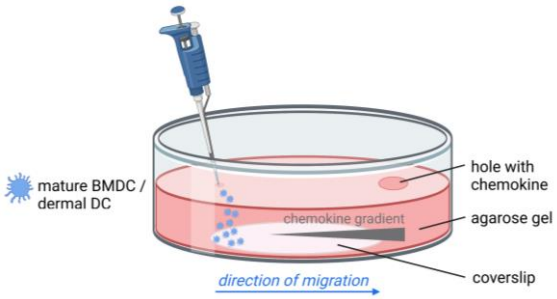
mature BMDC / dermal DC
hole with chemokine
chemokine gradient
agarose gel
direction of migration
coverslip

d

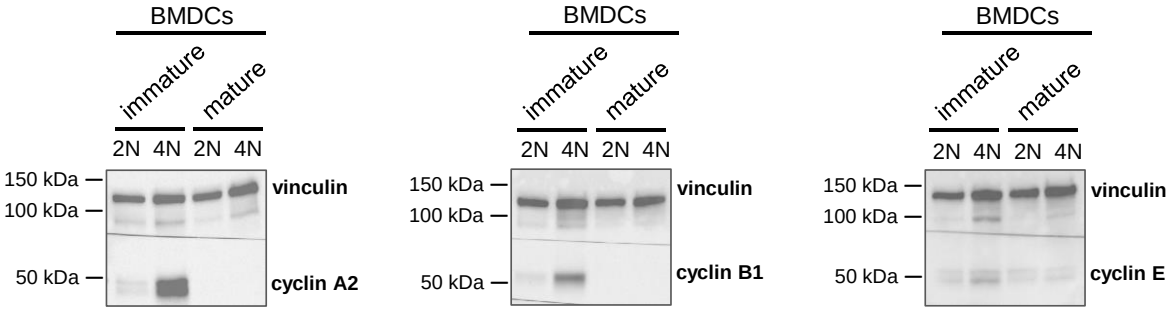
BMDCs
immature
mature
2N 4N 2N 4N
150 kDa
100 kDa
50 kDa
vinculin
cyclin A2
BMDCs
immature
mature
2N 4N 2N 4N
150 kDa
100 kDa
50 kDa
vinculin
cyclin B1
BMDCs
immature
mature
2N 4N 2N 4N
150 kDa
100 kDa
50 kDa
vinculin
cyclin E

Figure 16. G1 arrested DCs are a mixture of diploid and tetraploid cells

(**a**) Upper panel: Representative images of mature CETN2-GFP expressing BMDCs (left) and CETN2-GFP expressing dermal DCs (right) with indicated centrosome numbers migrating under agarose toward a chemokine source. BMDCs were fixed during migration, images of dermal DCs derive from time-lapse videos created during migration. Nuclei of BMDCs were stained with DAPI (pseudocolored in grey). Dotted white line marks cell outline. Boxes highlight area of magnification. Scale bars: 5 µm. Lower panel: Corresponding histograms of nuclear areas of mature BMDCs (left) and dermal DCs (right) with one centrosome (light blue), multiple centrosomes (dark blue) and sorted 2N BMDCs (orange, left) fixed under agarose. Black dotted line in BMDC histogram marks threshold value for distinguishing 2N and 4N BMDCs based on nuclear areas in the sorted 2N BMDC population. N = 60/67/213 (one/multiple/2N) BMDCs analyzed from two independent experiments and N = 29/21 (one/multiple) dermal DCs from four independent experiments with two and 12 mice, resepctively. BMDCs used for nuclear area analysis were stained and imaged by Michaela Limmer. (**b**) Mature CETN2-GFP expressing BMDCs fixed directly (left) and fixed while migrating under agarose toward a chemokine source (middle). WT dermal DCs (right) after IF staining against ac-tubulin (red). All nuclei were stained with DAPI (pseudocolored in grey). Dotted white line marks cell outline. Boxes highlight areas of magnification. Left and middle image were post-processed by deconvolution. Scale bar: 5 µm (left, right), 10 µm (middle). (**c**) Schematic illustration of a 2D under agarose migration assay with a chemokine gradient (created with BioRender.com). (**d**) Immunoblot analysis of cyclins in lysates generated from immature and mature CETN2-GFP expressing BMDCs sorted on DNA content into 2N and 4N subpopulations. Vinculin serves as loading control. One representative experiment out of three is shown. na: nuclear area. Cell sorting was done by Ann-Kathrin Weier.

3.2.4 Dendritic cells undergo mitotic slippage

The presence of tetraploid cells in G1 phase (Fig. 16 a and b) is an unusual event, since regular cell cycle transition is characterized by DNA duplication in S phase – leading to tetraploid cells in S/G2 – and subsequent DNA separation and distribution in M phase resulting in two diploid monoculeated daughter cells in G1 phase[371]. However, tetraploid cells in G1 indicate that they passed through S phase but have not completed mitosis.

To check for irregularities in mitosis we took a closer look at the *spindle assembly checkpoint* (SAC) and associated proteins that play a role in the progression or arrest of mitotic processes. The SAC monitors and promotes the attachment of spindle MTs to kinetochores usually being active in prometaphase when MT-kinetochore attachment processes take place[372,373]. The SAC detects errors in the attachment of kinetochores to the spindle, such as insufficient occupancy of MTs and lack of tension across bi-oriented kinetochore pairs[374]. The proteins *mitotic-arrest deficient 2* (Mad2), *budding uninhibited by benzimidazoles 3* (Bub3) and *Bub1-related kinase* (BubR1) together with Cdc20 form the *mitotic checkpoint complex* (MCC) that acts as an effector of the SAC[372].

During early mitosis, the MCC delays mitotic progress by inhibiting the *anaphase-promoting complex/cyclosome* (APC/C) due to SAC's sensing of unattached or improperly attached kinetochores (unsatisfied SAC)[372,375]. This prevents the degradation of cyclin B1[372] ensuring that mitotic progression only takes place when all sister chromatids have aligned to the mitotic spindle in a bipolar fashion[376] (Fig. 17 a). Typically, the SAC becomes inactive in metaphase,

when proper attachment is achieved (satisfied SAC). This in turn releases APC/C inhibition and initiates the degradation of cyclin B resulting in its depletion[372] and anaphase progression[377] (Fig. 17 a). However, if there are problems with kinetochore-MT attachment cells stay longer in (pro)metaphase leading to high concentrations of BubR1 and other SAC proteins[378,379] at kinetochores of unaligned chromosomes[378,379]. If a SAC mediated mitotic arrest lasts too long, cells can escape and exit mitosis without finishing M phase properly (premature exit). This process requires the degradation of cyclin B and is known as "mitotic slippage"[380,381] leading to mononucleated 4N cells with two centrosomes.

Based on our findings, it is conceivable that DCs exit mitosis although their SAC is active indicative of mitotic slippage. To test this hypothesis, we prepared lysates from LPS stimulated BMDCs over a period of 36 hrs and followed the levels of BubR1 and cyclin B1 in immunoblot analysis. As a control, we conducted the same time course with unstimulated, immature BMDCs. Levels of BubR1 and cyclin B1 in cells without LPS treatment fluctuated in the time window studied as is to be expected for a population of non-synchronized cells (Fig. 17 b, left panel). However, during maturation, BubR1 levels increased remarkably 6 hrs after LPS treatment and remained high until the end of the study period pointing to an active SAC in fully mature cells (Fig. 17 b, right panel). Cyclin B levels, on the other hand, were relatively high up to 60 min after stimulation, before they started to decrease and disappeared after 6 hrs. The combination of both band patterns revealed that cyclin B is degraded in the presence of an active SAC demonstrating mitotic slippage upon cell activation.

To visualize BubR1's spatial distribution and validate the results from the immunoblot analysis, we conducted IF experiments and stained for BubR1 in immature BMDCs that were injected under agarose (activated BMDCs). While pH3-staining ensured that we examine cells that are in M phase, an antibody against α-tubulin allowed visualization of the mitotic spindle. As characteristic for a regular prometaphase[374], we found strong BubR1 accumulation at chromosomes (Fig. 17 c, left panel). While in metaphase under regular conditions, the BubR1 signal is expected to diminish[374,382], our metaphase BMDCs still show strong BubR1 signals at chromosomes (Fig. 17 c, middle panel) pointing to an unsatisfied checkpoint. A potentially resulting SAC induced mitotic arrest increases the probability for mitotic slippage leading to polyploid cells in G1 phase as we observed. Besides BubR1 signals in (pro)metaphase cells, we also found cases of strong chromosomal BubR1 signals in anaphase (Fig. 17 c, right panel) indicating that the cells progressed into anaphase even in the presence of an active SAC. In line with these observations, we found mitotic figures such as large chromosome bridges (Fig. 17 d) which result from premature onset of anaphase without prolonged mitotic arrest[383] leading to abortive cytokinesis and polyploid cells[384].

Our data suggest that BMDCs that are transiting from an immature to a mature state and have passed the G1 restriction point undergo an unusual division cycle supressing mitosis in the presence of an active SAC. One proportion of these cells is assumend not to pass through a complete M phase after DNA (and centrosome) duplication. Instead, cells seem to exit mitosis prematurely via mitotic slippage. The following entry in G1 phase without DNA separation results in mononucleated tetraploid cells with two centrosomes. A second proportion of BMDCs seems to accumulate centrosomes due to cytokinesis failure leading to polyploid mono- or bi-nucleated cells.

Since centrosome duplication takes place simultaneously with DNA replication[385] the occurrence of two centrosomes is expected from tetraploid cells. However, the presence of 4N cells (with two centrosomes) in G1 arrested DCs due to a suppressed mitosis only partly explains the existence of multinumerous centrosomes in DCs since we also found G1 arrested diploid cells with two or more centrosomes (Fig. 16 a, left panel, middle) and tetraploid cells with more than two centrosomes (Fig. 12, c-e, Fig. 16 b, middle). Independent from ploidy (2N, 4N) the emergence of 5 and more centrioles (more than 2 centrosomes) (Fig. 17 d, right) suggests that there is a second mechanism for the formation of multinumerous centrosomes beside suppression of mitosis and associated centrosome accumulation. Indeed, we found evidence for centriole overduplication[370].

In summary, we showed that mature G1 arrested BMDCs contain multiple centrosomes due to a process of accumulation, including mitotic slippage and cytokinesis failure, and due to a mechanism of centrosomal overduplication or a combination of both processes. These processes result in a relatively stable proportion of 20-30 % cells with additional centrosomes in terminally differentiated DCs, raising the question of the impact of extra centrosomes at the functional level. In the present work, we addressed the process of migration and associated parameters.

a

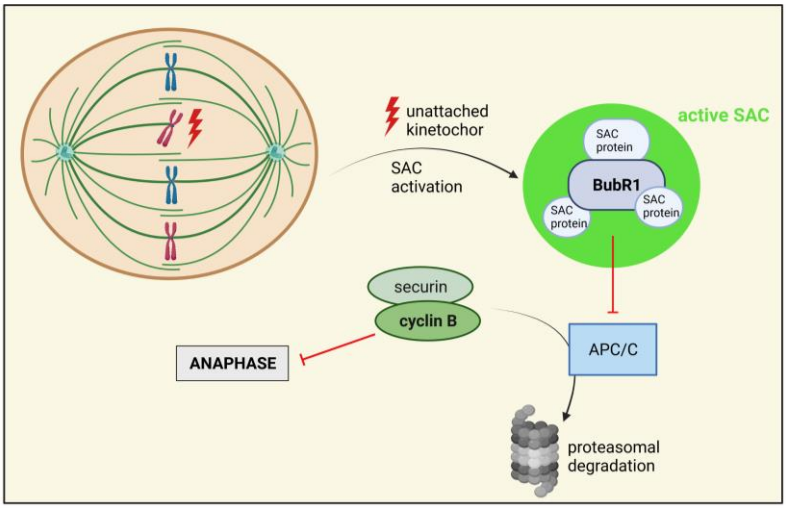

b

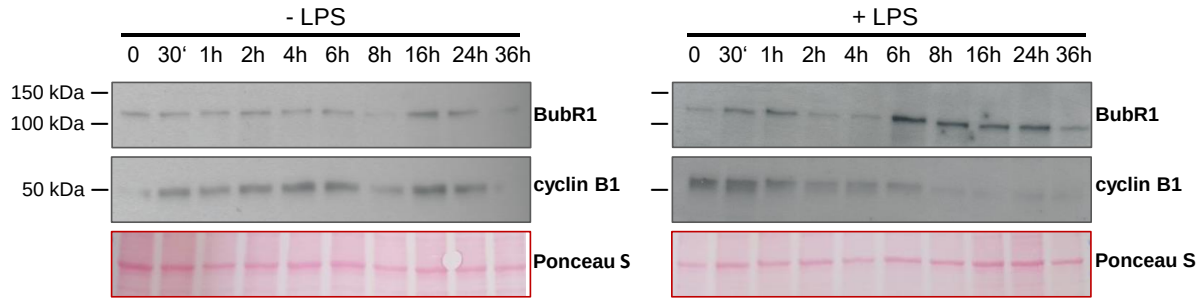

c

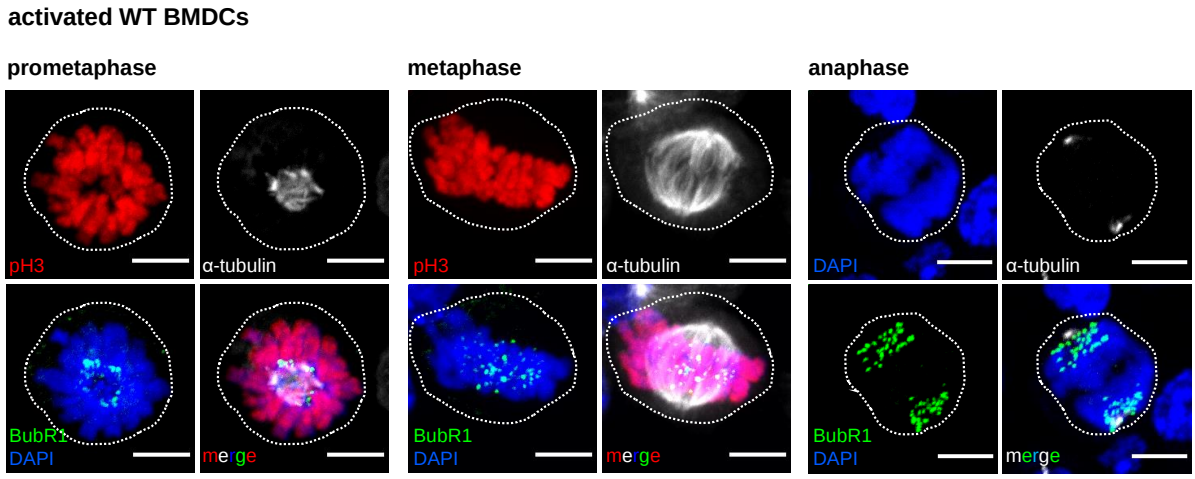

d

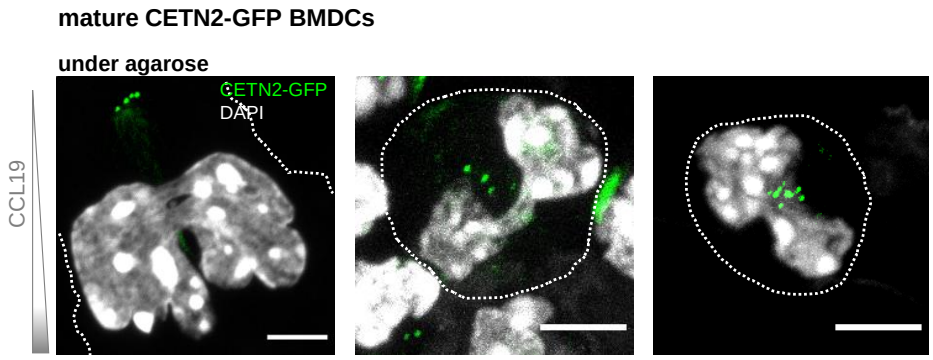

Figure 17. Centrosomes in DCs accumulate by mitotic slippage and cytokinesis failure

(**a**) Schematic illustration of the role of the SAC in regulating cell cycle progression (created with BioRender.com). (**b**) Immunoblot analysis of BubR1 and cyclin B1 in lysates generated from unstimulated (left, - LPS) and stimulated (right, + LPS) WT BMDCs at indicated timepoints. Ponceau S-stained membranes serve as loading control. One representative experiment out of two is shown. (**c**) IF staining of M phase indicator pH3, mitotic spindle (α-tubulin) and SAC (represented by BubR1) in activated WT BMDCs under agarose in indicated stages of mitosis. Individual and merged channels of pH3 (red), α-tubulin (grey) and BubR1 (green) are shown. DNA was stained with DAPI (blue). Dotted white line marks the cell outline. Scale bar: 5 µm. (**d**) Mature CETN2-GFP expressing BMDCs fixed under agarose during migration along a chemokine gradient (left) or fixed on a coverslip without having migrated beforehand (middle, right). Nuclei were stained with DAPI (pseudocolored in grey). Dotted white line marks cell outline. Left image was post-processed by deconvolution. Scale bars: 5 µm.

3.3 Dendritic cell migration is altered in the presence of additional centrosomes

3.3.1 Multiple centrosomes cluster during migration

As APCs, DCs reside as sentinels within peripheral tissues in an immature state. After antigen contact, they mature and migrate rapidly to secondary lymphoid organs, particularly the draining lymph nodes, where the interaction with T cells takes place[3,61,386]. In these processes, DCs must be able to travel through different environments in a target-oriented manner[67,77]. Since these processes rely, among other things, on efficient motility, which in DCs in turn depends on a functional centrosome as MTOC (see *Introduction*), we were interested whether or how additional centrosomes affect migration along gradients of chemotactic cues. So far, the role of multinumerous centrosomes during migration, their spatial organization and their impact on migration parameters in DCs is unknown.

Our first aim was to better characterize centrosome configuration in DCs with supernumerary centrosomes. To this end, we assessed the distance between the centrioles of a centrosome (**intra**centrosomal distance) as well as the distance between centrosomes (**inter**centrosomal distance, recorded as distance between the centers of centriole pairs) (Fig. 18 a, left). In case of more than two centrosomes, we captured the distance between the centrosomes furthest away from each other (not shown). In a first step, we conducted this analysis in fixed mature CETN2-GFP expressing BMDCs after the cells were injected under a layer of agarose and have migrated toward a chemokine source[219]. Distance measurements revealed that not only intra- but also intercentrosomal mean distances were small (0.6 and 1.4 µm, respectively) showing that centrosomes were located in close proximity to each other (clustered configuration) (Fig. 18 a, right).

Beside the situation of centrosomes in *fixed cells*, we examined the dynamic behavior of centrosomes *during migration* using mature CETN2-GFP BMDCs that were injected under agarose and exposed to a chemokine gradient. Similar to fixed samples, we found that extra centrosomes also cluster during migration: Following one representative cell with multiple centrosomes over time revealed a mean intercentrosomal distance of 2.25 µm (intracentrosomal distance: 0.86 µm) (Fig. 18 b). We also analyzed the distances between centrioles (intracentrosomal) in migrating cells with one and excess centrosomes and got almost the same numerical values (1.5 and 1.15 µm, respectively) leading to perfectly overlapping frequency distributions of intracentrosomal distances of both cell populations (Fig. 18 c, upper panel). Imaging migrating cells with multinumerous centrosomes for analysis of intra- and intercentrosomal distances unveiled that, similar to fixed cells (Fig. 18 a), distances

between centrosomes were higher than intracentrosomal distances (1.15 vs. 4.7 µm) (Fig. 18 c, lower panel).

Regarding the subcellular localization, we found that centrosomes in most cases were located close to the nucleus – in fixed cells as well as in migrating cells (Fig. 18 a, see also Fig. 12, c-e; Fig. 13, a-c and Fig. 14 a). This observation was also made in other cell types[237–239] and several ways of an association between the centrosome and the nucleus during interphase have been suggested[241]. However, whether this also applies to DCs, remains to be clarified.

Taken together, our analyses of fixed and migrating BMDCs showed that supernumerary centrosomes have a clustered configuration and are located in close proximity to the nucleus. Since in DCs the centrosome acts as the major MTOC[91], we wondered whether this task could also be fulfilled with extra centrosomes and examined this aspect in a next step.

a

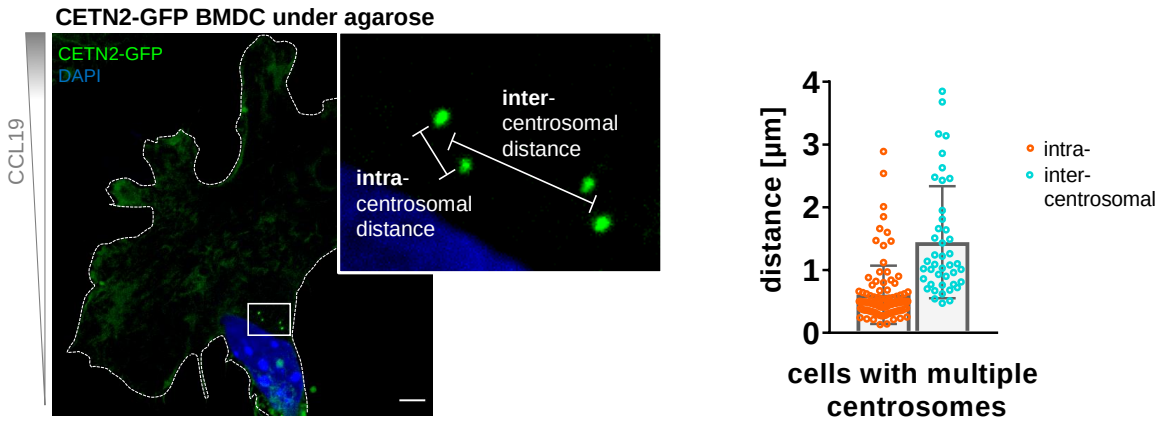

b

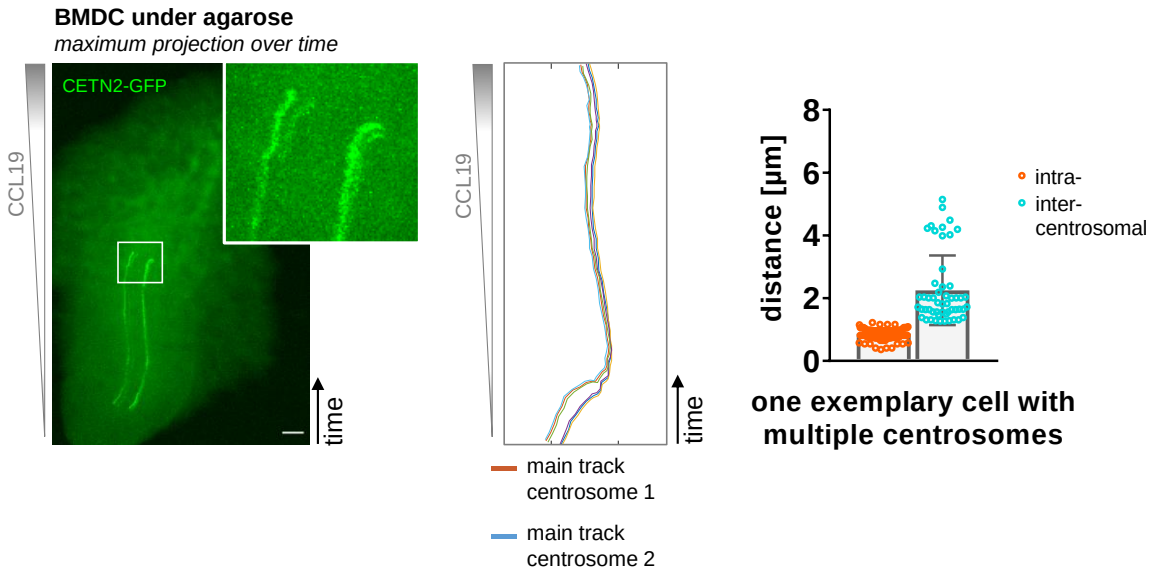

c

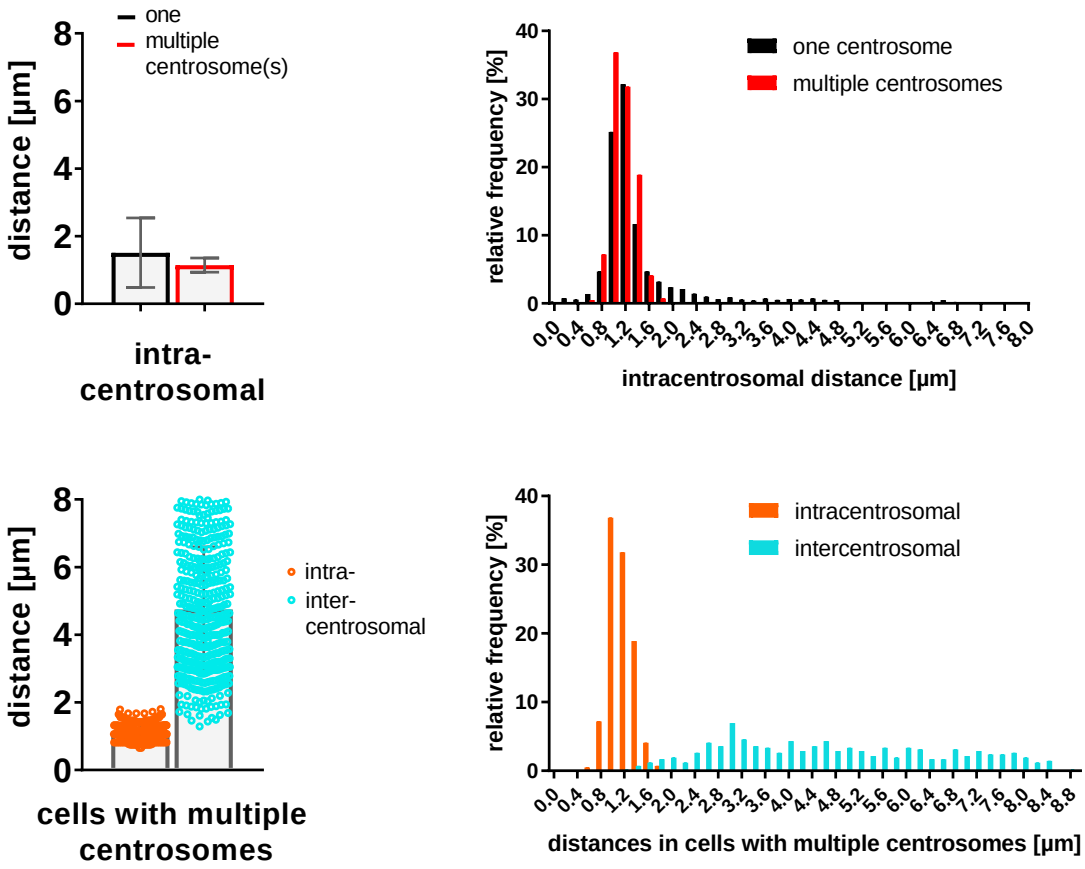

Figure 18. Multiple centrosomes cluster in migrating BMDCs

(**a**) Left: mature CETN2-GFP expressing BMDC fixed during migration under agarose toward a chemokine source. Nucleus was stained with DAPI (blue). White dotted line marks cell outline. Scale bar: 5 µm. White box highlights area of magnification showing multiple centrosomes. Lines exemplarily illustrate distances between centrioles (intracentrosomal) and between centrosomes (intercentrosomal). Right: Quantification of intra (orange)- and intercentrosomal (cyan) distances in CETN2-GFP expressing BMDCs with multiple centrosomes fixed during migration under agarose. Graph shows mean values ± SD with N = 50 cells pooled from 2 independent experiments. (**b**) Left: representative mature CETN2-GFP expressing BMDC with multiple centrosomes during migration under agarose along a chemotactic gradient (maximum projection of time frames). Scale bar: 5 µm. White box indicates area of magnification displaying tracks of four centrioles (two centrosomes). Middle: centriole tracks of one representative CETN2-GFP expressing BMDC with multiple centrosomes during migration under agarose toward a chemokine source. Plot was created by Robert Hauschild using Matlab. Right: Corresponding quantification of intra (orange)- and intercentrosomal (cyan) distances. Graph displays mean values ± SD. (**c**) Upper panel: Quantification of intracentrosomal distances in CETN2-GFP expressing BMDCs with one (black) and multiple (red) centrosomes during migration under agarose toward a chemokine source (left). Corresponding histogram (right). Lower panel: Quantification of intra- (orange) and intercentrosomal (cyan) distances in mature CETN2-GFP expressing BMDCs with multiple centrosomes during migration (left). Corresponding histogram (right). Both bar charts show mean values ± SD with N = 130 cells (one centrosome) and 12 cells (extra centrosomes) pooled from 3 independent experiments. Cells from analyses depicted in (**b**) and (**c**) were tracked and analyzed (manually/automatically) by Robert Hauschild.

3.3.2 MTOCs with extra centrosomes nucleate more microtubule filaments

To further approach the functional aspect of DC migration with additional centrosomes, we investigated centrosome associated cytoskeletal components that are indispensable for cell locomotion. While actin filaments generate protrusive and contractile forces that move the cell forward, MTs establish stable cell polarization and are mainly responsible for cell shape and directed cell locomotion[91,134]. Both scaffolding filaments are at least partly coordinated by the centrosome which in leukocytes acts as major MTOC nucleating and anchoring MT filaments, but also promotes actin filament assembly[91,326].

We wondered whether extra centrosomes act as functional MTOCs and if there are differences in the number of MTs between DCs with one and mulitnumerous centrosome(s). Moreover, we were interested whether the amount of centrosomal actin differs between these two cell subpopulations. To resolve these questions, we injected mature CETN2-GFP BMDCs under agarose and fixed the cells after a time of stable migration toward a chemokine source for subsequent stainings and microscopic analyses. In order to have the possibility to exclusively analyze effects that are due to different centrosome numbers and not due to ploidy it was important to be able to separate 2N from 4N cells. Therefore, we analyzed the nuclear sizes of unsorted cells to draw conclusions about ploidy as depicted in Fig. 16 a. As “reference” for nuclear sizes of diploid cells we analyzed sorted, pure 2N BMDCs in parallel to find out the order of magnitude of 2N cells’ nuclei. As shown in the frequency distribution of nuclear areas, unsorted BMDCs consist of two populations indicative for 2N and 4N cells (Fig. 16 a). While cells with only one centrosome (light blue) are represented by one Gaussian curve, BMDCs with multinumerous centrosomes appear as two bell curves (dark blue). All three curves – nuclear areas of sorted 2N cells, unsorted cells with one centrosome and unsorted BMDCs with multiple centrosomes – end at the same point (around 180 μm^2), while simultaneously, the second curve of cells with additional centrosomes begins marking the point where separation of 2N and 4N population takes place. This allowed us to derive a threshold for the nuclear area that enabled us to distinguish between 2N and 4N BMDCs defining all BMDCs with a nuclear size below 180 μm^2 (dotted black line) as diploid. In contrast to BMDCs, we were not able to obtain a clear frequency distribution for dermal DCs that would allow us to derive a threshold to distinguish 2N from 4N cells here as well (Fig. 16 a, lower right panel).

IF stainings of α-tubulin unveiled that 2N MTOCs with supernumerary centrosomes nucleate MTs in the same way 2N MTOCs with only one centrosome do; in both cases MTs align along the axis of migration allowing the conclusion that extra centrosomes act as functional MTOCs (Fig. 19 a, left). Counting single MT filaments radiating from individual centrosomes revealed

that 2N DCs with multiple centrosomes nucleate significantly more MTs at their MTOC than 2N DCs with only one centrosome (Fig. 19 a, right).

We next analyzed MT nucleation *in situ* using ears from WT mice. Ears were split and the obtained sheets were cultured for 24 hrs in full medium before the tissue was fixed. MHC-II staining allowed us to identify dermal DCs while ac-tubulin and α-tubulin visualized individual centrioles and MTs, respectively. Similar to *in vitro* stainings of mature BMDCs we observed MT nucleation of MTOCs with one and multiple centrosome(s) (Fig. 19 b). However, α-tubulin staining in ear tissue did not allow for quantification of individual MT filaments in DCs. Note that MT visualization via α-tubulin worked well in fibroblasts (Fig. 19 b, upper panel, dotted lined cell) suggesting that the antibody itself works, but not in every cell type.

In addition to organizing MTs, the centrosome also organizes part of actin polymerization[326,327]. For studying centrosomal actin, we conducted phalloidin stainings in 2N DCs with one and two or more centrosomes (Fig. 19 c, left). Analysis of normalized fluorescent intensity revealed that centrosomal actin density was significantly lower in 2N cells with extra centrosomes than in 2N cells with only one centrosome (Fig. 19 c, right).

In summary, we showed *in vitro* and *in situ* that multinumerous centrosomes act as functional MTOC. Moreover, examination of mature BMDCs revealed that cells with excess centrosomes have a significantly higher MT nucleation capacity than cells with one centrosome, whereas 2N BMDCs with one centrosome harbor more centrosomal actin than 2 N BMDCs with extra centrosomes. Because both filament types are critical for directional migration, we hypothesized that the different filament amounts in DCs with single and multiple centrosomes might influence migration behavior.

a

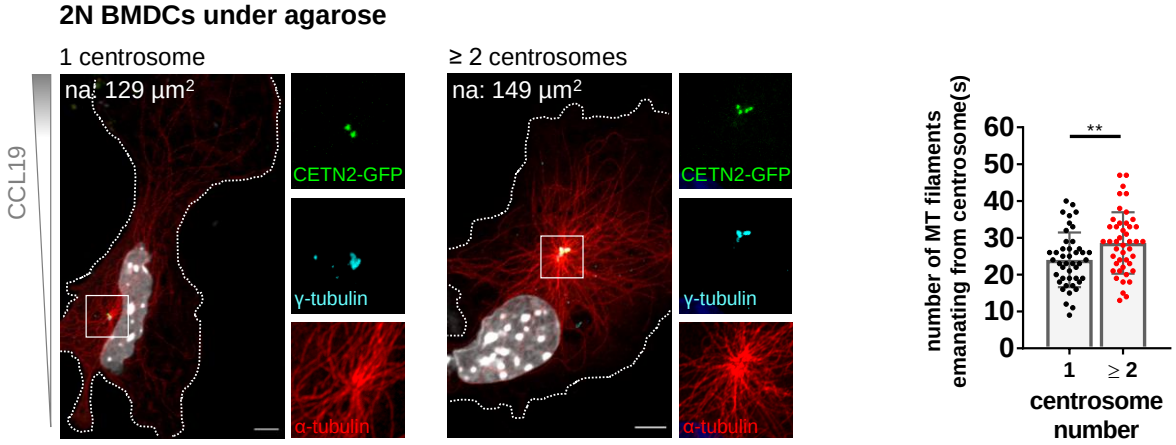

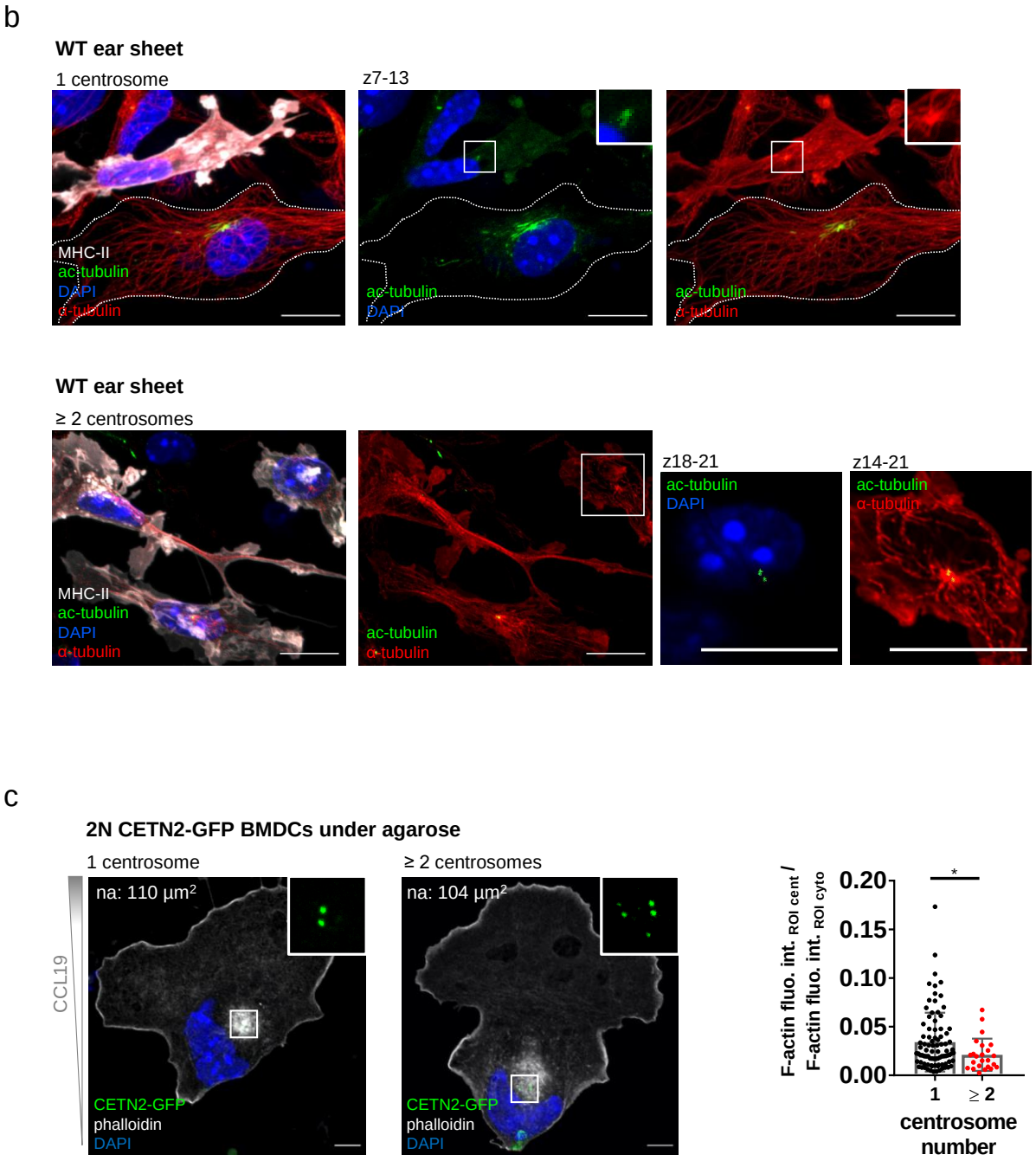

Figure 19. Dendritic cells with extra centrosomes harbor more centrosomal microtubules and less actin than cells with one centrosome

(**a**) Left: IF staining of MT filaments in mature 2N CETN2-GFP expressing BMDCs with different centrosome numbers fixed during migration under agarose toward a chemokine source. Merged and individual channels of CETN2-GFP (green), γ-tubulin (cyan) and α-tubulin (red) are shown. Nuclei were stained with DAPI (pseudocolored in grey). Dotted white line marks cell outline. White boxes highlight areas of magnification showing MT nucleating centrosomes. Post-processing of images: deconvolution. Scale bar: 5 µm. Right: Quantification of MT filaments in mature 2N CETN2-GFP expressing BMDCs emanating from one or multiple centrosome(s). Graph displays mean values ± SD with N = 44 (one centrosome) and 45 (multiple centrosomess) cells pooled from 7 independent experiments. **, P = 0.0073 (two-tailed, unpaired Student's t-test). BMDCs from two experiments were stained and imaged by Michaela Limmer. (**b**) IF stainings of centrioles and MTs in ear explants from WT mice. Merged channels of MHC-II (grey), ac-tubulin (green) and α-tubulin (red) are shown on the left, single channels and merging of two channels as indicated. White boxes show magnification of indicated region. Nuclei were stained with DAPI (blue). Scale bars: 10 µm. Upper panel: Left and right: complete Z-stack (maximum projection), middle: projection of indicated

z-planes. White dotted line marks fibroblast outline. Lower panel: Magnification of boxed region (right) shows only indicated z-plane projections. (**c**) Left: IF staining of centrosomal actin via phalloidin staining in mature 2N CETN2-GFP expressing BMDCs with indicated centrosome numbers fixed during migration under agarose toward a chemokine source. Merged and individual channels of CETN2-GFP (green) and phalloidin (grey) are shown. Nuclei were stained with DAPI (blue). White box marks area of magnification showing centrosomes. Scale bar: 5 µm. Right: quantification of centrosomal actin in mature 2N CETN2-GFP expressing BMDCs with one (black) or multiple (red) centrosome(s). Graph displays mean values ± SD with N = 88 (one centrosome) and 24 (multiple centrosomes) cells pooled from 4 independent experiments. *, P = 0.0395 (Mann-Whitney test). na: nuclear area; fluo. int.: fluorescence intensity; ROI: region of interest; cent.: centrosome; cyto: cytosol

3.3.3 Dendritic cells with excess centrosomes show enhanced persistent locomotion

After establishing differences in cytoskeletal components between (fixed) DCs with one and multinumerous centrosome(s) we investigated the impact of centrosome numbers on the migratory behavior of DCs under live conditions focussing on **velocity** and **directional persistence**. In a first step, we injected mature CETN2-GFP expressing BMDCs under agarose containing a chemokine gradient and imaged the cells during migration at a single cell level (Fig. 20 a). From the obtained tracks (Fig. 20 b, upper part) we determined migration velocity and directional persistence and directly compared the behavior of cells with one and supernumerary centrosome(s). As in the analysis of MTs and actin, we analyzed the cells according to ploidy and compared 2N cells with one and multiple centrosome(s) to exclude potential effects that could derive from ploidy.

Between the two groups of 2N BMDCs we could not find noticeable differences regarding velocity, but persistent locomotion of cells with extra centrosomes was significantly increased implying that those cells show less changes in direction during migration (Fig. 20 b, lower part). The analysis of Euclidean distance does not provide significant results but indicates that 2N BMDCs with additional centrosomes moved further away from their starting point in a given time period than cells with one centrosome (Fig. 20 b, right). This does not result from increased speed (since velocities were similar, see above), but from a migratory behavior with less distractions.

To confirm our results, we repeated this assay in a more physiological environment using dermal DCs from murine ear explants. Split ear sheets from CETN2-GFP reporter mice were placed on chemokine containing medium for three days and activated DCs emigrated from the tissue. Cells were harvested and injected under agarose for live cell imaging as described above (Fig. 20 c). It has to be noted that the limited number of dermal DCs did not allow to distinguish between di- and tetraploid cells with multinumerous centrosomes (Fig. 16 a, right). Similar to BMDCs, the persistence of dermal DCs with a surplus of centrosomes was

significantly higher showing that those cells changed direction less often than cells with only one centrosome, whereas velocities were comparable (Fig. 20 d).

Overall, we found that DCs with multiple centrosomes, when exposed to a CCL19 gradient, migrate more persistently and thus cover greater distances over time than DCs with only one centrosome. These findings show that additional clustered centrosomes do not hinder DCs in performing their functions (at least with regard to migration), but rather may even have an immune function-enhancing effect, which was investigated in a next step.

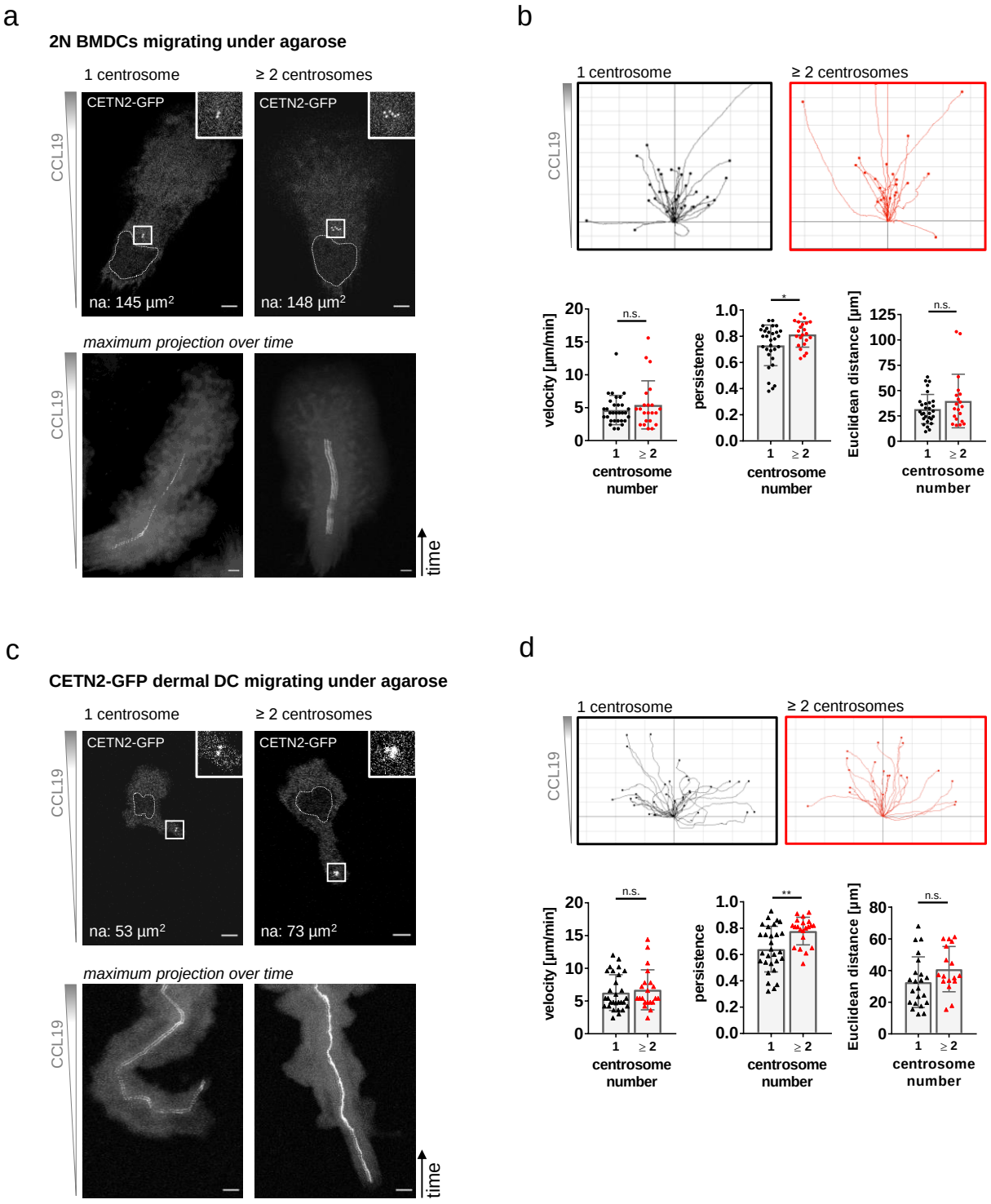

Figure 20. The persistence in locomotion of dendritic cells with multiple centrosomes is enhanced

(**a**) Upper panel: mature 2N CETN2-GFP expressing BMDCs with indicated centrosome numbers during migration under agarose along a chemotactic gradient. White dotted line marks nucleus. Boxes denote area of magnification showing centrioles. Lower panel: Corresponding maximum projections of time frames. Scale bars: 5 µm. (**b**) Upper panel: single-cell tracks of mature 2N CETN2-GFP expressing BMDCs with indicated centrosome numbers migrating under agarose along a chemotactic gradient. Lower panel: corresponding quantification of migration velocity (left), persistence (middle) and Euclidean distance (right). Graphs display mean values ± SD with N = 31 (one centrosome) and N = 22 (multiple centrosomes) cells pooled from 6 independent experiments. *, P = 0.0198, n.s., not significant (two-tailed, unpaired Student's t-test with Welch's correction (persistence), Mann-Whitney test (velocity, Euclidean distance)). (**c**) Upper panel: CETN2-GFP expressing dermal DCs with indicated centrosome numbers during migration under agarose along a chemotactic gradient. White dotted line marks nucleus. Boxes denote area of magnification showing centrioles. Lower panel: Corresponding maximum projections of time frames. Scale bars: 5 µm. (**d**) Upper panel: single-cell tracks of CETN2-GFP expressing dermal DCs with indicated centrosome numbers migrating under agarose along a chemotactic gradient. Lower panel: corresponding quantification of migration velocity (left), persistence (middle) and Euclidean distance (right). Graphs display mean values ± SD with N = 29 (one centrosome) and N = 21 (multiple centrosomes) cells for velocity and persistence analysis and N = 22 (one centrosome) and N = 17 (multiple centrosomes) cells for Euclidean distance analysis. Cells were pooled from 4 independent experiments. **, P = 0.0011, n.s., not significant (Mann-Whitney test (velocity); two-tailed, unpaired Student's t-test with Welch's correction (persistence); two-tailed, unpaired Student's t-test (Euclidean distance)). na: nuclear area

3.3.4 Multiple centrosomes are causally linked to enhanced persistent locomotion

The finding that DCs with multiple centrosomes migrate more persistently than cells with only one centrosome raises the question whether extra centrosomes are causal for enhanced persistent locomotion. To address this issue we sought to remove (additional) centrosomes during cell migration using laser ablation techniques[387,388] and examine migration velocity and directional persistence before and after the ablation process. Prior to these studies, we explored the settings required for efficient centrosome ablation: After injecting mature CETN2-GFP BMDCs under a block of agarose containing a chemokine gradient, we imaged the cells during migration at a single cell level and destroyed centrosomes with different laser intensities. Maximum intensity Z-stack projections of CETN2-GFP signals prior to and after the ablation process enabled us to judge if there was any GFP-signal left. We found technical conditions that allowed the removal of the centrosome(s) without killing the cells. After ablation, the centrosome was not or barely visible anymore (Fig. 21 a, left) and quantification of fluorescence intensities showed a loss of fluorescence signal at the irradiated region immediately after laser exposure (Fig. 21 a, right).

Next, we investigated whether laser exposure can efficiently disrupt MTOC function of centrosomes. During under agarose migration toward a chemokine source, centrosomes of mature CETN2-GFP BMDCs were ablated and the cells were instantaneously fixed through the agarose. Since we used gridded glass coverslips on which the cells migrated, we were

able to retrieve individual cells after laser intervention. Subsequent staining against α-tubulin provided a clear picture of MT integrity (Fig. 21 b, left). For analyses, we quantified MT numbers and configuration after laser ablation and compared these parameters with data from untreated cells. We found that treated cells have less MT filaments emanating from ablated centrosomes than control cells (Fig. 21 b, right). Moreover, the remaining filaments after laser treatment were shorter than MTs in control cells showing a disorganized structure with a curly architecture (Fig. 21 b left, c). These results confirmed that our laser ablation settings successfully eliminate the centrosome and its function as MTOC paving the way for the final step of the experiment.

In the following studies, we examined the migration behavior of migrating mature CETN2-GFP BMDCs before and after removal of the centrosome(s), thereby distinguishing between *full* and *partial* ablation. While *full ablation* implies the complete destruction of the centrosomes (Fig. 21 a), partial ablation leads to the elimination of only one of multiple centrosomes while the remaining one(s) stay/s intact (Fig. 21 d, lower panel).

Cells were injected under a layer of agarose, exposed to a chemokine gradient and imaged during migration at a single cell level while being exposed to laser treatment. To be able to assess the effect of laser shooting itself and to expose all cells to similar stresses we conducted control interventions by shooting in close proximity to centrosomes with identical laser settings resulting in three conditions: control shots, complete centrosomal ablation and partial ablation.

We observed that control treated cells were not affected by laser exposure at all showing stable migration even after the intervention (Fig. 21 d, upper and middle panel). Analyses of velocity and directional locomotion confirmed these obervations showing no significant changes (Fig. 21 e). Complete ablation of centrosomes (Fig. 21 a) as well as partial ablation (Fig. 21 d, lower panel) decreased the cells' velocity compared to control cells, but not to a significant extent (Fig. 21 e). However, both full and partial ablation strongly affected persistent cell movement compared to control-ablated cells resulting in a significant decrease of persistent locomotion. Thereby, the effect of full centrosomal ablation was even stronger than the consequences of partial ablation.

In summary, these data show that multinumerous centrosomes are causally linked to enhanced persistent locomotion of BMDCs that migrate in a chemokine gradient setting. From these results and the findings from the other functional assays, we conclude that extra centrosomes in terminal differentiated DCs are not a side effect the cells have to cope with, but that they may have a physiological role in mature DCs where they can be used to promote centrosome/MT-associated processes, such as directional locomotion.

a

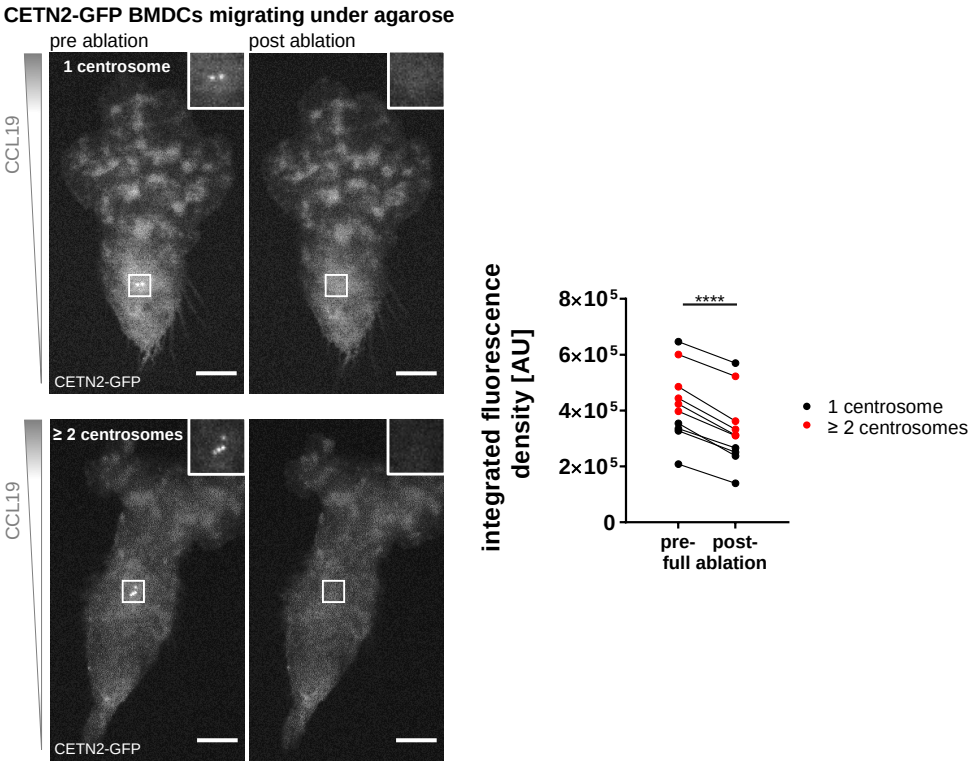
CETN2-GFP BMDCs migrating under agarose
pre ablation
post ablation
1 centrosome
CCL19
CETN2-GFP
≥ 2 centrosomes
integrated fluorescence density [AU]
8×10⁵
6×10⁵
4×10⁵
2×10⁵
0
****
pre-
post-
full ablation
1 centrosome
≥ 2 centrosomes

b

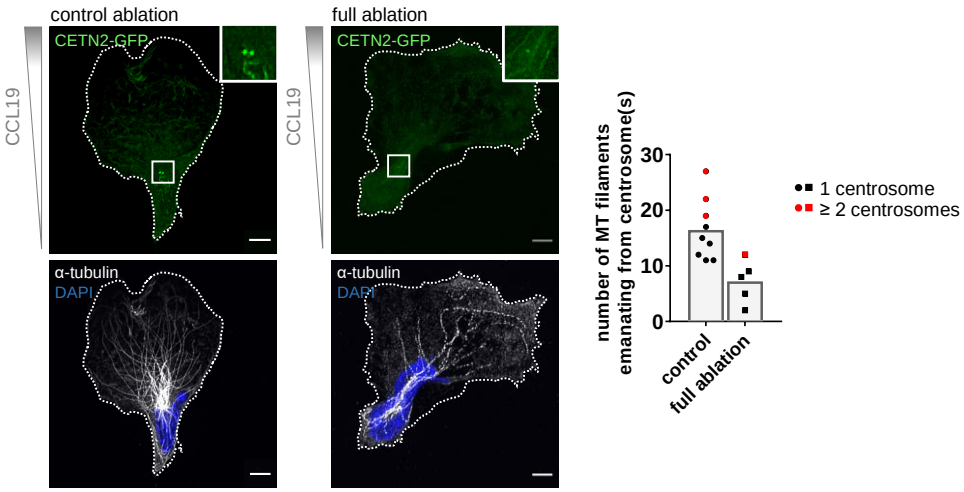
CETN2-GFP BMDCs migrating under agarose
control ablation
full ablation
CCL19
CETN2-GFP
α-tubulin
DAPI
number of MT filaments emanating from centrosome(s)
30
20
10
0
control
full ablation
1 centrosome
≥ 2 centrosomes

c

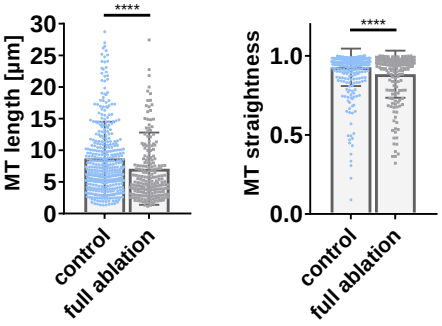
MT length [µm]
30
25
20
15
10
5
0
****
control
full ablation
MT straightness
1.0
0.5
0.0
****
control
full ablation

d

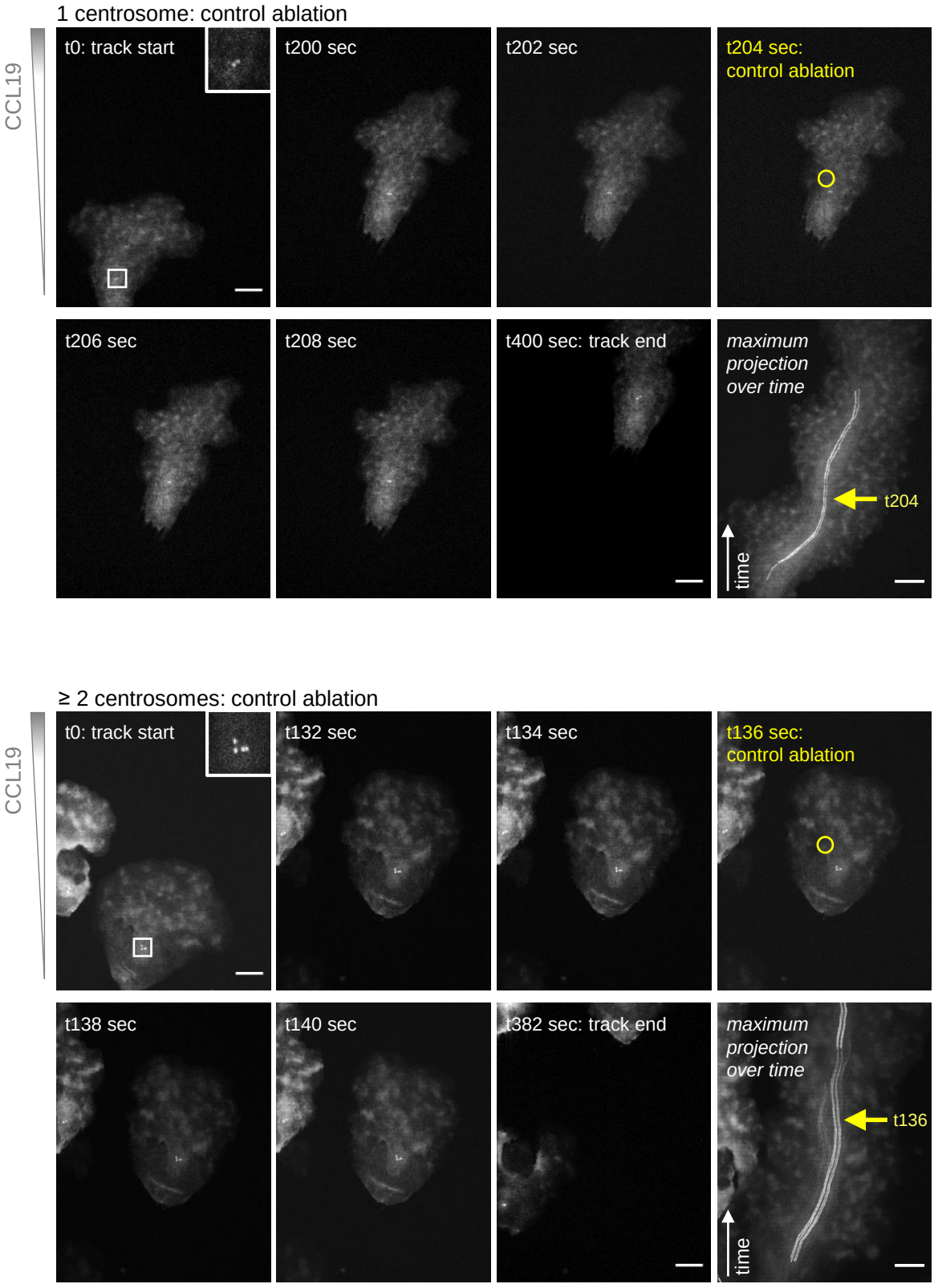
1 centrosome: control ablation
CCL19
t0: track start
t200 sec
t202 sec
t204 sec:
control ablation
t206 sec
t208 sec
t400 sec: track end
maximum
projection
over time
t204
time
≥ 2 centrosomes: control ablation
CCL19
t0: track start
t132 sec
t134 sec
t136 sec:
control ablation
t138 sec
t140 sec
t382 sec: track end
maximum
projection
over time
t136
time

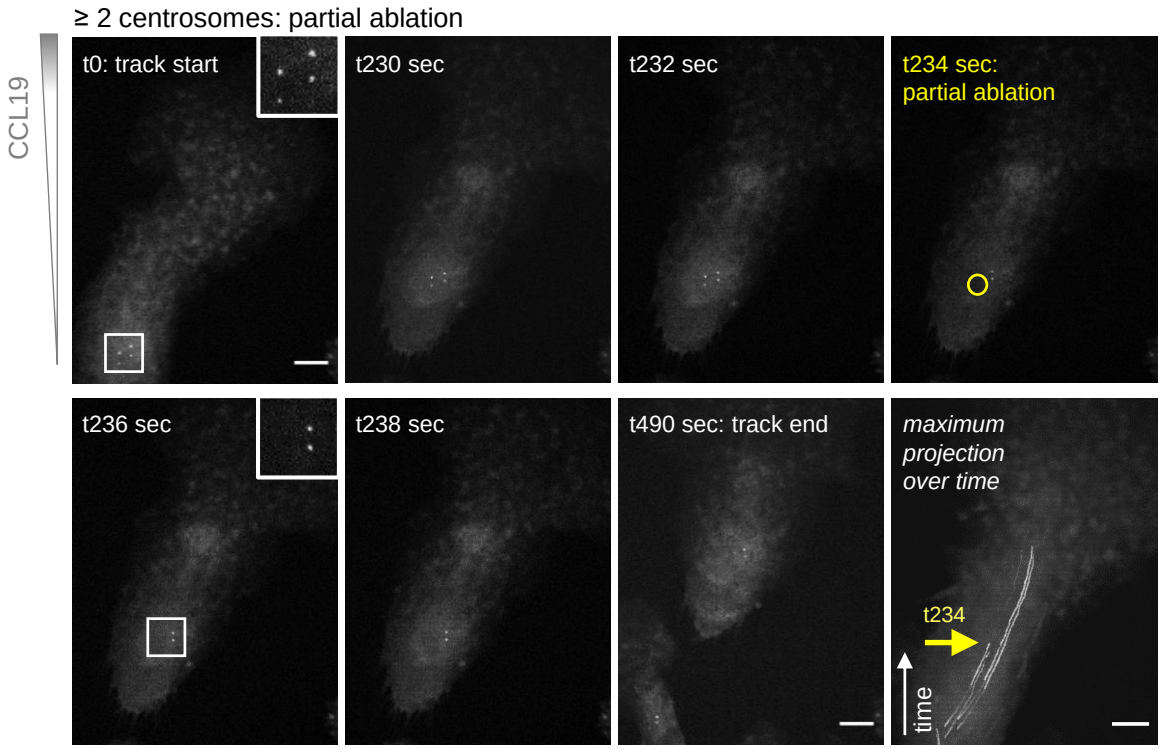

e

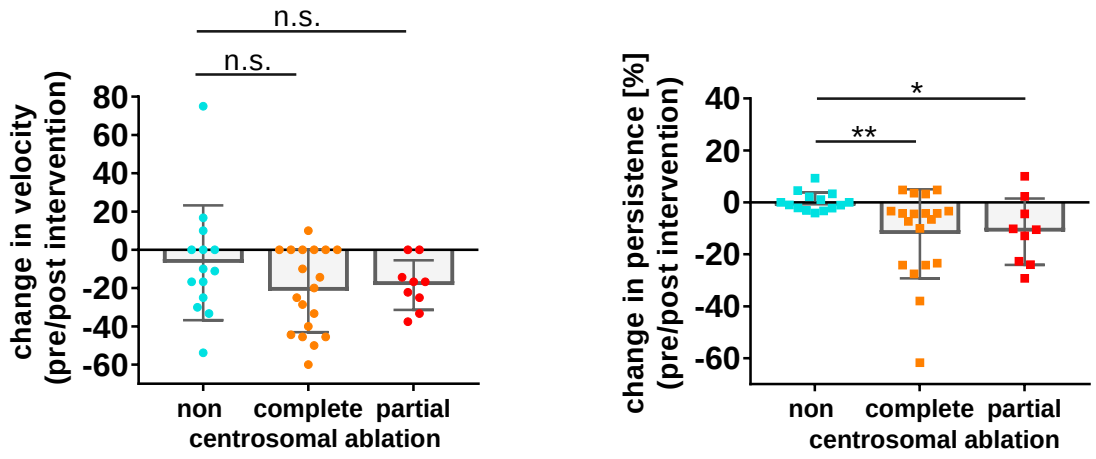

Figure 21. Persistence of locomotion decreases after ablating multiple centrosomes during migration

(**a**) Left: Complete laser ablation of one (upper panel) and multiple (lower panel) centrosome(s) in CETN2-GFP expressing BMDCs migrating under agarose toward a chemokine source. Pre- and post-ablation images of two representative BMDCs are shown (maximum intensity Z-stack projections). White boxes mark area of magnification showing the place the centrioles (pseudocolored in grey) are/were located. Scale bars: 10 µm. Right: quantification of integrated CETN2-GFP signal densities in defined *regions of interest* (ROIs) around one (black) and multiple (red) centrosome(s). Graph shows cell pairs before and after the ablation process. N = 5/5 cells (one/multiple centrosome(s)). ****, P < 0.0001 (two-tailed, paired Student's t-test). (**b**) Left: IF staining against α-tubulin in CETN2-GFP expressing BMDCs migrating under agarose along a chemotactic gradient. Images of cells experiencing control (left) and full (right) centrosomal ablation are shown. Cells were fixed instantaneously after the ablation process. Individual and merged channels of CETN2-GFP (green) and α-tubulin (grey) are shown. Nuclei were stained with DAPI (blue). Post-processing of images: deconvolution. White boxes mark areas of magnification showing region of the

centrosome. White dotted line depicts cell outline. Scale bars: 10 µm. Right: Corresponding quantification of MT filaments emanating from one (black) or multiple (red) centrosome(s) in BMDCs experiencing control (dots, N = 9) or full (squares, N = 5) centrosomal ablation. Graph shows mean values. One data point = one cell. (**c**) Quantification of MT length (left) and straightness (right) in CETN2-GFP expressing BMDCs experiencing control (light blue) or complete (grey) centrosomal ablation during migration under agarose. Straightness = end-to-end distance/total length of MT filament. Graphs display mean values ± SD with N = 413/205 filaments traced from 9 or 5 different cells (control/full ablation). ****, P < 0.0001 (Mann-Whitney test). (**d**) Illustration of control ablation of one (upper panel) and multiple (middle panel) centrosome(s) and partial ablation of multiple centrosomes (lower panel) in CETN2-GFP expressing BMDCs migrating under agarose along a chemotactic gradient. First image of each panel shows the first picture taken in an image series of a cell (t0: track start) followed by two images before the intervention (control, partial ablation). Time point of intervention is indicated in yellow. Time intervals: 2 sec. Yellow circle represents area of laser ablation. Two pictures following intervention display the cell directly after treatment followed by the last image of a series (track end). The last picture of every panel is a maximum intensity projection over time showing centriolar tracks. Yellow arrow marks place and timepoint of ablation. White boxes highlight area of magnification showing centrioles. Centrioles are pseudocolored in grey. Scale bars: 10 µm. (**e**) Quantification of migration velocity (left) and persistence (right) as change between the timepoint before and after indicated laser ablation treatments. Graphs show changes as mean values ± SD with N = 14/19/9 (non/complete/partial ablation) cells pooled from 6 independent experiments. *, P = 0.015 and **, P = 0.009 (Kruskal-Wallis test followed by Dunn's test), n.s.: not significant; t: timepoint

3.4 Disturbance of centrosomal clustering is accompanied by impaired cell migration

3.4.1 Clustering is the preferred configuration of multiple centrosomes in dendritic cells

In the studies shown so far, such as the 2D DC migration experiments *in vitro*, we observed clustering of multiple centrosomes (Fig. 22 a, left; see also Fig. 18 b and c, Fig. 20 a and c). This configuration was also detectable in fixed DCs – regardless of whether the cells had migrated before fixation (Fig. 22 a middle, see also Fig. 19 a) or not (Fig. 22 a right; see also Fig. 12 c-e, Fig. 13 a and b). Besides interphase, we also found centrosomal clustering during mitosis (data not shown). With this preferred centrosomal configuration, DCs exhibit parallels to cancer cells, whose multiple centrosomes are also predominantly clustered in interphase and mitosis[389,390].

We were interested in whether supernumerary centrosomes in DCs stay in close proximity to each other even in an environment that is more challenging than the 2D under agarose setting and thus more closely reflect the physiological environment in which DCs move. As DCs in tissues have to navigate through a complex system of fibers and pores constantly deciding which path to take[121,131], we switched to an *in vitro* migration system that allows us to study extra centrosomes during decision making, i.e., at a point where the cell undergoes drastic changes in shape. Therefore, we used microfabricated PDMS-based devices in form of Y-shaped decision channels providing cell confinement[126,133,226]. To visualize centrosomes, we

worked with CETN2-GFP expressing BMDCs that were chemotactically guided through the channels, and monitored centrosomes by time-lapse video fluorescence microscopy (60 sec intervals) (Fig. 22 b).

After a cell has entered the channel of a Y-shaped device (Fig. 22 b, transmitted light image, yellow circle, and timepoint (t) t0) it migrates along the chemotactic gradient and reaches the bifurcation at which the channel splits into two arms (t14). At this point, the decision takes place (transmitted light image, red circle), which path is chosen. While migrating cells extend protrusions into both channel arms[126] (t30, t39), the MTOC building centrosome acts as a side selector[131] showing occasional changes of direction at the Y-junction (t39, t43, t45). Once the decision for a direction has been made, the protrusion in the "loser arm" is retracted (t51, yellow arrow) and the cell follows the "winner" path (t45-t58). We found, that despite these challenging movements, multinumerous centrosomes were not torn apart, but stayed close together at any time point of imaging (see magnifications).

In contrast, we very rarely found DCs with additional centrosomes exhibiting large gaps between individual centrosomes (high intercentrosomal distance) and/or between single centrioles (intracentrosomal distance). In these cases of "declustered" centrosomes, cells exhibited problems with polarization and stable migration (Fig. 22 c) suggesting a correlation between a clustered centrosomal configuration and proper migration. MT stainings revealed that single declustered centrosomes can act as individual MTOCs (Fig. 22 d).

a

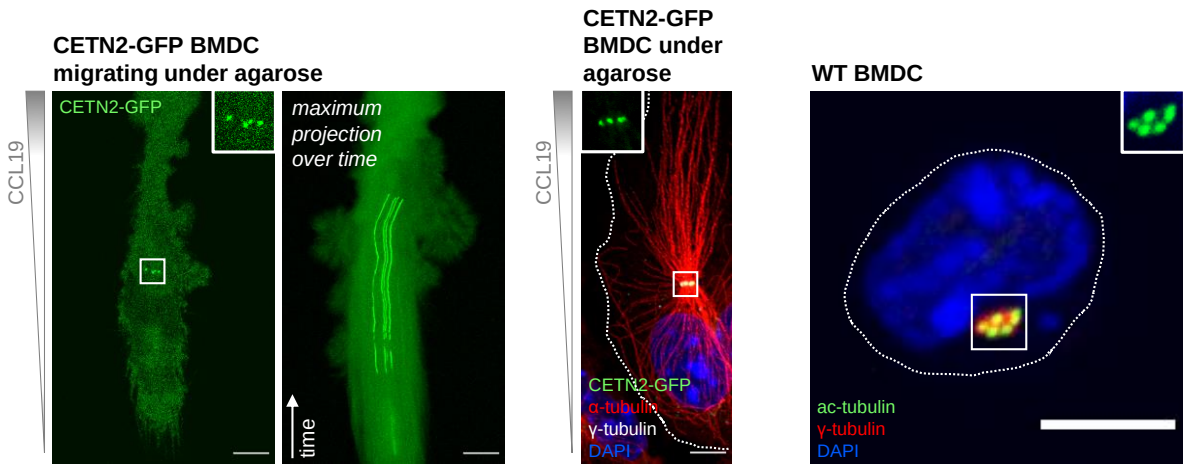

b

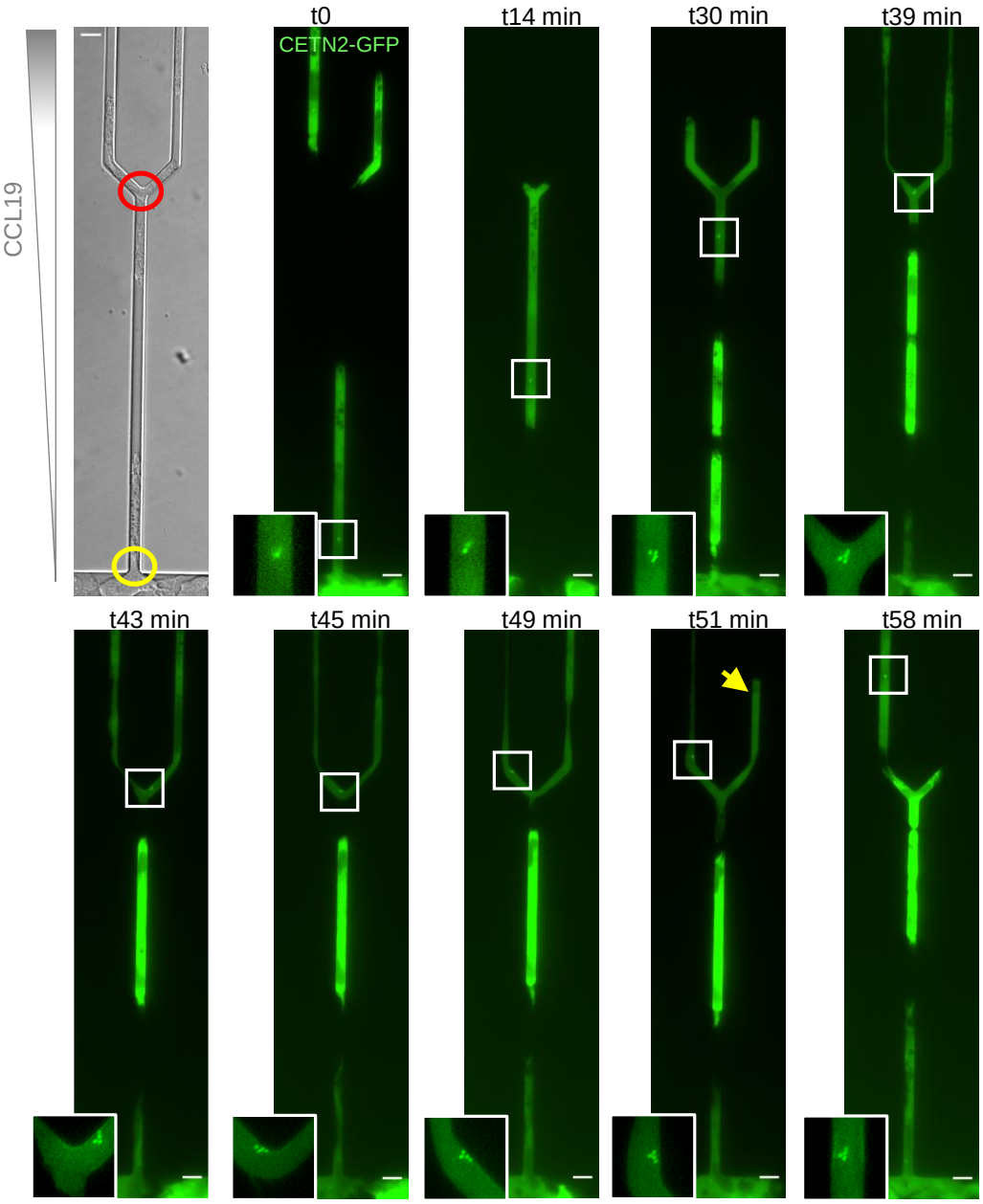
CCL19
t0
CETN2-GFP
t14 min
t30 min
t39 min
t43 min
t45 min
t49 min
t51 min
t58 min

c

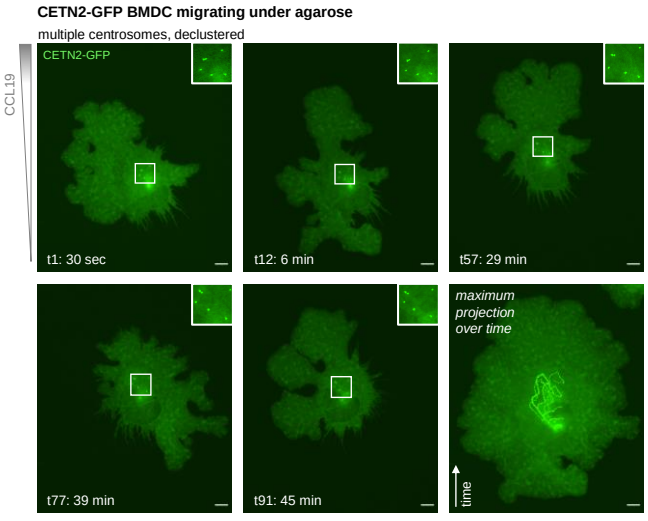
CETN2-GFP BMDC migrating under agarose
multiple centrosomes, declustered
CCL19
CETN2-GFP
t1: 30 sec
t12: 6 min
t57: 29 min
t77: 39 min
t91: 45 min
maximum projection over time
time

d

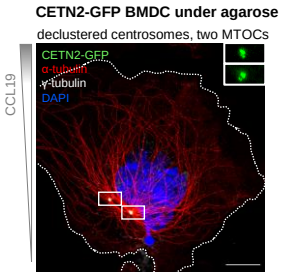
CETN2-GFP BMDC under agarose
declustered centrosomes, two MTOCs
CCL19
CETN2-GFP
γ-tubulin
DAPI

Figure 22. Clustering is the preferred configuration of multiple centrosomes in migrating and non-migrating dendritic cells

(**a**) Left: Mature CETN2-GFP expressing BMDC with multiple centrosomes during migration under agarose along a chemotactic gradient (left) and corresponding maximum projection of time frames (right). White box shows magnification of multiple centrosomes. Scale bar: 10 µm. Middle: IF staining of MT filaments and PCM in mature CETN2-GFP expressing BMDC with multiple centrosomes fixed during migration under agarose toward a chemokine source. Individual CETN2-GFP channel (green) and merged channels of CETN2-GFP, γ-tubulin (grey) and α-tubulin (red) are shown. Nucleus was stained with DAPI. Post-processing of image: deconvolution. Dotted white line marks cell outline. White box highlights area of magnification showing centrosomes. Scale bar: 5 µm. Right: IF staining of centrioles and PCM (represented by γ-tubulin) in mature WT BMDC. Individual ac-tubulin channel (green) and merged channels of ac-tubulin and γ-tubulin (red) are shown. Nucleus was stained with DAPI. Scale bar: 5 µm. Dotted white line marks cell outline. White box outlines area of magnification showing multiple centrosomes. (**b**) Mature CETN2-GFP expressing BMDCs with multiple centrosomes migrating in a Y-formed PDMS channel (4 × 4 µm) along a chemotactic gradient. First image shows setting under transmitted light, with yellow circle marking site of cell entrance in the unbranched channel and red circle marking site of channel bifurcation. The following 9 images are part of a time-lapse video fluorescence microscopy series (60 sec intervals) showing the cell of interest from entering the channel to passing the bifurcation at different time points (t), with the first selected image defined as t0. Centrosomes are marked by white boxes showing magnification of this region. Yellow arrow marks “loser protrusion” that retracts from the channel arm. Scale bars: 5 µm. (**c**) Representative images of a time-lapse video fluorescence microscopy series of a mature CETN2-GFP expressing BMDC with declustered centrososmes at different time points trying to migrate under agarose along a chemotactic gradient. The cell has problems to polarize. Time interval: 30 sec. The last picture is a maximum intensity projection over time showing centriolar tracks. White boxes highlight area of magnification showing centrioles. Scale bars: 10 µm. (**d**) IF staining of MT filaments and PCM in mature CETN2-GFP expressing BMDC with declustered centrosomes fixed during migration under agarose toward a chemokine source. Individual CETN2-GFP channel (green) and merged channels of CETN2-GFP, γ-tubulin (grey) and α-tubulin (red) are shown. Nucleus was stained with DAPI. Post-processing of image: deconvolution. White boxes mark areas of magnification showing centrosomes. Dotted white line depicts cell outline. Scale bar: 10 µm.

3.4.2 The clustered configuration of centrosomes can be chemically disturbed

We found that DCs usually cluster multinumerous centrosomes and retain this clustered configuration even during remarkable shape changes in the course of migration. In contrast, a declustered centrosomal architecture occurs naturally very rarely in DCs and cells with declustered centrosomes exhibited problems with polarization and persistent migration. Due to these findings, we assumed a correlation between a clustered centrosomal configuration and efficient migration. To investigate a potential dependence of proper DC migration on clustering of extra centrosomes, different approaches are conceivable. We decided to chemically disturb the clustered configuration and provoke the declustering of multiple centrosomes. Therefore, we made use of chemicals that are established as **declustering agents** in (mainly mitotic) experiments in cancer research (Fig. 23 a)[390–402] and examined the migratory behavior of treated and non-treated DCs.

Declustering agents take advantage of the difference known so far in centrosome numbers between normal and cancer cells and inhibit the formation of a pseudo-bipolar spindle in mitosis by preventing the clustering of additional centrosomes, thus provoking a multipolar

spindle with its fatal consequences (Fig. 23 a; see also section 4.4.2). The drugs are considered a promising approach in cancer treatment as they are thought to act specifically on (cancer) cells with multiple centrosomes achieving selective eradication of cancer cells without harming non-malignant cells[337,403]. The way in which declustering drugs disturb excess centrosome coordination depends on the chemical structure of the drug and is not fully understood for every substance. There are a number of declustering compounds with different mechanisms of action that are in various stages of study[391,393].

To test our hypothesis that efficient DC migration depends on a clustered configuration of extra centrosomes we used declustering substances named “GF-15” and “PJ-34” (Fig. 23 b). **GF-15** ((2*S*,6'*R*)-(7-chloro-4,6-dimethoxy-benzofuran-3-one)-2-spiro-1'-(2'-benzyloxy-6'-methylcyclo-hex-2'-en-4'-one)) is a small synthetic derivative of the antimycotic benzofuran derivative griseofulvin and leads to reduced spindle tension, spindle multipolarity and the inhibition of centrosomal clustering resulting in apoptosis in malignant cells *in vitro* and *in vivo*[397]. **PJ-34** (2-(dimethylamino)-N-(6-oxo-5H-phenanthridin-2-yl) acetamide hydrochloride) is a synthetically produced water-soluble inhibitor of *poly-ADP-ribose polymerase 1* (PARP1) and derives from phenanthrene, a polycyclic aromatic hydrocarbon (Fig. 23 b). PARPs play a crucial role in DNA repair and the inhibition of PARP-1 by PJ-34 was shown to cause cell death via the induction of multipolar spindles and extra centrosome declustering thereby not affecting normal cell proliferation[391,395,396,398,404,405].

In a first step, we tested the declustering potency of GF-15 and PJ-34 by determining the proportion of BMDCs with extra centrosomes that showed a declustered configuration after drug treatment. For this purpose, the definition of a threshold value was required that specifies at which intercentrosomal distance declustering exists. After treating mature CETN2-GFP expressing BMDCs with a declustering drug or the corresponding control (dimethyl sulfoxide (DMSO), ddH_2O) we fixed the cells on coverslips and conducted nuclear DAPI staining. Following image acquisition, the distance between multiple centrosomes (intercentrosomal distance) (Fig. 23 c, IF image, left magnification) in control and treated cells was measured. In case of more than two centrosomes or scattering of single centrioles throughout the cell, we captured the distance between centrosomes/centrioles furthest away from each other (Fig. 23 c, IF image, right magnification). To set a threshold defining the intercentrosomal distance above which declustering is present, we chose the mean intercentrosomal distance of untreated cells (Fig. 23 c, histograms, blue bars) and added two standard deviations (SDs). The upper border of the resulting interval represents the threshold value (Fig. 23 c, histograms, dotted black line). All drug treated cells (Fig. 23 c, histograms, red/orange bars) with intercentrosomal/intercentriolar distances above this cutoff value (Fig. 23 c, histograms, red/orange arrow) were considered declustered (Fig. 23 d).

For the application of GF-15 and PJ-34 we followed the previously published concentrations and incubation times[395–399,402]. For GF-15, it has been shown that the drug inhibits tubulin polymerization only at concentrations of or above 25 µM[397]. However, to be sure to avoid these undesirable side effects, we further halved the dosage (12.5 µM, 6 hrs incubation period). In case of PJ-34, we increased the concentration compared to the published data while considerably shortening the incubation period (50 µM, 3 hrs).

After manual measurement of the intercentrosomal distances of control and drug treated fixed CETN2-GFP expressing BMDCs, we calculated the means and SDs of the different populations. For DMSO treated cells, we obtained a mean of 1.53 µm (mean GF treated cells: 3.91 µm) and a SD of 0.68 µm. Adding two SDs to the mean, we calculated a threshold value of 2.89 µm. Applying this cutoff, we found that 64 % of GF-15 treated cells with multiple centrosomes exhibit intercentrosomal distances above this value and thus had a declustered centrosomal configuration. Calculating the corresponding values for water treated cells we obtained a mean of 1.61 µm (mean PJ-34 treated cells: 2.11 µm) and a SD of 0.79 µm resulting in a threshold value of 3.20 µm and a proportion of cells with declustered centrosomes of 15 %.

Since declustering potency analyses revealed that GF-15 in the tested conditions led to more declustering events (Fig. 23 c, histograms), we decided to focus on this drug in the subsequent functional assays.

a

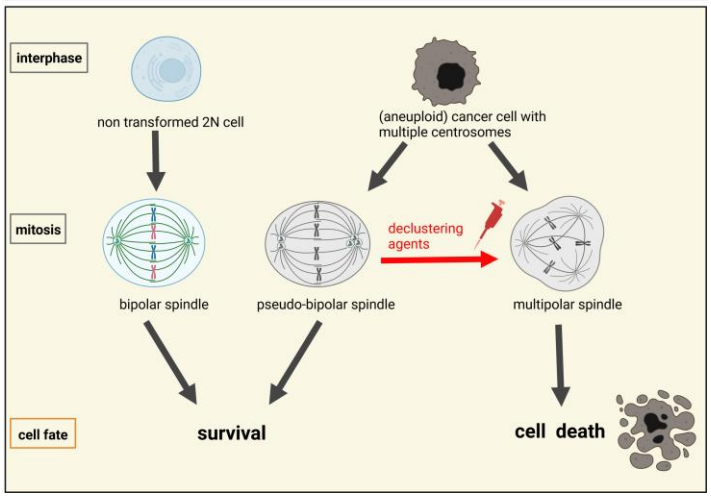

b

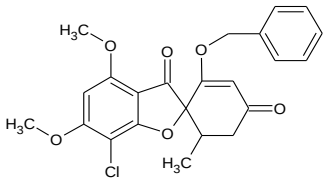

GF-15

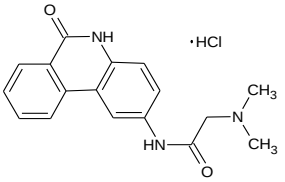

PJ-34

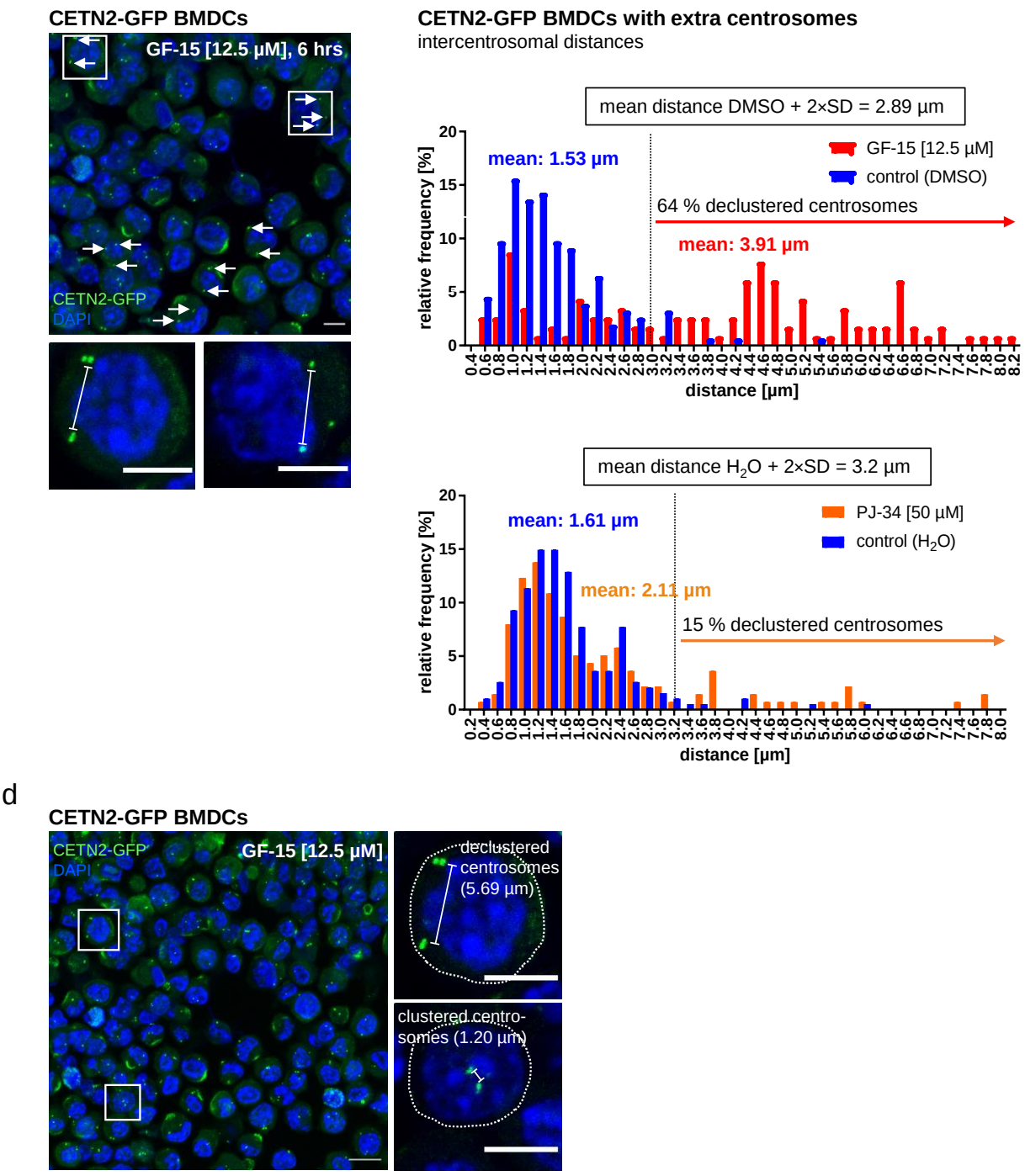

Figure 23. Declustering agents disturb the clustered configuration of multiple centrosomes

(**a**) Mode of action of declustering agents. The drugs have been tested in cancer cells, where they interfere with the formation of pseudo-bipolar mitotic spindles that the cells seek to form through centrosomal clustering in order to proceed with mitosis. Multipolar spindles are not well tolerated and lead to cell death. Illustration created with BioRender.com. (**b**) Chemical structure of the two declustering agents GF-15 and PJ-34. (**c**) IF image: fixed mature CETN2-GFP expressing BMDCs after treatment with GF-15 (12.5 µM) for 6 hrs. Centrioles appear as green foci. Nuclei were stained with DAPI. Arrows mark multinumerous centrosomes/centrioles (≥ 4 CETN2-GFP positive foci) that are scattered throughout the cells. White boxes mark areas of magnification showing two exemplary cells depicted below to clarify the procedure of distance measuring in cells with extra centrosomes. Left cell: if the centrosomes were separated in pairs, the distance between the pairs was measured. In case of three or more pairs, the distance between the two centrosomes furthest apart was measured (not shown here). Right cell: when the centrosomal structure was destroyed and the centrioles were distributed in the cell, the distance between the two

most distant centrioles was measured. Scale bars: 5 µm. Histograms: relative frequencies of intercentrosomal distances in DMSO treated (control, blue) and drug treated (red/orange) fixed mature CETN2-GFP expressing BMDCs with extra centrosomes. Based on the means of the distances in control cells and the corresponding *standard deviation* (SD), a threshold was defined (black dotted line), beyond which centrosomes were considered to be declustered. Numbers of analyzed cells: N = 152 (DMSO), N = 115 (GF-15) and N = 194 (water), N = 140 (PJ-34), respectively. (**d**) Fixed mature CETN2-GFP expressing BMDCs after treatment with GF-15. Nuclei were stained with DAPI. White boxes mark areas of magnification showing two exemplary cells on the right to illustrate the situation of clustered (lower cell) and declustered (upper cell) centrosomes. Dotted white line marks cell outline. Scale bars: 5 µm.

3.4.3 Declustering agents impair migration *in vitro* and *in situ*

To examine DC locomotion after treatment with GF-15 in a physiological environment, we conducted *in situ* migration studies. Ears from WT mice were split into two sheets and placed on full medium supplemented with GF-15 (12.5 µM) or DMSO (control) for 48 hrs. The splitting process induces an inflammatory state leading to activation of dermal DCs, which subsequently migrate into the lymphatic vessels. After fixation of the whole tissue, we stained for lymphatic vessels and DCs. High-resolution microscopy allowed us to count individual cells in, on and around the lymphatic vessels (Fig. 24 a, left). Subsequently, we determined the proportion of cells in/on the vessels in treated and untreated ear sheets and revealed that after treatment significantly less cells managed to reach the lymphatics (Fig. 24 a, right), which may indicate an impairment of migration by GF-15.

In order to dissect the effects of declustering agents and to collect individual migration parameters, we switched to an *in vitro* system and conducted 3D and 2D migration assays for life cell imaging. A 3D environment for cells was created with the help of collagen which mimicks ECM scaffolds by building a mesh of fibers and pores[121]. Devices for 3D assays were constructed as shown in Fig. 12 a and filled with collagen, GF-15 or DMSO, and mature BMDCs previously treated with GF-15 (12.5 µM) or DMSO for 6 hrs. CCL19 on top of the collagen cell mixture provides a chemotactic gradient. Additionally, we conducted 2D under agarose migration assays with imageable glass bottom dishes. Here, too, cells were pretreated with GF-15 (12.5 µM) or DMSO for 6 hrs prior to injection under agarose which was also mixed with the declustering drug or DMSO. A gradient of CCL19 was created for chemotactic locomotion. DC migration toward the chemokine source was visualized by time-lapse video brightfield-microscopy (3D collagen assay: 60 sec intervals, 2D under agarose assay: 40 sec intervals; imaging period: 4 hrs).

Using a migration analysis software, we manually tracked individual migrating cells and determined migration parameters such as velocity and persistence. Analyses of the cells in collagen gels showed that persistence as well as migration velocity was slightly decreased after drug treatment (Fig. 24 b). In contrast, cells migrating under agarose exhibited a severe impairment of their locomotion after drug treatment, manifested by a strong decrease in

persistence and velocity (Fig. 24 c). Strikingly, in 2D under agarose migration assays *all* drug treated cells – not only the fraction with supernumerary centrosomes on which the drug is supposed to act – were barely able to migrate.

In summary, we found that the declustering agent GF-15 impairs cell migration *in situ* and in various *in vitro* migration assays. However, it has to be clarified whether the declustering of extra centrosomes is the cause of the impaired migration. The overall effect observed in treated cells in 2D under agarose assays suggests that the drug might target something other than only multiple centrosomes and requires further elucidation.

a

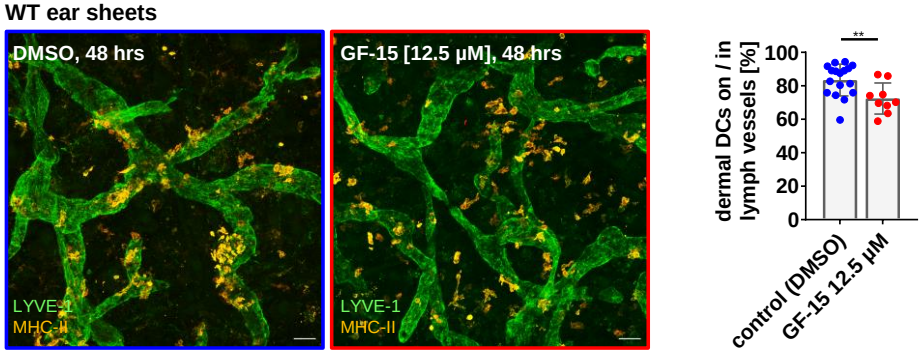

b

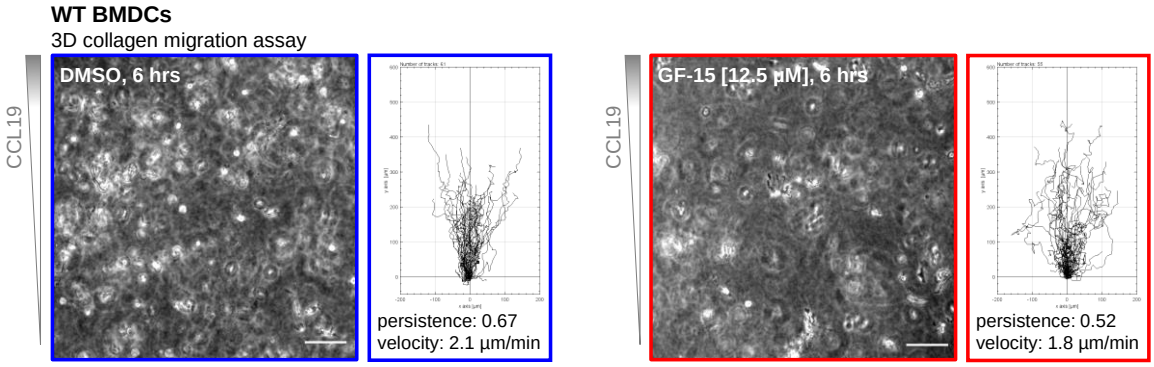

c

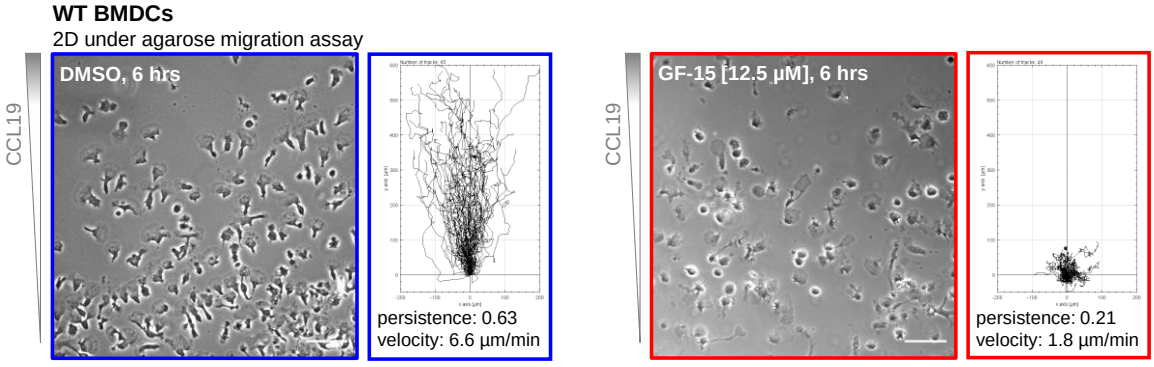

Figure 24. Dendritic cells exhibit an impaired migratory phenotype *in situ* and *in vitro* after treatment with the declustering agent GF-15

(**a**) Left: IF *in situ* staining of lymphatic vessels via LYVE-1 (green) and dermal DCs via MHC-II (orange) after control (DMSO, left) or GF-15 treatment (12.5 µM) for 48 hrs (right). Scale bar: 50 µm. Right: Quantification of dermal DCs that are located on or in the vessels. Graph displays mean values ± SD with cells from N = 17 (DMSO, blue) and N = 9 (GF-15, red) images of ear sheets from 3 different mice (counted cells: 1339 control, 760 GF-15 treated). **, P = 0.0091 (two-tailed, unpaired Student's t-test). (**b**) 3D collagen migration assay along chemotactic gradients with control (DMSO, 6 hrs, left) and GF-15 (12.5 µM, 6 hrs, right) treated mature WT BMDCs from one mouse. Scale bar: 100 µm. Next to each representative image from the time-lapse videos representative single-cell tracks of cells from one well of a multiwell plate are displayed with N = 61 (DMSO) and N = 55 (GF-15) tracks. For analysis of persistence and velocity, single-cell tracks of cells pooled from 2 wells per condition were analyzed with N = 116 (DMSO) and N = 113 (GF-15). (**c**) 2D under agarose migration assay along chemotactic gradients with control (DMSO, 6 hrs, left) and GF-15 (12.5 µM, 6 hrs, right) treated mature WT BMDCs from one mouse. Scale bar: 100 µm. Next to each representative image from the time-lapse videos single-cell tracks of cells from one (DMSO) well and cells pooled from 2 wells (GF-15) of a multiwell plate are displayed with N = 65 (DMSO) and N = 49 (GF-15) tracks. For analysis of persistence and velocity, single-cell tracks of cells pooled from 2 wells were analyzed in both conditions with N = 133 (DMSO) and N = 49 (GF-15).

3.4.4 Declustering drugs have severe side effects on cytoskeletal components

We observed moderate impairment of migration of dermal DCs *in situ* and BMDCs in 3D collagen assays after GF-15 exposure (12.5 µM), whereas treated BMDCs under agarose (2D) were not able to migrate properly at all. The results from the latter assay were surprising because it was not expected that *all* cells, but only those with supernumerary centrosomes, would exhibit an impaired migratory phenotype. In addition to impaired migration in under agarose assays, we observed only very few cases of successful cell polarization (Fig. 24 c, right panel) – a process in large part depending on MTOCs and MTs[91]. Although it has been published that GF-15 does not inhibit tubulin polymerization up to a concentration of 25 µM (in human cancer cells)[397], our observations could indicate impaired MT integrity in DCs. This suspicion prompted us to examine DCs' cytoskeleton more closely.

To visualize MTs, we conducted under agarose migration assays with GF-15 and DMSO treated mature WT BMDCs as described above. After fixing the cells through the agarose, we conducted IF stainings against α-tubulin. Additionally, we stained for centrioles (ac-tubulin), PCM (γ-tubulin) and the nucleus (DAPI). As expected from GF-15 treatment, cells with multiple centrosomes showed centrosomal scattering (Fig. 25 a, upper panel). However, MTs exhibited a non-intact and atrophied phenotype: MTs did nucleate/anchor at centrosomal MTOCs, but the filaments seemed to be considerably shorter than control MTs and did not extend across the cell (Fig. 25 a, upper panel) as we observed in untreated cells (Fig. 22 a, middle). This could at least partly explain migration and polarization effects. Likewise, DCs with normal centrosome content showed the same MT abnormalities (Fig. 25 a, lower panel). Moreover, different from what is reported in the literature[397], we observed that GF-15 (12.5 µM) causes

centrosomal declustering not only in cells with extra centrosomes, but also in those with normal centrosome content, leading to a dispersion of the two centrioles of a centrosome (Fig. 25 a, lower panel, Fig. 25 b, left panel). Distance measurements between individual centrioles in cells with only one centrosome (intracentrosomal distance), analogous to intercentrosomal distance analyses in cells with multiple centrosomes (Fig. 23 c), yielded considerably larger values after drug treatment with a proportion of dispersed centrioles of more than 60 % (mean DMSO treated cells: 0.7 µm, SD: 0.28 µm) (Fig. 25 b, right panel). Given that two centrioles in most cells were kept close together (< 2 µm)[406], as we observed also for DMSO treated BMDCs (Fig. 25 b, histogram, blue bars), it is conceivable that GF-15 might impair the linker fibers that connect a pair of centrioles.

To examine whether the observed adverse effects were concentration-dependent and might be diminished by reducing the amount of drug, we tested GF-15 in a concentration of 1 µM maintaining an incubation time of 6 hrs. In a first step, we investigated declustering potency via intercentrosomal distance analyses in fixed mature CETN2-GFP expressing BMDCs with additional centrosomes. In parallel, we measured intracentrosomal distances for potential linker impairment in cells with regular centrosome content. In contrast to GF-15 at a concentration of 12.5 µM, the lower amount of drug caused declustering in only about 6 % of cells with extra centrosomes (declustering potency decreased). However, the proportion of cells with only one centrosome that showed potential linker integrity impairment was substantially smaller as well (3 %) (side effects decreased) (Fig. 25 c). Next, we conducted IF stainings and found that low-dose GF-15 had no obvious effect on MTs, but led to mild spreading of the PCM even after shortening the incubation time from 6 to 3 hrs resulting in “empty” (acentrosomal) MTOCs (Fig. 25 d, white arrows). Since the PCM carries the MT organization activity of centrosomes[252,253] PCM spreading created even more MTOCs than the declustering already did. Additionally, we observed polarization problems of cells with multiple dispersed MTOCs (Fig. 25 d).

These experiments led us to conclude that GF-15 has undesirable side effects in addition to the intended declustering effect: impairment of the MT cytoskeleton and probably also the centrosomal linker as well as spreading of the PCM generating more (acentrosomal) MTOCs. Side effects could only be partially prevented by a reduction of the drug concentration, but at the expense of declustering potency. Because of the multiple side effects that affect or prevent polarization and proper cell locomotion, the extent to which centrosome declustering itself contributes to impaired DC migration could not be addressed with GF-15.

a

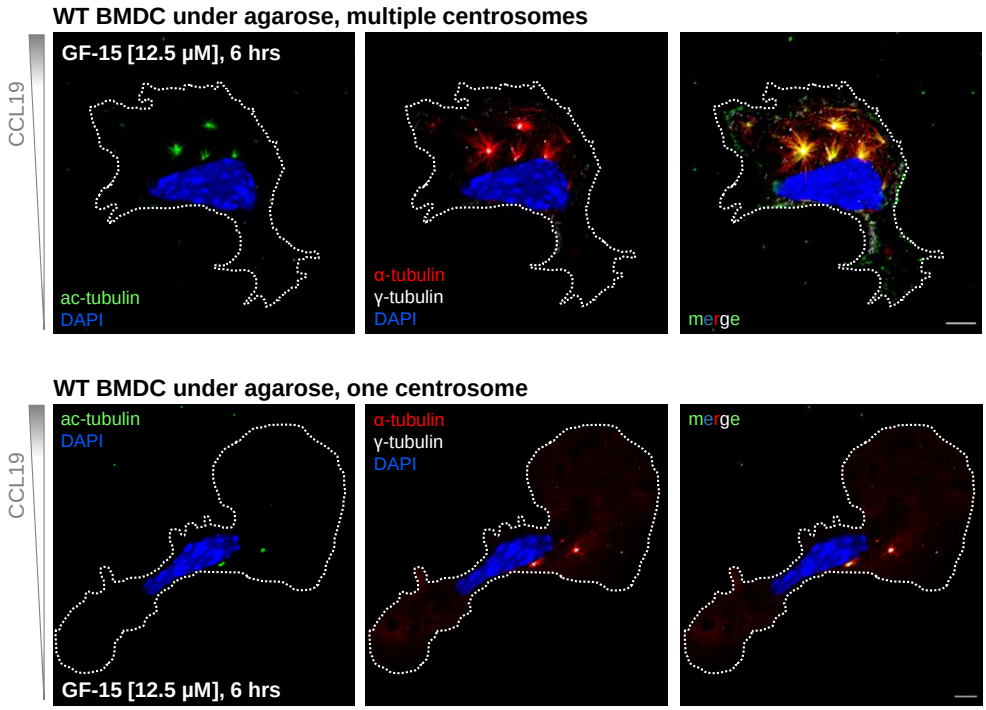
WT BMDC under agarose, multiple centrosomes
GF-15 [12.5 µM], 6 hrs
CCL19
ac-tubulin
DAPI
α-tubulin
γ-tubulin
DAPI
merge
WT BMDC under agarose, one centrosome
ac-tubulin
DAPI
α-tubulin
γ-tubulin
DAPI
merge
CCL19
GF-15 [12.5 µM], 6 hrs

b

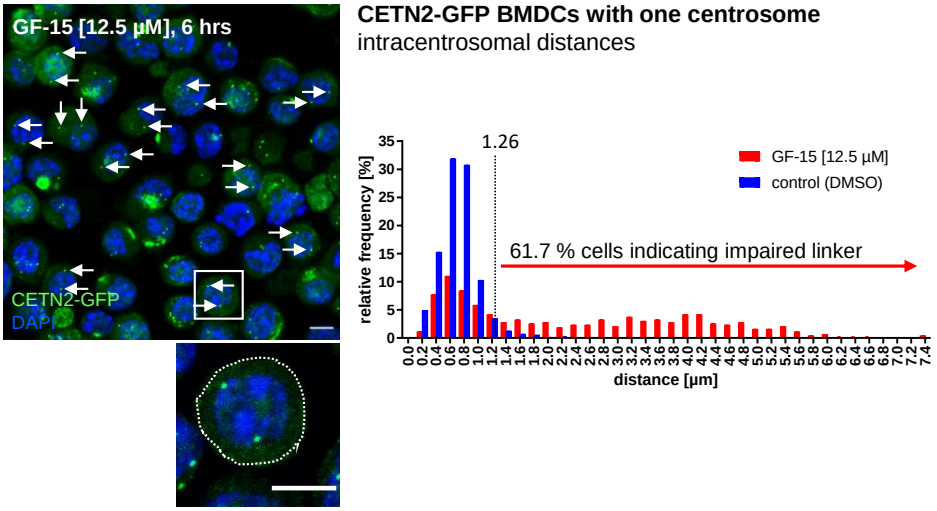
GF-15 [12.5 µM], 6 hrs
CETN2-GFP
DAPI
CETN2-GFP BMDCs with one centrosome
intracentrosomal distances
1.26
GF-15 [12.5 µM]
control (DMSO)
61.7 % cells indicating impaired linker
relative frequency [%]
distance [µm]

c

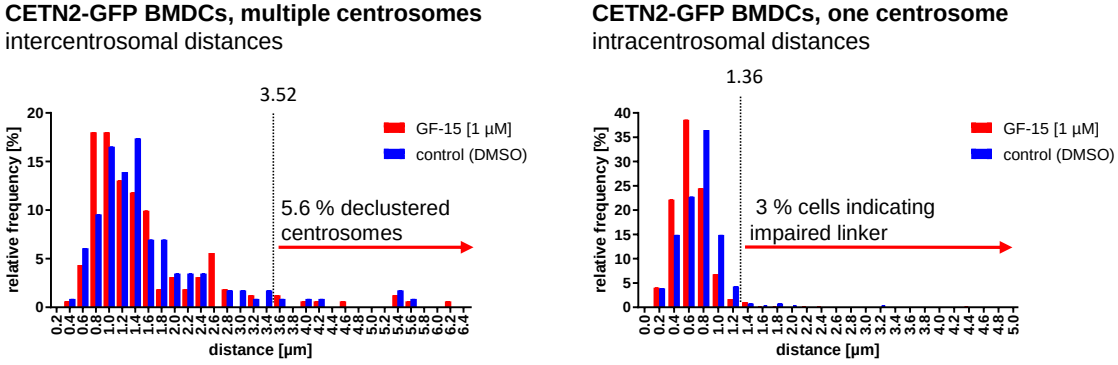
CETN2-GFP BMDCs, multiple centrosomes
intercentrosomal distances
3.52
GF-15 [1 µM]
control (DMSO)
5.6 % declustered centrosomes
relative frequency [%]
distance [µm]
CETN2-GFP BMDCs, one centrosome
intracentrosomal distances
1.36
GF-15 [1 µM]
control (DMSO)
3 % cells indicating impaired linker
relative frequency [%]
distance [µm]

d

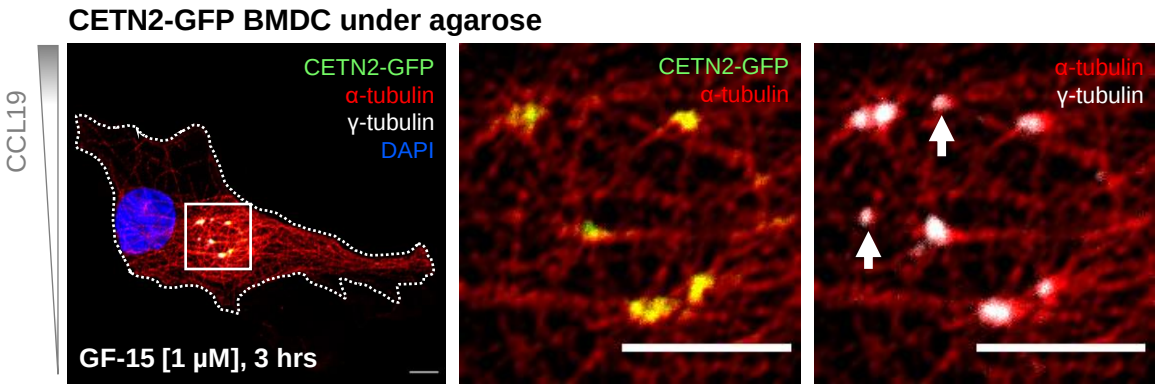

Figure 25. GF-15 has severe side effects on dendritic cells with one and multiple centrosomes

(**a**) IF staining of MT filaments in GF-15 treated (12.5 µM, 6 hrs) mature WT BMDCs with multiple (upper panel) and one centrosome(s) (lower panel) fixed during migration under agarose toward a chemokine source. Individual and indicated merged channels of ac-tubulin (green), γ-tubulin (grey) and α-tubulin (red) are shown. Nuclei were stained with DAPI. Post-processing of images: deconvolution. Dotted white lines mark cell outline. Scale bars: 5 µm. (**b**) Left: Representative image of mature fixed CETN2-GFP expressing BMDCs after treatment with GF-15 (12.5 µM, 6 hrs). Nuclei were stained with DAPI. White arrows mark scattered centrioles in cells with only one centrosome. White box marks region of magnification showing one representative cell with one centrosome and scattered centrioles. Dotted white line depicts cell outline. Scale bars: 5 µm. Right: Corresponding histogram showing relative frequencies of intracentrosomal distances from N = 541 DMSO treated (control, blue) and N = 426 GF-15 treated (12.5 µM, 6 hrs,red) fixed mature CETN2-GFP expressing BMDCs with one centrosome. Based on the mean of the distances in control cells and the corresponding standard deviation (SD), a threshold was defined (mean + 2× SD, black dotted line), beyond which centrosomal integrity is considered destroyed. (**c**) Histograms showing relative frequencies of intercentrosomal (left) and intracentrosomal (right) distances in fixed mature CETN2-GFP expressing BMDCs with multiple and one centrosome(s), respectively, after treatment with a lower concentration of GF-15 (1 µM, 6 hrs, red) or control treatment (DMSO, blue). The threshold for defining when centrosomes are considered declustered (left) and centrosomal integrity is considered destroyed (right) is calculated as described in b). Numbers of analyzed cells with multiple and one centrosome(s): N = 115 (DMSO), N = 161 (GF-15) and N = 255 (DMSO), N = 469 (GF-15), respectively. (**d**) IF staining against α-tubulin and γ-tubulin for visualization of MT filaments and PCM, respectively, in mature CETN2-GFP expressing BMDC with multiple centrosomes fixed during migration under agarose toward a chemokine source after treatment with GF-15 in a lower concentration and shorter incubation time than previously (1 µM, 3 hrs). Indicated merged channels of CETN2-GFP (green), α-tubulin (red) and γ-tubulin (grey) are shown. Nucleus was stained with DAPI. Post-processing of image: deconvolution. Dotted white line represents cell outline. White box marks area of magnification showing scattered centrosomes/centrioles. White arrows indicate acentrosomal PCM. Cell does not show a polarized morphology. Scale bars: 5 µm.

To test whether the observed side effects depend on the drug type, we switched to PJ-34, a compound of a different chemical class inducing centrosomal declustering to a lesser extent than GF-15 (15 vs. 64 %), as shown in fixed BMDCs (Fig. 23 c). We found that PJ-34 (50 µM, 3 hrs incubation) also showed a much lower impairment of the integrity of single centrosomes, as analyses of intracentrosomal distances demonstrate (Fig. 26 a). *In situ* ear sheet assays with PJ-34 (25 and 50 µM, 48 hrs) and water control showed a concentration-dependent impairment of DC migration (Fig. 26 b). IF stainings of PJ-34 treated mature CETN2-GFP expressing BMDCs that have migrated under agarose revealed that multiple centrosomes were successfully declustered (Fig. 26 c, green arrows) and MTs themselves showed an intact appearance, but PCM spreading was very pronounced, resulting in a large number of additional acentrosomal MTOCs similar to GF-15 (Fig. 26 c, white arrows). In the light of these side effects, it is difficult to dissect to what extent declustering contributes to migration effects, such as those we observed in the ear sheet assay (Fig. 26 b).

a

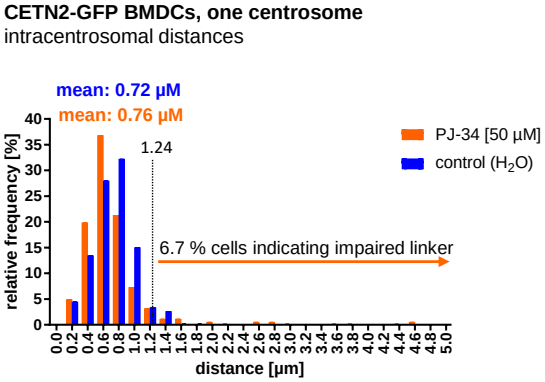

b

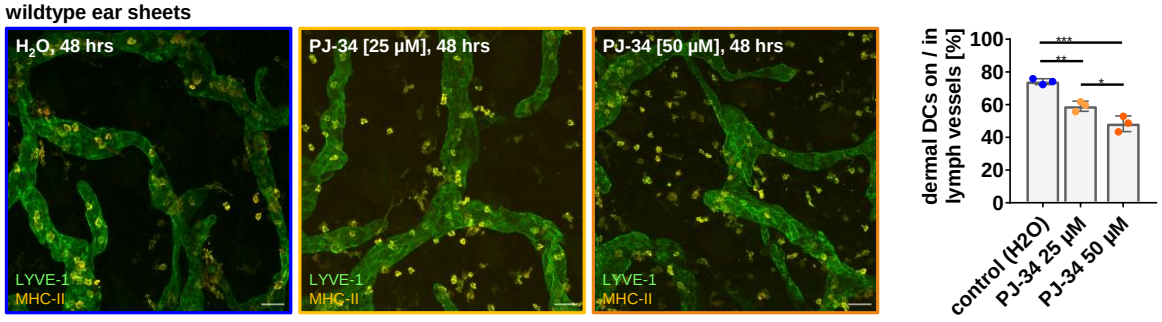

c

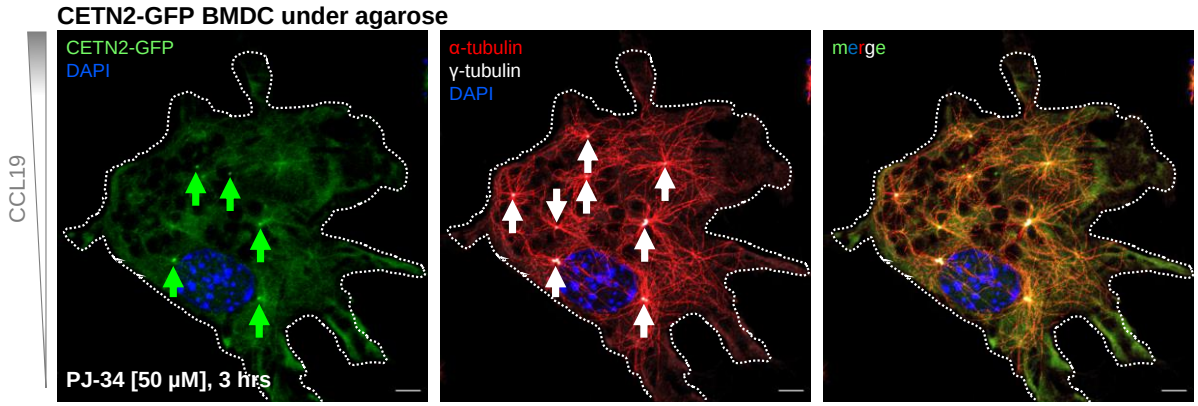

Figure 26. PJ-34 as an alternative declustering agent to GF-15 has less severe but still adverse side effects on dendritic cells

(**a**) Histogram showing relative frequencies of intracentrosomal distances from N = 378 control treated (water, blue) and N = 342 PJ-34 treated (50 µM, 3 hrs, orange) fixed mature CETN2-GFP expressing BMDCs with one centrosome. Threshold beyond which centrosomal integrity is considered destroyed (mean distance in control cells + 2× SD) is depicted as black dotted line. (**b**) Left: IF *in situ* staining of lymphatic vessels via LYVE-1 (green) and dermal DCs via MHC-II (orange) after control (water, left) or PJ-34 treatment (25 µM middle, 50 µM right) for 48 hrs. Scale bar: 50 µm. Right: Quantification of dermal DCs that are located on or in the vessels. Graph displays mean values ± SD with cells from N = 28 (water, blue), N = 27 (PJ-34, 25 µM, light orange) and N = 26 (PJ-34, 50 µM, dark orange) images of ear sheets from 5 different mice (counted cells: 3068 control, 2478 PJ-34 25 µM, 2734 PJ-34 25 µM treated). */**/***, P = 0.0205/0.0042/0.0002 (one-way ANOVA followed by Tukey-Kramer test). (**c**) IF staining against α-tubulin and γ-tubulin for visualization of MT filaments and PCM, respectively, in mature CETN2-GFP expressing BMDC with multiple centrosomes fixed during migration under agarose toward a chemokine source after treatment with PJ-34 (50 µM, 3 hrs). Indicated merged channels of CETN2-GFP (green), α-tubulin (red) and γ-tubulin (grey) are shown. Nucleus was stained with DAPI. Post-processing of image: deconvolution. Dotted white line marks cell outline. Green and white arrows indicate single scattered centrioles and acentrosomal MTOCs, respectively. Cell does not show a polarized configuration. Scale bars: 5 µm

Table 1 provides an overview of some of the experiments performed with the declustering compounds GF-15 and PJ-34, thereby listing side effects, drug potency, inter- and intracentrosomal distances, among others. Figure 27 summarizes the distance analyses graphically. Note that, with the exception of treatment with GF-15 (12.5 µM), the variance of the values was very low in cells with only one centrosome regardless of drug or control treatment, and also in untreated cells with multiple centrosomes hardly any variance was found.

Table 1. Overview declustering conditions

CETN2-GFP BMDCs

treatment	AC [%]	decl. cells [%]	thresh -old [µm]	side effects	1 centros.: mean intra-centr. dist. [µm] (SD)	≥ 2 centros.: mean inter-centr. dist. [µm] (SD)	analyzed cells total
DMSO, 6 hrs	22		2.89		0.7 (0.28)	1.53 (0.68)	695
GF-15 12.5 µM, 6 hrs	21.3	64		MTs atrophied, linker impaired*	2.43 (1.7)	3.91 (2.06)	541
GF-15 6.25 µM, 6 hrs				MTs atrophied			
DMSO, 3 hrs	25.5		3.36		0.72 (0.26)	1.59 (0.89)	499
DMSO, 6 hrs	31.1		3.52		0.74 (0.31)	1.6 (0.96)	370
GF-15 1 µM, 3 hrs	30.6	3.8		MTs intact, linker impaired*, PCM spreaded	0.70 (0.31)	1.37 (0.74)	431
GF-15 1 µM, 6 hrs	25.6	5.6			0.65 (0.31)	1.54 (1.0)	630
DMSO, 3 hrs	31.7		3.19		0.71 (0.29)	1.54 (0.82)	536
GF-15 0.5 µM, 3 hrs	30.2	10.6		MTs intact, few cases of impaired linker* + spreaded PCM	0.7 (0.27)	1.7 (1.02)	563
GF-15 0.1 µM, 3 hrs				MTs curly/ tensionless, rare cases of spreaded PCM + impaired linker*			
H_2O	33.9		3.2		0.72 (0.26)	1.61 (0.79)	572
PJ-34 50 µM, 3 hrs	28.8	15		MT intact, PCM spreaded, linker impaired*	0.76 (0.63)	2.11 (1.48)	480
H_2O	22		3.0		0.68 (0.25)	1.46 (0.77)	541
PJ-34 50 µM, 16/24 hrs	23.5	13.4		inconspicuous, only 5 images	0.74 (0.67)	1.77 (1.56)	285
PJ-34 25 µM, 3+6 hrs				MT intact, few cases of PCM spreading + impaired linker*			

AC: additional centrosomes (> 1); centros.: centrosome; decl.: declustered; dist.: distance; hrs: hours; intercent.: intercentriolar; intracent.: intracentriolar; MTs: microtubules; PCM: pericentriolar material; SD: standard deviation. Related test series are separated from each other by thick black lines.

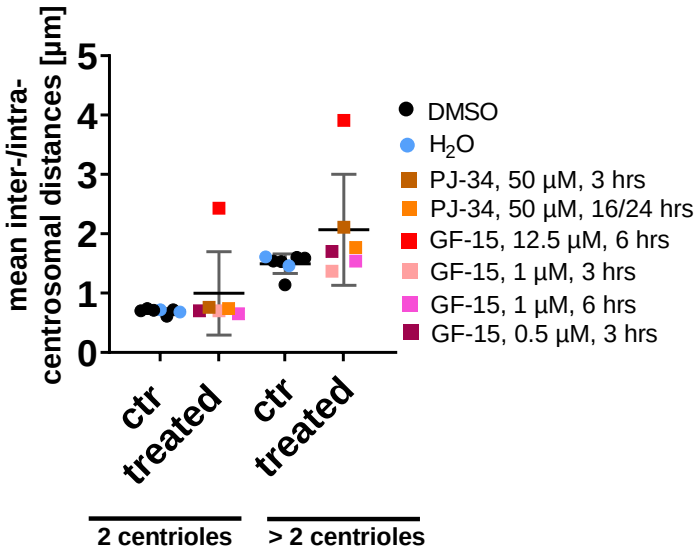

Figure 27. Inter- and intracentrosomal distances in declustering agent treated and control BMDCs

Visualization of inter- and intracentrosomal distances listed in Tab. 1, displayed by centriole number. Data derive from experiments with fixed mature CETN2-GFP expressing BMDCs previously treated with the indicated declustering agent or the corresponding control (ctr).

Overall, we found that declustering drugs cause varying degrees of centrosomal declustering in BMDCs with extra centrosomes and impair migration of dermal DCs in tissues as well as locomotion of BMDCs *in vitro*. Due to drug-induced side effects that affect cell polarization and directed migration, such as potential centrosomal linker impairment and PCM spreading, it was not possible to decipher the contribution of centrosome declustering to the observed migratory impairment. Therefore, the approach of chemical declustering in its present form cannot help to unequivocally answer the question of whether a clustered centrosomal configuration is required for proper cell migration. However, we found that the drugs – known for their effects in cancer cells – also induce declustering in non-malignant cells (BMDCs) with supernumerary centrosomes. Here, we observed that drug induced adverse events in BMDCs occur already far below drug concentrations that are considered side effect-free in trials with cancer cells. Moreover, we found that declustering agents were not specific for cells with extra centrosomes as stated in the literature[395–397]; instead, they also affect cells with normal centrosome numbers, as we have seen from the disturbance of the configuration of centriole pairs in BMDCs with one centrosome.

4 Discussion

4.1 Primary and peripheral dendritic cells have excess centrosomes

Most non-malignant cells harbor one centrosome in G1 phase and – after duplication in S phase – two centrosomes in G2 and M phase[255,349]. The presence of two or more centrosomes is a typical feature of cancer cells and is rarely found in non-malignant cells[336,337]. Interestingly, analysis of centrosome numbers in mature primary DCs, generated from murine bone marrow, and tissue resident DCs revealed that, at 20-30 %, a non-negligible proportion of cells carries two and more centrosomes[370]. In contrast, centrosome numbers in immature BMDCs were predominantly regular, suggesting that the emergence of excess centrosomes is related to the process of maturation. Quantification of centrosome numbers required high resolution of centriolar structures allowing us to resolve distinct centrioles. Although many of the tested antibodies gave unsatisfying results when trying to label single centrioles (data not shown) we were able to assess centrosome numbers with antibodies against ac-tubulin, CEP135 and with the use of cells generated from CETN2-GFP reporter mice that express a GFP-labeled version of the cetriolar protein centrin2. Visualizing the PCM worked well by staining the PCM proteins Cdk5Rap2 (not shown) and γ-tubulin, but is not well suited to resolve individual centrioles because of the diffuse staining pattern. Since ac-tubulin is not a genuine centriolar marker and to prove that CETN2-GFP overexpression does not trigger centrosome amplification, we verified our analysis by staining the centriolar protein CEP135. We demonstrated a clear “triple-colocalization” of ac-tubulin, CEP135, γ-tubulin in WT cells and CETN2-GFP, CEP135, γ-tubulin in CETN2-GFP cells, ensuring that we precisely stained and counted *bona fide* centrosomes.

Deviations in counting centrosomes when using different proteins for visualization and counting most likely are a result of the spatial organization of the respective centriolar marker. While the whole centriolar cylinder consists of ac-tubulin units, CEP135 and centrin are localized at the proximal and distal end of a centriole, respectively (see Fig. 10). Due to the small distance between the two proximal centriole ends, the two cylinders may not be resolved properly when staining CEP135 potentially leading to an underestimation of centrosome numbers[407].

Multinumerous centrosomes were not only observed in BMDCs and isolated dermal DCs but also in DCs within tissues suggesting that the phenomenon of additional centrosomes is not caused by the crawl out process or culture conditions. To our knowledge, the presence of extra

centrosomes has not yet been detected in immune cells and opens a multitude of questions, some of which have been further addressed in this work.

Multiple centrosomes have previously been observed in trophoblasts[408,409], megakaryocytes[410] and cycling progenitors of olfactory sensory neurons[411]. In addition, some highly differentiated cell types such as hepatocytes[412] and osteoclasts[413] show supernumerary centrosomes, as do multiciliated cells, for instance, in the ventricles of the adult brain, the respiratory and reproductive tracts of vertebrates[414]. While these findings suggest that cells with excess centrosomes are part of physiological developmental and differentiation processes, the presence of multinumerous centrosomes is also well known from cancer/malignant cells[336]. It has long been debated whether aberrant centrosome numbers are a cause or consequence of tumorigenesis, but there is increasing evidence that centrosome amplification can cause chromosomal instability and tumor onset[328–330]. Moreover, amplified centrosomes have been shown to confer beneficial properties to malignant cells and are positively associated with tumor aggressiveness[328,329,337,392,415–418]. Indeed, cell division of cancer cells with multiple centrosomes often leads to lagging chromosomes and low-grade (non-lethal) chromosome missegregation[419] which can result in aneuploid daughter cells that have a proliferation or survival advantage conferring (more) malignant properties to the cell[419,420].

To expand the knowledge of supernumerary centrosomes and their origin, it might be informative to look for additional centrosomes in pDCs, which develop differently from cDCs and leave the bone marrow as terminally differentiated cells. Furthermore, the study of mo-DCs and other immune cells beyond DCs may provide deeper insights into the occurrence of multinumerous centrosomes in the immune system and the potential uniqueness of the phenomenon for specific cell types. In addition, it would be interesting to study the situation of centrosomes in DCs of other species, especially in human samples. Also, systematic analysis of different TLR agonists to stimulate DCs together with the respective stimulus-specific transcriptional programs may provide further insight into the biology of supernumerary centrosomes in DCs.

Beside the number of centrosomes, it might be interesting to take a closer look at structural aspects of excess centrosomes in DCs trying to find out whether there are differences to “regular” centrosomes. Cancer cells, for instance, often exhibit structural abnormalities of centrosomes in addition to numerical aberrations, which is reflected by altered centrosome size/shape or centriole length[332,421,422]. In these cases, the regulation of centrosomal proteins and/or their PTMs is disrupted[423,424] which can lead to enhanced or suppressed intracellular MT nucleation thus potentially influencing cell shape, polarity, motility and/or the potential to metastasize[424,425].

4.2 Cell cycle modifications are responsible for the emergence of extra centrosomes in dendritic cells

4.2.1 Activated dendritic cells arrest in G1 phase of the cell cycle

Differentiated DCs were shown to have a low turnover rate[42], making it unlikely that the excess of centrosomes we observed in mature BMDCs and tissue resident DCs arise from ongoing cell proliferation. However, to investigate this issue, we stained for the proliferation markers EdU in mature BMDCs and dermal DCs in murine ear sheets as well as pH3 in mature BMDCs. IF analysis revealed only few positive signals in the analyzed cell populations indicating that multinumerous centrosomes are not a result of ongoing cell cycling processes.

In a next step, we examined whether the cells arrest during the cell cycle, for which we made use of cyclins, Cdks and Cdk inhibitors. In contrast to mature BMDCs and dermal DCs, only immature BMDCs expressed high levels of the typical S/G2/M phase cyclins (A2 and B1), confirming that only immature DCs are actively cycling; cyclin E1, on the other hand, was found in all maturation stages. While immature cells showed high levels of cyclin E1 as a snap shot from the cell cycle when the cells pass G1 phase during cycling, mature/activated (arrested) DCs *retain* high levels of cyclin E in G1 phase.

Compared to other cyclins, cyclin D1 expression levels do not reach a high or distinct expression peak in proliferating cells (see Fig. 15 a). Thus, this cyclin is not an optimal marker to distinguish cell cycle phases from one another – a fact that also applies to its binding partner Cdk4. Additionally, cyclin D1's minor expression levels may explain why overall Cdk4 levels were comparatively low (see Fig. 15 b, middle panel). The insufficient informative value of Cdk4 as well as its low protein levels in dermal DCs and the limited number of dermal cells prompted us to test Cdks only in BMDCs but not in dermal DCs.

In addition to the cyclins, Cdks and Cdk inhibitors shown, we tested further markers to obtain information about a cell cycle arrest. Preferred markers were geminin and *chromatin licensing and DNA replication factor 1* (Cdt1), replication licensing factors whose levels oscillate inversely during the cell cycle[426]; while Cdt1 levels peak during G1 and drop after initiation of S phase[427], geminin levels are highest during S/G2/M phase[428,429]. Unfortunately, no antibody against Cdt1 worked in our assays (data not shown). Finally, we received the possibility to get information about the phase of the cell cycle arrest with a more elegant method, the use of *fluorescent ubiquitination-based cell cycle indicator* (FUCCI) transgenic mice. The principle according to which phases are distinguished is also based on the cell cycle regulators Cdt1 and geminin: A fragment of Cdt 1 and geminin, respectively, is fused to different fluorescing proteins[426] resulting in FUCCI cell-nuclei that fluoresce in different colors depending on the cell

cycle phase they are in (G1: red, S/G2/M: green). Newly generated daughter cells are colorless since geminin degrades rapidly in late M phase while Cdt1 is expressed in early G1 phase. Orange cells, on the other hand, appear when both Cdt1 and geminin are present (G1-S transition)[426]. After generating BMDCs from FUCCI mice, we quantified all cells according to their colors and showed that 25 hrs after LSP stimulation the majority (about 98 %) of cells appeared red or colorless indicating that mature BMDCs rest in G1 phase of the cell cycle (Fig. 28)[370].

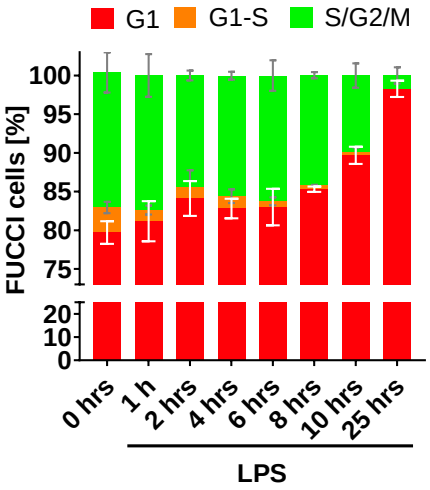

Figure 28. Determination of the cell cycle phase in which mature BMDCs and dermal DCs arrest

Quantification of the proportions of FUCCI-derived BMDCs in the indicated cell cycle phases after different time periods of stimulation with LPS. Graph displays mean values ± SD of three independent experiments (analyzed cells per condition: ≥ 228). Bone marrow from FUCCI mice was kindly provided by Prof. Andreas Villunger, Institute for Developmental Immunology, Biocenter, Medical University of Innsbruck, Austria. Generation and cultivation of FUCCI-derived BMDCs was done by Ann-Kathrin Weier.
FUCCI: fluorescent ubiquitination-based cell cycle indicator

A similar arrest of the cell cycle after stimulation is known from studies with lentiviruses and CD4 T lymphocytes, a T lymphoblastoid cell line and several mammalian cell lines[430–432]. The human *immunodeficiency virus type 1* (HIV-1) protein *Viral Protein R* (Vpr) for example as well as primate lentiviruses other than HIV-1 induce a cell cycle arrest in G2/M by keeping Cdk1 in the phosphorylated (inactive) state thus preventing the activation of the Cdk1/cyclin B complex which is required for entry into M phase[430,431]. The aim behind is thought to be the delay or prevention of apoptosis of infected cells increasing the amount of virus[431].

In summary, using different approaches, we showed that the proliferative capacity of DCs after activation is negligible *in vitro* and *in situ* and we reliably demonstrated that mature DCs arrest in G1 phase of the cell cycle.

4.2.2 Additional centrosomes in dendritic cells emerge through several pathways

4.2.2.1 Premature mitotic exit

With the help of the FUCCI system[426] we were able to clearly show that mature BMDCs arrest in G1 phase of the cell cycle. Additionally, we unraveled that the population of G1 arrested cells consists of 2N and 4N cells rising the question of how tetraploid cells (carrying two or more centrosomes) can occur in G1. The presence of 4N cells in G1 phase indicates an incomplete mitosis.

To investigate mitosis of DCs in more detail, we analyzed the levels of BubR1 and cyclin B1 during maturation in immunoblot analysis and found an opposite development: While cyclin B levels continued to decrease and eventually became undetectable, BubR1 levels increased and persisted on the same level in the absence of cyclin B indicating mitotic slippage (see Fig. 17 b, right panel). These findings are in line with the current paradigm stating that a mechanism behind/triggering this process is the successive degradation of cyclin B1 during prolonged mitotic arrest[381]. There are currently two hypotheses as to why cyclin B1 can be degraded in the presence of an active SAC: The first one suggests a low APC/C activity, which is able to escape SAC-mediated inhibition leading to the leakage of cyclin B1 degradation[376]. A second hypothesis proposes that a fatigue in SAC activation and/or strengthening of SAC-inactivating mechanisms weakens the SAC gradually leading to cyclin B1 degradation[376]. Recently, data appeared that support the second hypothesis: Reduction of Mad2 at kinetochores of cells during mitotic arrest weakens the SAC, which in turn enables the proteasomal degradation of cyclin B by APC/C promoting mitotic slippage[376].

In accordance with the indications on mitotic slippage from immunoblot analysis, IF stainings in BMDCs revealed that chromosomal accumulation of BubR1 did not decrease at metaphase and was even clearly detectable in anaphase, a stage in which BubR1 signals are normally absent[374,382]. At this point, kinetochore stainings would have been advantageous, but were not successful so that we restricted ourselves to visualizing the DNA using DAPI. Although our IF findings do not *prove* the presence of mitotic slippage due to lack of kinetochore stainings, they strongly indicate a premature mitotic exit in combination with the results from our immunoblot experiments explaining the presence of mononucleted 4N cells with two centrosomes in G1 phase. A BubR1 reporter construct for live cell imaging could be suitable to study the process of mitotic slippage in more detail.

A modified cell cycle with conversion from diploidy to polyploidy (and the emergence of multiple centrosomes), as it is known from the development of other highly differentiated cells, can be part of a developmental program that physiologically produces polyploid progeny. In this

context, a mitotic slippage like phenomenon, also known as “endomitosis”[343], is for example used by **megakaryocytes** upon maturation leading to globulated polyploid nuclei[433–435]. After entering mitosis, the cells start to condense chromosomes and at most anaphase A can be achieved, but then fully separation of sister chromatids does not occur, nor cytokinesis[436–438]. Instead, cells enter a G1-like state, re-enter S phase and start another round of endomitosis[439]. Besides this form of endomitosis (no nuclear division, no cytokinesis), an endomitotic cycle variant is known, in which nuclear division occurs without cytokinesis leading to multinucleated polyploid giant cells[440]. This form of abortive mitosis occurs in postnatal **cardiomyocytes**[441], mammalian **hepatocytes**[412,442] and **osteoclasts**[443]. **Placental trophoblast giant cells** in turn have skipped mitosis altogether (endocycling or endoreduplication) and appear as mononucleated polyploid cells[436,444]. Another mechanism that leads to multinumerous centrosomes is **cell fusion**. These fusion events occur in very specific processes during development, such as syncytiotrophoblast cell formation in the mammalian placenta through the fusion of post-mitotic diploid progenitor cells[408,444] or the formation of osteoclasts from precursors[445]. Similarly, mature skeletal myotubes arise from the fusion of myoblasts[413,446]. The pathway of cell fusion is also being discussed for the emergence of polyploidy in hepatocytes[447]. Most of the described pathways are accompanied by the emergence of multiple centrosomes, however, this is not necessarily the case, as shown by the differentiation process of muscle cells, in which centrioles are lost upon fusion[312,448,449].

The process of mitotic slippage is also known from non-physiological conditions. Prolonged mitosis can result in cell death – a fate **cancer cells** try to avoid and therapeutic approaches are taking advantage of. Antimitotic therapies such as antimicrotubule drugs perturbe MT dynamics leading to sustained activation of the SAC and mitotic arrest[344,450]. In some cases, arrested cells undergo mitotic cell death (“mitotic catastrophe“) explaining the anti-proliferative effect of antimicrotubule drugs[344]. However, cancer cells often acquire resistance mechanisms helping them to circumvent mitotic cell death and prematurely exit mitosis via mitotic slippage[343]. When “slipping” from mitosis to interphase without undergoing proper chromosome segregation and cytokinesis, tetraploid multinucleated cells arise that either arrest in G1 phase, die as post-slippage cells or continue cycling as genomically unstable cells[344]. The premature exit from drug-induced mitotic arrest to avoid subsequent cell death is thought to be a major mechanism contributing to patient resistance to such drugs[343].

Just like the non-malignant and malignant cells listed above, activated DCs undergo an alternative mitosis thereby increasing their centrosome number, but different from many of the others, they arrest in G1 afterwards. This might be a reason why DCs – in contrast to cancer cells[420,451] that can go on cycling with a magnitude of centrioles potentially promoting their

malignancy – can "afford" multiple centrosomes without running the risk of accumulating defects and becoming malignant (see next section).

4.2.2.2 Cytokinesis failure

Beside the process of mitotic slippage, which is mainly responsible for the presence of mononucleated 4N DCs[370], we observed some other mitotic peculiarities after LPS stimulation. We found evidence of cytokinesis failure in BMDCs, resulting in mononucleated and binucleated 4N cells with excess centrosomes. Other outgrowth of and reason for abortive cytokinesis was the presence of anaphase bridges, i.e., chromatin structures in the cleavage plane leading to polyploid cells[384]. Binucleated cells as well as chromosome bridges or lagging chromosomes (not shown) can be caused by overriding the checkpoint leading to premature chromosome separation and anaphase onset without prolonged mitotic arrest[383,452]. The presence of BubR1 at chromosomes of anaphase BMDCs (see Fig. 17 c, right panel) indicates that the cells progressed into mitosis in the presence of an active SAC. Overriding the SAC implies a weak checkpoint and might be dangerous, since there are still unattached or not properly attached kinetochores potentially resulting in aneuploidy[453]. Aneuploidy is considered a hallmark of cancer[454] and can drive tumorigenesis although recent findings show that an aneuploid karyotype is not a universal promoter of tumorigenesis[455,456]. For activated DCs, the occurrence of aneuploidy is most likely not a dangerous event to the organism since mature BMDCs and tissue resident DCs are terminally differentiated cells with only low proliferative capacity[42] and a short life-span[457,458] reducing the risk of malignant cell transformation. Accordingly, tumors very rarely arise from DCs. DC neoplasms can affect the lymphatic system as well as extranodal sites[459] but due to the small number of patients and the incompleteness of published data only little is known about incidences and prevalences (for example, the incidence of blastic plasmacytoid DC neoplasm is 0.000045 %)[459,460]. Moreover, cancer originating from DCs is very heterogeneous making it difficult to draw conclusions from single case studies.

In summary, we found that mature BMDCs and dermal DCs arrest in G1 phase and we demonstrated for BMDCs that this population contains diploid and tetraploid cells. One proportion of 4N cells arises from a modified cell division cycle the cells go through. After LPS stimulation, the cells that have already passed the G1 restriction point duplicate their DNA and centrosome in S phase, before they enter M phase. Here, suppression of mitosis takes place with a proportion of cells exiting mitosis prematurely via mitotic slippage ending up as mononucleated 4N cells in G1 phase carrying two centrosomes. Another proportion of G1 arrested 4N cells results from cytokinesis failures during mitosis giving rise to mono- and

binucleated cells with double number of centrosomes as well as mitotic figures such as chromosome bridges or lagging chromosomes. Similar to what we observed in activated murine DCs, some non-malignant human cells were shown to exit the cell cycle and undergo polyploidization in response to physiological or pathological stimuli, such as injury, hypoxia, starvation, temperature, and aging[440]. For instance, there is evidence that hypertension is associated with polyploidization of heart muscle and vascular smooth muscle cells[461,462]. Whether LPS or mechanical stimuli that we use to induce murine DC activation can be classified as comparable stimuli to those described above is not yet known.

4.2.2.3 Centriole overduplication

In addition to differentiated tetraploid DCs with two centrosomes, we found 4N cells with more than two centrosomes and 2N BMDCs with two and more centrosomes suggesting that centrosome accumulation due to incomplete mitosis is not the only mechanism for the emergence of multinumerous centrosomes in G1 arrested DCs.

Besides the centrosome, the DNA is also duplicated exactly once per cell cycle. Under physiological conditions, the two cycles are coordinated: In case of a delay of the chromosome cycle, the centrosome cycle stops preventing the production of extra centrosomes[252]. If this coordination gets lost, a mechanism called “(over)duplication” can cause extra centrosomes. Overduplication is a phenomenon well known from cancer cells[338–340] and has been identified in melanoma cells as the major pathway for the development of excess centrosomes[338]. During overduplication observed in cancer cells, DNA and centriole duplication are uncoupled[333,463] resulting in an untimely centriole duplication, i.e., centrioles continue to duplicate while DNA duplication has stopped[341,342]. Keyplayers of the centriole duplication cycle are PLK2 and PLK4. Experimentally, centrosome amplification was induced by PLK4 overexpression in a human osteosarcoma cell line[267,464] and in flies[465], whereby this occurs through the simultaneous generation of multiple procentrioles in S phase[464]. Similar evidence was found for PLK2 overexpression in malignant and non-malignant cells[269].

While suppressed mitosis and cell fusion are mostly accompanied by tetraploidy and two centrosomes (four centrioles), overduplication can cause considerably more centrioles and is independent from ploidy. This is exactly what we observed in a proportion of differentiated DCs, giving a first hint that centriole overduplication may play a role for the emergence of excess centrosomes in DCs. This suspicion was supported by our group by showing that PLK2 upregulation upon LPS stimulation leads to centriolar overduplication in BMDCs[370]. In this context, it might be also worthwhile to further investigate the nucleolar protein nucleophosmin, which is involved in the process of centriole duplication [466].

In summary, multinumerous centrosomes in activated DCs arise by two pathways, occurring in equal proportions of about 50 %[370]. 2N cells in G1 phase have acquired their extra centrosomes through **centriole overduplication**, while 4N cells harbor multiple centrosomes due to **centrosome accumulation** during abortive (incomplete) mitosis or due to a combination of both processes resulting in approximately 30 % of cells having additional centrosomes[370]. Both pathways are known from neoplasia development[467], but the combined occurrence has not yet been described in a physiological context.

It has not yet been clarified whether it would in principle be possible for DCs to increase the proportion of cells with extra centrosomes beyond 30 % after LPS stimulation. This issue is for instance also related to the question of whether *all* cells that have passed the restriction point in G1 at the time of stimulus acquire additional centrosomes or whether there might be a “cell reservoir” from which further cells with multiple centrosomes can arise. Moreover, in preliminary experiments with different TLR agonists, we observed that the proportion of DCs with additional centrosomes varies depending on the stimulus. In addition, we discovered that mature BMDCs stored under non-optimal culture conditions, in our case in a *non-humidified* environment, had a strikingly higher poportion of cells with multiple centrosomes and, moreover, remarkably more centrosomes per cell. This suggests that the formation of extra centrosomes may be related in some way to adaptation processes and/or stress responses. Therefore, it might be of interest to systematically expose DCs to different stimuli and cellular stressors and investigate the percentage of cells with extra centrosomes and the amount of extra centrosomes per cell.

4.3 Supernumerary centrosomes affect dendritic cell migration

4.3.1 Multiple centrosomes stay close together during drastic cell shape changes

To get an impression of the spatial organization of centrosomes in DCs with one and multiple centrosome(s), we determined intracentrosomal and intercentrosomal distances in fixed BMDCs that have migrated under agarose as well as in BMDCs during migration along chemotactic gradients. Both parameters were slightly lower in fixed cells than during migration, possibly because forces acting on the centrioles during migration pull them apart. Intracentrosomal distances in migrating BMDCs were comparable in cells with one and multiple centrosome(s) while intercentrosomal distances were found to exceed intracentrosomal distances (see Fig. 18 c, lower panel). The latter finding might be explainable by the linker fibers that connect the two centrioles of a G1 phase centrosome and/or the

significant shape changes that DCs undergo during migration, which may also affect the localization of the centrosomes leading to higher intercentrosomal distances. However, considering the distances in absolute terms rather than comparing intra- and intercentrosomal distances, it is apparent that multiple centrosomes are located in close proximity to each other.

In DCs, we almost exclusively found intracentrosomal distances below 2 µm – a value that in many studies serves as threshold for intact centrosome cohesion. Regardless of the cell cycle stage, in case of an intracentrosomal (intercentriolar) distance of more than 2 µm, the connection is assumed to be destroyed ("centrosome splitting") as deduced from experiments with cancer cell lines[278,468,469]. Moreover, experiments with human *retinal pigmented epithelial* (RPE1) cells revealed that in the majority of cells, the two centrioles stay close together (< 2 µm) during interphase[406]. In outer hair cells, stereocilia-bearing sensory cells of the mammalian cochlea, the intercentriolar distance is less than 1 µm[470]. Similar results were found in centrosomes isolated from human, calf, mouse and rat thymocytes, bovine peripheral lymphocytes and from a human cell line of T lymphoblastic origin[471]. Besides, many other studies examining centrosomal cohesion with a plethora of cell types use an intercentriolar distance of 2 µm for the definition of centrosome splitting[276,468,472–475].

Centrosome splitting was observed, for instance, in cells lacking the linker (associated) proteins C-NAP1, rootletin or Cep68[277,472,473,475–477]. However, there are findings from experiments with human RPE1 cells suggesting that the loss of centrosomal linker function is a reversible event[406] indicating that the linker between two centrioles is a highly flexible structure[406]. Consistent with these findings are observations from experiments with neutrophils: After activation with a chemoattractant, transient centrosomal splitting occurs reaching intercentriolar distances of 8-10 µm, in some cells even higher[478]. It should be noted however, that the results of the migration studies come from experiments that – in contrast to our studies – were conducted in a uniform chemokine field leading to non-directional migration.

We also conducted preliminary studies with mature BMDCs migrating under agarose in a homogeneous chemokine field and observed that, as expected, the cells did not maintain their direction of migration for long and changed their shape permanently and sometimes drastically; nevertheless, the centrioles of single centrosomes as well as multiple centrosomes stayed close together all the time (not shown). Thus, we concluded that neither the chemokine gradient provides signals for the grouping (clustering) of centrosomes, nor are centrosomes passively forced together by the shape of the cells as they migrate toward the highest chemokine concentration. Furthermore, due to the low cell density in those assays (and later also confirmed in migration assays with a chemokine gradient and low cell density), we

excluded the possibility that migrating cells under agarose – and with them their centrioles/centrosomes – are squeezed together by neighboring cells.

Additionally, we demonstrated in mature BMDCs migrating in Y-formed channels that even during path decision making processes, which are often accompanied by extreme changes in cell shape due to mechanical deformations, multiple centrosomes stay close together. We do not assume that the narrow canals of the Y-channels foster a clustered configuration of extra centrosomes, since, for example, in under agarose migration assays multiple centrosomes also remained close together. Moreover, at the bifurcation, i.e., the point of decision making, cells showed two competing protrusions and the centrosome was subject to directional changes at this point (see Fig. 22 b), which opposes centrosomal compression by constriction. Despite this challenging circumstances, we found that the centrosomes stay close together suggesting that they are actively hold together.

In summary, using different assays and migration models, we were able to demonstrate that multiple centrosomes are located in close proximity to each other in fixed cells as well as during migration.

4.3.2 Dendritic cells with extra centrosomes show more microtubules and less actin around the centrosomes

Having confirmed the presence of multiple centrosomes in different types of DCs, we turned to functional aspects and investigated the significance of additional centrosomes for DC biology focussing on directional migration. To exclude potential effects of ploidy, we only included 2N cells in our analyses. In a first step, we analyzed the role of excess centrosomes as MTOC. After having found that MTOCs with multiple centrosomes are as functional in organizing MTs as their counterparts with one centrosome, we investigated in BMDCs whether there is a correlation between the surplus of centrosomes and the number of MTOC nucleated MTs (nucleation capacity). Analysis revealed a statistically significant difference between these two groups with cells carrying extra centrosomes nucleating about 33 % more MTs than cells with normal centrosome numbers. Performing this analysis in dermal DCs would have strengthened this finding, however, stainings of MT filaments in ear explants only worked well for fibroblasts and we did not succeed in resolving individual MTs in dermal DCs making valid MT counting impossible. What we have not yet investigated, but which may be of interest, is whether the structure of MTs in BMDCs with multiple centrosomes is altered in addition to the number.

Since centrosomes do not only function as MTOC but also as actin filament organizing center[326,327] we investigated the amount of centrosomal actin in BMDCs and found that, unlike

MTs, there was less centrosomal actin in cells with a surplus of centrosomes than in cells with normal centrosome content. This observation of an inverse relationship is in line with findings from other groups showing, for example, in interphase lymphocytes, that increasing density of centrosomal actin correlates with reduced amounts of MTs[327]. Others studied centrosomal actin nucleation during mitosis and found a burst in centrosomal actin as cells enter anaphase, which was accompanied by a decrease in centrosomal MT density[479]. Since the two filament types seem to compete for space around the centrosome, it is conceivable that steric issues could arise, such that "a plus of MTs filaments" as we found in 2N DCs with extra centrosomes may lower the capacity for actin polymerization.

Since the PCM plays an important role in MT nucleation, it seems worthwhile to study this component of the centrosome more intensively. Preliminary results from immunoblot experiments with 2N BMDCs indicate that cells with multinumerous centrosomes have more γ-tubulin than cells with only one centrosome. Since γ-tubulin is one of the PCM proteins that promote MT nucleation[298], more γ-tubulin could point to more PCM, which in turn could lead to more space for MTs (and consequently less for actin). Therefore, it might be interesting to pursue the question of whether more centrosomes are associated with more PCM (and therefore with enhanced MT nucleation capacity). In this context, PLK1 and whether altered levels lead to altered amounts of γ-tubulin may be of interest since PLK1 facilitates the recruitment of γ-tubulin[480].

The findings regarding MT nucleation capacity and the amount of PCM are diverse in the literature. Analysis of tissue from high grade human breast tumors, for example, revealed that multinumerous centrosomes exhibited increased MT nucleation compared to centrosomes of normal breast tissues, while centrosomes were characterized by an excess of PCM[332]. Studies from *tumor endothelial cells* (TECs) which often carry multinumerous centrosomes, showed that cells with supernumerary centrosomes had significantly less centrosomal γ-tubulin than control cells which was supposed to decrease MT nucleation[481]. However, it should be mentioned that we analyzed γ-tubulin levels in immunoblot analysis detecting total cell γ-tubulin, whereas the results from TECs come from IF analysis of centrosomal γ-tubulin. Another important difference to our results is that DCs predominantly exhibit a clustered centrosomal configuration whereas multiple centrosomes in the mentioned examples were scattered within the cytoplasm showing high intercentrosomal distances[332,481]. When comparing studies in terms of the number of nucleated MTs, it should be noted that in the presence of declustered centrosomes, there can be two types of quantification, counting MTs per cell and MTs per centrosome. Moreover, classification of centrosome status regarding "normal content" and "excess centrosomes" can differ between studies.

As an example of non-malignant cells where similar results to our DCs were found, studies with a human mammary epithelial cell line with inducible centrosome amplification/ accumulation can serve. Analysis revealed a clustered configuration of multiple centrosomes in interphase, elevated centrosomal γ-tubulin levels and increased centrosomal MT nucleation capacity[337]. However, in contrast to our findings, additional centrosomes in these cells were shown to promote features of malignant transformation (see also 4.3.4).

4.3.3 Directional persistence is significantly higher in dendritic cells with additional centrosomes

To explore the functional relevance of multinumerous centrosomes in DCs we followed activated 2N BMDCs during chemotactic migration under agarose and analyzed migration parameters at a single cell level. The same was done with dermal DCs isolated from ear sheets, but it was not possible to derive a threshold for ploidy via nucleus size here, as it was the case with BMDCs (see Fig. 16 a). It can be assumed that this might be feasible with higher numbers of dermal DCs, however, these experiments require a not insignificant number of test animals, which must be kept in mind. In both BMDCs and dermal DCs, we found no appreciable difference in migration velocity between cells with multiple and one centrosome(s), but directional persistence was significantly higher in cells with two or more centrosomes.

Euclidean distance analyses showed a trend of higher values in cells with additional centrosomes suggesting that these cells have moved further away from the starting point (point at which the cells were located at the start of the analysis) within the same time period than cells with only one centrosome. Transferred to a “real life setting“, such as the dermis of the skin, this could mean that activated DCs with excess centrosomes have already reached the lymphatic vasculature while cells with regular centrosome content have not yet come so far. To study this issue in more detail and strengthen our findings, *in vitro* migration assays in a competitive setting would be an option. Here, we would expect, that the first cells that arrive at a designated destination carry predominantly multinumerous centrosomes. However, such approaches require a common or comparable starting point and a sufficient number of cells to be retrieved, both of which are technically difficult to achieve. As a corresponding *in vivo* experiment, DCs could conceivably be sorted on diploid cells with one and multiple centrosomes, stained differently, and then injected as a mixture into the footpad of a mouse. After a defined period of time, the ears would then be analyzed to see if there are more cells with additional centrosomes in/on the lymphatic vessels of the dermis. However, this approach is experimentally very challenging.

At this point, modeling approaches and the inclusion of DC migration beyond a gradient setting can be useful. Modeling can help to overcome limitations in study design that may occur with certain questions. Preliminary results from studies with ear sheets, for example, revealed that direct analyses (e.g., the time cells with one and more centrosome(s) require to enter the lymphatics) in this physiological environment were not possible: Although imaging of centrioles in skin DCs located in/on lymphatic vessels was possible in principle, valid determination of centrosome numbers was not due to overlapping of the cells preventing a reliable assignment of the centrioles to the cells. In addition, extending analyses by *in vitro* migration experiments with homogeneously distributed or without chemokine seem necessary in this context, since *in vivo*, for example in dermal tissue, DCs do not permanently reside in a gradient environment. Instead, they are predominantly located somewhere between the lymphatics where they are not in close proximity to a vessel with its perilymphatic chemokine gradient (see Fig. 6). Therefore, it is important to understand the contribution of extra centrosomes to non-guided migration. Beyond the perilymphatic chemokine gradient, DCs have to migrate and find the vessel without external guidance cues, exhibiting a mode of locomotion described as persistent random walk motility, which is characterized by alternating phases of persistent movements and random walks (see section 1.2.3). The physiological relevance behind the mentioned *in vitro* assays is based on the questions I) how efficiently can DCs with different centrosome numbers navigate in uniform chemokine fields after activation and approach the zone of chemokine gradient in order to enter the lymphatic vessels and II) whether DCs with additional centrosomes also show a migration advantage under these conditions. In addition to velocity/accumulated distance and directional persistence as readout parameters, it would be interesting to determine and compare the scanned area of cells with one and multinumerous centrosome(s). From a physiological point of view, the interest behind this is to find out how comprehensively, accurately and quickly DCs scan their environment.

Here, migration parameters obtained from these assays, such as velocity and directional persistence, can be used for the calculation of the *mean square displacement* (MSD) which represents the squared distance between the cell and the tracking origin over time. The MSD as a measure of how far cells can move in time gives an impression on how directional persistence affects the distance that cells travel during a defined timeperiod. Migration data obtained can then be fitted to a suitable migration model, which for DCs would be a persistent random walk model. From the MSD analysis, the persistence time can be derived which is the time the cells migrate persistently before changing direction, i.e., the time until the next random walk phase begins, thus being a measure of the ability of a cell to maintain its direction of motion. With the mentioned parameters, it is possible to investigate the effect of extra centrosomes on migration using mathematical modeling. This provides information about the

time it takes for DCs with one and more centrosome(s) until they enter the lymphatic vessels and answers the questions, whether and to which extent cells with multiple centrosomes possess an advantage over cells with only one centrosome.

4.3.4 Enhanced persistent cell migration is caused by excess centrosomes

In order to ascertain whether multiple centrosomes are not only associated with, but also cause enhanced persistent locomotion we sought to remove (extra) centrosomes in migrating CETN2-GFP BMDCs via laser ablation techniques. The project required the identification of suitable laser settings that were sufficient to destroy centrosomes but mild enough to ensure cell function. To this end, we performed several pre-tests, including the analysis of remaining fluorescence intensity of the centrosome after laser exposure, which revealed a clear reduction of the fluorescence signal. Even though we could not definitely rule out the possibility that this was merely bleaching, we were able to switch off the centrosome as MTOC, as following IF stainings revealed: We performed control and full centrosomal laser ablations in CETN2-GFP expressing BMDCs migrating under agarose and stained the cells for MTs. Cells experiencing control ablations, consisting of laser treatment of an area in close proximity to the centrosomes, showed a normal cellular shape as well as regular looking MTs emanating from the centrosome. It is conceivable that a few MT filaments might have been destroyed by the control laser treatment but probably have regrown from the centrosome. After complete centrosomal ablation, however, the centrosome in its function as MTOC was destroyed, very likely going back to the fact that the loss of centrioles usually leads to PCM dispersal[266,296,482], which prevents the regrowth of MTs resulting in reduced MTs numbers. Moreover, we observed a decrease in MT filament length and a curly configuration after full centrosomal ablation compared to control treatment indicating a loss of tension. These findings led us to conclude that the technical conditions were suitable to efficiently switch off the centrosome as MTOC, so we used these settings for the following ablation experiments. Alternatives to laser ablation to eliminate centrosome's MTOC function could be *chromophore-assisted light inactivation* (CALI), which uses a phototoxic fluorescent protein for the light-induced inactivation of target proteins (in our study, centrosomal proteins including PCM components)[483], or the *PROteolysis TArgeting Chimera* (PROTAC) technique, that utilizes endogenous E3 ligases to degrade target proteins via the ubiquitin-proteasome system. PROTACs have also been available for some time with a light-inducible switch (opto-PROTACs) enabling the degradation of protein targets in a spatiotemporal manner[484]. Both approaches could be gentler than laser ablation techniques, but cannot be applied in primary cells, requiring another cellular system, such as *Homeobox B8* (HoxB8)-derived DCs.

We conducted laser ablation experiments in CETN2-GFP BMDCs during migration under agarose toward a chemokine source and measured migration velocity and persistence before and after laser treatment. We were not able to distinguish between 2N and 4N BMDCs, but since we analyzed migration parameters of one and the same cell before and after laser intervention, this was not mandatory. Control ablations that did not target the centrosomes did not influence persistent migration at all and velocity only showed a marginal decrease, the latter could be due to a disturbance of actin, the main driving force of DC locomotion[82,87]. Complete as well as partial centrosomal ablation led to a significant decrease in directional persistence compared with control-ablated cells; velocity, on the other hand, was only slightly reduced. These results demonstrate that the centrosome is decisive for directional persistent locomotion and, moreover, revealed a causal relationship between supernumerary centrosomes and enhanced persistent migration.

After having demonstrated that extra centrosomes lead to more efficient chemotaxis of BMDCs compared to BMDCs with one centrosome the question arises as to how exactly additional centrosomes improve persistent migration. One conceivable mechanism would be that multinumerous centrosomes contribute to stable polarization. Against the backdrop, that MTs are mainly responsible for persistent migration it is conceivable that our findings are due to the enhanced capacity of extra centrosomes to nucleate/anchor MT filaments. In addition to the function of MTs as asymmetric structure in generating front-back polarity, it is also worth recalling their function as tracks for the directed transport of new membrane and cytoskeletal components and signaling molecules to the leading edge to maintain polarity and directional persistent cell migration. Not to forget, MTs are able to resist high compressive loads thereby contributing to the formation and maintenance of membrane protrusions. Moreover, there is growing evidence that not only actin is driver of the pushing forces required for cell protrusions, but also MTs seem to contribute to providing pushing forces for cell protrusions/migration (reviewed in [87]). To prove the hypothesis that multiple centrosomes contribute to stable polarization, one of the next steps could be to analyze the amount and the size of lateral protrusions in DCs with one and multiple centrosome(s) to decipher whether lateral membrane extensions are correlated with the number of centrosomes. Based on our findings so far, we would expect that DCs with additional centrosomes exhibit fewer lateral protrusions being more “focused” on their goal giving preference to the protruding central membrane part over all lateral membrane outgrowths. MTs may also be an indirect driver of enhanced migration by influencing the Golgi apparatus, which is explained by the fact that centrosome nucleated radial MT arrays are crucial for the organization of a polarized Golgi apparatus during cell migration. There is evidence from cancer cells, that cells with multiple centrosomes nucleate more MT filaments and that this might provide an enriched signal for polarized Golgi assembly with a

possibly more pronounced cis-trans Golgi polarization allowing enhanced trafficking of vesicles with migration promoting factors to the leading edge (reviewed in [416]).

While we identified a potentially positive/advantageous role of supernumerary centrosomes for immune effector functions of DCs showing that additional centrosomes promote persistent chemotactic migration, multiple centrosomes in cancer cells have similar yet quite different effects. The excess of centrosomes in malignant cells appears to confer cytoskeletal advantages that enhance cell polarization and Golgi-dependent vesicular trafficking, but this favors stromal invasion and other aspects of metastatic progression. There is evidence from a human mammary epithelial cell line that acquires malignant characteristics after induced generation of extra centrosomes, as well as from tumor cells, that increased centrosomal MT nucleation occurring via clustered extra centrosomes results in increased Rac1 activity. This in turn can lead to invasive protrusions that disrupt normal cell-cell adhesions[337,485,486]. These findings illustrate that multinumerous centrosomes not only play a role in mitotic processes in the context of cancer, but also can profoundly disrupt interphase activities, such as migration.

Interestingly, TECs, which are not malignant themselves but differ from healthy endothelial cells and also harbor a surplus of centrosomes, show potentially malignant features even though MT nucleation is decreased[481]. Multiple centrosomes in TECs, however, exhibit a dispersed configuration throughout the cytoplasm, which seems to be critical for the potentially harmful properties of the cell. As the underlying model, it is assumed that decreased MT nucleation capacity compromises centrosome clustering at the MTOC leading to fragmentation of the Golgi apparatus due to scattered centrosomes and randomized vesicle trafficking[481]. In consequence, the cells show impaired cell polarity, disrupted cell migration and perturbed vessel sprouting thereby contributing to tissue disorganization and pathology. In addition, reduced MT nucleation capacity itself is assumed to directly impair cell migration. The ablation of excess centrosomes partially rescued centrosome scattering and restored directed cell migration demonstrating how important a clustered configuration of extra centrosomes is for proper cell locomotion[481].

In line with these findings, we observed problems with polarization and stable migration in DCs whose extra centrosomes showed a declustered configuration (see Fig. 22 c), even though these cases are very rare. This led us to hypothesize that the postulated relationship between multiple centrosomes and enhanced migration only exists when centrosomes are clustered (further discussed in the next sections).

4.4 Scattering of multiple centrosomes in dendritic cells has negative effects on migration

4.4.1 Centrosomal clustering is beneficial for dendritic cells

DCs predominantly show a clustered configuration of their supernumerary centrosomes as proven in fixed samples as well as in DCs migrating in different *in vitro* approaches. In the rare cases of DCs with declustered centrosomes, the cells have problems with polarization and stable migration. Preliminary quantification of migration parameters of mature BMDCs in a bulk under agarose migration assay supports the assumption of migration impairment in the presence of declustered centrosomes (Fig. 29). Therefore, we hypothesized that a clustered configuration of multiple centrosomes is required for proper cell migration.

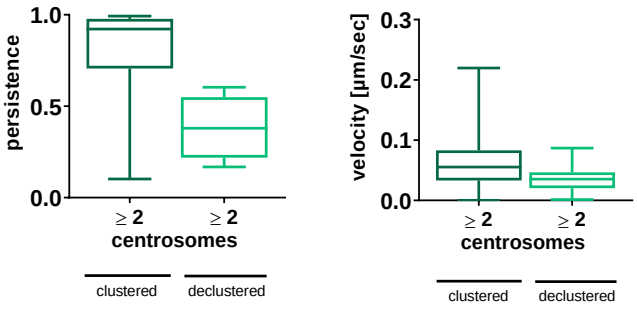

Figure 29. A declustered centrosomal configuration adversely affects cell migration

Quantification of persistence and velocity of mature CETN2-GFP expressing BMDCs with multiple centrosomes in the indicated configuration during migration under agarose toward a chemokine source. Box plot diagrams display median, 25% and 75 % percentile with whiskers marking minimum and maxium. Graph is based on N = 19 (clustered) and N = 4 (declustered) cells pooled from 8 independent experiments.

Indications of a possible mechanism behind disturbed migration in the presence of declustered centrosomes came from MT stainings revealing that single declustered centrosomes can act as individual MTOCs (see Fig. 22 d). This phenomenon has been observed in many different cell types and also applies to single centrioles in DCs (see Fig. 26c and Fig. 30). The presence of multiple MTOCs potentially influences the spatial alignment of the cell during polarization and/or hinders directed migration. MTOCs together with MTs are indispensable for inducing and maintaining cell polarity and are known to act as pathfinder during cell locomotion by stabilizing a selected direction of movement[325,487]. The scattering of centrosomes therefore generates multiple sites of MT nucleation and pathfinders, which could lead to difficulties in MT coordination, problems with polarizaiton, or conflicts in decision making about which direction to take. Interestingly, we observed (rare) cases of mature BMDCs under agrose, which exhibited a well-polarized shape and appeared to migrate properly, although their

centrosomes were declustered and formed multiple MTOCs. Unlike in most BMDCs with declustered centrosomes, the declustered centrosomes/MTOCs in the successfully polarized cells were not spreaded throughout the cell, but aligned on an imaginary line along the axis of migration, suggesting that the geometric/spatial arrangement of supernumerary centrosomes plays an important role (Fig. 30, left). As a side note, persistent migration was also observed in DCs with two split centrioles when both cylinders were aligned along the axis of migration (Fig. 30, right).

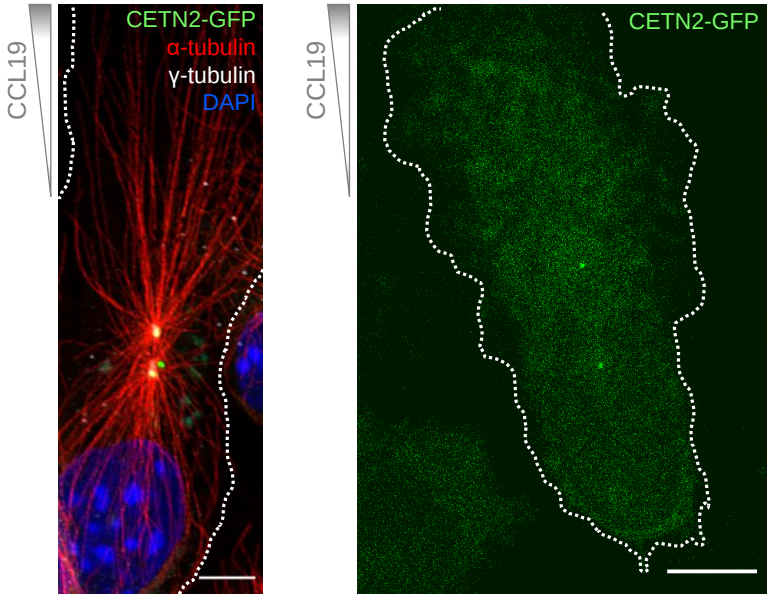

Figure 30. Successful polarization is possible when multiple centrosomes/scattered centrioles are aligned along the migration axis

Left: IF staining of MT filaments and PCM in mature CETN2-GFP expressing BMDC with multiple centrosomes/MTOCs fixed during migration under agarose toward a chemokine source. Merged channels of CETN2-GFP (green), α-tubulin (red) and γ-tubulin (grey) are shown. Nucleus was stained with DAPI. Post-processing of image: deconvolution. Dotted white line marks cell outline. Scale bar: 5 µm. Right: mature CETN2-GFP expressing BMDCs with scattered centrosome during migration under agarose along a chemotactic gradient. White dotted line indicates cell outline. Scale bar: 10 µm.

The occurrence of multiple MTOCs in non-malignant motile cells is rarely reported. In zebrafish primordial germ cells, duplicated MTOCs lead to impaired organization and dynamics of MTs, thereby interfering with cell polarization and migration[488]. Studies with baby hamster kidney fibroblasts that were fused into syncitia revealed that more than 3/4 of the cells harbor multiple MTOCs and that the syncitia were able to locomote if the MTOCs aggregated into a common cluster[489] pointing to an important role of centrosomal clustering for migration.

4.4.2 Centrosomal clustering is a known phenomenon in cancer cells

In contrast to the majority of non-malignant cells, tumor cells frequently carry multinumerous centrosomes[331,336] which they acquire by centriole overduplication or divison failure[336]. In malignant diseases, extra centrosomes are associated with various features of tumor aggressiveness, such as chromosomal instability, aneuploidy, increased invasiveness, tumor grade and size, aberrant stem cell divisions or recurrence in various types of cancer[328,329,337,392,415–418]. Indeed, supernumerary centrosomes are sufficient to drive spontaneous tumorigenesis in mammals[330], raising the question of the link. At first glance, the connection between additional centrosomes and the ambition of cancer cells to survive and proliferate appears contradictory, since extra centrosomes pose a great danger to a cell as they promote the formation of a multipolar spindle during mitosis[451]. This is not well tolerated by the cell and leads to mitotic catastrophe (cell death during mitosis) or multipolar mitosis[394,490]. If the cell resists mitotic catastrophe and divides in a multipolar fashion, this often results in high-grade aneuploid daughters that are very likely to go into apoptosis[491,492]. To avoid these tumor-suppressive events, cancer cells have developed a strategy to deal with extra centrosomes and avert the emergence of a multipolar spindle. By clustering their extra centrosomes into two functional poles (MTOCs), they generate a “pseudo-bipolar spindle” which ensures bipolar mitosis and cell survival similar to normal diploid cells[389,394,493] (see Fig. 23 a). Although the SAC presumably provides enough time for effective clustering prior to anaphase[394], a transient multipolar spindle intermediate occurs during the process of bipolar spindle creation promoting the formation of merotelic kinetochore attachments (one kinetochore is connected to MTs emanating from opposite spindle poles)[328,394,494]. Since these irregular MT kinetochore attachments are not detected by the SAC, the emergence of lagging chromosomes and low-grade (non-lethal) chromosome missegregation is promoted[419]. This might give rise to aneuploid daughter cells with a proliferation advantage or survival benefit conferring (more) malignant properties to the cell[419,420].

Against this backdrop, it becomes obvious that molecules that disturb centrosomal clustering are of great interest for research into anti-cancer therapies. Several substances are known from cancer research to induce centrosomal declustering in mitosis[393], which prompted us to try these drugs as tool in interphase DCs to prove the hypothesis that a clustered configuration of multiple centrosomes is a prerequisite for persistent DC migration.

4.4.3 Declustering drugs are not suitable for analyzing the dependence of proper dendritic cell migration on centrosomal clustering

We designed experiments to perturb centrosomal clusters in BMDCs to study the migratory behavior of DCs with scattered centrosomes and check for a potential connection between successful clustering and proper migration. Therefore, we used declustering agents, which are mainly used in cancer research to study mitotic processes, and planned to establish the drugs for our interphase settings. From the variety of substances available, we have selected the declustering compounds GF-15 and PJ-34. The griseofulvin derivative GF-15 is in pre-clinical development and has been shown – at concentrations that do not significantly affect tubulin polymerization – to reduce spindle tension in mitotic cancer cells, possibly by inhibiting MT dynamic stability[397]. Since spindle tension is necessary for centrosome clustering, cells with supernumerary centrosomes experience centrosome declustering, multipolar cell division, and ultimately cell death[397,495,496]. *In vitro* and *in vivo* studies revealed that GF-15 potently inhibits tumor cell growth[397]. PJ-34 is a PARP inhibitor in pre-clinical state and was shown to induce a G2/M arrest in human cancer cells *in vitro* via activation of p21 and subsequent cell death via disrupting the bipolar clustering of extra centrosomes[391,393,395,396]. It should be mentioned that some PJ-34 related PARP inhibitors are already approved for marketing as first-line, second-line, third-line or maintenance therapy for some specific cancer entities or are tested in clinical trials[497,498]. Both declustering agents were said to affect exclusively cancer cells harboring multiple centrosomes without affecting normal cell proliferation[395–397].

We oriented ourselves to the published concentrations, but ultimately set them significantly downward in our assays to prevent potential toxic effects on DCs. In fixed BMDCs, we analyzed the potency of the drugs by determining the proportion of cells with multiple centrosomes that have declustered centrosomes. We approached this topic by measuring the distances between centrosomes (intercentrosomal), which we first recorded in control treated cells (DMSO, H_2O) to get an idea, which distances are “normal“. Note that the obtained mean values from this analysis (see Fig. 23 c, right panel) are very similar to the mean intercentrosomal distances recorded in completely untreated fixed cells (see Fig. 18 a and Fig. 27) demonstrating that control treatments had no influence on the process of (de)clustering.

It could be worth considering cell size in the analysis, as distances between centrosomes/centrioles may be greater in larger cells. Alternatively, separation of 2N and 4N cells based on nuclear size could be targeted with subsequent exclusive analysis of 2N cells, similar to the procedure used in untreated BMDCs under agarose (see Fig. 16 a). In addition to this procedure, other approaches are conceivable to determine when a centrosome is

declustered. A recent study in osteoclasts, for example, defines a cluster as “having 3 or more adjacent CEP164 signals within 1 µm of each other”[445]. Others worked with 3D reconstructions of Z-stack images and quantitated the spread of interphase centrosomal clusters using an appropriate software[390]. After calculating the volume of the cluster, the ratio of the average volume of clusters to the average volume of the corresponding cell was determined.

Since GF-15 led to higher percentages of centrosomal declustering in fixed BMDCs than PJ-34, we initially focused on that drug and used it in different migration assays. *In situ* migration assays in skin explants revealed a migration disadvantage of drug treated DCs compared to control-treated cells as evidenced by the fact that fewer of the treated cells reached the lymphatic vessels. We have attempted to resolve centrioles at higher magnification (40×), but since the cells partially overlap, making it impossible to assign the centrioles to specific cells, we were unable to make a statement about a relationship between migratory phenotype and centrosomal declustering; here, it would be worth considering whether a 3D reconstruction could be an option. Although the finding that after drug treatment fewer cells have reached the lymphatic vessels supports our hypothesis, it is important to keep in mind that the drugs could also have effects other than centrosomal declustering and that DCs may be less able to reach the lymphatic vasculature after treatment because, for example, the cells may have problems with gradient sensing.

The following *in vitro* migration assays in live imaging mode allowed us to quantify migration parameters, such as persistence and velocity, and to better dissect the cause of the impaired migratory phenotype. The limitation with the 3D collagen and 2D under agarose migration assays performed is that both are bulk assays in which the centrosomes could not be resolved. Since "only" about 30 % of BMDCs contain multinumerous centrosomes, potential impact could be lost in the mass, which limits the significance of the assays. However, if enough cells are analyzed, effects should still be reflected in the results. Sorting by cells with multiple centrosomes was not considered as an option because the stress on the cells from the sorting process, drug treatment, and live cell migration assays would have been too high. To overcome the aforementioned limitations of bulk assays, we attempted under agarose live cell migration assays at single cell level, as individual centrioles can be resolved here and cells with different centrosome numbers can be distinguished. However, all attempts failed since the cells were too stressed after drug treatment for the following, also stressful, migration assay.

Cell migration analysis in artificial 3D systems better reflects physiological cell behavior than results obtained from 2D *in vitro* systems[121], but as can be seen from the comparison of the two assay types, the impairment of migration after treatment with GF-15 was more evident in the 2D setting (see Fig. 24 b and c). The observed difference in migration ability might go back

to the fact that DCs in geometrically more complex environments, such as tissue or artificial collagen fiber networks, were able to compensate migration impairment with the help of the surrounding structures and pores, while in the simpler 2D settings they lack compensation possibilities and migration defects become fully apparent. Since after drug treatment, no BMDC did migrate at all in under agarose assays we assumed an overall effect of the drug that is independent from its declustering capacity and targets *all* cells. Therefore, we decided to study the cytoskeleton, in particular MTs, which are needed by all cells for persistent migration, and took a closer look at the centrosomal configuration in cells with only one centrosome.

IF stainings of BMDCs with multiple centrosomes revealed that after treatment with GF-15 (12.5 µM, 6 hrs) the declustering of centrosomes was induced successfully resulting in multiple scattered centrosomes. We do not know whether the centrosomes are "ejected" from the PCM cloud during the process of declustering or whether they are distributed in the cell together with the PCM. However, this made no difference for our investigations, since single centrioles, and even small centrioles, can recruit PCM[499–501] and it is conceivable that “naked” centrosomes/centrioles just recruit new PCM and therefore can nucelate MTs. In addition to the expected effect of centrosome declustering, we observed that MTs were almost completely atrophied. A similar pattern of MT degeneration was found in cells with one centrosome. GF-15 was reported to inhibit tubulin polymerization only above concentrations of 25 µM, which is 25-fold higher than required for the induction of spindle multipolarity[397]. Although we reduced this concentration by half in our experiments, it appears to be sufficient to inhibit tubulin polymerization in interphase DCs, suggesting that DCs’ drug response may be different from that of tumor cells.

In addition, we found scattering of centrioles in GF-15 treated cells with one centrosome, whereas the mean intracentrosomal distance in control (DMSO) treated cells (see Fig. 25 b, right panel) was almost the same as in completely untreated fixed cells (see Fig. 18 a and Fig. 27), showing – as already in cells with multiple centrosomes – that control treatment had no effect on the process of (de)clustering. Scattering of centrioles is possible when the linker is impaired and when MTs, that were reported to position centrioles relatively close together in the absence of the linker[475], cannot perform this task. However, in case of linker impairment, it might be possible that this is only a transient event as reported from other cells[406]. Further information about the situation of the linker fibers can be obtained from the proteins C-Nap1, rootletin, and CEP68, but this aspect was of secondary importance for our purpose. What was shown with certainty, and what differs from what is reported by cancer cells, is that GF-15 not only targets cells with multinumerous centrosomes.

Further reduction of drug concentration or switching to PJ-34 abolished the occurrence of scattered centrioles in BMDCs with one centrosome and, moreover, left MTs intact in cells with one and multiple centrosome(s). However, the proportion of cells with declustered centrosomes was remarkably smaller after these drug modifications, illustrating the challenge of finding a drug concentration that is high enough to produce a significant effect, i.e., a high proportion of cells with declustered centrosomes, on the one hand, and low enough to avoid undesired side effects on the other. That low drug concentrations are not a guarantee for the absence of side effects was shown by the fact that we still observed undesirable side effects in cells with extra centrosomes even at low GF-15 or PJ-34 concentrations, such as spreading of the PCM with the formation of acentrosomal MTOCs. It was shown very early that MTs nucleate mainly from the PCM and not from centrioles explaining the presence of both centriolar and acentriolar MTOCs[294]. The organization of MTs without centrosomes is known, for example, from mitotic spindle assembly in mammalian cells[502]. Furthermore, there are examples of acentriolar MTOCs that organize MTs during meiosis and early development in some animal species[503,504].

Additional sites of MT nucleation due to PCM spreading represent for us an undesirable side effect of the drugs, which makes it difficult to investigate a potential dependence of proper migration on clustered centrosomes. This is explained by the relationship between MT nucleation and proper migration: Declustering substances lead to the (intended) declustering of centrosomes and, in some cases of cells with extra centrosomes, we additionally observed scattered centrioles (see Fig. 26 c). In both cases, higher numbers of MTOCs occur, so that MT nucleation and coordination occurs at many sites in the cell, with the numerous MTOCs presumably "working in different directions", which might lead to impaired polarization and thus disturbed migration (see above). With additional MTOCs due to empty PCM, there are even more sites for MT nucleation, which increases the probability of disrupted cell migration, but is not due to declustering per se. In summary, at low drug concentrations, we found intact MTs, but due to the side effect of PCM spreading, more MTOCs were generated than would have been caused by declustering of centrosomes alone.

Following the study of TECs that have excess centrosomes in a scattered configuration[481,505] and exhibit reduced MT nucleation capacity compared to TECs with 1-2 centrosomes[481], we repeated our study of MT nucleation capacity in untreated BMDCs (see Fig. 19 a) with drug treated cells. Although it is questionable whether the naturally occurring centrosomal scattering in TECs is comparable to the drug-induced declustering in BMDCs, preliminary results from 2N BMDCs treated with PJ-34 (50 µM, 3 hrs) show that the effect of increased centrosomal MT nucleation capacity we observed in untreated BMDCs with extra centrosomes (see Fig. 19 a) was abolished after drug treatment (both cell populations nucleate equal numbers of

MTs) (Fig. 31). Thereby, it did not matter whether we looked at *all* MTOCs (i.e., including empty MTOCs) or only at the pure centrioles and centrosomes that nucleate MTs. Moreover, reduced MT nucleation in TECs was observed to correlate with impaired Golgi integrity[481], which is essential for cell migration, and therefore excess centrosomes in TECs were supposed to disturb cell migration by Golgi scattering. In BMDCs treated with declustering agents, we observed that the Golgi apparatus was slightly dispersed (not shown), but systematic analysis is still pending.

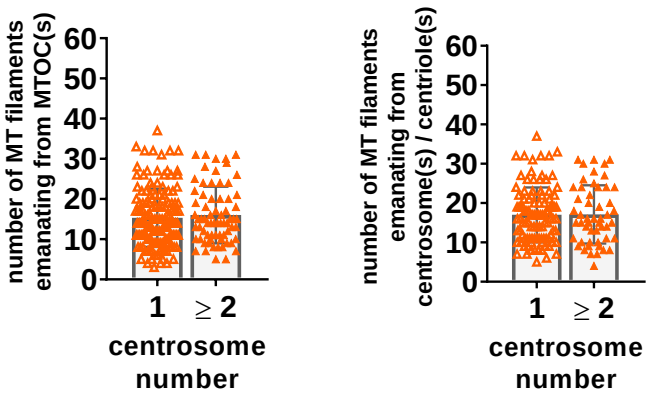

Figure 31. Extra centrosomes do not nucleate more MT filaments after treatment with declustering agents

Preliminary data: Quantification of nucleated MTs per MTOC (left) and of nucleated MTs per centrosome(s)/centriole(s) (right) in 2N CETN2-GFP expressing BMDCs under agarose. Graph displays mean values ± SD with N = 73 (one centrosome) and 27 (multiple centrosomes) cells pooled from 2 independent experiments.

Experiments with nocodazole to manipulate MT numbers in BMDCs also led to centrosome declustering in BMDCs with supernumerary centrosomes as well as massive PCM spreading. Since MTs undergo constant depolymerization processes and nocodazole prevents the addition of tubulin subunits, MT filaments disappear indicating that MTs keep the centrosome clusters together.

In summary, we observed that declustering agents have multiple side effects in BMDCs, such as MT degeneration or PCM spreading with the generation of additional empty MTOCs. While we could avoid the former by lowering the drug concentration – which unfortunately resulted in only a few cells having declustered centrosomes – spreading of the PCM also occurred at lower drug concentrations. Therefore, we were not able to assess whether the migration effects we saw after drug treatment were caused by the declustering of centrosomes or by the side effects of the drug.

It is stated that GF-15 and PJ-34 specifically affect cells with multiple centrosomes, which were cancer cells in the drug studies. Not investigated in these studies and very likely not known at all are DCs with additional centrosomes, which we found to be impaired by the drugs, as well as DCs with only one centrosome. Thus, our results "contradict" the literature, respectively, we see that the drugs seem to act differently in immune cells than in cancer cells. It is conceivable that DCs (with additional centrosomes) are more sensitive to (certain) drugs than, for example, cancer cells. In this context, it is important to keep in mind that everything that is known about declustering of extra centrosomes comes from experiments with cancer cells or cancer cell lines, focusing on mitosis and not on interphase processes as we study.

It is conceivable that the search for appropriate drug concentrations or declustering agents for the study of interphase processes in DCs will have to be extended. In any case, the data from the literature do not seem to be easily transferable (from cancer cells to DCs, from mitotic to interphase processes). Conversely, the question arises to what extent our findings are transferable to *in vivo* situations. However, on the basis of our experiments, it should be kept in mind that when declustering agents are administered, non-cancer cells that have extra centrosomes, namely DCs, and cells with only one centrosome (DCs and possibly also other cells) could also be targeted. This raises the question of what the side effects of therapy with declustering agents would be, assuming that humans also have DCs with multiple centrosomes. To evaluate the extent to which the side effect profile of declustering agents is justifiable, a careful risk-benefit assessment and further research is required.

4.4.4 Alternative approaches and complementary experiments

The statement "*Declustering drugs, such as griseofulvin […] and PJ34, all appear to selectively eradicate tumor cells, sparing healthy ones, since only cancer cells harbor excess centrosomes that can be declustered.*" published in a review from 2013[416] can be clearly contradicted with our results. What we can see from the experiments with declustering agents – which we initially conducted to investigate DCs' dependence of proper migration on clustering of extra centrosomes – is that the drugs do not only affect cancer cells with their supernumerary centrosomes, but also non-malignant cells with extra centrosomes. Moreover, these substances are not that specific for cells with a surplus of centrosomes as they were awarded in the literature, as they also affect cells with normal centrosome numbers. This not only raises questions regarding clinical use, but also excludes declustering agents (at least GF-15 and PJ-34) in the manner used for our studies, since we cannot assess where the observed migration defects come from (whether from declustering or side effects). While we

know that MT integrity is not an issue since it is intact at lower drug concentrations, we cannot rule out PCM spreading, making alternatives to the current approaches necessary.

One possibility would be to further vary the concentrations and incubation times of the drugs to find suitable conditions, or to change the compound class of declustering agents. One candidate, with which some preliminary assays have also been run, is the substance CW069. This declustering agent is in pre-clinical development and acts as an allosteric inhibitor of the protein *human spleen embryonic tissue and testis* (HSET)[391,506]. HSET, which is also known as *kinesin family member C1* (KIFC1), is part of the kinesin-14 family whose members are specific minus-end MT directed motors that cross-link MTs and coordinate spindle assembly[507,508]. Beside dynein, HSET/KIFC1 belongs to the major MT motors and was found to be crucial for centrosome clustering[329,394]. In cancer cell lines, CW069 was shown to increase multipolar mitotic spindles by inducing centrosome declustering in cells containing supernumerary centrosomes without compromising the formation of bipolar mitosis in non-malignant cells[506,509–511]. In our studies, the effect of CW069 on multiple centrosomes in interphase BMDCs was inconsistent, which might have several reasons. On the one hand, it is reported that knockdown of HSET in non-malignant cells or cancer cells with 'low-level' centrosome amplification does not inhibit bipolar spindle formation, allowing the cells to undergo normal division[394,464], suggesting that DCs whose centrosome numbers we would classify as low are therefore not affected either. On the other hand, studies with a murine cancer cell line revealed that HSET is crucially involved in mitotic centrosome clustering, but dynein has the major role in maintaining the centrosomal clusters during interphase[390]. So for us, dynein would be the protein of interest, but targeting this protein would have severe side effects, so no conclusions could be drawn about (de)clustering.

To determine the proportion of migration effects due to centrosomal declustering and effects due to drug side effects, a proper control is needed. One idea, which however does not allow working with primary cells, is to tether the centrosomes together and treat the cells with declustering agents, so that declustering is excluded as reason for migration effects, before the migration behavior of the cells are checked. As a tether, an anti-GFP nanobody in an inducible lentiviral vector would seem appropriate and HoxB8-derived CETN2-GFP DCs could serve as a cell model.

The approaches presented below can help to learn more about a potential dependence of proper migration on a clustered centrosomal configuration, but require the natural occurrence of declustered centrosomes. Since this is very rare, experiments would be very inefficient in their yield and are therefore not the first choice. In a correlative approach, directional persistence and intercentrosomal distances of BMDCs migrating along a gradient would be

recorded and correlated. A negative correlation (the greater the distance between centrosomes (declustered configuration), the lower the persistence) would indicate that clustering is required. If it turns out that centrosome clustering is indeed needed for persistent cell migration, a possible next step could be to look for a causal link between clustering and persistent migration. For this, declustered centrosomes could be laser ablated during cell migration. Readout in this “rescue experiment” would be the persistence of locomotion before and after the ablation process to answer the question of whether persistence increases after removal of "disturbing" centrosomes. As mentioned before, natural declustering rarely occurs in BMDCs. Inducing declustering first with declustering agents seems to be problematic due to the side effects of the drugs. In addition, it can be assumed that the cells would not survive laser ablation at all due to the additional stress caused by the drugs.

Another approach we have considered and taken initial steps in, is a CRISPR-based screen to find out which components are required for centrosome clustering in DCs. With the knowledge gained therefrom, it would be possible to design experiments in which relevant structures and molecules could be specifically targeted. Drug-wash-out experiments could possibly help provide helpful information on needed (re)clustering factors.

In any case, it is worthwhile to further investigate the process of centrosomal cluster formation, as the data collected so far suggest that this process plays an important role in the effector functions of DCs. Probably the most obvious and simplest option would initially be to expand the spectrum of declustering agents to include substances from other drug classes and/or to further titrate the drugs already in use.

4.5 Conclusion and outlook

Our results show that 20-30 % of activated BMDCs and dermal DCs harbor two or more centrosomes. We found that this phenomenon is neither a result of ongoing cell cyle progression nor the artifact of *in vitro* culturing conditions by demonstrating that both cell types no longer have appreciable proliferative activity and proving that supernumerary centrosomes are also present *in situ*. Rather, we unraveled that activation of primary DCs leads to an arrest in G1 phase of the cell cycle and an accumulation of centrosomes due to suppressed karyokinesis or cytokinesis. At the functional level, we looked at the migratory behavior of DCs with multiple centrosomes compared to DCs with one centrosome. Here, we found that multinumerous centrosomes form a functional MTOC nucleating more MT filaments than MTOCs with only one centrosome. While migration velocity between both cell populations was comparable, a surplus of centrosomes led to enhanced persistent migration. In addition, we observed that multiple centrosomes predominantly exhibited a clustered configuration, which prompted us to examine whether proper DC migration depends on the clustering of extra centrosomes. Treatment with declustering agents caused an impaired migration behavior of DCs; however, these substances had serious side effects on DCs, e.g., on the cytoskeleton, which did not allow attributing any migration effects to centrosomal declustering and necessitates the search for alternative approaches.

We found in these experiments that declustering agents – at least in DCs – already caused adverse effects far below the concentration considered to be side effect-free for cancer cells. Moreover, our studies revealed that declustering agents, which are said to exclusively target cells with excess centrosomes, as assumed so far from experiments with malignant cells (that typically have many centrosomes), I) also act on non-malignant cells and II) target cells with only one centrosome.

In summary, our results overcome the paradigm that cells in G1 phase have only one centrosome by showing that the phenomenon of additional centrosomes is present in terminally differentiated immune cells. The emergence of multinumerous centrosomes goes back to two paths, one of which is described in the present work. Known for their potential in cancer cells to drive malignancy, extra centrosomes in mature DCs appear to be part of a physiological program. They contribute to the regular tasks of the cell by conferring beneficial properties to it with respect to centrosome- and MT-associated immune processes, such as directional locomotion. Thus, our findings open up a completely new perspective on supernumerary centrosomes for regular cell and tissue homeostasis.

Although DCs are in a way the "counterparts" of tumor cells, both cell types share many parallels. Starting with the presence of multiple centrosomes and the two pathways of origin[339,512] to the clustering of centrosomes and the ability to switch between an amoeboid and a mesenchymal migration mode, to the phenomenon of enhanced migration when extra centrosomes are present. Still, there is hardly any cancer from DCs; on the contrary, the listed aspects that worsen the nature of tumor cells have positive aspects for the organism in DCs. Nevertheless, for research on the phenomenon of extra centrosomes, we currently only have cancer cells to look at, because most data on additional centrosomes and declustering come from experiments with malignant cells and the appearance of extra centrosomes in DCs was previously unknown. Our experiments with declustering agents show that it is not always possible to use findings from cancer cells as a guide.

Future research approaches could involve other organelles in DCs with multinumerous centrosomes, such as mitochondria and especially the Golgi apparatus, whose state may play a major role in locomotion during centrosomal declustering. Metabolism could also be an interesting subject of investigation associated with the question of whether DCs with a surplus of centrosomes generate energy differently than DCs with only one centrosome. It is further of great interest whether the phenomenon of extra centrosomes also occurs in human DCs. In addition, the finding that 70 % of DCs have only one centrosome, although the presence of additional centrosomes has obvious advantages, leaves some questions to be answered. Do the 30 % of cells with extra centrosomes represent only a subset of a larger number of cells that could theoretically have multiple centrosomes? Is it conceivable that the organism retains some flexibility here that allows it to further increase the proportion of cells with excess centrosomes under certain circumstances?

The selection of questions and possible approaches, as well as the results presented in this work, make clear that there is a great need for further research on the phenomenon of extra centrosomes. Since supernumerary centrosomes have so far been known mainly from cancer cells and not from immune cells, this opens up a wide field of research that needs to be explored.

References

1. Turvey, S E&Broide, D H (2010). Innate immunity. *The Journal of allergy and clinical immunology* 125, S24-32
2. Banchereau, J&Steinman, R M (1998). Dendritic cells and the control of immunity. *Nature* 392, 245–252
3. Banchereau, J *et al.* (2000). Immunobiology of dendritic cells. *Annual review of immunology* 18, 767–811
4. Mildner, A&Jung, S (2014). Development and function of dendritic cell subsets. *Immunity* 40, 642–656
5. Waisman, A *et al.* (2017). Dendritic cells as gatekeepers of tolerance. *Seminars in immunopathology* 39, 153–163
6. Zhang, J *et al.* (2019). Bone marrow dendritic cells regulate hematopoietic stem/progenitor cell trafficking. *The Journal of clinical investigation* 129, 2920–2931
7. Guilliams, M *et al.* (2014). Dendritic cells, monocytes and macrophages: a unified nomenclature based on ontogeny. *Nature reviews. Immunology* 14, 571–578
8. Merad, M *et al.* (2013). The dendritic cell lineage: ontogeny and function of dendritic cells and their subsets in the steady state and the inflamed setting. *Annual review of immunology* 31, 563–604
9. Hong, W *et al.* (2022). New Insights of CCR7 Signaling in Dendritic Cell Migration and Inflammatory Diseases. *Frontiers in pharmacology* 13, 841687
10. Worbs, T *et al.* (2017). Dendritic cell migration in health and disease. *Nature reviews. Immunology* 17, 30–48
11. Colonna, M *et al.* (2004). Plasmacytoid dendritic cells in immunity. *Nature immunology* 5, 1219–1226
12. Sichien, D *et al.* (2017). Development of conventional dendritic cells: from common bone marrow progenitors to multiple subsets in peripheral tissues. *Mucosal immunology* 10, 831–844
13. Manz, M G *et al.* (2001). Dendritic cell potentials of early lymphoid and myeloid progenitors. *Blood* 97, 3333–3341
14. Akashi, K *et al.* (2000). A clonogenic common myeloid progenitor that gives rise to all myeloid lineages. *Nature* 404, 193–197
15. Wu, L *et al.* (2001). Development of thymic and splenic dendritic cell populations from different hemopoietic precursors. *Blood* 98, 3376–3382
16. Corcoran, L *et al.* (2003). The lymphoid past of mouse plasmacytoid cells and thymic dendritic cells. *Journal of immunology (Baltimore, Md. : 1950)* 170, 4926–4932
17. Pelayo, R *et al.* (2005). Derivation of 2 categories of plasmacytoid dendritic cells in murine bone marrow. *Blood* 105, 4407–4415

18. Onai, N *et al.* (2007). Identification of clonogenic common Flt3+M-CSFR+ plasmacytoid and conventional dendritic cell progenitors in mouse bone marrow. *Nature immunology* 8, 1207–1216

19. Naik, S H *et al.* (2007). Development of plasmacytoid and conventional dendritic cell subtypes from single precursor cells derived in vitro and in vivo. *Nature immunology* 8, 1217–1226

20. Onai, N *et al.* (2013). A clonogenic progenitor with prominent plasmacytoid dendritic cell developmental potential. *Immunity* 38, 943–957

21. Diao, J *et al.* (2004). Characterization of distinct conventional and plasmacytoid dendritic cell-committed precursors in murine bone marrow. *Journal of immunology (Baltimore, Md. : 1950)* 173, 1826–1833

22. Liu, K *et al.* (2009). In vivo analysis of dendritic cell development and homeostasis. *Science (New York, N.Y.)* 324, 392–397

23. Ginhoux, F *et al.* (2009). The origin and development of nonlymphoid tissue CD103+ DCs. *The Journal of experimental medicine* 206, 3115–3130

24. Diao, J *et al.* (2006). In situ replication of immediate dendritic cell (DC) precursors contributes to conventional DC homeostasis in lymphoid tissue. *Journal of immunology (Baltimore, Md. : 1950)* 176, 7196–7206

25. Bursch, L S *et al.* (2007). Identification of a novel population of Langerin+ dendritic cells. *The Journal of experimental medicine* 204, 3147–3156

26. Del Rio, M-L *et al.* (2007). CD103- and CD103+ bronchial lymph node dendritic cells are specialized in presenting and cross-presenting innocuous antigen to CD4+ and CD8+ T cells. *Journal of immunology (Baltimore, Md. : 1950)* 178, 6861–6866

27. Crowley, M *et al.* (1989). The cell surface of mouse dendritic cells: FACS analyses of dendritic cells from different tissues including thymus. *Cellular Immunology* 118, 108–125

28. Vremec, D *et al.* (1992). The surface phenotype of dendritic cells purified from mouse thymus and spleen: investigation of the CD8 expression by a subpopulation of dendritic cells. *The Journal of experimental medicine* 176, 47–58

29. Gurka, S *et al.* (2015). Mouse Conventional Dendritic Cells Can be Universally Classified Based on the Mutually Exclusive Expression of XCR1 and SIRPα. *Frontiers in immunology* 6, 35

30. Murphy, T L *et al.* (2016). Transcriptional Control of Dendritic Cell Development. *Annual review of immunology* 34, 93–119

31. Schlitzer, A *et al.* (2013). IRF4 transcription factor-dependent CD11b+ dendritic cells in human and mouse control mucosal IL-17 cytokine responses. *Immunity* 38, 970–983

32. Bachem, A *et al.* (2010). Superior antigen cross-presentation and XCR1 expression define human CD11c+CD141+ cells as homologues of mouse CD8+ dendritic cells. *The Journal of experimental medicine* 207, 1273–1281

33. Crozat, K *et al.* (2010). The XC chemokine receptor 1 is a conserved selective marker of mammalian cells homologous to mouse CD8alpha+ dendritic cells. *The Journal of experimental medicine* 207, 1283–1292

34. Dorner, B G *et al.* (2009). Selective expression of the chemokine receptor XCR1 on cross-presenting dendritic cells determines cooperation with CD8+ T cells. *Immunity* 31, 823–833

35. Lutz, M B *et al.* (1999). An advanced culture method for generating large quantities of highly pure dendritic cells from mouse bone marrow. *Journal of Immunological Methods* 223, 77–92

36. Inaba, K *et al.* (1992). Generation of large numbers of dendritic cells from mouse bone marrow cultures supplemented with granulocyte/macrophage colony-stimulating factor. *The Journal of experimental medicine* 176, 1693–1702

37. Scheicher, C *et al.* (1992). Dendritic cells from mouse bone marrow: In vitro differentiation using low doses of recombinant granulocyte-macrophage colony-stimulating factor. *Journal of Immunological Methods* 154, 253–264

38. Inaba, K *et al.* (1993). Granulocytes, macrophages, and dendritic cells arise from a common major histocompatibility complex class II-negative progenitor in mouse bone marrow. *Proceedings of the National Academy of Sciences of the United States of America* 90, 3038–3042

39. Gilliet, M *et al.* (2002). The development of murine plasmacytoid dendritic cell precursors is differentially regulated by FLT3-ligand and granulocyte/macrophage colony-stimulating factor. *The Journal of experimental medicine* 195, 953–958

40. Xu, Y *et al.* (2007). Differential development of murine dendritic cells by GM-CSF versus Flt3 ligand has implications for inflammation and trafficking. *Journal of immunology (Baltimore, Md. : 1950)* 179, 7577–7584

41. Helft, J *et al.* (2015). GM-CSF Mouse Bone Marrow Cultures Comprise a Heterogeneous Population of CD11c(+)MHCII(+) Macrophages and Dendritic Cells. *Immunity* 42, 1197–1211

42. Cabeza-Cabrerizo, M *et al.* (2019). Tissue clonality of dendritic cell subsets and emergency DCpoiesis revealed by multicolor fate mapping of DC progenitors. *Science immunology* 4

43. Ng, L G *et al.* (2008). Migratory dermal dendritic cells act as rapid sensors of protozoan parasites. *PLoS pathogens* 4, e1000222

44. Farache, J *et al.* (2013). Luminal bacteria recruit CD103+ dendritic cells into the intestinal epithelium to sample bacterial antigens for presentation. *Immunity* 38, 581–595

45. Amigorena, S&Bonnerot, C (1999). Fc receptor signaling and trafficking: a connection for antigen processing. *Immunological reviews* 172, 279–284

46. Garrett, W S *et al.* (2000). Developmental Control of Endocytosis in Dendritic Cells by Cdc42. *Cell* 102, 325–334

47. Albert, M L *et al.* (1998). Immature dendritic cells phagocytose apoptotic cells via alphavbeta5 and CD36, and cross-present antigens to cytotoxic T lymphocytes. *The Journal of experimental medicine* 188, 1359–1368

48. Reis e Sousa, C *et al.* (1993). Phagocytosis of antigens by Langerhans cells in vitro. *The Journal of experimental medicine* 178, 509–519

49. Sallusto, F *et al.* (1995). Dendritic cells use macropinocytosis and the mannose receptor to concentrate macromolecules in the major histocompatibility complex class II compartment: downregulation by cytokines and bacterial products. *The Journal of experimental medicine* 182, 389–400

50. Janeway, C A (1992). The immune system evolved to discriminate infectious nonself from noninfectious self. *Immunology Today* 13, 11–16

51. Akira, S *et al.* (2001). Toll-like receptors: critical proteins linking innate and acquired immunity. *Nature immunology* 2, 675–680

52. van Vliet, S J *et al.* (2008). Dendritic cells and C-type lectin receptors: coupling innate to adaptive immune responses. *Immunology and cell biology* 86, 580–587

53. Takeuchi, O&Akira, S (2010). Pattern recognition receptors and inflammation. *Cell* 140, 805–820

54. Kawai, T&Akira, S (2009). The roles of TLRs, RLRs and NLRs in pathogen recognition. *International immunology* 21, 317–337

55. Gallo, P M&Gallucci, S (2013). The dendritic cell response to classic, emerging, and homeostatic danger signals. Implications for autoimmunity. *Frontiers in immunology* 4, 138

56. Silva-Gomes, S., Decout, A. & Nigou, J. Pathogen-Associated Molecular Patterns (PAMPs). In *Encyclopedia of Inflammatory Diseases,* edited by M. Parnham (Springer Basel, Basel, 2015), pp. 1–16

57. Chow, J C *et al.* (1999). Toll-like receptor-4 mediates lipopolysaccharide-induced signal transduction. *The Journal of biological chemistry* 274, 10689–10692

58. Zelenay, S&Reis e Sousa, C (2013). Adaptive immunity after cell death. *Trends in immunology* 34, 329–335

59. Krysko, O *et al.* (2013). Many faces of DAMPs in cancer therapy. *Cell death & disease* 4, e631

60. Di Virgilio, F *et al.* (2020). Purinergic signaling, DAMPs, and inflammation. *American journal of physiology. Cell physiology* 318, C832-C835

61. Steinman, R M *et al.* (1997). Dendritic cells in the T-cell areas of lymphoid organs. *Immunological reviews* 156, 25–37

62. Winde, C M de *et al.* (2020). Molecular mechanisms of dendritic cell migration in immunity and cancer. *Medical microbiology and immunology* 209, 515–529

63. Liu, J *et al.* (2021). Dendritic cell migration in inflammation and immunity. *Cellular & molecular immunology* 18, 2461–2471

64. Ohl, L *et al.* (2004). CCR7 governs skin dendritic cell migration under inflammatory and steady-state conditions. *Immunity* 21, 279–288

65. Tal, O *et al.* (2011). DC mobilization from the skin requires docking to immobilized CCL21 on lymphatic endothelium and intralymphatic crawling. *The Journal of experimental medicine* 208, 2141–2153

66. Förster, R *et al.* (1999). CCR7 Coordinates the Primary Immune Response by Establishing Functional Microenvironments in Secondary Lymphoid Organs. *Cell* 99, 23–33

67. Vargas, P *et al.* (2016). Innate control of actin nucleation determines two distinct migration behaviours in dendritic cells. *Nature cell biology* 18, 43–53

68. West, M A *et al.* (2004). Enhanced dendritic cell antigen capture via toll-like receptor-induced actin remodeling. *Science (New York, N.Y.)* 305, 1153–1157

69. Théry, C&Amigorena, S (2001). The cell biology of antigen presentation in dendritic cells. *Current Opinion in Immunology* 13, 45–51

70. Roche, P A&Furuta, K (2015). The ins and outs of MHC class II-mediated antigen processing and presentation. *Nature reviews. Immunology* 15, 203–216

71. Cella, M *et al.* (1997). Inflammatory stimuli induce accumulation of MHC class II complexes on dendritic cells. *Nature* 388, 782–787

72. Kotsias, F *et al.* (2019). Antigen processing and presentation. *International review of cell and molecular biology* 348, 69–121

73. Inaba, K *et al.* (1997). High levels of a major histocompatibility complex II-self peptide complex on dendritic cells from the T cell areas of lymph nodes. *The Journal of experimental medicine* 186, 665–672

74. Embgenbroich, M&Burgdorf, S (2018). Current Concepts of Antigen Cross-Presentation. *Frontiers in immunology* 9, 1643

75. Joffre, O P *et al.* (2012). Cross-presentation by dendritic cells. *Nature reviews. Immunology* 12, 557–569

76. Alvarez, D *et al.* (2008). Mechanisms and consequences of dendritic cell migration. *Immunity* 29, 325–342

77. Heuzé, M L *et al.* (2013). Migration of dendritic cells: physical principles, molecular mechanisms, and functional implications. *Immunological reviews* 256, 240–254

78. Girard, J-P *et al.* (2012). HEVs, lymphatics and homeostatic immune cell trafficking in lymph nodes. *Nature reviews. Immunology* 12, 762–773

79. Braun, A *et al.* (2011). Afferent lymph-derived T cells and DCs use different chemokine receptor CCR7-dependent routes for entry into the lymph node and intranodal migration. *Nature immunology* 12, 879–887

80. Kameritsch, P&Renkawitz, J (2020). Principles of Leukocyte Migration Strategies. *Trends in cell biology* 30, 818–832

81. Yamada, K M&Sixt, M (2019). Mechanisms of 3D cell migration. *Nature reviews. Molecular cell biology* 20, 738–752

82. Moreau, H D *et al.* (2018). Integrating Physical and Molecular Insights on Immune Cell Migration. *Trends in immunology* 39, 632–643

83. Andrian, U H von&Mempel, T R (2003). Homing and cellular traffic in lymph nodes. *Nature reviews. Immunology* 3, 867–878

84. Nourshargh, S&Alon, R (2014). Leukocyte migration into inflamed tissues. *Immunity* 41, 694–707

85. Lämmermann, T&Germain, R N (2014). The multiple faces of leukocyte interstitial migration. *Seminars in immunopathology* 36, 227–251

86. Weninger, W *et al.* (2014). Leukocyte migration in the interstitial space of non-lymphoid organs. *Nature reviews. Immunology* 14, 232–246

87. Garcin, C&Straube, A (2019). Microtubules in cell migration. *Essays in biochemistry* 63, 509–520

88. Hsu, J C *et al.* (2013). Region-specific epithelial cell dynamics during branching morphogenesis. *Developmental dynamics : an official publication of the American Association of Anatomists* 242, 1066–1077

89. Auffray, C *et al.* (2007). Monitoring of blood vessels and tissues by a population of monocytes with patrolling behavior. *Science (New York, N.Y.)* 317, 666–670

90. Friedl, P&Weigelin, B (2008). Interstitial leukocyte migration and immune function. *Nature immunology* 9, 960–969

91. Kopf, A&Kiermaier, E (2021). Dynamic Microtubule Arrays in Leukocytes and Their Role in Cell Migration and Immune Synapse Formation. *Frontiers in cell and developmental biology* 9, 635511

92. Ringer, P *et al.* (2017). Sensing the mechano-chemical properties of the extracellular matrix. *Matrix biology : journal of the International Society for Matrix Biology* 64, 6–16

93. Gardel, M L *et al.* (2010). Mechanical integration of actin and adhesion dynamics in cell migration. *Annual review of cell and developmental biology* 26, 315–333

94. Kloc, M *et al.* (2014). The newly found functions of MTOC in immunological response. *Journal of leukocyte biology* 95, 417–430

95. Wolf, K *et al.* (2013). Physical limits of cell migration: control by ECM space and nuclear deformation and tuning by proteolysis and traction force. *The Journal of cell biology* 201, 1069–1084

96. Lämmermann, T *et al.* (2008). Rapid leukocyte migration by integrin-independent flowing and squeezing. *Nature* 453, 51–55

97. Huttenlocher, A (1995). Adhesion in cell migration. *Current opinion in cell biology* 7, 697–706

98. Yumura, S *et al.* (1984). Localization of actin and myosin for the study of ameboid movement in Dictyostelium using improved immunofluorescence. *The Journal of cell biology* 99, 894–899

99. Mihlan, M *et al.* (2022). Neutrophils: Amoeboid Migration and Swarming Dynamics in Tissues. *Frontiers in cell and developmental biology* 10, 871789

100. Lämmermann, T&Sixt, M (2009). Mechanical modes of 'amoeboid' cell migration. *Current opinion in cell biology* 21, 636–644

101. Friedl, P *et al.* (1998). CD4+ T lymphocytes migrating in three-dimensional collagen lattices lack focal adhesions and utilize β1 integrin-independent strategies for polarization, interaction with collagen fibers and locomotion. *Eur. J. Immunol.* 28, 2331–2343

102. Stossel, T P (1994). The E. Donnall Thomas Lecture, 1993. The machinery of blood cell movements. *Blood* 84, 367–379

103. Wilkinson, P C (1985). Random locomotion; chemotaxis and chemokinesis. A guide to terms defining cell locomotion. *Immunology Today* 6, 273–278

104. Allan, R B&Wilkinson, P C (1978). A visual analysis of chemotactic and chemokinetic locomotion of human neutrophil leucocytes. *Experimental cell research* 111, 191–203

105. Lämmermann, T&Kastenmüller, W (2019). Concepts of GPCR-controlled navigation in the immune system. *Immunological reviews* 289, 205–231

106. Friedl, P *et al.* (2001). Amoeboid leukocyte crawling through extracellular matrix: lessons from the Dictyostelium paradigm of cell movement. *Journal of leukocyte biology* 70, 491–509

107. Lämmermann, T *et al.* (2009). Cdc42-dependent leading edge coordination is essential for interstitial dendritic cell migration. *Blood* 113, 5703–5710

108. Zigmond, S H *et al.* (1981). Cell polarity: an examination of its behavioral expression and its consequences for polymorphonuclear leukocyte chemotaxis. *The Journal of cell biology* 89, 585–592

109. Jørgensen, A S *et al.* (2018). CCL19 with CCL21-tail displays enhanced glycosaminoglycan binding with retained chemotactic potency in dendritic cells. *Journal of leukocyte biology* 104, 401–411

110. Weber, M *et al.* (2013). Interstitial dendritic cell guidance by haptotactic chemokine gradients. *Science (New York, N.Y.)* 339, 328–332

111. Paz, J L de *et al.* (2007). Profiling heparin-chemokine interactions using synthetic tools. *ACS chemical biology* 2, 735–744

112. Luther, S A *et al.* (2000). Coexpression of the chemokines ELC and SLC by T zone stromal cells and deletion of the ELC gene in the plt/plt mouse. *Proceedings of the National Academy of Sciences of the United States of America* 97, 12694–12699

113. Ngo, V N *et al.* (1998). Epstein-Barr virus-induced molecule 1 ligand chemokine is expressed by dendritic cells in lymphoid tissues and strongly attracts naive T cells and activated B cells. *The Journal of experimental medicine* 188, 181–191

114. Willimann, K *et al.* (1998). The chemokine SLC is expressed in T cell areas of lymph nodes and mucosal lymphoid tissues and attracts activated T cells via CCR7. *Eur. J. Immunol.* 28, 2025–2034

115. Luther, S A *et al.* (2002). Differing activities of homeostatic chemokines CCL19, CCL21, and CXCL12 in lymphocyte and dendritic cell recruitment and lymphoid neogenesis. *Journal of immunology (Baltimore, Md. : 1950)* 169, 424–433

116. Kriehuber, E *et al.* (2001). Isolation and characterization of dermal lymphatic and blood endothelial cells reveal stable and functionally specialized cell lineages. *The Journal of experimental medicine* 194, 797–808

117. Britschgi, M R *et al.* (2010). CCL21 is sufficient to mediate DC migration, maturation and function in the absence of CCL19. *European journal of immunology* 40, 1266–1271

118. Haessler, U *et al.* (2011). Dendritic cell chemotaxis in 3D under defined chemokine gradients reveals differential response to ligands CCL21 and CCL19. *Proceedings of the National Academy of Sciences of the United States of America* 108, 5614–5619

119. Sánchez-Madrid, F&Del Pozo, M A (1999). Leukocyte polarization in cell migration and immune interactions. *The EMBO journal* 18, 501–511

120. Insall, R H (2010). Understanding eukaryotic chemotaxis: a pseudopod-centred view. *Nature reviews. Molecular cell biology* 11, 453–458

121. Sixt, M&Lämmermann, T (2011). In vitro analysis of chemotactic leukocyte migration in 3D environments. *Methods in molecular biology (Clifton, N.J.)* 769, 149–165

122. Hauser, M A&Legler, D F (2016). Common and biased signaling pathways of the chemokine receptor CCR7 elicited by its ligands CCL19 and CCL21 in leukocytes. *Journal of leukocyte biology* 99, 869–882

123. Merino-Casallo, F *et al.* (2022). Unravelling cell migration: defining movement from the cell surface. *Cell adhesion & migration* 16, 25–64

124. Howard, T H&Oresajo, C O (1985). The kinetics of chemotactic peptide-induced change in F-actin content, F-actin distribution, and the shape of neutrophils. *The Journal of cell biology* 101, 1078–1085

125. Coates, T D *et al.* (1992). Relationship of F-actin distribution to development of polar shape in human polymorphonuclear neutrophils. *The Journal of cell biology* 117, 765–774

126. Kopf, A *et al.* (2020). Microtubules control cellular shape and coherence in amoeboid migrating cells. *The Journal of cell biology* 219

127. Nogales, E (2000). Structural insights into microtubule function. *Annual review of biochemistry* 69, 277–302

128. Wu, J&Akhmanova, A (2017). Microtubule-Organizing Centers. *Annual review of cell and developmental biology* 33, 51–75

129. Eddy, R J *et al.* (2002). Microtubule asymmetry during neutrophil polarization and migration. *Molecular biology of the cell* 13, 4470–4483

130. Malech, H L *et al.* (1977). Structural analysis of human neutrophil migration. Centriole, microtubule, and microfilament orientation and function during chemotaxis. *The Journal of cell biology* 75, 666–693

131. Renkawitz, J *et al.* (2019). Nuclear positioning facilitates amoeboid migration along the path of least resistance. *Nature* 568, 546–550

132. Renkawitz, J *et al.* (2009). Adaptive force transmission in amoeboid cell migration. *Nature cell biology* 11, 1438–1443

133. Leithner, A *et al.* (2016). Diversified actin protrusions promote environmental exploration but are dispensable for locomotion of leukocytes. *Nature cell biology* 18, 1253–1259

134. Schaks, M *et al.* (2019). Actin dynamics in cell migration. *Essays in biochemistry* 63, 483–495

135. van Helvert, S *et al.* (2018). Mechanoreciprocity in cell migration. *Nature cell biology* 20, 8–20

136. Bouchet, B P&Akhmanova, A (2017). Microtubules in 3D cell motility. *Journal of cell science* 130, 39–50

137. Laan, L *et al.* (2008). Force-generation and dynamic instability of microtubule bundles. *Proceedings of the National Academy of Sciences of the United States of America* 105, 8920–8925

138. Inoué, S&Salmon, E D (1995). Force generation by microtubule assembly/disassembly in mitosis and related movements. *Molecular biology of the cell* 6, 1619–1640

139. Dogterom, M&Koenderink, G H (2019). Actin-microtubule crosstalk in cell biology. *Nature reviews. Molecular cell biology* 20, 38–54

140. Dogterom, M&Yurke, B (1997). Measurement of the force-velocity relation for growing microtubules. *Science (New York, N.Y.)* 278, 856–860

141. Rodriguez, O C *et al.* (2003). Conserved microtubule-actin interactions in cell movement and morphogenesis. *Nature cell biology* 5, 599–609

142. Chang, F *et al.* (2005). Regulation of actin assembly by microtubules in fission yeast cell polarity. *Novartis Foundation symposium* 269, 59-66; discussion 66-72, 223-30

143. Hayles, J&Nurse, P (2001). A journey into space. *Nature reviews. Molecular cell biology* 2, 647–656

144. Hind, L E *et al.* (2016). Leading from the Back: The Role of the Uropod in Neutrophil Polarization and Migration. *Developmental cell* 38, 161–169

145. Vicente-Manzanares, M *et al.* (2009). Non-muscle myosin II takes centre stage in cell adhesion and migration. *Nature reviews. Molecular cell biology* 10, 778–790

146. Ridley, A J *et al.* (2003). Cell migration: integrating signals from front to back. *Science (New York, N.Y.)* 302, 1704–1709

147. Case, L B&Waterman, C M (2015). Integration of actin dynamics and cell adhesion by a three-dimensional, mechanosensitive molecular clutch. *Nature cell biology* 17, 955–963

148. Lehtimäki, J *et al.* (2017). Actin Filament Structures in Migrating Cells. *Handbook of experimental pharmacology* 235, 123–152

149. Krause, M&Gautreau, A (2014). Steering cell migration: lamellipodium dynamics and the regulation of directional persistence. *Nature reviews. Molecular cell biology* 15, 577–590

150. Bokoch, G M (1995). Chemoattractant signaling and leukocyte activation. *Blood* 86, 1649–1660

151. Abercrombie, M *et al.* (1971). The locomotion of fibroblasts in culture. *Experimental cell research* 67, 359–367

152. Lauffenburger, D A&Horwitz, A F (1996). Cell Migration: A Physically Integrated Molecular Process. *Cell* 84, 359–369

153. Friedl, P&Wolf, K (2010). Plasticity of cell migration: a multiscale tuning model. *The Journal of cell biology* 188, 11–19

154. Reversat, A *et al.* (2020). Cellular locomotion using environmental topography. *Nature* 582, 582–585

155. Petrie, R J&Yamada, K M (2016). Multiple mechanisms of 3D migration: the origins of plasticity. *Current opinion in cell biology* 42, 7–12

156. Te Boekhorst, V *et al.* (2016). Plasticity of Cell Migration In Vivo and In Silico. *Annual review of cell and developmental biology* 32, 491–526

157. Stoitzner, P *et al.* (2002). A close-up view of migrating Langerhans cells in the skin. *The Journal of investigative dermatology* 118, 117–125

158. Wolf, K *et al.* (2003). Amoeboid shape change and contact guidance: T-lymphocyte crawling through fibrillar collagen is independent of matrix remodeling by MMPs and other proteases. *Blood* 102, 3262–3269

159. Paluch, E K *et al.* (2016). Focal Adhesion-Independent Cell Migration. *Annual review of cell and developmental biology* 32, 469–490

160. Pollard, T D&Borisy, G G (2003). Cellular Motility Driven by Assembly and Disassembly of Actin Filaments. *Cell* 112, 453–465

161. Barbier, L *et al.* (2019). Myosin II Activity Is Selectively Needed for Migration in Highly Confined Microenvironments in Mature Dendritic Cells. *Frontiers in immunology* 10, 747

162. Liu, B P *et al.* (1998). Microtubule depolymerization induces stress fibers, focal adhesions, and DNA synthesis via the GTP-binding protein Rho. *Cell adhesion and communication* 5, 249–255

163. Gundersen, G G&Worman, H J (2013). Nuclear positioning. *Cell* 152, 1376–1389

164. Luxton, G W G&Gundersen, G G (2011). Orientation and function of the nuclear-centrosomal axis during cell migration. *Current opinion in cell biology* 23, 579–588

165. Saeki, H *et al.* (1999). Cutting edge: secondary lymphoid-tissue chemokine (SLC) and CC chemokine receptor 7 (CCR7) participate in the emigration pathway of mature dendritic cells from the skin to regional lymph nodes. *Journal of immunology (Baltimore, Md. : 1950)* 162, 2472–2475

166. Gunn, M D *et al.* (1999). Mice lacking expression of secondary lymphoid organ chemokine have defects in lymphocyte homing and dendritic cell localization. *The Journal of experimental medicine* 189, 451–460

167. Schwarz, J *et al.* (2017). Dendritic Cells Interpret Haptotactic Chemokine Gradients in a Manner Governed by Signal-to-Noise Ratio and Dependent on GRK6. *Current biology : CB* 27, 1314–1325

168. Zöltzer, H (2003). Initial lymphatics--morphology and function of the endothelial cells. *Lymphology* 36, 7–25

169. Baluk, P *et al.* (2007). Functionally specialized junctions between endothelial cells of lymphatic vessels. *The Journal of experimental medicine* 204, 2349–2362

170. Banerji, S *et al.* (1999). LYVE-1, a new homologue of the CD44 glycoprotein, is a lymph-specific receptor for hyaluronan. *The Journal of cell biology* 144, 789–801

171. Mummert, M E *et al.* (2002). Synthesis and surface expression of hyaluronan by dendritic cells and its potential role in antigen presentation. *Journal of immunology (Baltimore, Md. : 1950)* 169, 4322–4331

172. Johnson, L A *et al.* (2017). Dendritic cells enter lymph vessels by hyaluronan-mediated docking to the endothelial receptor LYVE-1. *Nature immunology* 18, 762–770

173. Russo, E *et al.* (2016). Intralymphatic CCL21 Promotes Tissue Egress of Dendritic Cells through Afferent Lymphatic Vessels. *Cell reports* 14, 1723–1734

174. Nitschké, M *et al.* (2012). Differential requirement for ROCK in dendritic cell migration within lymphatic capillaries in steady-state and inflammation. *Blood* 120, 2249–2258

175. Ulvmar, M H *et al.* (2014). The atypical chemokine receptor CCRL1 shapes functional CCL21 gradients in lymph nodes. *Nature immunology* 15, 623–630

176. Link, A *et al.* (2007). Fibroblastic reticular cells in lymph nodes regulate the homeostasis of naive T cells. *Nature immunology* 8, 1255–1265

177. Bajénoff, M *et al.* (2003). The strategy of T cell antigen-presenting cell encounter in antigen-draining lymph nodes revealed by imaging of initial T cell activation. *The Journal of experimental medicine* 198, 715–724

178. MARCHESI, V T&GOWANS, J L (1964). THE MIGRATION OF LYMPHOCYTES THROUGH THE ENDOTHELIUM OF VENULES IN LYMPH NODES: AN ELECTRON MICROSCOPE STUDY. *Proceedings of the Royal Society of London. Series B, Biological sciences* 159, 283–290

179. Girard, J-P&Springer, T A (1995). High endothelial venules (HEVs): specialized endothelium for lymphocyte migration. *Immunology Today* 16, 449–457

180. Gunn, M D *et al.* (1998). A chemokine expressed in lymphoid high endothelial venules promotes the adhesion and chemotaxis of naive T lymphocytes. *Proceedings of the National Academy of Sciences of the United States of America* 95, 258–263

181. Comerford, I *et al.* (2013). A myriad of functions and complex regulation of the CCR7/CCL19/CCL21 chemokine axis in the adaptive immune system. *Cytokine & growth factor reviews* 24, 269–283

182. Winzler, C *et al.* (1997). Maturation stages of mouse dendritic cells in growth factor-dependent long-term cultures. *The Journal of experimental medicine* 185, 317–328

183. Stankevicins, L *et al.* (2020). Deterministic actin waves as generators of cell polarization cues. *Proceedings of the National Academy of Sciences of the United States of America* 117, 826–835

184. Rot, A&Andrian, U H von (2004). Chemokines in innate and adaptive host defense: basic chemokinese grammar for immune cells. *Annual review of immunology* 22, 891–928

185. Arai, H *et al.* (1997). Chemotaxis in a lymphocyte cell line transfected with C-C chemokine receptor 2B: evidence that directed migration is mediated by betagamma dimers released by activation of Galphai-coupled receptors. *Proceedings of the National Academy of Sciences of the United States of America* 94, 14495–14499

186. Neptune, E R&Bourne, H R (1997). Receptors induce chemotaxis by releasing the betagamma subunit of Gi, not by activating Gq or Gs. *Proceedings of the National Academy of Sciences of the United States of America* 94, 14489–14494

187. Huang, Y E *et al.* (2003). Receptor-mediated regulation of PI3Ks confines PI(3,4,5)P3 to the leading edge of chemotaxing cells. *Molecular biology of the cell* 14, 1913–1922

188. Gardiner, E M *et al.* (2002). Spatial and Temporal Analysis of Rac Activation during Live Neutrophil Chemotaxis. *Current Biology* 12, 2029–2034

189. Welch, M D&Mullins, R D (2002). Cellular control of actin nucleation. *Annual review of cell and developmental biology* 18, 247–288

190. Dong, X *et al.* (2005). P-Rex1 is a primary Rac2 guanine nucleotide exchange factor in mouse neutrophils. *Current Biology* 15, 1874–1879

191. Roberts, A W *et al.* (1999). Deficiency of the Hematopoietic Cell-Specific Rho Family GTPase Rac2 Is Characterized by Abnormalities in Neutrophil Function and Host Defense. *Immunity* 10, 183–196

192. Bear, J E *et al.* (1998). SCAR, a WASP-related protein, isolated as a suppressor of receptor defects in late Dictyostelium development. *The Journal of cell biology* 142, 1325–1335

193. Miki, H *et al.* (1998). WAVE, a novel WASP-family protein involved in actin reorganization induced by Rac. *The EMBO journal* 17, 6932–6941

194. Cory, G O C&Ridley, A J (2002). Cell motility: braking WAVEs. *Nature* 418, 732–733

195. Weber, K S C *et al.* (1998). Chemokine-induced monocyte transmigration requires cdc42-mediated cytoskeletal changes. *Eur. J. Immunol.* 28, 2245–2251

196. Haddad, E *et al.* (2001). The interaction between Cdc42 and WASP is required for SDF-1-induced T-lymphocyte chemotaxis. *Blood* 97, 33–38

197. Allen, W E *et al.* (1998). A role for Cdc42 in macrophage chemotaxis. *The Journal of cell biology* 141, 1147–1157

198. Jones, G E (2000). Cellular signaling in macrophage migration and chemotaxis. *Journal of leukocyte biology* 68, 593–602

199. Etienne-Manneville, S&Hall, A (2002). Rho GTPases in cell biology. *Nature* 420, 629–635

200. Deakin, N O&Turner, C E (2008). Paxillin comes of age. *Journal of cell science* 121, 2435–2444

201. Li, Z *et al.* (2003). Directional Sensing Requires Gβγ-Mediated PAK1 and PIXα-Dependent Activation of Cdc42. *Cell* 114, 215–227

202. Higgs, H N&Pollard, T D (2000). Activation by Cdc42 and PIP(2) of Wiskott-Aldrich syndrome protein (WASp) stimulates actin nucleation by Arp2/3 complex. *The Journal of cell biology* 150, 1311–1320

203. Bokoch, G M (2003). Biology of the p21-activated kinases. *Annual review of biochemistry* 72, 743–781

204. Kamp, M E *et al.* (2016). Function and Regulation of Heterotrimeric G Proteins during Chemotaxis. *International journal of molecular sciences* 17

205. Wang, F (2009). The signaling mechanisms underlying cell polarity and chemotaxis. *Cold Spring Harbor perspectives in biology* 1, a002980

206. Xu, J *et al.* (2003). Divergent Signals and Cytoskeletal Assemblies Regulate Self-Organizing Polarity in Neutrophils. *Cell* 114, 201–214

207. Rossman, K L *et al.* (2005). GEF means go: turning on RHO GTPases with guanine nucleotide-exchange factors. *Nature reviews. Molecular cell biology* 6, 167–180

208. Krendel, M *et al.* (2002). Nucleotide exchange factor GEF-H1 mediates cross-talk between microtubules and the actin cytoskeleton. *Nature cell biology* 4, 294–301

209. Ren, Y *et al.* (1998). Cloning and characterization of GEF-H1, a microtubule-associated guanine nucleotide exchange factor for Rac and Rho GTPases. *The Journal of biological chemistry* 273, 34954–34960

210. Hart, M J *et al.* (1998). Direct stimulation of the guanine nucleotide exchange activity of p115 RhoGEF by Galpha13. *Science (New York, N.Y.)* 280, 2112–2114

211. Nalbant, P *et al.* (2009). Guanine nucleotide exchange factor-H1 regulates cell migration via localized activation of RhoA at the leading edge. *Molecular biology of the cell* 20, 4070–4082

212. Chang, Y-C *et al.* (2008). GEF-H1 couples nocodazole-induced microtubule disassembly to cell contractility via RhoA. *Molecular biology of the cell* 19, 2147–2153

213. Evers, E *et al.* (2000). Rho family proteins in cell adhesion and cell migration. *European Journal of Cancer* 36, 1269–1274

214. Pruenster, M *et al.* (2015). Extracellular MRP8/14 is a regulator of β2 integrin-dependent neutrophil slow rolling and adhesion. *Nature communications* 6, 6915

215. Quast, T *et al.* (2022). A Stable Chemokine Gradient Controls Directional Persistence of Migrating Dendritic Cells. *Frontiers in cell and developmental biology* 10, 943041

216. Wolf, K *et al.* (2009). Collagen-based cell migration models in vitro and in vivo. *Seminars in cell & developmental biology* 20, 931–941

217. Doyle, A D *et al.* (2013). Dimensions in cell migration. *Current opinion in cell biology* 25, 642–649

218. Faure-André, G *et al.* (2008). Regulation of dendritic cell migration by CD74, the MHC class II-associated invariant chain. *Science (New York, N.Y.)* 322, 1705–1710

219. Heit, B&Kubes, P (2003). Measuring chemotaxis and chemokinesis: the under-agarose cell migration assay. *Science's STKE : signal transduction knowledge environment* 2003, PL5

220. Garcia-Arcos, J M *et al.* (2019). Reconstitution of cell migration at a glance. *Journal of cell science* 132

221. Fujii, T (2002). PDMS-based microfluidic devices for biomedical applications. *Microelectronic Engineering* 61-62, 907–914

222. Vargas, P *et al.* (2014). Study of cell migration in microfabricated channels. *Journal of visualized experiments : JoVE,* e51099

223. Sala, F *et al.* (2022). Microfluidic Lab-on-a-Chip for Studies of Cell Migration under Spatial Confinement. *Biosensors* 12

224. Saxena, N *et al.* (2021). Fabrication of a microfluidic device for studying the combinatorial effect of physical and chemical cues on cell migration. *STAR protocols* 2, 100310

225. Vesperini, D *et al.* (2021). Characterization of immune cell migration using microfabrication. *Biophysical reviews* 13, 185–202

226. Renkawitz, J *et al.* (2018). Micro-engineered "pillar forests" to study cell migration in complex but controlled 3D environments. *Methods in cell biology* 147, 79–91

227. Leithner, A *et al.* (2016). Geometrically complex microfluidic devices for the study of cell migration. *Protocol Exchange*

228. Friedl, P&Bröcker, E B (2000). The biology of cell locomotion within three-dimensional extracellular matrix. *Cellular and molecular life sciences : CMLS* 57, 41–64

229. Varennes, J *et al.* (2019). Physical constraints on accuracy and persistence during breast cancer cell chemotaxis. *PLoS computational biology* 15, e1006961

230. Petrie, R J *et al.* (2009). Random versus directionally persistent cell migration. *Nature reviews. Molecular cell biology* 10, 538–549

231. Bornens, M *et al.* (1987). Structural and chemical characterization of isolated centrosomes. *Cell motility and the cytoskeleton* 8, 238–249

232. Chevrier, V *et al.* (2002). The Rho-associated protein kinase p160ROCK is required for centrosome positioning. *The Journal of cell biology* 157, 807–817

233. Doxsey, S (2001). Re-evaluating centrosome function. *Nature reviews. Molecular cell biology* 2, 688–698

234. Azimzadeh, J&Marshall, W F (2010). Building the centriole. *Current biology : CB* 20, R816-25

235. Gönczy, P (2012). Towards a molecular architecture of centriole assembly. *Nature reviews. Molecular cell biology* 13, 425–435

236. Paintrand, M *et al.* (1992). Centrosome organization and centriole architecture: Their sensitivity to divalent cations. *Journal of Structural Biology* 108, 107–128

237. Malone, C J *et al.* (2003). The C. elegans Hook Protein, ZYG-12, Mediates the Essential Attachment between the Centrosome and Nucleus. *Cell* 115, 825–836

238. Bornens, M (1977). Is the centriole bound to the nuclear membrane? *Nature* 270, 80–82

239. Fais, D *et al.* (1984). Evidence for the nucleus-centriole association in living cells obtained by ultracentrifugation. *European journal of cell biology* 33, 190–196

240. Tzur, Y B *et al.* (2006). SUN-domain proteins: 'Velcro' that links the nucleoskeleton to the cytoskeleton. *Nature reviews. Molecular cell biology* 7, 782–788

241. Burakov, A V&Nadezhdina, E S (2013). Association of nucleus and centrosome: magnet or velcro? *Cell biology international* 37, 95–104

242. Kuriyama, R&Borisy, G G (1981). Centriole cycle in Chinese hamster ovary cells as determined by whole-mount electron microscopy. *The Journal of cell biology* 91, 814–821

243. Guichard, P *et al.* (2021). The centriolar tubulin code. *Seminars in cell & developmental biology*

244. Lutz, W *et al.* (2001). Phosphorylation of centrin during the cell cycle and its role in centriole separation preceding centrosome duplication. *The Journal of biological chemistry* 276, 20774–20780

245. Janke, C&Bulinski, J C (2011). Post-translational regulation of the microtubule cytoskeleton: mechanisms and functions. *Nature reviews. Molecular cell biology* 12, 773–786

246. Piperno, G&Fuller, M T (1985). Monoclonal antibodies specific for an acetylated form of alpha-tubulin recognize the antigen in cilia and flagella from a variety of organisms. *The Journal of cell biology* 101, 2085–2094

247. Eddé, B *et al.* (1990). Posttranslational glutamylation of alpha-tubulin. *Science (New York, N.Y.)* 247, 83–85

248. Wang, J T *et al.* (2017). Centriole triplet microtubules are required for stable centriole formation and inheritance in human cells. *eLife* 6

249. Kochanski, R S&Borisy, G G (1990). Mode of centriole duplication and distribution. *The Journal of cell biology* 110, 1599–1605

250. Rousselet, A *et al.* (2001). Structural and functional effects of hydrostatic pressure on centrosomes from vertebrate cells. *Cell motility and the cytoskeleton* 48, 262–276

251. Nigg, E A&Holland, A J (2018). Once and only once: mechanisms of centriole duplication and their deregulation in disease. *Nature reviews. Molecular cell biology* 19, 297–312

252. Bettencourt-Dias, M&Glover, D M (2007). Centrosome biogenesis and function: centrosomics brings new understanding. *Nature reviews. Molecular cell biology* 8, 451–463

253. Lawo, S *et al.* (2012). Subdiffraction imaging of centrosomes reveals higher-order organizational features of pericentriolar material. *Nature cell biology* 14, 1148–1158

254. Sonnen, K F *et al.* (2012). 3D-structured illumination microscopy provides novel insight into architecture of human centrosomes. *Biology open* 1, 965–976

255. Tsou, M-F B&Stearns, T (2006). Controlling centrosome number: licenses and blocks. *Current opinion in cell biology* 18, 74–78

256. Marshall, W F *et al.* (2001). Kinetics and regulation of de novo centriole assembly. *Current Biology* 11, 308–317

257. Brabander, M de *et al.* (1982). Microtubule stability and assembly in living cells: the influence of metabolic inhibitors, taxol and pH. *Cold Spring Harbor symposia on quantitative biology* 46 Pt 1, 227–240

258. Piel, M *et al.* (2000). The respective contributions of the mother and daughter centrioles to centrosome activity and behavior in vertebrate cells. *The Journal of cell biology* 149, 317–330

259. Debec, A *et al.* (2010). Centrioles: active players or passengers during mitosis? *Cellular and molecular life sciences : CMLS* 67, 2173–2194

260. Conduit, P T *et al.* (2015). Centrosome function and assembly in animal cells. *Nature reviews. Molecular cell biology* 16, 611–624

261. Haren, L *et al.* (2009). Plk1-dependent recruitment of gamma-tubulin complexes to mitotic centrosomes involves multiple PCM components. *PloS one* 4, e5976

262. Lee, K&Rhee, K (2011). PLK1 phosphorylation of pericentrin initiates centrosome maturation at the onset of mitosis. *The Journal of cell biology* 195, 1093–1101

263. Joukov, V *et al.* (2014). The Cep192-organized aurora A-Plk1 cascade is essential for centrosome cycle and bipolar spindle assembly. *Molecular cell* 55, 578–591

264. Terada, Y *et al.* (2003). Interaction of Aurora-A and centrosomin at the microtubule-nucleating site in Drosophila and mammalian cells. *The Journal of cell biology* 162, 757–763

265. Meng, L *et al.* (2015). Bimodal Interaction of Mammalian Polo-Like Kinase 1 and a Centrosomal Scaffold, Cep192, in the Regulation of Bipolar Spindle Formation. *Molecular and cellular biology* 35, 2626–2640

266. Bettencourt-Dias, M *et al.* (2005). SAK/PLK4 is required for centriole duplication and flagella development. *Current Biology* 15, 2199–2207

267. Habedanck, R *et al.* (2005). The Polo kinase Plk4 functions in centriole duplication. *Nature cell biology* 7, 1140–1146

268. Fu, J *et al.* (2015). The centrosome and its duplication cycle. *Cold Spring Harbor perspectives in biology* 7, a015800

269. Warnke, S *et al.* (2004). Polo-like kinase-2 is required for centriole duplication in mammalian cells. *Current Biology* 14, 1200–1207

270. Guichard, P *et al.* (2010). Procentriole assembly revealed by cryo-electron tomography. *The EMBO journal* 29, 1565–1572

271. Wong, C&Stearns, T (2003). Centrosome number is controlled by a centrosome-intrinsic block to reduplication. *Nature cell biology* 5, 539–544

272. Schmidt, T I *et al.* (2009). Control of Centriole Length by CPAP and CP110. *Current Biology* 19, 1005–1011

273. Tang, C-J C *et al.* (2009). CPAP is a cell-cycle regulated protein that controls centriole length. *Nature cell biology* 11, 825–831

274. Chrétien, D *et al.* (1997). Reconstruction of the centrosome cycle from cryoelectron micrographs. *Journal of Structural Biology* 120, 117–133

275. Blangy, A *et al.* (1995). Phosphorylation by p34cdc2 regulates spindle association of human Eg5, a kinesin-related motor essential for bipolar spindle formation in vivo. *Cell* 83, 1159–1169

276. Yang, J *et al.* (2006). Rootletin interacts with C-Nap1 and may function as a physical linker between the pair of centrioles/basal bodies in cells. *Molecular biology of the cell* 17, 1033–1040

277. Bahe, S *et al.* (2005). Rootletin forms centriole-associated filaments and functions in centrosome cohesion. *The Journal of cell biology* 171, 27–33

278. Mayor, T *et al.* (2000). The centrosomal protein C-Nap1 is required for cell cycle-regulated centrosome cohesion. *The Journal of cell biology* 151, 837–846

279. Fry, A M *et al.* (2017). Recent advances in pericentriolar material organization: ordered layers and scaffolding gels. *F1000Research* 6, 1622

280. Watanabe, K *et al.* (2019). The Cep57-pericentrin module organizes PCM expansion and centriole engagement. *Nature communications* 10, 931

281. Asteriti, I A *et al.* (2015). Cross-Talk between AURKA and Plk1 in Mitotic Entry and Spindle Assembly. *Frontiers in oncology* 5, 283

282. Pimenta-Marques, A&Bettencourt-Dias, M (2020). Pericentriolar material. *Current biology : CB* 30, R687-R689

283. Tsou, M-F B&Stearns, T (2006). Mechanism limiting centrosome duplication to once per cell cycle. *Nature* 442, 947–951

284. Tsou, M-F B *et al.* (2009). Polo kinase and separase regulate the mitotic licensing of centriole duplication in human cells. *Developmental cell* 17, 344–354

285. La Terra, S *et al.* (2005). The de novo centriole assembly pathway in HeLa cells: cell cycle progression and centriole assembly/maturation. *The Journal of cell biology* 168, 713–722

286. Riparbelli, M G&Callaini, G (2003). Drosophila parthenogenesis: a model for de novo centrosome assembly. *Developmental biology* 260, 298–313

287. Stinchcombe, J C&Griffiths, G M (2014). Communication, the centrosome and the immunological synapse. *Philosophical transactions of the Royal Society of London. Series B, Biological sciences* 369

288. Fourriere, L *et al.* (2020). The role of microtubules in secretory protein transport. *Journal of cell science* 133

289. Chabin-Brion, K *et al.* (2001). The Golgi complex is a microtubule-organizing organelle. *Molecular biology of the cell* 12, 2047–2060

290. Efimov, A *et al.* (2007). Asymmetric CLASP-dependent nucleation of noncentrosomal microtubules at the trans-Golgi network. *Developmental cell* 12, 917–930

291. Rodionov, V *et al.* (1999). Centrosomal control of microtubule dynamics. *Proceedings of the National Academy of Sciences of the United States of America* 96, 115–120

292. Kobayashi, T&Dynlacht, B D (2011). Regulating the transition from centriole to basal body. *The Journal of cell biology* 193, 435–444

293. Preble, A. M., Giddings, T. M. & Dutcher, S. K. Basal bodies and centrioles: Their function and structure. In *The Centrosome in Cell Replication and Early Development* (Elsevier1999), Vol. 49, pp. 207–233

294. Gould, R R&Borisy, G G (1977). The pericentriolar material in Chinese hamster ovary cells nucleates microtubule formation. *The Journal of cell biology* 73, 601–615

295. Bornens, M&Gönczy, P (2014). Centrosomes back in the limelight. *Philosophical transactions of the Royal Society of London. Series B, Biological sciences* 369

296. Bobinnec, Y *et al.* (1998). Centriole disassembly in vivo and its effect on centrosome structure and function in vertebrate cells. *The Journal of cell biology* 143, 1575–1589

297. Moritz, M *et al.* (1995). Microtubule nucleation by γ-tubulin-containing rings in the centrosome. *Nature* 378, 638–640

298. Zheng, Y *et al.* (1995). Nucleation of microtubule assembly by a gamma-tubulin-containing ring complex. *Nature* 378, 578–583

299. Delgehyr, N *et al.* (2005). Microtubule nucleation and anchoring at the centrosome are independent processes linked by ninein function. *Journal of cell science* 118, 1565–1575

300. Akhmanova, A&Kapitein, L C (2022). Mechanisms of microtubule organization in differentiated animal cells. *Nature reviews. Molecular cell biology* 23, 541–558

301. Oakley, C E&Oakley, B R (1989). Identification of γ-tubulin, a new member of the tubulin superfamily encoded by mipA gene of Aspergillus nidulans. *Nature* 338, 662–664

302. Martin, M&Akhmanova, A (2018). Coming into Focus: Mechanisms of Microtubule Minus-End Organization. *Trends in cell biology* 28, 574–588

303. Haren, L *et al.* (2006). NEDD1-dependent recruitment of the gamma-tubulin ring complex to the centrosome is necessary for centriole duplication and spindle assembly. *The Journal of cell biology* 172, 505–515

304. Muroyama, A&Lechler, T (2017). Microtubule organization, dynamics and functions in differentiated cells. *Development (Cambridge, England)* 144, 3012–3021

305. Mennella, V *et al.* (2012). Subdiffraction-resolution fluorescence microscopy reveals a domain of the centrosome critical for pericentriolar material organization. *Nature cell biology* 14, 1159–1168

306. Akhmanova, A&Steinmetz, M O (2015). Control of microtubule organization and dynamics: two ends in the limelight. *Nature reviews. Molecular cell biology* 16, 711–726

307. Muroyama, A *et al.* (2016). Divergent regulation of functionally distinct γ-tubulin complexes during differentiation. *The Journal of cell biology* 213, 679–692

308. Stiess, M *et al.* (2010). Axon extension occurs independently of centrosomal microtubule nucleation. *Science (New York, N.Y.)* 327, 704–707

309. Leask, A *et al.* (1997). Synaptically coupled central nervous system neurons lack centrosomal gamma-tubulin. *Neuroscience letters* 229, 17–20

310. Bugnard, E *et al.* (2005). Reorganization of microtubule nucleation during muscle differentiation. *Cell motility and the cytoskeleton* 60, 1–13

311. Becker, R *et al.* (2020). Microtubule Organization in Striated Muscle Cells. *Cells* 9

312. Tassin, A M *et al.* (1985). Fate of microtubule-organizing centers during myogenesis in vitro. *The Journal of cell biology* 100, 35–46

313. Oddoux, S *et al.* (2013). Microtubules that form the stationary lattice of muscle fibers are dynamic and nucleated at Golgi elements. *The Journal of cell biology* 203, 205–213

314. Sanchez, A D&Feldman, J L (2017). Microtubule-organizing centers: from the centrosome to non-centrosomal sites. *Current opinion in cell biology* 44, 93–101

315. Bacallao, R *et al.* (1989). The subcellular organization of Madin-Darby canine kidney cells during the formation of a polarized epithelium. *The Journal of cell biology* 109, 2817–2832

316. Bartolini, F&Gundersen, G G (2006). Generation of noncentrosomal microtubule arrays. *Journal of cell science* 119, 4155–4163

317. Keating, T J *et al.* (1997). Microtubule release from the centrosome. *Proceedings of the National Academy of Sciences of the United States of America* 94, 5078–5083

318. Hartman, J J *et al.* (1998). Katanin, a Microtubule-Severing Protein, Is a Novel AAA ATPase that Targets to the Centrosome Using a WD40-Containing Subunit. *Cell* 93, 277–287

319. Ahmad, F J *et al.* (1999). An essential role for katanin in severing microtubules in the neuron. *The Journal of cell biology* 145, 305–315

320. Mogensen, M M *et al.* (2000). Microtubule minus-end anchorage at centrosomal and non-centrosomal sites: the role of ninein. *Journal of cell science* 113 (Pt 17), 3013–3023

321. Yu, W *et al.* (1993). Microtubule nucleation and release from the neuronal centrosome. *The Journal of cell biology* 122, 349–359

322. Mogensen, M M *et al.* (1997). Centrosomal deployment of γ-tubulin and pericentrin: Evidence for a microtubule-nucleating domain and a minus-end docking domain in certain mouse epithelial cells. *Cell motility and the cytoskeleton* 36, 276–290

323. Wu, J *et al.* (2016). Molecular Pathway of Microtubule Organization at the Golgi Apparatus. *Developmental cell* 39, 44–60

324. Meiring, J C M *et al.* (2020). Generation and regulation of microtubule network asymmetry to drive cell polarity. *Current opinion in cell biology* 62, 86–95

325. Ueda, M *et al.* (1997). Centrosome positioning and directionality of cell movements. *Proceedings of the National Academy of Sciences of the United States of America* 94, 9674–9678

326. Farina, F *et al.* (2016). The centrosome is an actin-organizing centre. *Nature cell biology* 18, 65–75

327. Inoue, D *et al.* (2019). Actin filaments regulate microtubule growth at the centrosome. *The EMBO journal* 38

328. Ganem, N J *et al.* (2009). A mechanism linking extra centrosomes to chromosomal instability. *Nature* 460, 278–282

329. Basto, R *et al.* (2008). Centrosome amplification can initiate tumorigenesis in flies. *Cell* 133, 1032–1042

330. Levine, M S *et al.* (2017). Centrosome Amplification Is Sufficient to Promote Spontaneous Tumorigenesis in Mammals. *Developmental cell* 40, 313-322.e5

331. Pihan, G A *et al.* (1998). Centrosome defects and genetic instability in malignant tumors. *Cancer research* 58, 3974–3985

332. Lingle, W L *et al.* (1998). Centrosome hypertrophy in human breast tumors: implications for genomic stability and cell polarity. *Proceedings of the National Academy of Sciences of the United States of America* 95, 2950–2955

333. Nigg, E A (2002). Centrosome aberrations: cause or consequence of cancer progression? *Nature reviews. Cancer* 2, 815–825

334. Bettencourt-Dias, M *et al.* (2011). Centrosomes and cilia in human disease. *Trends in genetics : TIG* 27, 307–315

335. Hansemann, D. Ueber pathologische Mitosen. In *Band 123* (De Gruyter1891), pp. 356–370

336. Chan, J Y (2011). A clinical overview of centrosome amplification in human cancers. *International journal of biological sciences* 7, 1122–1144

337. Godinho, S A *et al.* (2014). Oncogene-like induction of cellular invasion from centrosome amplification. *Nature* 510, 167–171

338. Denu, R A *et al.* (2018). Centriole Overduplication is the Predominant Mechanism Leading to Centrosome Amplification in Melanoma. *Molecular cancer research : MCR* 16, 517–527

339. Prosser, S L *et al.* (2009). Molecular dissection of the centrosome overduplication pathway in S-phase-arrested cells. *Molecular and cellular biology* 29, 1760–1773

340. Kim, S-J *et al.* (2020). ATAD5 suppresses centrosome over-duplication by regulating UAF1 and ID1. *Cell cycle (Georgetown, Tex.)* 19, 1952–1968

341. Balczon, R *et al.* (1995). Dissociation of centrosome replication events from cycles of DNA synthesis and mitotic division in hydroxyurea-arrested Chinese hamster ovary cells. *The Journal of cell biology* 130, 105–115

342. Gard, D L *et al.* (1990). Centrosome duplication continues in cycloheximide-treated Xenopus blastulae in the absence of a detectable cell cycle. *The Journal of cell biology* 110, 2033–2042

343. Sinha, D *et al.* (2019). Mitotic slippage: an old tale with a new twist. *Cell cycle (Georgetown, Tex.)* 18, 7–15

344. Cheng, B&Crasta, K (2017). Consequences of mitotic slippage for antimicrotubule drug therapy. *Endocrine-related cancer* 24, T97-T106

345. Behrndt, M *et al.* (2012). Forces driving epithelial spreading in zebrafish gastrulation. *Science (New York, N.Y.)* 338, 257–260

346. Schindelin, J *et al.* (2012). Fiji: an open-source platform for biological-image analysis. *Nature methods* 9, 676–682

347. Schneider, C A *et al.* (2012). NIH Image to ImageJ: 25 years of image analysis. *Nature methods* 9, 671–675

348. Pflicke, H&Sixt, M (2009). Preformed portals facilitate dendritic cell entry into afferent lymphatic vessels. *The Journal of experimental medicine* 206, 2925–2935

349. Nigg, E A (2007). Centrosome duplication: of rules and licenses. *Trends in cell biology* 17, 215–221

350. Higginbotham, H *et al.* (2004). Transgenic mouse line with green-fluorescent protein-labeled Centrin 2 allows visualization of the centrosome in living cells. *Transgenic research* 13, 155–164

351. Piperno, G *et al.* (1987). Microtubules containing acetylated alpha-tubulin in mammalian cells in culture. *The Journal of cell biology* 104, 289–302

352. Balashova, E E *et al.* (2009). Distribution of tyrosinated and acetylated tubulin in centrioles during mitosis of 3T3 and SV40-3T3 cells. *Cell Tiss. Biol.* 3, 359–368

353. Sulimenko, V *et al.* (2017). Regulation of microtubule nucleation mediated by γ-tubulin complexes. *Protoplasma* 254, 1187–1199

354. Holzmann, S *et al.* (2004). A model system using tape stripping for characterization of Langerhans cell-precursors in vivo. *The Journal of investigative dermatology* 122, 1165–1174

355. Malumbres, M&Barbacid, M (2005). Mammalian cyclin-dependent kinases. *Trends in biochemical sciences* 30, 630–641

356. García-Reyes, B *et al.* (2018). The Emerging Role of Cyclin-Dependent Kinases (CDKs) in Pancreatic Ductal Adenocarcinoma. *International journal of molecular sciences* 19

357. Pagano, M *et al.* (1992). Cyclin A is required at two points in the human cell cycle. *The EMBO journal* 11, 961–971

358. Gérard, C&Goldbeter, A (2009). Temporal self-organization of the cyclin/Cdk network driving the mammalian cell cycle. *Proceedings of the National Academy of Sciences of the United States of America* 106, 21643–21648

359. Sherr, C J&Roberts, J M (2004). Living with or without cyclins and cyclin-dependent kinases. *Genes & development* 18, 2699–2711

360. Ohtsubo, M *et al.* (1995). Human cyclin E, a nuclear protein essential for the G1-to-S phase transition. *Molecular and cellular biology* 15, 2612–2624

361. Nurse, P (2000). A Long Twentieth Century of the Cell Cycle and Beyond. *Cell* 100, 71–78

362. Harbour, J *et al.* (1999). Cdk Phosphorylation Triggers Sequential Intramolecular Interactions that Progressively Block Rb Functions as Cells Move through G1. *Cell* 98, 859–869

363. Huang, X *et al.* (2012). Prolonged early G(1) arrest by selective CDK4/CDK6 inhibition sensitizes myeloma cells to cytotoxic killing through cell cycle-coupled loss of IRF4. *Blood* 120, 1095–1106

364. Fung, T K&Poon, R Y C (2005). A roller coaster ride with the mitotic cyclins. *Seminars in cell & developmental biology* 16, 335–342

365. Wade Harper, J (1993). The p21 Cdk-interacting protein Cip1 is a potent inhibitor of G1 cyclin-dependent kinases. *Cell* 75, 805–816

366. El-Deiry, W (1993). WAF1, a potential mediator of p53 tumor suppression. *Cell* 75, 817–825

367. Harper, J W *et al.* (1995). Inhibition of cyclin-dependent kinases by p21. *Molecular biology of the cell* 6, 387–400

368. Abukhdeir, A M&Park, B H (2008). P21 and p27: roles in carcinogenesis and drug resistance. *Expert reviews in molecular medicine* 10, e19

369. Sherr, C J&Roberts, J M (1999). CDK inhibitors: positive and negative regulators of G1-phase progression. *Genes & development* 13, 1501–1512

370. Weier, A-K *et al.* (2022). Multiple centrosomes enhance migration and immune cell effector functions of mature dendritic cells. *The Journal of cell biology* 221

371. Schafer, K A (1998). The cell cycle: a review. *Veterinary pathology* 35, 461–478

372. Musacchio, A&Salmon, E D (2007). The spindle-assembly checkpoint in space and time. *Nature reviews. Molecular cell biology* 8, 379–393

373. Overlack, K *et al.* (2015). A molecular basis for the differential roles of Bub1 and BubR1 in the spindle assembly checkpoint. *eLife* 4, e05269

374. Logarinho, E *et al.* (2004). Different spindle checkpoint proteins monitor microtubule attachment and tension at kinetochores in Drosophila cells. *Journal of cell science* 117, 1757–1771

375. Musacchio, A (2015). The Molecular Biology of Spindle Assembly Checkpoint Signaling Dynamics. *Current biology : CB* 25, R1002-18

376. Lok, T M *et al.* (2020). Mitotic slippage is determined by p31comet and the weakening of the spindle-assembly checkpoint. *Oncogene* 39, 2819–2834

377. Bolanos-Garcia, V M&Blundell, T L (2011). BUB1 and BUBR1: multifaceted kinases of the cell cycle. *Trends in biochemical sciences* 36, 141–150

378. Cleveland, D W *et al.* (2003). Centromeres and Kinetochores. *Cell* 112, 407–421

379. Maiato, H *et al.* (2004). The dynamic kinetochore-microtubule interface. *Journal of cell science* 117, 5461–5477

380. Koepp, D M *et al.* (1999). How the Cyclin Became a Cyclin. *Cell* 97, 431–434

381. Brito, D A&Rieder, C L (2006). Mitotic checkpoint slippage in humans occurs via cyclin B destruction in the presence of an active checkpoint. *Current biology : CB* 16, 1194–1200

382. Taylor, S S *et al.* (2001). Kinetochore localisation and phosphorylation of the mitotic checkpoint components Bub1 and BubR1 are differentially regulated by spindle events in human cells. *Journal of cell science* 114, 4385–4395

383. Hayashi, M T&Karlseder, J (2013). DNA damage associated with mitosis and cytokinesis failure. *Oncogene* 32, 4593–4601

384. Pampalona, J *et al.* (2012). Progressive telomere dysfunction causes cytokinesis failure and leads to the accumulation of polyploid cells. *PLoS genetics* 8, e1002679

385. Stearns, T (2001). Centrosome Duplication. *Cell* 105, 417–420

386. Randolph, G J *et al.* (2005). Dendritic-cell trafficking to lymph nodes through lymphatic vessels. *Nature reviews. Immunology* 5, 617–628

387. Magidson, V *et al.* (2007). Laser microsurgery in the GFP era: a cell biologist's perspective. *Methods in cell biology* 82, 239–266

388. Khodjakov, A *et al.* (1997). A synergy of technologies: Combining laser microsurgery with green fluorescent protein tagging. *Cell motility and the cytoskeleton* 38, 311–317

389. Quintyne, N J *et al.* (2005). Spindle multipolarity is prevented by centrosomal clustering. *Science (New York, N.Y.)* 307, 127–129

390. Pannu, V *et al.* (2014). Centrosome-declustering drugs mediate a two-pronged attack on interphase and mitosis in supercentrosomal cancer cells. *Cell death & disease* 5, e1538

391. Prakash, A *et al.* (2018). Clinically Applicable Inhibitors Impacting Genome Stability. *Molecules (Basel, Switzerland)* 23

392. Ogden, A *et al.* (2012). Let's huddle to prevent a muddle: centrosome declustering as an attractive anticancer strategy. *Cell death and differentiation* 19, 1255–1267

393. Bhakta-Guha, D *et al.* (2015). Dis-organizing centrosomal clusters: specific cancer therapy for a generic spread? *Current medicinal chemistry* 22, 685–694

394. Kwon, M *et al.* (2008). Mechanisms to suppress multipolar divisions in cancer cells with extra centrosomes. *Genes & development* 22, 2189–2203

395. Castiel, A *et al.* (2011). A phenanthrene derived PARP inhibitor is an extra-centrosomes de-clustering agent exclusively eradicating human cancer cells. *BMC cancer* 11, 412

396. Visochek, L *et al.* (2019). The phenanthrene derivative PJ34 exclusively eradicates human pancreatic cancer cells in xenografts. *Oncotarget* 10, 6269–6282

397. Raab, M S *et al.* (2012). GF-15, a novel inhibitor of centrosomal clustering, suppresses tumor cell growth in vitro and in vivo. *Cancer research* 72, 5374–5385

398. Inbar-Rozensal, D *et al.* (2009). A selective eradication of human nonhereditary breast cancer cells by phenanthridine-derived polyADP-ribose polymerase inhibitors. *Breast cancer research : BCR* 11, R78

399. Bai, X T *et al.* (2015). Small PARP inhibitor PJ-34 induces cell cycle arrest and apoptosis of adult T-cell leukemia cells. *Journal of hematology & oncology* 8, 117

400. Cohen-Armon, M (2020). The Modified Phenanthridine PJ34 Unveils an Exclusive Cell-Death Mechanism in Human Cancer Cells. *Cancers* 12

401. Madison, D L *et al.* (2011). The PARP inhibitor PJ34 causes a PARP1-independent, p21 dependent mitotic arrest. *DNA repair* 10, 1003–1013

402. Stępnik, M *et al.* (2017). Cytotoxicity of anticancer drugs and PJ-34 (poly(ADP-ribose)polymerase-1 (PARP-1) inhibitor) on HL-60 and Jurkat cells. *Advances in clinical and experimental medicine : official organ Wroclaw Medical University* 26, 379–385

403. Leber, B *et al.* (2010). Proteins required for centrosome clustering in cancer cells. *Science translational medicine* 2, 33ra38

404. Vos, M de *et al.* (2012). The diverse roles and clinical relevance of PARPs in DNA damage repair: current state of the art. *Biochemical pharmacology* 84, 137–146

405. Huang (2008). PJ34, an inhibitor of PARP-1, suppresses cell growth and enhances the suppressive effects of cisplatin in liver cancer cells. *Oncol Rep*

406. Vlijm, R *et al.* (2018). STED nanoscopy of the centrosome linker reveals a CEP68-organized, periodic rootletin network anchored to a C-Nap1 ring at centrioles.

Proceedings of the National Academy of Sciences of the United States of America 115, E2246-E2253

407. Lin, Y-C *et al.* (2013). Human microcephaly protein CEP135 binds to hSAS-6 and CPAP, and is required for centriole assembly. *The EMBO journal* 32, 1141–1154

408. Huppertz, B *et al.* (2006). Trophoblast fusion: fusogenic proteins, syncytins and ADAMs, and other prerequisites for syncytial fusion. *Micron (Oxford, England : 1993)* 37, 509–517

409. Buss, G *et al.* (2022). Postmitotic centriole disengagement and maturation leads to centrosome amplification in polyploid trophoblast giant cells. *Molecular biology of the cell* 33, ar118

410. Wilkie, A R *et al.* (2019). KIFC1 Mediates Centrosome Clustering Prior to Proplatelet Formation from Megakaryocytes. *Blood* 134, 721

411. Ching, K&Stearns, T (2020). Centrioles are amplified in cycling progenitors of olfactory sensory neurons. *PLoS biology* 18, e3000852

412. Guidotti, J-E *et al.* (2003). Liver cell polyploidization: a pivotal role for binuclear hepatocytes. *The Journal of biological chemistry* 278, 19095–19101

413. Oren-Suissa, M&Podbilewicz, B (2007). Cell fusion during development. *Trends in cell biology* 17, 537–546

414. Brooks, E R&Wallingford, J B (2014). Multiciliated cells. *Current biology : CB* 24, R973-82

415. Lingle, W L *et al.* (2002). Centrosome amplification drives chromosomal instability in breast tumor development. *Proceedings of the National Academy of Sciences of the United States of America* 99, 1978–1983

416. Ogden, A *et al.* (2013). Heading off with the herd: how cancer cells might maneuver supernumerary centrosomes for directional migration. *Cancer metastasis reviews* 32, 269–287

417. Arnandis, T *et al.* (2018). Oxidative Stress in Cells with Extra Centrosomes Drives Non-Cell-Autonomous Invasion. *Developmental cell* 47, 409-424.e9

418. Thompson, S L *et al.* (2010). Mechanisms of chromosomal instability. *Current biology : CB* 20, R285-95

419. Sluder, G *et al.* (1997). The checkpoint control for anaphase onset does not monitor excess numbers of spindle poles or bipolar spindle symmetry. *Journal of cell science* 110 (Pt 4), 421–429

420. Gönczy, P (2015). Centrosomes and cancer: revisiting a long-standing relationship. *Nature reviews. Cancer* 15, 639–652

421. Marteil, G *et al.* (2018). Over-elongation of centrioles in cancer promotes centriole amplification and chromosome missegregation. *Nature communications* 9, 1258

422. Lingle, W L&Salisbury, J L (1999). Altered centrosome structure is associated with abnormal mitoses in human breast tumors. *The American journal of pathology* 155, 1941–1951

423. Lingle, W L *et al.* (2005). Deregulation of the centrosome cycle and the origin of chromosomal instability in cancer. *Advances in experimental medicine and biology* 570, 393–421

424. Casenghi, M *et al.* (2003). Polo-like kinase 1 regulates Nlp, a centrosome protein involved in microtubule nucleation. *Developmental cell* 5, 113–125

425. Nigg, E A *et al.* (2014). The centrosome duplication cycle in health and disease. *FEBS letters* 588, 2366–2372

426. Sakaue-Sawano, A *et al.* (2008). Visualizing spatiotemporal dynamics of multicellular cell-cycle progression. *Cell* 132, 487–498

427. Li, X *et al.* (2003). The SCF(Skp2) ubiquitin ligase complex interacts with the human replication licensing factor Cdt1 and regulates Cdt1 degradation. *The Journal of biological chemistry* 278, 30854–30858

428. McGarry, T J&Kirschner, M W (1998). Geminin, an Inhibitor of DNA Replication, Is Degraded during Mitosis. *Cell* 93, 1043–1053

429. Nishitani, H *et al.* (2004). Proteolysis of DNA replication licensing factor Cdt1 in S-phase is performed independently of geminin through its N-terminal region. *The Journal of biological chemistry* 279, 30807–30816

430. Planelles, V *et al.* (1996). Vpr-induced cell cycle arrest is conserved among primate lentiviruses. *Journal of virology* 70, 2516–2524

431. He, J *et al.* (1995). Human immunodeficiency virus type 1 viral protein R (Vpr) arrests cells in the G2 phase of the cell cycle by inhibiting p34cdc2 activity. *Journal of virology* 69, 6705–6711

432. Jowett, J B *et al.* (1995). The human immunodeficiency virus type 1 vpr gene arrests infected T cells in the G2 + M phase of the cell cycle. *Journal of virology* 69, 6304–6313

433. Nagata, Y *et al.* (1997). Thrombopoietin-induced polyploidization of bone marrow megakaryocytes is due to a unique regulatory mechanism in late mitosis. *The Journal of cell biology* 139, 449–457

434. Vitrat, N *et al.* (1998). Endomitosis of Human Megakaryocytes Are Due to Abortive Mitosis. *Blood* 91, 3711–3723

435. Fox, D T&Duronio, R J (2013). Endoreplication and polyploidy: insights into development and disease. *Development (Cambridge, England)* 140, 3–12

436. Davoli, T&Lange, T de (2011). The causes and consequences of polyploidy in normal development and cancer. *Annual review of cell and developmental biology* 27, 585–610

437. Gentric, G *et al.* (2012). Hepatocytes polyploidization and cell cycle control in liver physiopathology. *International journal of hepatology* 2012, 282430

438. Edgar, B A&Orr-Weaver, T L (2001). Endoreplication Cell Cycles. *Cell* 105, 297–306

439. Lee, H O *et al.* (2009). Endoreplication: polyploidy with purpose. *Genes & development* 23, 2461–2477

440. Zhang, J *et al.* (2022). Human cell polyploidization: The good and the evil. *Seminars in cancer biology* 81, 54–63

441. Milliron, H-Y Y *et al.* (2019). Isolation of Cardiomyocytes Undergoing Mitosis With Complete Cytokinesis. *Circulation research* 125, 1070–1086

442. Margall-Ducos, G *et al.* (2007). Liver tetraploidization is controlled by a new process of incomplete cytokinesis. *Journal of cell science* 120, 3633–3639

443. Takegahara, N *et al.* (2016). Involvement of Receptor Activator of Nuclear Factor-κB Ligand (RANKL)-induced Incomplete Cytokinesis in the Polyploidization of Osteoclasts. *The Journal of biological chemistry* 291, 3439–3454

444. El-Hashash, A H K *et al.* (2010). Genes and signals regulating murine trophoblast cell development. *Mechanisms of development* 127, 1–20

445. Philip, R *et al.* (2022). Terminally differentiated osteoclasts organize centrosomes into large clusters for microtubule nucleation and bone resorption. *Molecular biology of the cell* 33, ar68

446. Pajcini, K V *et al.* (2008). Myoblasts and macrophages share molecular components that contribute to cell-cell fusion. *The Journal of cell biology* 180, 1005–1019

447. Faggioli, F *et al.* (2011). Single-cell analysis of ploidy and centrosomes underscores the peculiarity of normal hepatocytes. *PloS one* 6, e26080

448. Connolly, J A *et al.* (1986). Centrioles are lost as embryonic myoblasts fuse into myotubes in vitro. *European journal of cell biology* 39, 341–345

449. Ng, D C H *et al.* (2021). Cilia, Centrosomes and Skeletal Muscle. *IJMS* 22, 9605

450. Rieder, C L&Maiato, H (2004). Stuck in division or passing through: what happens when cells cannot satisfy the spindle assembly checkpoint. *Developmental cell* 7, 637–651

451. Sluder, G&Nordberg, J J (2004). The good, the bad and the ugly: the practical consequences of centrosome amplification. *Current opinion in cell biology* 16, 49–54

452. Mourón, S *et al.* (2010). RINGO C is required to sustain the spindle-assembly checkpoint. *Journal of cell science* 123, 2586–2595

453. Weaver, B A A&Cleveland, D W (2005). Decoding the links between mitosis, cancer, and chemotherapy: The mitotic checkpoint, adaptation, and cell death. *Cancer cell* 8, 7–12

454. Weaver, B A A&Cleveland, D W (2006). Does aneuploidy cause cancer? *Current opinion in cell biology* 18, 658–667

455. Ben-David, U&Amon, A (2020). Context is everything: aneuploidy in cancer. *Nature reviews. Genetics* 21, 44–62

456. Gordon, D J *et al.* (2012). Causes and consequences of aneuploidy in cancer. *Nature reviews. Genetics* 13, 189–203

457. McLellan, A D *et al.* (2000). Differential susceptibility to CD95 (Apo-1/Fas) and MHC class II-induced apoptosis during murine dendritic cell development. *Cell death and differentiation* 7, 933–938

458. Ingulli, E *et al.* (1997). In vivo detection of dendritic cell antigen presentation to CD4(+) T cells. *The Journal of experimental medicine* 185, 2133–2141

459. Kairouz, S *et al.* (2007). Dendritic cell neoplasms: an overview. *American journal of hematology* 82, 924–928

460. Sapienza, M R *et al.* (2019). Blastic Plasmacytoid Dendritic Cell Neoplasm: State of the Art and Prospects. *Cancers* 11

461. Hixon, M L *et al.* (2000). Cks1 mediates vascular smooth muscle cell polyploidization. *The Journal of biological chemistry* 275, 40434–40442

462. Vliegen, H W *et al.* (1995). Polyploidy of myocyte nuclei in pressure overloaded human hearts: a flow cytometric study in left and right ventricular myocardium. *The American journal of cardiovascular pathology* 5, 27–31

463. Krämer, A *et al.* (2005). Centrosome aberrations in hematological malignancies. *Cell biology international* 29, 375–383

464. Kleylein-Sohn, J *et al.* (2007). Plk4-induced centriole biogenesis in human cells. *Developmental cell* 13, 190–202

465. Sabino, D *et al.* (2015). Moesin is a major regulator of centrosome behavior in epithelial cells with extra centrosomes. *Current biology : CB* 25, 879–889

466. Budhu, A S&Wang, X W (2005). Loading and unloading: orchestrating centrosome duplication and spindle assembly by Ran/Crm1. *Cell cycle (Georgetown, Tex.)* 4, 1510–1514

467. Cosenza, M R&Krämer, A (2016). Centrosome amplification, chromosomal instability and cancer: mechanistic, clinical and therapeutic issues. *Chromosome research : an international journal on the molecular, supramolecular and evolutionary aspects of chromosome biology* 24, 105–126

468. Meraldi, P&Nigg, E A (2001). Centrosome cohesion is regulated by a balance of kinase and phosphatase activities. *Journal of cell science* 114, 3749–3757

469. Xia, Y *et al.* (2018). CCDC102B functions in centrosome linker assembly and centrosome cohesion. *Journal of cell science* 131

470. Haag, N *et al.* (2018). The Actin Nucleator Cobl Is Critical for Centriolar Positioning, Postnatal Planar Cell Polarity Refinement, and Function of the Cochlea. *Cell reports* 24, 2418-2431.e6

471. Tournier, F *et al.* (1991). The intercentriolar linkage is critical for the ability of heterologous centrosomes to induce parthenogenesis in Xenopus. *The Journal of cell biology* 113, 1361–1369

472. Conroy, P C *et al.* (2012). C-NAP1 and rootletin restrain DNA damage-induced centriole splitting and facilitate ciliogenesis. *Cell cycle (Georgetown, Tex.)* 11, 3769–3778

473. Graser, S *et al.* (2007). Cep68 and Cep215 (Cdk5rap2) are required for centrosome cohesion. *Journal of cell science* 120, 4321–4331

474. Fang, G *et al.* (2014). Centlein mediates an interaction between C-Nap1 and Cep68 to maintain centrosome cohesion. *Journal of cell science* 127, 1631–1639

475. Panic, M *et al.* (2015). The centrosomal linker and microtubules provide dual levels of spatial coordination of centrosomes. *PLoS genetics* 11, e1005243

476. Flanagan, A-M *et al.* (2017). Centriole splitting caused by loss of the centrosomal linker protein C-NAP1 reduces centriolar satellite density and impedes centrosome amplification. *Molecular biology of the cell* 28, 736–745

477. Mazo, G *et al.* (2016). Spatial Control of Primary Ciliogenesis by Subdistal Appendages Alters Sensation-Associated Properties of Cilia. *Developmental cell* 39, 424–437

478. Schliwa, M *et al.* (1982). Centrosome splitting in neutrophils: an unusual phenomenon related to cell activation and motility. *Cell* 31, 705–717

479. Farina, F *et al.* (2019). Local actin nucleation tunes centrosomal microtubule nucleation during passage through mitosis. *The EMBO journal* 38

480. Eot-Houllier, G *et al.* (2010). Plk1 regulates both ASAP localization and its role in spindle pole integrity. *The Journal of biological chemistry* 285, 29556–29568

481. Kushner, E J *et al.* (2014). Excess centrosomes disrupt endothelial cell migration via centrosome scattering. *The Journal of cell biology* 206, 257–272

482. Basto, R *et al.* (2006). Flies without centrioles. *Cell* 125, 1375–1386

483. Bulina, M E *et al.* (2006). Chromophore-assisted light inactivation (CALI) using the phototoxic fluorescent protein KillerRed. *Nature protocols* 1, 947–953

484. Liu, J *et al.* (2020). Light-induced control of protein destruction by opto-PROTAC. *Science advances* 6, eaay5154

485. LoMastro, G M&Holland, A J (2019). The Emerging Link between Centrosome Aberrations and Metastasis. *Developmental cell* 49, 325–331

486. Bid, H K *et al.* (2013). RAC1: an emerging therapeutic option for targeting cancer angiogenesis and metastasis. *Molecular cancer therapeutics* 12, 1925–1934

487. Xu, J *et al.* (2005). Neutrophil microtubules suppress polarity and enhance directional migration. *Proceedings of the National Academy of Sciences of the United States of America* 102, 6884–6889

488. Pfeiffer, J *et al.* (2018). Rapid progression through the cell cycle ensures efficient migration of primordial germ cells - The role of Hsp90. *Developmental biology* 436, 84–93

489. Lewis, L&Albrecht-Buehler, G (1987). Distribution of multiple centrospheres determines migration of BHK syncitia. *Cell motility and the cytoskeleton* 7, 282–290

490. Löffler, H *et al.* (2006). Structure meets function--centrosomes, genome maintenance and the DNA damage response. *Experimental cell research* 312, 2633–2640

491. Holland, A J&Cleveland, D W (2009). Boveri revisited: chromosomal instability, aneuploidy and tumorigenesis. *Nature reviews. Molecular cell biology* 10, 478–487

492. Galimberti, F *et al.* (2011). Anaphase catastrophe is a target for cancer therapy. *Clinical cancer research : an official journal of the American Association for Cancer Research* 17, 1218–1222

493. Brinkley, B (2001). Managing the centrosome numbers game: from chaos to stability in cancer cell division. *Trends in cell biology* 11, 18–21

494. Yang, Z *et al.* (2008). Extra centrosomes and/or chromosomes prolong mitosis in human cells. *Nature cell biology* 10, 748–751

495. Rønnest, M H *et al.* (2009). Synthesis and structure-activity relationship of griseofulvin analogues as inhibitors of centrosomal clustering in cancer cells. *Journal of medicinal chemistry* 52, 3342–3347

496. Kawamura, E *et al.* (2013). Identification of novel small molecule inhibitors of centrosome clustering in cancer cells. *Oncotarget* 4, 1763–1776

497. ÄrzteZeitung, S M. PARP-Inhibitoren „neuer Standard in der Primärtherapie“. PARP-Inhibitoren sind beim fortgeschrittenen Ovarialkarzinom in die Erstlinie aufgestiegen. Available at https://www.aerztezeitung.de/Medizin/PARP-Inhibitoren-neuer-Standard-in-der-Primaertherapie-409311.html (2020)

498. Eckstein, N&Weber--Lassalle, K. PARP-Inhibitoren als neue Option. Available at https://www.pharmazeutische-zeitung.de/index.php?id=55260 (2014)

499. Kirkham, M *et al.* (2003). SAS-4 is a C. elegans centriolar protein that controls centrosome size. *Cell* 112, 575–587

500. Leidel, S&Gönczy, P (2003). SAS-4 is essential for centrosome duplication in C elegans and is recruited to daughter centrioles once per cell cycle. *Developmental cell* 4, 431–439

501. Sluder, G&Rieder, C L (1985). Centriole number and the reproductive capacity of spindle poles. *The Journal of cell biology* 100, 887–896

502. Khodjakov, A *et al.* (2000). Centrosome-independent mitotic spindle formation in vertebrates. *Current Biology* 10, 59–67

503. Courtois, A *et al.* (2012). The transition from meiotic to mitotic spindle assembly is gradual during early mammalian development. *The Journal of cell biology* 198, 357–370

504. Baumbach, J *et al.* (2015). Dissecting the function and assembly of acentriolar microtubule organizing centers in Drosophila cells in vivo. *PLoS genetics* 11, e1005261

505. Hida, K *et al.* (2004). Tumor-associated endothelial cells with cytogenetic abnormalities. *Cancer research* 64, 8249–8255

506. Watts, C A *et al.* (2013). Design, synthesis, and biological evaluation of an allosteric inhibitor of HSET that targets cancer cells with supernumerary centrosomes. *Chemistry & biology* 20, 1399–1410

507. Mountain, V *et al.* (1999). The kinesin-related protein, HSET, opposes the activity of Eg5 and cross-links microtubules in the mammalian mitotic spindle. *The Journal of cell biology* 147, 351–366

508. Cai, S *et al.* (2009). Kinesin-14 family proteins HSET/XCTK2 control spindle length by cross-linking and sliding microtubules. *Molecular biology of the cell* 20, 1348–1359

509. Wu, J *et al.* (2013). Discovery and mechanistic study of a small molecule inhibitor for motor protein KIFC1. *ACS chemical biology* 8, 2201–2208

510. Xiao, Y-X&Yang, W-X (2016). KIFC1: a promising chemotherapy target for cancer treatment? *Oncotarget* 7, 48656–48670

511. Myers, S M&Collins, I (2016). Recent findings and future directions for interpolar mitotic kinesin inhibitors in cancer therapy. *Future medicinal chemistry* 8, 463–489

512. Nigg, E A (2006). Origins and consequences of centrosome aberrations in human cancers. *International journal of cancer* 119, 2717–2723

Acknowledgements

First of all, I would like to deeply thank Prof. Dr. Eva Kiermaier for giving me the opportunity to work in this fascinating project, for her scientific support and guidance throughout my PhD time. In addition, I am grateful for encouraging any continuing education to expand my skills and helping me not to get lost in the details but thinking more conceptional.

I would also like to extend my gratitude to my thesis committee, Prof. Dr. Oliver Gruß as second reviewer, and PD Dr. Heike Weighardt and Prof. Dr. Anton Bovier as members of the examination board for the evaluation of my work.

Moreover, I would like to express my gratefulness to all the past and present members of the Kiermaier and Kolanus group, who supported me with inspiring discussions, helpful ideas and delicious food. Many thanks go to Ann-Kathrin Weier for her endless patience with the cell sorter promoting the paper project and for the best Snickers cake I have ever tested. A special thanks to Stephanie Ebbinghaus for her great lab management, but especially for always having a hand to help and an ear to listen.

I am grateful to all the timed lab members for their contribution to my project and the nice times we had together, especially thanks to Michaela Limmer, Tabea Elschner, Annika Breuer and Simeon Wessler.

A very big thank you goes to Dr. Thomas Quast for much valuable advice and his support in all small and bigger issues, not least in setting up new microscope stuff.

I would like to express my gratitude to Prof. Dr. Michael Sixt for hosting me in his lab several times and giving me the opportunity to discuss my project. Many thanks go to Julian Stopp, who introduced me to the depths of PDMS device production, and Ingrid de Vries for facilitating my integration into the Sixt group. Furthermore, I would also like to sincerely thank the IST Imaging Facility, especially Robert Hauschild for data analysis and answering thousands of questions, and Anna Hapek, for never giving up on tracking down undetectable cells.

In addition, I would like to thank Sarah Förster, who has always been a great help to me in all scientific and non-scientific matters, and has proofread parts of the thesis. Furthermore, I thank Andy Zielinski for proofreading, discussing statistical issues, and solving computer problems, and Jonas Kahn for his spontaneous and competent help with formatting. A last but especially big thank you goes to my family, Björn Weiershausen, Julia Schöppach, Anne Böcking, Antje Fehr, Corinna Hees, Wiebke Aden, Jaqueline Rosinke, Matthias Bender and Helmut Müller for supporting and encouraging me.